Manipulation of malate biosynthesis and exudation in *Arabidopsis thaliana*

Dissertation

zur Erlangung des

Doktorgrades der Naturwissenschaften (Dr. rer. nat.)

der

Naturwissenschaftlichen Fakultät I – Biowissenschaften –

der Martin-Luther-Universität

Halle-Wittenberg

vorgelegt

von Frau Ranju Chutia, M.Sc.

geb. am 16.11.1990 in Sabarmati, Indien

1. Gutachter: Prof. Dr. Steffen Abel

2. Gutachter: Prof. Dr. Ingo Heilmann

3. Gutachter: Prof. Dr. Paul B. Larsen

Tag der öffentlichen Verteidigung: 10.12.2019

Nothing in life is to be feared, it is only to be understood. Now it is the time to understand more, so that we may fear less.

-**Marie Curie**

TABLE OF CONTENTS

LIST OF FIGURES……vi

LIST OF TABLES……vii

LIST OF SUPPLEMENTARY FIGURES……viii

LIST OF SUPPLEMENTARY TABLES……x

ABBREVIATIONS AND SYMBOLS……xi

1 INTRODUCTION 1

1.1 Importance of phosphorus 1

1.2 Plant adaptation to low Pi-stress 1

1.3 Organic acids and their importance during nutrient stresses 3

1.4 Biosynthesis of organic acids 6

1.4.1 Biosynthesis of malate 7

1.5 Phosphoenolpyruvate carboxylase (PPC) 8

1.5.1 Regulation of PPC 9

1.6 Phosphoenolpyruvate carboxylase kinase (PPCK) 10

1.6.1 Regulation of PPCK 11

1.7 Pi-deficiency and metabolic bypass via PPC 11

1.8 Manipulation of malate and citrate biosynthesis and their transport 13

1.9 Manipulation of PPC/PPCK pathway 15

1.10 Hypothesis and objectives 17

2 RESULTS 19

2.1 Influence of Pi-starvation on PPC/PPCK pathway in Arabidopsis 19

2.1.1 Malate and citrate content after Pi-starvation in Arabidopsis 19

2.1.2 Malate and citrate exudation after Pi-starvation in Arabidopsis 19

2.1.3 Expression analysis of *PPC*s and *PPCK*s by RT-qPCR 21

2.1.4 Expression analysis of *PPC*s and *PPCK*s in *phr1phl1* mutant by RT-qPCR 22

2.1.5 Tissue-specific expression analysis of *PPCK1* and *PPCK2* 22
2.1.5.1 Expression analysis of *PPCKs* by promoter GUS reporter lines 23
2.1.5.2 Expression analysis of *PPCKs* by promoter GFP reporter lines 23
2.1.6 Expression analysis of *PPCK1* and *PPCK2* in root-tips after different time points of Pi-deficiency treatment 24
2.1.7 Expression analysis of *PPCKs* in root-tips of plants growing on split plates 25
2.1.8 Characterization of transgenic lines having translational fusion construct of PPCK1 under its native promoter 25
2.1.8.1 Malate content in transgenic lines having translational fusion construct of PPCK1 under its native promoter 26
2.1.9 Western blot analysis to detect PPCK1 protein levels after Pi-starvation 27
2.1.9.1 Detection of PPCK1 protein in *pPPCK1$_{long}$::gDNA-GFP/ppck1-1* lines 27
2.1.10 Expression analysis of *MDH*s by RT-qPCR 28
2.1.11 Characterization of plants deficient in PPCs 30
2.1.11.1 Malate and citrate content in plants deficient in *PPC*s 30
2.1.12 Characterization of transgenic lines having GFP tagged PPCKs 31
2.1.12.1 Western blot analysis of transgenic lines having GFP-tagged PPCKs 31
2.1.12.2 Malate content in transgenic lines having GFP-tagged PPCKs 32
2.1.12.3 Subcellular localization of PPCK1 and PPCK2 33
2.2 Manipulation of PPC/PPCK pathway by misexpression of *PPCK*s 34
2.2.1 Modification of PPC/PPCK pathway by overexpression of *PPCK*s 34
2.2.1.1 Characterization of transgenic lines overexpressing *PPCKs* 34
2.2.1.2 Growth analysis of transgenic lines overexpressing *PPCK1* and *PPCK2* 35
2.2.1.3 Malate and citrate content in transgenic lines overexpressing *PPCKs* 36
2.2.1.4 Malate and citrate exudation in transgenic lines overexpressing *PPCKs* 37
2.2.2 Modification of PPC/PPCK pathway by downregulation of *PPCK1* 39
2.2.2.1 Malate and citrate content in *ppck1-1* line 42
2.2.2.2 Phenotypic analysis of *ppck1-1* line 43
2.2.2.3 Malate and citrate exudation in *ppck1-1* line 45
2.2.2.4 Hypersensitive root growth response of *ppck1-1* line and *ALMT1* overexpressor after Pi-starvation 46
2.2.2.5 Malate and citrate content in *almt1* and *ALMT1^{OE}* 47
2.2.2.6 Expression analysis of *ALMT1* in roots of *ppck1-1* line 48
2.2.2.7 Characterization of transgenic lines generated to complement *ppck1-1* 49

2.2.2.8 Detection of a second site insertion in *ppck1-1* line 52
2.2.2.9 Characterization of T-DNA insertion lines of *ALMT2* 54
2.2.2.10 Characterization of other T-DNA insertion lines of *PPCK1* 54
2.2.2.11 Expression analysis of *ALMT1* and *ALMT2* in *ppck1-4* line 59
2.2.2.12 Expression analysis of *PPCK2* and *PPCs* in *ppck1-1 and ppck1-4* lines 59
2.3 Effect of malate exudation on Pi-solubilization capacity of plants 60
2.3.1 Pi content in *PPCK1* and *PPCK2* overexpressors 61
2.3.2 Pi content in *ppck1-1* and complementation lines 62
2.3.3 Pi content in *ppck1-4*, *almt1*, and *ALMT1^{OE}* 62
2.3.4 Performance of K- and C-lines on media supplemented with insoluble Pi-source, calcium-phosphate 62
2.3.4.1 Pi content in K- and C-lines 62
2.3.4.2 Malate content in K- and C-lines 64
2.4 Analysis of other metabolites in all the generated transgenic lines 65
2.4.1 Metabolites altered in transgenic plants overexpressing *PPCKs* 65
2.4.2 Metabolites altered in *ppck1-1* line 66
2.4.3 Metabolites altered in complementation lines 67
2.4.4 Metabolites altered in *ppck1-4* line 67
2.4.5 Metabolites altered in *ALMT1^{OE}* 68
3 DISCUSSION 69
3.1 Role of individual PPC isoforms in Arabidopsis 69
3.2 Role of PPCK isoforms in Arabidopsis 72
3.3 Subcellular localization of PPCKs in Arabidopsis 74
3.4 Contribution of PPCK1 and PPCK2 to malate and citrate generation 75
3.5 Effect of *PPCK* overexpression on malate content under Pi-sufficient conditions 77
3.6 Effect of *PPCK* overexpression on citrate content under Pi-sufficient conditions 79
3.7 Effect of *PPCK* overexpression on malate and citrate content under Pi-deficient conditions 81
3.8 Effect of altered *PPCK* expression on the morphology of plants 83

3.9 Effect of malate exudation on primary root length during low Pi stress....84

3.10 Pi-solubilization capacity of transgenic lines....87

4 SUMMARY AND OUTLOOK....89

5 MATERIALS AND METHODS....92

5.1 Materials....92

5.1.1 Chemicals, Reagents, and standards....92

5.1.2 Bacterial strains and plasmid vectors....92

5.2 Media....92

5.3 Plant material and cultivation....94

5.3.1 Plant lines....94

5.3.2 Plant cultivation on soil....94

5.3.3 Plant cultivation under aseptic conditions....94

5.3.4 Transformation of Arabidopsis....94

5.3.5 Selection of transformed Arabidopsis plants....95

5.4 Bacterial culture and transformation....95

5.4.1 *Escherichia coli* and *Agrobacterium tumefaciens* cultivation....95

5.4.2 *Escherichia coli* and *Agrobacterium tumefaciens* transformation....95

5.5 Molecular Biology methods....96

5.5.1 Isolation of genomic DNA....96

5.5.2 Isolation of plasmid DNA from *E. coli*....96

5.5.3 Polymerase chain reaction (PCR)....96

5.5.3.1 Standard PCRs....97

5.5.3.2 High fidelity PCR for molecular cloning....97

5.5.4 Agarose gel electrophoresis....98

5.5.5 Extraction of DNA fragments from agarose gel....98

5.5.6 Gateway cloning....98

5.5.6.1 Directional cloning in pENTR/D-TOPO vector system....98

5.5.6.2 Generation of expression clones via the Gateway system....99

5.5.7 Restriction enzyme digestion....99

5.5.8 Analysis of transcript levels from Arabidopsis seedlings 99
5.5.8.1 Isolation of RNA 99
5.5.8.2 Processing of RNA samples to prevent contamination by genomic DNA 100
5.5.8.3 cDNA synthesis 100
5.5.8.4 Semi-quantitative PCR (RT-PCR) 100
5.5.8.5 Quantitative Real-Time-PCR (RT-qPCR) 100
5.6 Biochemical Methods 101
5.6.1 Analysis of metabolites from plant tissues and exudates 101
5.6.1.1 Extraction of samples for targeted metabolite profiling 101
5.6.1.2 Analysis of amino acids 101
5.6.1.3 Analysis of organic acids 102
5.6.1.4 Water incubation experiment for root exudate analysis 103
5.6.1.5 Preparation of exudates for organic acid analysis 103
5.6.2 Treatment of plants with calcium phosphate as insoluble Pi-source 103
5.6.3 Analysis of protein from plant tissues 104
5.6.3.1 Extraction of protein from plant material 104
5.6.3.2 Protein quantification 104
5.6.3.3 Sodium dodecyl sulfate polyacrilamide gel electrophoresis (SDS-PAGE) 104
5.6.3.4 Immunoblotting (Western Blot) 105
5.6.4 Histochemical analysis 105
5.6.4.1 Iron staining 105
5.6.4.2 Callose staining 106
5.6.4.3 GUS (β-glucuronidase) staining 106
5.6.4.4 Confocal laser microscopy 106
5.6.5 Physiological assays 106
5.6.5.1 Root length measurement assay 106
5.7 Data analysis 106
6 REFERENCES 107
7 APPENDIX 124
ACKNOWLEDGEMENT xiv
CURRICULUM VITAE xvi
STATUTORY DECLARATION xvii

LIST OF FIGURES

Figure 1-1: ALMT1 mediated malate efflux in local Pi sensing at Arabidopsis root tips 4

Figure 1-2: Enzymes involved in the biosynthesis and degradation of malate in Arabidopsis..... 8

Figure 1-3: Model highlighting role of PPCs and PPCKs during plant acclimatization to Pi-starvation 13

Figure 2-1: Normalized malate and citrate content after Pi-starvation in WT seedlings 20

Figure 2-2: Normalized malate and citrate content in root exudates after Pi-starvation in WT seedlings 20

Figure 2-3: Expression analysis of *PPCs* and *PPCKs* in WT seedlings by RT-qPCR 22

Figure 2-4: Tissue-specific expression analysis of *PPCK1* and *PPCK2* by GUS staining 24

Figure 2-5: Expression analysis of *PPCK1* and *PPCK2* in root-tips after Pi-deficiency treatment 25

Figure 2-6: Expression analysis of *PPCK1* and *PPCK2* in roots of seedlings growing on split plates..... 26

Figure 2-7: Normalized content of malate in *pPPCK1$_{long}$::gDNA-GFP/ppck1-1* lines 27

Figure 2-8: Detection of PPCK1 protein in *pPPCK1$_{long}$::gDNA-GFP/ppck1-1* lines grown under Pi-sufficient and Pi-deficient conditions 28

Figure 2-9: Detection of PPCK1 in *pPPCK1$_{long}$::gDNA-GFP/ppck1-1* lines grown under Pi-sufficient and Pi-deficient condition in Arabidopsis 29

Figure 2-10: Detection of GFP-tagged PPCK1 and PPCK2 in stably transformed Arabidopsis by immunoblot analysis 32

Figure 2-11: Subcellular localization of PPCK1 and PPCK2 33

Figure 2-12: Expression analysis of *PPCK1* and *PPCK2* in roots of untagged overexpression lines grown under Pi-sufficient and Pi-deficient conditions by RT-qPCR 35

Figure 2-13: Model showing elevated generation of malate and citrate by overexpression of *PPCKs* 36

Figure 2-14: Normalized content of malate and citrate in transgenic lines overexpressing *PPCK1* and *PPCK2* 38

Figure 2-15: Normalized content of malate and citrate in root exudates of plants overexpressing *PPCK*s 39

Figure 2-16: Characterization of T-DNA insertion mutants of *PPCK1* 40

Figure 2-17: Characterization of T-DNA insertion mutants of *PPCK2* 41

Figure 2-18: Model showing reduced generation of malate and citrate in plants due to absence of *PPCK1* 42

Figure 2-19: Normalized content of malate and citrate in *ppck1-1* compared to WT seedlings..... 43

Figure 2-20: Comparison of total root length between *ppck1-1* and WT seedlings..... 44

Figure 2-21: Comparison of root-tip morphology between Pi-starved *ppck1-1* and WT seedlings 45

Figure 2-22: Normalized content of malate and citrate in root exudates of *ppck1-1* line compared to WT 46

Figure 2-23: Normalized malate and citrate content in root exudates of *almt1* and *ALMT1^{OE}* compared to WT..... 47

Figure 2-24: Expression analysis of *ALMT1* in roots of *ppck1-1* seedlings 48

Figure 2-25: Expression analysis of *PPCK1* in *pPPCK1$_{long}$::gDNA/ppck1-1* lines by RT-qPCR 49

Figure 2-26: Normalized malate and citrate content in *pPPCK1$_{long}$::gDNA/ppck1-1* lines 51

Figure 2-27: Normalized malate and citrate content in root exudates of *pPPCK1$_{long}$::gDNA/ppck1-1* lines 52

Figure 2-28: Position of the second site insertion in *ppck1-1* line 53

Figure 2-29: Expression analysis of *ALMT2* in roots of *ppck1-1* seedlings by RT-qPCR 54

Figure 2-30: Characterization of *ppck1-4* and *ppck1-5* lines 55

Figure 2-31: Normalized malate and citrate content in *ppck1-4* and *ppck1-5* lines compared to WT. 57

Figure 2-32: Normalized content of malate and citrate in root exudates of *ppck1-4* line compared to WT 58

Figure 2-33: Comparison of total root length between *ppck1-4* and WT seedlings 59

Figure 2-34: Comparison of root-tip morphology between Pi-starved *ppck1-4* and WT seedlings 59

Figure 2-35: Normalized Pi content in transgenic lines overexpressing *PPCK1* and *PPCK2*, and in *ppck1-1* and *pPPCK1$_{long}$::gDNA/ppck1-1 lines* compared to WT 61

Figure 2-36: Normalized Pi content in *ppck1-4*, *almt1*, and *ALMT1^{OE}* compared to WT 63

Figure 2-37: Pi content in *pPPCK1$_{long}$::gDNA/ppck1-1* and *35S::PPCK1* lines compared to WT when grown on insoluble Pi source, calcium phosphate 64

Figure 3-1: Possible routes of citrate generation in plants overexpressing *PPCK1* under Pi-sufficient condition 80

Figure 3-2: Possible route of elevated citrate generation in shoots of Pi-depleted *PPCK1* overexpressors 82

LIST OF TABLES

Table 5-1: Plasmid vectors used in this study and their purpose and feature 93

Table 5-2: Media composition 93

Table 5-3: Components of standard PCR and colony PCR reaction 97

Table 5-4: Thermal profile for DreamTaq PCR 97

Table 5-5: Components of high fidelity PCR 97

Table 5-6: Thermal profile Phusion High-Fidelity PCR 98

Table 5-7: Components of RT-qPCR reaction 101

Table 5-8: Thermal cycling conditions for RT-qPCR 101

Table 5-9: Composition of SDS-PAGE Gel 105

LIST OF SUPPLEMENTARY FIGURES

Supplementary Figure 7-1: Expression analysis of *PPC* and *PPCK* isoforms in roots of *phr1phl1* seedlings by RT-qPCR 124

Supplementary figure 7-2: GFP-flourescence detected in roots and leaves of *pPPCK1$_{long}$::GFP-GUS* reporter lines grown under Pi-sufficient and Pi-deficient conditions 125

Supplementary figure 7-3: GFP-flourescence detected in roots and leaves of *pPPCK2$_{long}$::GFP-GUS* reporter lines grown under Pi-sufficient and Pi-deficient conditions 126

Supplementary figure 7-4: Expression analysis of *PPCK1* in *pPPCK1$_{long}$::gDNA-GFP* lines by RT-qPCR 127

Supplementary figure 7-5: Subcellular localization of PPCK1 *in pPPCK1$_{long}$::gDNA-GFP/ppck1-1* lines 127

Supplementary figure 7-6: Expression analysis of *MDH*s in WT seedlings by RT-qPCR 128

Supplementary figure 7-7: Expression analysis of *PPC*s in their respective T-DNA insertion lines by RT-qPCR 128

Supplementary figure 7-8: Normalized malate and citrate content in *ppc* mutants compared to WT 129

Supplementary figure 7-9: Expression analysis of *PPCK1* and *PPCK2* by RT-qPCR in transgenic lines transformed with N or C-terminally tagged GFP protein construct 130

Supplementary figure 7-10: Normalized root malate content in transgenic lines overexpressing GFP-tagged PPCKs 130

Supplementary Figure 7-11: Expression analysis of *PPCK1* and *PPCK2* by RT-qPCR in transgenic lines overexpressing *PPCK1* and *PPCK2* 131

Supplementary Figure 7-12: Comparison of fresh weight of plants overexpressing *PPCK1* and *PPCK2* to WT 131

Supplementary Figure 7-13: Comparison of rosette fresh weight of plants overexpressing *PPCK1* and *PPCK2* to WT 132

Supplementary Figure 7-14: Comparison between fresh weight of *ppck1-1* and WT seedlings 132

Supplementary Figure 7-15: Comparison of rosette fresh weight between *ppck1-1* and WT plants 132

Supplementary Figure 7-16: Iron accumulation and callose deposition in Pi-depleted primary roots of *ppck1-1* seedlings 133

Supplementary Figure 7-17: Normalized malate and citrate content in *almt1* and *ALMT1^{OE}* compared to WT 133

Supplementary Figure 7-18: Comparison of fresh weight of *pPPCK1$_{long}$::gDNA/ppck1-1* lines to WT and *ppck1-1* 134

Supplementary Figure 7-19: Comparison of total root length of *pPPCK1$_{long}$::gDNA/ppck1-1* lines to WT and *ppck1-1* 134

Supplementary Figure 7-20: Comparison of root-tip morphology of Pi-starved *pPPCK1$_{long}$::gDNA/ppck1-1* lines to WT and *ppck1-1* seedlings 135

Supplementary Figure 7-21: Comparison of iron deposition in primary roots of Pi-depleted *pPPCK1$_{long}$::gDNA/ppck1-1* lines to WT and *ppck1-1* seedlings 135

Supplementary Figure 7-22: Comparison of callose deposition in primary roots of Pi-starved *pPPCK1$_{long}$::gDNA/ppck1-1* lines to WT and *ppck1-1* seedlings 136

Supplementary figure 7-23: Characterization of T-DNA insertion mutants of *ALMT2* 137

Supplementary Figure 7-24: Normalized content of malate and citrate in *almt2* lines compared to WT 137

Supplementary figure 7-25: Normalized malate and citrate content in root exudates of *almt2* lines compared to WT 138

Supplementary Figure 7-26: Comparison between fresh weight of *ppck1-4* and WT seedlings 138

Supplementary figure 7-27: Iron accumulation and callose deposition in Pi-depleted primary roots of *ppck1-4* seedlings 139

Supplementary figure 7-28: Expression analysis of *ALMT1* and *ALMT2* in roots of *ppck1-4* seedlings by RT-qPCR 140

Supplementary figure 7-29: Expression analysis of *PPCK2* in *ppck1-1* and *ppck1-4* seedlings by RT-qPCR 140

Supplementary figure 7-30: Expression analysis of *PPC*s in *ppck1-1* and *ppck1-4* seedlings by RT-qPCR 141

Supplementary figure 7-31: Expression analysis of *ALMT1* and *ALMT2* in roots of plants overexpressing *PPCK1* and *PPCK2* by RT-qPCR 141

Supplementary figure 7-32: Expression analysis of *ALMT1* and *ALMT2* in roots of *pPPCK1$_{long}$::gDNA/ppck1-1* lines 142

Supplementary figure 7-33: Malate content in *pPPCK1$_{long}$::gDNA/ppck1-1* and *35S::PPCK1* lines compared to WT when grown on insoluble Pi source, calcium phosphate 142

LIST OF SUPPLEMENTARY TABLES

Supplementary table 7-1: Comparison of metabolite levels in roots of *35::PPCK1* lines to the levels detected in WT 143

Supplementary table 7-2: Comparison of metabolite levels in roots of *35S::PPCK2* lines to the levels detected in WT 144

Supplementary table 7-3: Comparison of metabolite levels in shoots of *35S::PPCK1* lines to the levels detected in WT 145

Supplementary table 7-4: Comparison of metabolite levels in shoots of *35S*::*PPCK2* lines to the levels detected in WT 146

Supplementary table 7-5: Comparison of metabolite levels in *ppck1-1* seedlings to the levels detected in WT 147

Supplementary table 7-6: Comparison of metabolite levels in roots of *pPPCK1$_{long}$::gDNA*/*ppck1-1* grown under Pi-sufficient condition to the levels detected in WT and *ppck1-1* roots 148

Supplementary table 7-7: Comparison of metabolite levels in roots of *pPPCK1$_{long}$::gDNA*/*ppck1-1* grown under Pi-deficient condition to the levels detected in WT and *ppck1-1* roots 149

Supplementary table 7-8: Comparison of metabolite levels in shoots of *pPPCK1$_{long}$::gDNA*/*ppck1-1* grown under Pi-sufficient condition to the levels detected in WT and *ppck1-1* shoots 150

Supplementary table 7-9: Comparison of metabolite levels in shoots of *pPPCK1$_{long}$::gDNA*/*ppck1-1* grown under Pi-deficient condition to the levels detected in WT and *ppck1-1* shoots 151

Supplementary table 7-10: Comparison of metabolite levels in *ppck1-4* seedlings to the levels detected in WT 152

Supplementary table 7-11: Comparison of metabolite levels in *ALMT1^{OE}* grown under Pi-sufficient and Pi-deficient conditions to the levels detected in WT 153

Supplementary table 7-12: T-DNA insertion lines analyzed in this study 154

Supplementary table 7-13: Primers used for genotyping 155

Supplementary table 7-14: Transgenic lines generated during the course of this study 156

Supplementary table 7-15: Primers used for amplification of products for Directional TOPO cloning 157

Supplementary table 7-16: Primers used for colony PCR 158

Supplementary table 7-17: Primers used for sequencing of pENTR clones 159

Supplementary table 7-18: Restriction enzymes used to digest entry and destination cassette 160

Supplementary table 7-19: Primers used in RT-PCR and RT-qPCR 161

Supplementary table 7-20: MS parameters for MRM-transitions of organic acids (Ziegler et al., 2016) 162

ABBREVIATIONS AND SYMBOLS

AACT	ALUMINUM ACTIVATED CITRATE TRANSPORTER
ADP	Adenosine diphosphate
Al	Aluminum
ALMT	*ALUMINUM-ACTIVATED MALATE TRANSPORTER*
ALMT1^{OE}	Transgenic line overexpressing ALMT1
ANOVA	Analysis of variance
At[gene name]	*Arabidopsis thaliana*[gene name]
ATP	Adenosine triphosphate
AtP5A	P5-type ATPase
bp	Base pairs
BTPC	'Bacterial-type' PPC
C3	Cavin cycle
C4	Hatch and Slack cycle
CAM	Crassulacean Acid Metabolism
CaMKs	Ca^{2+}/CALMODULIN-REGULATED GROUP OF PROTEIN KINASES
CaP	Tricalcium diphosphate [$Ca_3(PO_4)_2$]
cDNA	Complementary deoxyribonucleic acid
CDPKs	Ca^{2+} DEPENDENT PROTEIN KINASES
Col-0	Columbia-0
Col-2	Columbia-2
Col-3	Columbia-3
CS	CITRATE SYNTHASE
Ct	Cycle threshold
C-terminal	Carboxyterminal
DDR	DNA damage responses
DIC	Dicarboxylate carrier
DNA	Deoxyribonucleic acid
DTC	Dicarboxylate-tricarboxylate carrier
e.g.	*exempli gratia* – for example
EDTA	Ethylenediaminetetraacetic acid
et al.	*et alii*- and others
etc	*et cetera*
FBPase	FRUCTOSE 1,6-BISPHOSPHATASE
Fe	Iron
FUM	Fumarase
FW	Fresh weight
gDNA	Genomic deoxyribonucleic acid
GFP	Green fluorescent protein
GUS	B-glucuronidase

h	Hour(s)
i.e.	*id est* - that is
kb	Kilo bases
kDa	Kilodaltons
K_m	Michaelis constant
KP	Potassium dihydrogen phosphate (KH_2PO_4)
LPR1	LOW PHOSPHATE RESPONSE 1
LSM	Laser scanning microscope
M	Molar
MATE	MULTIDRUG AND TOXIC COMPOUND
MDH	MALATE DEHYDROGENASE
ME	MALIC ENZYME
MEP	Methylerythritol-4-phosphate
mg	Milligram
min	Minute(s)
mM	Milli molar
mm	Millimetre
Mr	Relative molecular mass
mRNA	Messenger ribonucleic acid
MS	Malate Synthase
MW	Molecular weight
NAD-ME	NAD-Malic enzyme
NADP-ICDH	NADP-DEPENDENT ISOCITRATE DEHYDROGENASE
NADP-ME	NADP-Malic enzyme
NASC	Nottingham Arabidopsis Stock Centre
nmol	Nano molar
N-terminal	Aminoterminal
OAA	Oxaloacetate
OD_{600}	Optical density at 600 nm wavelength
P	Phosphorus
p	Probability value
PA	Phosphatidic acid
PDR2	PHOSPHATE DEFICIENCY RESPONSE 2
PEP	Phosphoenolpyruvate
PEPCK	PHOSPHOENOLPYRUVATE CARBOXYKINASE
PHL1	PHR1 LIKE
PHR1	PHOSPHATE STARVATION RESPONSE 1
PHT1	PHOSPHATE TRANSPORTER 1
Pi	Inorganic phosphate
PK	PYRUVATE KINASE
pmol	Pico molar

PP2A	PROTEIN PHOSPHATASE 2A
PPC	PHOSPHOENOLPYRUVATE CARBOXYLASE
PPCK	PHOSPHOENOLPYRUVATE CARBOXYLASE KINASE
PTPC	'Plant-type' PPCs
RAM	Root apical meristem
ROS	Reactive oxygen species
rpm	Rotations per minute
RT-PCR	Reverse transcription polymerase chain reaction
RT-qPCR	Reverse transcription quantitative real-time polymerase chain reaction
SCN	Stem cell niche
SD	Standard deviation
SDS	Sodium dodecyl sulfate
SDS-PAGE	Sodium dodecyl sulfate polyacrylamide gel electrophoresis
s	Second(s)
SHR	SHORT-ROOT
SIGnAL	Salk Institute Genomic Analysis Laboratory
SPS	SUCROSE PHOSPHATE SYNTHASE
STOP1	SENSITIVE TO PROTON RHIZOTOXICITY 1
TCA	Tricarboxylic acid cycle
T-DNA	Transfer deoxyribonucleic acid
UBQ10	*UBIQUITIN 10*
UTR	Untranslated region
v/v	Volume per volume
vs	Versus
w/v	Weight per volume
WT	Wild-type
µl	Microliter
µg	Microgram
µM	Micro molar
35S CaMV	*Cauliflower Mosaic Virus 35S promoter*

Three letter abbreviations for amino acids are used throughout this thesis, except in supplementary tables where one letter code is used for amino acids. Non proteinogenic amino acids ornithine and citrulline are abbreviated as Orn and Citru, respectively. Organic acids fumarate, succinate, alpha-ketoglutarate, and aconitate are abbreviated as fum, suc, akg, and aco, respectively in the supplementary tables.

1 INTRODUCTION

1.1 Importance of phosphorus

Phosphorus (P) is a critical macro element required in various important processes like photosynthesis, respiration, signal transduction events, nucleic acids, and membrane biosynthesis in plants (Chiou and Lin, 2011; Péret et al., 2011). Inorganic phosphate (Pi) and its conjugated anhydrides constitute the major core of plant metabolism and bioenergetics. Therefore, plant performance and growth directly depends on Pi nutrition (Ticconi et al., 2009). At neutral pH, Pi is typically present as a mixture of $H_2PO_4^-$ and HPO_4^{2-}. It is predominantly transported as $H_2PO_4^-$ (Pi) into the plant system. Most of the soil P is present either as organic phosphate (e.g. inositol phosphates, sugar phosphates, DNA, phytates, and phospholipids) or as Pi (Plaxton and Lambers, 2015). Mobility of Pi in soil is severely limited with diffusion coefficients < 10^{-12} m^2 s^{-1} due to its high propensity to form insoluble complexes with metal ions like Al^{3+}, Fe^{3+}, Ca^{2+}, and Mg^{2+} depending on the soil pH (Lambers et al., 2015; Vance et al., 2003). Therefore, the bioavailability of free Pi in soil solutions is exceedingly low, typically around 1-10 µM (Abel, 2017; Shen et al., 2011). Thus, it is not surprising that in around 70% of global cultivated land, Pi-limitation is a common abiotic stress together with metal toxicities, critically limiting crop performance and yield (Kochian et al., 2015; López-Arredondo et al., 2014).

1.2 Plant adaptation to low Pi-stress

Plants activate a set of coordinated morphological, biochemical, and molecular responses to reprioritize internal Pi distribution and external Pi acquisition in order to cope with low Pi availability (Abel, 2011; Baker et al., 2015; Chiou and Lin, 2011; Péret et al., 2011). Plant's responses to low Pi are broadly categorized as systemic and local (Chiou and Lin, 2011). Even though these two responses are discussed as two separate events, they are often interrelated. Systemic responses depends on the global Pi status of the plant and involve processes like enhanced activation of root Pi transporters for efficient Pi uptake, secretion of phosphatases to solubilize Pi from organic phosphate complexes, exudation of organic acids to release Pi from insoluble Pi metal-complexes, and remodeling of Pi metabolism for enhanced Pi recycling, such as substitution of phospholipids in the membrane by sulfolipids and galactolipids (Lambers et al., 2012; Meyer et al., 2010; Remy et al., 2012; Robinson et al., 2012; Shin et al., 2004). On the other hand, local responses are dependent on the external Pi status of the soil and aim at enhanced Pi scavenging by remodeling the entire root system architecture (Chiou and Lin, 2011; Péret et al., 2011). The surface area of roots is also increased for better soil exploration by producing longer root hairs at higher density. Moreover, primary root growth is restricted with increased production and length of lateral roots in order to increase topsoil foraging where most of the soil P is available (Lynch and Brown, 2001). This phenotypic response in Arabidopsis is modulated

by external iron (Fe) availability and localized Fe accumulation in root meristems (Müller et al., 2015; Svistoonoff et al., 2007; Ward et al., 2008). Pi-deficiency leads to hyperaccumulation of Fe in roots, possibly a reactive consequence of increased Fe availability at low Pi (Abel, 2011). Moreover, omitting Fe from the growth medium rescues the short primary root phenotype of Arabidopsis in the Pi-deficient medium (Ward et al., 2008).

PHOSPHATE DEFICIENCY RESPONSE 2 (PDR2), LOW PHOSPHATE RESPONSE 1 (LPR1), and its close paralog LPR2 are known to play a central role in local Pi-sensing (Ticconi et al., 2009). *PDR2* codes for AtP5A, the single P5-type ATPase of undefined transport specificity in Arabidopsis which is localized to the endoplasmic reticulum (Palmgren and Nissen, 2011; Sørensen et al., 2015; Ticconi et al., 2009). *LPR1* encodes a cell wall-resident multicopper oxidase with ferroxidase activity (Müller et al., 2015). *PDR2* and *LPR1* are expressed in cell type-specific but overlapping domains of the root apical meristem (RAM) and the transition zone. *LPR1/2* and *PDR2* genetically interact because the *lpr1lpr2* double mutation, which causes unrestricted primary root growth on low Pi, suppresses the hypersensitive short root phenotype of *pdr2* in the triple mutant background (Müller et al., 2015; Ticconi et al., 2009). PDR2 is thought to control LPR1 function by an unknown mechanism (Müller et al., 2015). Upon Pi-deprivation, the PDR2-LPR1 module mediates apoplastic Fe-accumulation in the stem cell niche (SCN) and transition zone which correlate with the sites of reactive oxygen species (ROS) generation and callose deposition. Callose deposition blocks the symplastic connection between cells and thereby restricts the SHORT-ROOT (SHR) movement, a key transcription factor of root patterning and cell fate specification (Petricka et al., 2012), which is followed by reduced stem cell maintenance and RAM activity (Müller et al., 2015).

Pi-deficiency often coexists with Al-toxicity in soil and also elevated Al^{3+} and low Pi exerts similar effects on root with respect to callose deposition and inhibition of primary root elongation (Müller et al., 2015; Sivaguru et al., 2000; Sun et al., 2010). This suggests shared components for monitoring Pi-availability and its associated Al-toxicity (Abel, 2017). This was supported by a recent work where a genetic screen was performed to identify mutants with a significantly longer primary root when grown on Pi-depleted medium (Balzergue et al., 2017). This screen identified loss of function mutations in two genes, *ALUMINUM-ACTIVATED MALATE TRANSPORTER 1* (*ALMT1*) and *SENSITIVE TO PROTON RHIZOTOXICITY 1 (STOP1).* These two genes were also identified in a *pdr2* suppressor screen for rescue of the hypersensitive root growth response on low Pi (Ph.D. thesis of Dr Ahmed, 2015). *ALMT1* encodes a malate efflux channel and is known to play a very important function in Al exclusion during Al-toxicity (Hoekenga et al., 2006; Kochian et al., 2015). *ALMT1* is a direct target of STOP1 which is a zinc finger transcription factor. It has recently been shown that Pi-starvation enhances STOP1 abundance in the nucleus to activate *ALMT1* expression, which triggers malate efflux into the apoplast

of internal cell layers of root-tips (Balzergue et al., 2017). Induction in *ALMT1* expression is independent of PHR1 (PHOSPHATE STARVATION RESPONSE 1) and PHL1 (PHR1 Like), which are the two master transcription factors controlling the transcription of more than 60% of phosphate starvation responsive genes. ALMT1 mediated malate exudation into the rhizosphere and into the apoplast of root-tips might have different biochemical roles which are also explained by short root and long root phenotype of *almt1* in the presence of Al and in the absence of Pi, respectively. Unlike malate exuded in the rhizosphere which is thought to solubilize Pi from bound Pi source (Narang et al., 2000) and to detoxify Al^{3+} (Delhaize et al., 1993), exuded malate in the apoplast is thought to form complexes with Fe^{3+} by mobilizing it from Fe-Pi or Fe-pectin complexes for reduction by ascorbate (Grillet et al., 2014). Subsequently Fe^{2+} can be re-oxidized by LPR1 dependent Fe-redox cycling which ultimately leads to ROS generation and callose deposition [Figure 1-1]. Unlike the PDR2-LPR1 module, the STOP1-ALMT1 module regulates callose deposition only in the transition zone but not in the SCN (Abel, 2017; Balzergue et al., 2017). Sucrose, which is known to modify systemic Pi starvation responses (Chiou and Lin, 2011) was suggested to act through its conversion to malate (Abel, 2017) which can be exuded by ALMT1, thereby linking systemic malate generation with ALMT1 mediated local malate efflux into the apoplast of internal cell layers of root tips [Figure 1-1].

1.3 Organic acids and their importance during nutrient stresses

Plants modify their rhizosphere by secreting an array of primary and secondary metabolites in order to facilitate their interactions with the surrounding environment (Dam and J. Bouwmeester, 2016). Root exudates are often a complex mixture of many components like phenolics, amino acids, sugars, organic acids, extracellular enzymes, mucilages, root border cells, inorganic, or gaseous molecules (Dakora and Phillips, 2002). With respect to mobilization and uptake of nutrients and detoxification of heavy metals by plants, the role of organic acids has been studied in great detail (Jones, 1998).

Organic acids are carbon compounds possessing at least one carboxyl group and are often characterized by their low molecular weight (<250 MW). Some typical examples of organic acids which are known to be exuded by plants are citrate, malate, oxalate, fumarate, malonate, and acetate. At the near neutral pH of the cell, organic acids typically exist in their fully dissociated forms (carboxylates) and enter the soil solution as anions carrying one or several negative charges depending on the compound exuded (Jones et al., 2003). The relative amounts and the type of organic acid exuded depend on the plant species, the plant age, the physiological conditions, and the soil environment (Chen et al., 2017; Jones, 1998; Strobel, 2001).

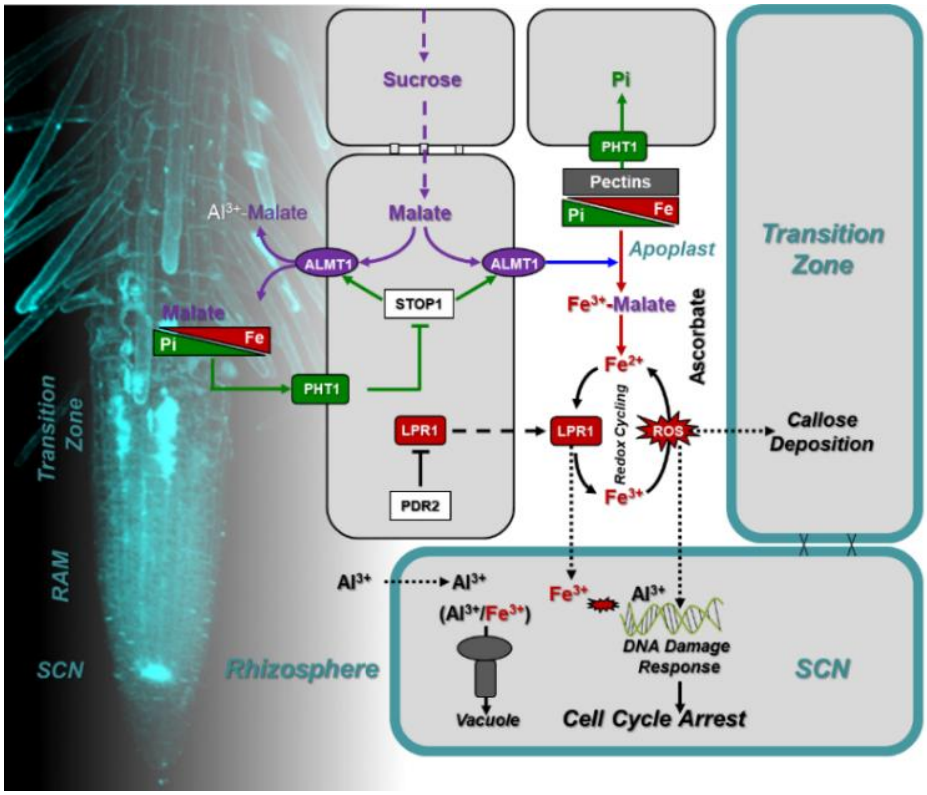

Figure 1-1: ALMT1 mediated malate efflux in local Pi sensing at Arabidopsis root tips

LPR1 is thought to generate ROS via Fe redox cycling during low Pi-stress leading to the induction of callose deposition in the transition zone and SCN. PDR2 restricts the function of LPR1. ALMT1 mediated malate efflux in the apoplast of interior root tip cell layers can mobilize Fe^{3+} from Fe-Pi and Fe-pectin complexes for reduction by ascorbate, and subsequent functioning of the redox cycling. The STOP1-ALMT1 module regulates callose deposition only in the transition zone. ALMT1 mediated malate exudation in the rhizosphere aids in solubilizing Pi and detoxifying Al^{3+}. The released Pi is taken up by PHT1 (PHOSPHATE TRANSPORTER 1) family members. Al^{3+} if not sequestered can directly bind the DNA and activate DNA damage responses (DDR) which may lead eventually to loss of stem cell. Fe^{3+} mediated ROS generation may also trigger DDR. The likely precursor of malate generation in roots may be sucrose. Adapted from Abel, 2017.

Exudation of carboxylates into the rhizosphere by plant roots is one of several strategies by which plants acquire Pi from soils (Hocking, 2001). Pi and organic phosphate adsorbed to the soil particles or complexed to metal ions such as Al^{3+}, Fe^{3+} or Ca^{2+} can be mobilized by carboxylates via ligand exchange, thereby releasing Pi which can then be taken up by plant roots (Jones, 1998; Lambers et al., 2006). The ability of carboxylates to release Pi depends on their capacity to compete for anion exchange sites in the soil which is ultimately reflected by the number of carboxyl groups and their configuration relative to other carboxyl and hydroxyl groups (Martin et al., 2014; Ryan et al., 2001). Therefore, the chelating capacity of carboxylates in soil is in the order- tricarboxylates ($citrate^{3-}$)> dicarboxylates ($malate^{2-}$, $oxalate^{2-}$, and $malonate^{2-}$)> monocarboxylates ($acetate^{-}$) (Jones et al., 2003; Ryan et al., 2001). Pioneering studies demonstrating the link between organic acid exudation and Pi-starvation was provided by Gardener and his group (Gardner et al., 1983; Gardener et al., 1982a, 1982b). They showed that proteoid or cluster roots of *Lupinus albus* (white lupin), belonging to the plant family Fabaceae, exude large amounts of citric acid in response to Pi-starvation. Several members of another

plant family- the Proteaceae (like Harsh hakea and Banskia), are also known to enhance Pi uptake from soil by exuding organic acids, especially malate and citrate from their cluster roots (Dinkelaker et al., 1995; Grierson, 1992; Keerthisinghe et al., 1998). Other crop species, which do not form cluster roots are also known to exude organic acids like oxalate and citrate by rice (Hoffland et al., 2006), citrate by cowpea (Jemo et al., 2007), malate and citrate by tea and rape (Hoffland et al., 1989; Lin et al., 2011), oxalate and malate by soybean (Dong et al., 2004; Liao et al., 2006), and citrate by chickpea (Neumann and Römheld, 1999). Recently, it has also been shown that Pi-starvation triggers malate and citrate exudation in the model plant Arabidopsis (Maruyama et al., 2019). Other than increasing the availability of Pi, organic acids can also change the available concentrations of micronutrients like iron (Fe^{3+}), manganese (Mn^{2+}), copper (Cu^{2+}), and zinc (Zn^{2+}) in the soil solution and thereby increase their uptake by plants (Jones and Darrah, 1994; Ryan et al., 2001; Ström et al., 2005; White et al., 2003).

Organic acids also play an important role in heavy metal tolerance. In response to lead (Pb^{2+}) and copper (Cu^{2+}), rice and Arabidopsis increase the exudation of oxalate and citrate**,** respectively (Murphy et al., 1999; Yang et al., 2000). In contrast to Pi deficiency, where the exuded organic acids release bound Pi from insoluble Pi-complexes, organic acids released in response to heavy metal stress confer heavy metal tolerance by chelating them in the rhizosphere, resulting in non-toxic complexes (Ryan et al., 2001). With regard to heavy metal stress, considerable progress has been made in unraveling the mechanism of Al^{3+} tolerance in plants. In acidic soils, Al^{3+} is very toxic and can inhibit plant growth already at µM concentrations (Yang et al., 2013). Citrate, malate, and oxalate were identified as the main organic acids released in response to Al^{3+} (Kochian et al., 2005, 2004). However, as for Pi deficiency, the kind of organic acid released in response to Al^{3+} is species specific (Ma et al., 2001) like malate in wheat (Kitagawa et al., 1986), citrate in maize and barley (Pellet et al., 1995; Zhao et al., 2003), oxalate in buckwheat (Zheng et al., 1998), malate and citrate in rye (Ma et al., 2000), or citrate, malate, and aconitate in sorghum (Cambraia et al., 1983; Gonçalves et al., 2005; Magalhaes et al., 2007). First evidence for Al^{3+} induced exudation of malate was provided by results which showed that Al^{3+} tolerance of near-isogenic wheat lines depended on their capacity to exude malate (Delhaize et al., 1993; Kitagawa et al., 1986). The gene conferring such tolerance was identified as a malate channel, which was named *ALUMINUM ACTIVATED MALATE TRANSPORTER* (*TaALMT1*) (Sasaki et al., 2004). Homologs of TaALMT1 have later been identified in other species such as Arabidopsis (AtALMT1) (Hoekenga et al., 2006), rape (BnALMT1 and BnALMT2) (Ligaba et al., 2006), rye (ScALMT1) (Fontecha et al., 2006) and barley (HvALMT1) (Gruber et al., 2011). Arabidopsis ALMT1, which belongs to a large ALMT family protein comprising 14 members, is expressed at the plasma membrane of the epidermal cells of the root tip and is the responsible transporter for malate exudation upon Al^{3+} stress. Upon Al^{3+} stress, malate exudation is enhanced by increased transcription of *AtALMT1* as well as by

allosteric activation of AtALMT1 driven malate transport by exogenous Al^{3+} (Hoekenga et al., 2006). Apart from malate transporter, genes encoding citrate transporters which belongs to MULTIDRUG AND TOXIC COMPOUND families (MATE), mediating secretion of citrate from plant roots in response to Al, have also been identified in several plant species, such as sorghum (Magalhaes et al., 2007), barley (Furukawa et al., 2007), maize (Maron et al., 2010), rye (Yokosho et al., 2010), and rice (Yokosho et al., 2011). In addition to AtALMT1, Arabidopsis AtMATE1 also contributes to Al resistance by releasing citrate from mature regions of the root (Liu et al., 2009), although Al^{3+}-induced citrate exudation is much smaller compared to Al^{3+}-induced malate exudation. Both *AtALMT1* and *AtMATE1* are under the transcriptional control of AtSTOP1 (Liu et al., 2009).

1.4 Biosynthesis of organic acids

Understanding the metabolism of organic acids is very important in plants because they are involved in crucial physiological functions like energy metabolism, maintenance of redox balance, biosynthesis of amino acids, and modulation of adaptation to the environment (López-Bucio et al., 2000). Organic acid content in roots of plants is typically in the range of 10-20 mM (1-4% of dry weight) and primarily depends on the photosynthetic pathway used [e.g. Crassulacean Acid Metabolism (CAM) , Calvin cycle (C3), or Hatch and Slack cycle (C4)], growth age, and nutritional status of the plant (Jones, 1998). The concentration of organic acids in soil solutions across a broad range of ecosystems is typically low in the range of 1-50 µM, but in soil surrounding cluster roots, it can also exceed 600 µM (Jones, 1998; Martin et al., 2014; Strobel, 2001).

Organic acids are mainly biosynthesized in the mitochondria through the tricarboxylic acid cycle (TCA cycle or Krebs cycle) and to a lower extent in the glyoxysomes via the glyoxylate cycle (Ap Rees, 1990; López-Bucio et al., 2000). They accumulate in plants due to incomplete oxidation of photosynthetic assimilates and they represent the transitory or stored forms of fixed carbon. During periods of active photosynthesis, particularly in the light, the redox level in the cell is increased, which results in the transformation of the TCA cycle to an open structure constituting two main branches- one branch produces citrate which can be transformed to isocitrate, 2-oxoglutarate, or their derivatives like glutamate (citrate valve), while the other branch produces malate that can be exported from mitochondria and accumulated in vacuoles (malate valve) (Igamberdiev and Eprintsev, 2016). Organic acids are stored in very small pools in the mitochondria, whereas the vacuole acts as the major storage site of organic acids. The vacuolar transport machinery ensures that the cytosolic pools of organic acids remain constant (López-Bucio et al., 2000; Meyer et al., 2011). Since the operation of malate and citrate valves involves mitochondria, cytosol, and other organelles, isoforms of several enzymes of the TCA cycle also operate in the cytosol and other cell organelles (Igamberdiev and Eprintsev, 2016).

Citrate is generated by the action of the enzyme citrate synthase (CS), which catalyzes the first committed step of the TCA cycle; the condensation of oxaloacetate (OAA) with acetyl-CoA (Fernie et al., 2004). Unlike other TCA cycle enzymes, CS is exclusively localized in mitochondria in green tissues (Schmidtmann et al., 2014). An isoform of CS is also present in peroxisomes; however, there, it plays an important role only during the glyoxylate cycle at the time of seed germination and post-germinative growth (Eastmond and Graham, 2001).

1.4.1 Biosynthesis of malate

Malate is known to play diverse roles in plant metabolism and is assumed to represent the ultimate product of glycolysis (Lance and Rustin, 1984; Martinoia and Rentsch, 1994; Schulze et al., 2002a). In C4 and CAM photosynthesis, malate is the key metabolite transiently storing carbon fixed from CO_2 (Maier et al., 2011). In C4 and CAM plants, the photosynthetic efficiency is improved by spatial (mesophyll cells and bundle sheath cells) and temporal (night and dark) separation of the biochemical components of CO_2 assimilation. The initial fixation of CO_2 in C4 and CAM plants is achieved by PHOSPHOENOLPYRUVATE CARBOXYLASE (PPC) which catalyzes the irreversible β-carboxylation of phosphoenolpyruvate (PEP) to OAA. In C4 plants, PPC is located in the cytosol of mesophyll cells and the produced C4 acid is then shuttled to the bundle sheath cells where CO_2 is released for the C3 cycle. Three variations of C4 photosynthesis are known depending on the decarboxylase enzymes acting on the C4 acid in the bundle sheath cells. These three enzymes are either NADP-MALIC ENZYME (NADP-ME), NAD-MALIC ENZYME (NAD-ME), or PHOSPHOENOLPYRUVATE CARBOXYKINASE (PEPCK) (Gowik and Westhoff, 2011). In CAM plants, the PPC reaction occurs during the night when stomata are open. The fixed carbon is stored as a C4 acid in a large central vacuole during the night. During the day, malate is released from the vacuole and decarboxylated via ME (Cook et al., 1995).

Enzymes and metabolite transporters involved in the photosynthetic machinery of C4 plants also occur in C3 plants, although with much lower activity and different tissue specificities (Häusler et al., 2002). Malate also constitutes a significant fraction of the fixed carbon in C3 plants (Maurino and Engqvist, 2015). Enzymes involved in the biosynthesis of malate in C3 plants include FUMARASE (FUM), MALATE SYNTHASE (MS), MALATE DEHYDROGENASE (MDH), and PHOSPHOENOLPYRUVATE CARBOXYLASE (PPC) [Figure 1-2]. FUM, also known as FUMARASE HYDRATASE catalyzes the reversible hydration of fumarate to malate. Both mitochondrial and cytosolic forms of FUM are known to exist in Arabidopsis (Heazlewood, 2004; Pracharoenwattana et al., 2010). MS is a key enzyme in the glyoxylate cycle and is localized to the peroxisomes where it irreversibly converts acetyl-CoA (from fatty acid β-oxidation) and glyoxylate to malate (Maurino and Engqvist, 2015). MDH is a widely distributed enzyme belonging to oxidoreductases group and catalyzes the reversible interconversion of OAA and malate. Several

isoforms of MDH occurs in higher plants which differs in their subcellular localization and cofactor specificity (Gietl, 1992). NADP-dependent MDHs (pIMDH) occur in the chloroplasts where they are involved in balancing reducing equivalents between the cytosol and stroma, maintaining redox homeostasis in plants (Gietl, 1992; Miller et al., 1998; Schulze et al., 2002; Selinski and Scheibe, 2014). NAD-dependent MDHs occur in the cytosol (cMDH), where they are involved in the malate-aspartate shuttle; the mitochondria (mMDH), where they are involved in the TCA cycle; and the peroxisomes (pMDH), where they participate in β-oxidation. In root nodules, MDH (neMDH) functions in nitrogen fixation and assimilation. In heterotrophic tissues, the cMDHs are involved in the generation of malate from OAA (Maurino and Engqvist, 2015).

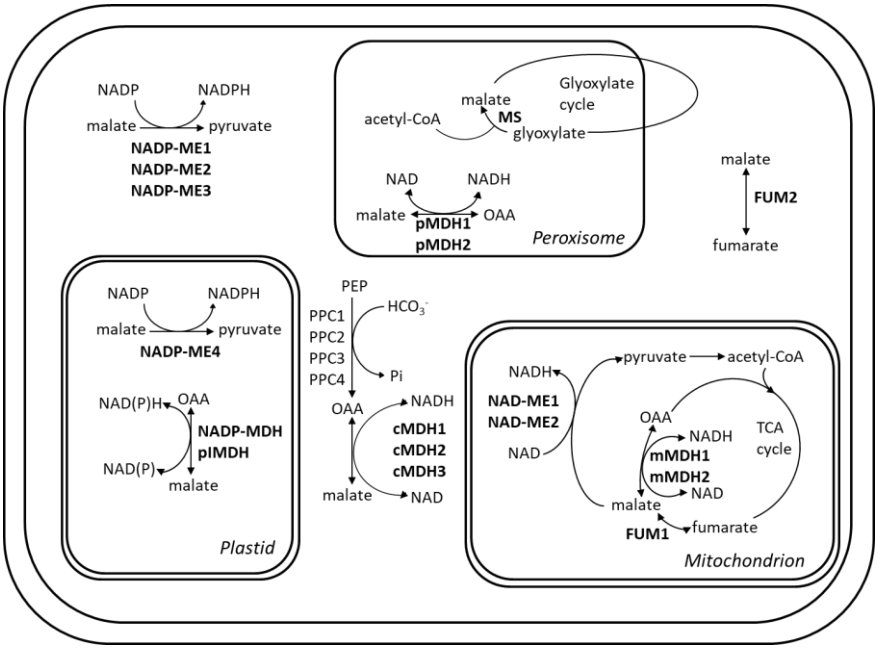

Figure 1-2: Enzymes involved in the biosynthesis and degradation of malate in Arabidopsis

Biosynthesis and degradation of malate take place in different subcellular components. Enzymes involved in malate biosynthesis are discussed in the text. Malic enzyme (ME) is a malate degrading enzyme which catalyzes the oxidative decarboxylation of malate to pyruvate. NADP-dependent ME are located in the cytosol and plastid, whereas NAD-dependent ME are present in mitochondria. Adapted from Maurino and Engqvist, 2015.

1.5 Phosphoenolpyruvate carboxylase (PPC)

PPC (EC 4.1.1.31) operates at a crucial branch point of plant carbohydrate metabolism. It catalyzes the irreversible β-carboxylation of PEP in the presence of HCO_3^- using Mg^{2+} as a cofactor to generate OAA and Pi (O'Leary et al., 2011). This enzyme is ubiquitous in plants and is also found in other organisms like cyanobacteria, green algae, most archaea, and nonphotosynthetic bacteria, but has not been identified in animals and fungi (Izui et al., 2004). In addition to their role in C4 and CAM photosynthesis where they catalyze the initial fixation of atmospheric CO_2, PPCs are involved in a broad range of functions in non-photosynthetic tissues and leaves of C3 plants, like in the anaplerotic replenishment of TCA cycle intermediates to provide precursors for amino acid biosynthesis (O'Leary et al., 2011), in

the modulation of the carbon-nitrogen balance in plants (Shi et al., 2015), in stomatal opening (Asai et al., 2000), in seed formation and germination (Nhiri et al., 2000), and in fruit ripening (Guillet et al., 2002). They also provide malate as a substrate to symbiotic nitrogen-fixing bacteroids of legume root nodule (Nomura et al., 2006), and they are involved in stress responses such as pH, salt, alkaline, and cadmium stress (Chen et al., 2008; Feria et al., 2016; Sun et al., 2014; Willick et al., 2019), or Pi and Fe deficiency (Feria et al., 2016; Gregory et al., 2009; Li and Lan, 2015). To fulfill these different functions, plant PPC belongs to a small multigene family, whose members exhibit predominant; but not exclusive tissue specific expression (Sánchez and Cejudo, 2003).

Two distinct classes of PPCs are known to occur in plants. They are 'Plant-type' PPCs (PTPC) and a distantly related 'Bacterial-type' PPC (BTPC) (Gennidakis et al., 2007; Igawa et al., 2010; Mamedov et al., 2005; Sánchez and Cejudo, 2003; Sullivan et al., 2004). PTPC genes encode 105-110 kDa polypeptides containing a conserved N-terminal serine phosphorylation and a lysine-monoubiquitination site and they assemble into homotetrameric 400 kDa complexes (Class-1 PPCs) (Izui et al., 2004; Kai et al., 2003). BTPC genes encode larger 116-118 kDa polypeptides containing a unique intrinsically disordered domain which mediates its tight interaction with PTPC monomers, forming an unusual 900 kDa hetero-octameric Class-2 PPC, which is desensitized to allosteric effectors. BTPC lacks the N-terminal serine phosphorylation sites (acid-base-XXSIDAQLR) characteristic of PTPCs and acts as the catalytic and regulatory subunits of Class-2 PPC that is subject to multi-site regulatory phosphorylation (Gennidakis et al., 2007; Igawa et al., 2010; O'Leary et al., 2011; Sánchez and Cejudo, 2003). The Arabidopsis genome encodes four PPCs- three PTPC's (AtPPC1, AtPPC2, AtPPC3) and one BTPC (AtPPC4). Sanchez and his group (2003) showed that *AtPPC1* transcripts are present in all organs, predominantly in roots. *AtPPC2* transcripts are also detectable in all plant organs, but most abundantly in green tissues. *AtPPC3* transcripts have exclusively been found in roots and siliques, whereas *AtPPC4* transcript levels were detected in siliques, flowers, and to a lower level in roots. Different PPC isoforms have also been shown in rice (Masumoto et al., 2010), maize (Dong et al., 1998; Kawamura et al., 1990), sorghum (Lepiniec et al., 1993), and flaveria (Ernst and Westhoff, 1997).

1.5.1 Regulation of PPC

PPC is subject to allosteric control by various metabolite effectors. Many Class 1 PPCs show allosteric activation by effector molecules like glucose-6-phosphate and allosteric feedback inhibition by L-malate, aspartate, and glutamate at physiological pH (Chollet et al., 1996; Izui et al., 2004). However, depending on the physiological function (photosynthetic or non-photosynthetic) of specific PPC isoenzymes and the cellular environment where they operate, their specific kinetic and allosteric properties are quite variable (O'Leary et al., 2011). A typical example is the increased substrate

saturation constant (K_m) for PEP of C4 PPCs, which is about ten times higher than of C3 PPCs (Ting and Osmond, 1973). Moreover, C4 PPCs are also less inhibited by malate compared to C3 PPCs (Bläsing et al., 2002; Dong et al., 1998; Svensson et al., 2003). Post-translational modifications of PPCs via reversible phosphorylation of its conserved N terminal Ser residue causes significant changes in the allosteric properties of the enzyme (Marsh et al., 2003). This modification decreases the sensitivity of PPCs to allosteric inhibitors while increasing its sensitivity to allosteric activators and affinity for PEP, thus activating the enzyme (Chollet et al., 1996; Nimmo, 2003; O'Leary et al., 2011; Vidal and Chollet, 1997). Although the BTPCs lack the conserved N terminal phosphorylation site of PTPCs, three novel phosphorylation sites (Thr^4 at the N terminus and Ser^{425} and Ser^{451} within its disordered region) were identified (O'Leary et al., 2011) in BTPC from germinating castor oil seeds (COS).

In C4 and CAM plants, the phosphorylation state of PPC increases in response to light and circadian rhythm, respectively (Nimmo, 2000; Ueno, 2001). In C3 plants, various factors like light, nitrogen supply, photosynthate supply to legume root nodules and to developing seeds, as well as Pi deprivation lead to the phosphorylation of C3 PPCs (Duff and Chollet, 1995; Le Van Quy et al., 1991; O'Leary et al., 2011). Phosphorylation and dephosphorylation of PTPCs in plants are catalyzed by PHOSPHOENOLPYRUVATE CARBOXYLASE KINASE (PPCK) and PROTEIN PHOSPHATASE 2A (PP2A), respectively (Carter et al., 1991, 1990; Hartwell et al., 1996; Nimmo, 2000). The signals leading to PPC phosphorylation and to increases in their activity also regulate the cytosolic turnover of PPCK proteins (Bakrim et al., 1992; Carter et al., 1991; Chollet et al., 1996; Echevarria et al., 1994; Gousset-Dupont et al., 2005; Hartwell et al., 1999; Jiao et al., 1991; Le Van Quy et al., 1991). In contrast, the activity of PP2A is relatively constant (Carter et al., 1996, 1991, 1990; Taybi et al., 2004), which emphasizes the importance of PPCK in controlling PPC activity and thereby its key role in controlling plant metabolism.

Apart from the regulation of PPCs by phosphorylation, monoubiquitination, and interaction with phosphatidic acid (PA) result in the inhibition of PPC activity (Monreal et al., 2010; O'Leary et al., 2011; Ruiz-Ballesta et al., 2014; Shane et al., 2013; Uhrig et al., 2008).

1.6 Phosphoenolpyruvate carboxylase kinase (PPCK)

PPCK is a low abundant protein and so far the smallest known protein kinase (Nimmo, 2003). Biochemical evidence argued for the presence of two types of PPCKs with Mr values of 30-33 kDa and 37-39 kDa in several plant species (Chollet et al., 1996; Nimmo, 2003; Saze et al., 2001; Vidal and Chollet, 1997). However, all *PPCK* genes identified so far from plants encode polypeptides with Mr values of 30-33 kDa (Nimmo, 2003). PPCK is a novel member of the Ca^{2+}/CALMODULIN-REGULATED GROUP OF PROTEIN KINASES (CaMKs) and is more closely related to the catalytic domains of plant Ca^{2+} DEPENDENT PROTEIN KINASES (CDPKs) than to other members of the CaMK family (Hartwell et

al., 1999). Although related to CDPKs, it is a Ca^{2+} independent protein kinase comprising only the Ser/Thr kinase catalytic domain and lacking the autoinhibitory region and Ca^{2+}-binding EF hands (Marsh et al., 2003; Nimmo, 2003). It also lacks other well-defined phosphorylation sites which are present in other protein kinases (Johnson et al., 1996). Plant PPCKs are encoded by a small gene family and at least two isoforms have been found in most species investigated so far (Fontaine et al., 2002; Nimmo, 2003; Shenton et al., 2006). In Arabidopsis, two isoforms of PPCKs- PPCK1 and PPCK2 are present showing different expression patterns (Fontaine et al., 2002). *PPCK1* transcripts were mainly detected in rosette leaves, to a lower extent in flowers and roots, and at a very low level in stems, cauline leaves, and siliques. In contrast, *PPCK2* transcripts were detected mainly in roots and flowers, and to a lower extent in cauline leaves, whereas they were undetectable in rosette leaves and stems.

1.6.1 Regulation of PPCK

Plant PPCKs are unusual protein kinases, known to be regulated only at the level of synthesis/degradation (Chollet et al., 1996; Johnson et al., 1996; Nimmo, 2003). In C4 plants, the transcript abundance of PPCK is regulated by light (Chollet et al., 1996; Hartwell et al., 1999, 1996; Vidal and Chollet, 1997), however, in maize, PPCK is also subject to circadian or metabolic control (Nimmo, 2003; Ueno et al., 2000). CAM PPCKs are known to be controlled by circadian regulation, with expression peaking at night (Hartwell et al., 1999; Nimmo, 2003; Taybi et al., 2000). However, Borland and his group showed that treatments affecting malate content or compartmentation like temperature manipulations or enclosing leaves in an atmosphere of nitrogen, circadian control of PPCK transcript or activity are modulated, possibly by feedback inhibition of *PPCK* expression by a high content of cytosolic malate (Borland et al., 1999). Mechanisms involving thioredoxin (Saze et al., 2001; Tsuchida et al., 2001) and a protein inhibitor (Nimmo et al., 2001) have also been reported to regulate PPCK activity. Expression of Arabidopsis PPCKs is moderately increased by light, pH, and carbon supply (Chen et al., 2008; Fontaine et al., 2002). Transcript levels of PPCK in developing endosperm of castor oil seeds and two PPCK isoforms of soybean in nodules are known to be markedly influenced by the photosynthate supply from shoots whereas another isoform of PPCK in soybean is reported to be under circadian control in leaves but not in roots (Murmu and Plaxton, 2007; Sullivan et al., 2004).

1.7 Pi-deficiency and metabolic bypass via PPC

As a consequence of severe Pi starvation, a strong decline in intracellular concentrations of Pi, ATP, and ADP occurs, which directly affects respiratory metabolism via the enzymes of the glycolytic pathway, which uses these factors as cosubstrates in their reaction mechanisms (Duff et al., 1989; Plaxton and Podestá, 2006). The ability of plants to adjust their metabolism under such conditions by bypassing such enzymes through alternative pathways can partially compensate for such metabolic

disruptions (Plaxton and Tran, 2011; Theodorou and Plaxton, 1993). One bypass reaction which has been extensively studied in several plant species grown under Pi-depleted condition involves PPCs and PPCKs (Duff et al., 1989; Gregory et al., 2009; Johnson et al., 1994; Toyota et al., 2003). They are suggested to secure pyruvate supply to the TCA cycle, by bypassing the ADP limited cytosolic PYRUVATE KINASE (PK). Concurrently, the PPC byproduct Pi from PEP can be recycled into the metabolism of Pi-deficient cells (Nagano et al., 1994; Plaxton and Carswell, 1999). Apart from this, increased phosphorylation of PPCs during low Pi-stress is suggested as a mechanism by which plants can adjust their metabolism to acquire more Pi from metal-Pi complexes by releasing organic acids, like malate and citrate into the rhizosphere (Gregory et al., 2009; Shane et al., 2013) [Figure 1-3]. Hoffland and his group showed that increase in citrate exudation from roots of Pi-starved rape plants (*Brassica napus*) correlated with increased activity of PPC (Hoffland et al., 1992). A similar increase in PPC activity upon Pi starvation has also been reported from other plant species like chickpea (Neumann and Römheld, 1999), Madagascar periwinkle (Nagano et al., 1994), tomato (Pilbeam et al., 1993), sesbania (Aono et al., 2001), and tobacco (Toyota et al., 2003). Enhanced exudation has often been correlated with the enhanced activities of not only PPC, but also of MDH and CS, and an elevated rate of dark CO_2 fixation in plants (Gregory et al., 2009; Plaxton and Tran, 2011; Vance et al., 2003).

Results in support of this bypass mechanism in Pi-starved Arabidopsis are provided by several independent transcriptomic and enzymatic studies. It has been reported that Pi-starvation triggers increased expression of *PPC*s and *PPCK*s in Arabidopsis (Chen et al., 2007; Feria et al., 2016; Gregory et al., 2009; Morcuende et al., 2007; Müller et al., 2007). *AtPPCK1* and *AtPPCK2* are among the most strongly induced genes in response to Pi starvation (Morcuende et al., 2007; Müller et al., 2007). Moreover, in Arabidopsis, an increase in PPCK protein abundance after 3 h of transfer to Pi-depleted medium has also been reported (Chen et al., 2007). In Arabidopsis suspension cells and seedlings, it has been shown that Pi-starvation enhances PPC specific activity and *in vivo* phosphorylation of the PTPC isoenzyme AtPPC1 at its conserved Ser11 phosphorylation site (Gregory et al., 2009). Although they could only identify AtPPC1 as the phosphorylated PTPC isoenzyme via MALDI-QqTOF-MS/MS of both tryptic and Asp-N digests, the possibility that other PTPCs could also be phosphorylated cannot be excluded. As such, it is still unknown, whether there is specificity of PPCK isoforms with respect to the phosphorylation of the different PPC isoforms.

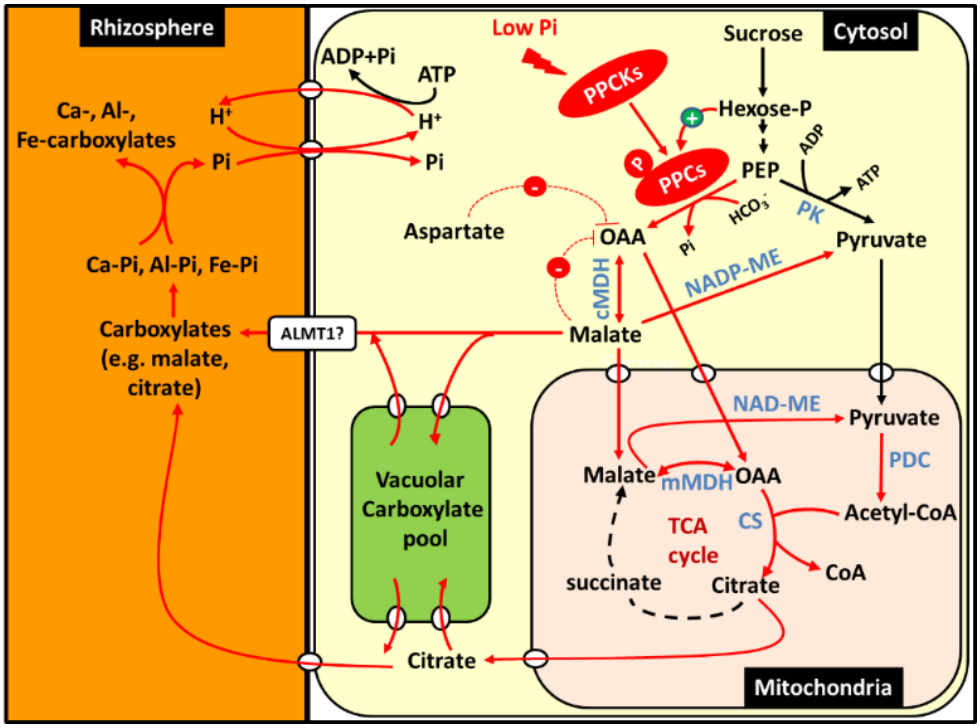

Figure 1-3: Model highlighting role of PPCs and PPCKs during plant acclimatization to Pi-starvation

PPC provides metabolic bypass to the ADP limited cytosolic PK to facilitate pyruvate supply to the TCA cycle, while concurrently releasing its by-product Pi to be reassimilated into the metabolism of Pi-starved plants. Induction of PPCs during low Pi-stress has been correlated to the synthesis and exudation of organic acids to the rhizosphere by plants. Exuded organic acids can chelate cations that immobilize Pi in the soil like Ca^{2+}, Al^{3+}, and Fe^{3+}, thereby solubilizing Pi. Role of ALMT1 in exuding malate into the rhizosphere during Pi-starvation is not known. Adapted from Shane et al., 2013.

1.8 Manipulation of malate and citrate biosynthesis and their transport

Considering the importance of organic acids exudation during Pi-starvation and heavy metal stress, several attempts had been made in developing transgenic plants showing enhanced tolerance to Al and increased Pi acquisition and use. Most researchers aimed at the manipulation of enzymes involved in organic acid biosynthesis, assuming that increased concentration of organic acids in the cytosol might be sufficient to enhance transport to the rhizosphere and that the rate-limiting step for organic acid efflux might be their biosynthesis and not transport. The first successful report on achieving increased organic acid production and exudation was provided by Fuente et al. (1997). They showed that transgenic tobacco plants expressing *CS* gene from *Pseudomonas aeruginosa* (*CSb*) exhibited increased citrate levels both in roots and in exudates and also showed enhanced tolerance to Al compared to the control plants. Moreover, the same plants also yielded more leaf and fruit biomass and acquired more Pi from poorly soluble forms present in alkaline soils (López-Bucio et al., 2000). However, the same transgenic tobacco line from De la Fuente et al. as well as additional transgenic tobacco lines expressing 100-fold greater *CSb* failed to show increased citrate content both in roots and exudates, suggesting that the activity of CS from *P. aeruginosa* in the generated tobacco lines was either dependent on the external environment, or alternatively, the previously observed effects were

due to some other variables (Delhaize et al., 2001). Similarly, overexpression of a mitochondrial *CS* gene in transgenic tobacco lines failed to accumulate more citrate in tissues and in exudates, although CS activity was higher compared to the activity detected in control plants (Delhaize et al., 2003). However, overexpression of a mitochondrial *CS* from Arabidopsis in carrot cells showed enhanced citrate exudation and improved growth on aluminum phosphate (Al-P) containing medium (Koyama et al., 1999). More reports on overexpression of *CS* in different plant species like canola (Anoop et al., 2003), alfalfa (Barone et al., 2008) and tobacco (Deng et al., 2009; Han et al., 2009) followed, showing enhanced tolerance to Al due to increased content of citrate in tissues and in root exudates. There are also reports on the overexpression of *MDH* in alfalfa (Tesfaye et al., 2001) and tobacco (Wang et al., 2010). In transgenic alfalfa plants, overexpression of nodule enhanced form of *MDH* increased malate, citrate, oxalate, succinate, and acetate levels both in roots and exudates, whereas in transgenic tobacco, overexpression of a *cMDH* from Arabidopsis and a *MDH* from *E. coli*. increased malate content in roots, leaves, and exudates compared to the levels in untransformed plants. Moreover, these plants also showed enhanced tolerance to Al and exhibited higher P levels. Other than *CS* and *MDH*, overexpression of *ME* is also reported to rescue plants from Al-toxicity by producing higher internal concentration and external efflux of malate and citrate (Sun et al., 2014; Zhou et al., 2018).

The first systemic study aimed to specifically improve the ability of a plant to utilize P from Al-P, Fe-P (iron phosphate), and Ca-P (calcium phosphate) complexes were performed by manipulation of malate generation in tobacco by overexpressing a *mMDH* gene from the mycorrhizal fungi *Penicillium oxalicum* (Lü et al., 2012). These plants exhibited significantly higher MDH activity and elevated content of malate in roots and exudates when grown in both low and high Pi conditions compared to the control plants. In medium containing insoluble P sources- Al-P, Fe-P, and Ca-P, these lines showed significant increases in their biomass, Pi uptake, and P content. A similar study conducted in cotton also showed similar results (Wang et al., 2015). This group also included knock-down lines for *MDH1* which showed opposite results to the lines overexpressing this gene.

Increasing organic acid biosynthesis alone might not always be sufficient to increase organic acid efflux, because the rate-limiting step for exudation could also be the transport of organic anions across the plasma membrane. Evidence supporting such a hypothesis was provided from several plant species. For example in tobacco where although endogenous citrate and isocitrate content in roots and shoots were elevated by reducing the activity of NADP-DEPENDENT ISOCITRATE DEHYDROGENASE (NADP-ICDH), which plays a major role in the catabolism of citrate, by antisense RNA approach, citrate exudation could not be elevated (Delhaize et al., 2003). In white lupin, the maximum in vitro activities of PPC and CS upon Pi-starvation did not correlate with the rate of citrate exudation (Watt and Evans, 1999). Also, although organic acid concentrations in roots and shoots of

Pi-starved wheat and tomato plants were higher, exudation of organic acids was not higher (Neumann and Römheld, 1999). These studies prompted several researchers to focus on the manipulation of transporters, such as ALMT and MATE in order to increase the exudation of organic acids. Following the discovery of ALMT1 in wheat (Sasaki et al., 2004), several successful attempts were made to enhance Al^{3+} mediated malate exudation and Al resistance by overexpressing *TaALMT1* in plant species like barley (Delhaize et al., 2009, 2004), Arabidopsis (Ryan et al., 2011), and wheat (Pereira et al., 2010). Homologs of *TaALMT1* from other plants were also successfully used to enhance malate exudation and Al tolerance of plants (Gruber et al., 2011; Ligaba et al., 2006; Ryan et al., 2011; Zhang et al., 2018). In addition to malate transporter, several researchers also enhanced citrate efflux and Al tolerance of plants by overexpressing citrate transporters like MATE and ALUMINUM ACTIVATED CITRATE TRANSPORTER (AACT); for example, overexpression of sorghum *MATE- SbMATE*, maize *MATE- ZmMATE1*, and cabbage *MATE- BoMATE* in arabidopsis (Magalhaes et al., 2007; Maron et al., 2010; Wu et al., 2014); *SbMATE* in barley (Zhou et al., 2014); rice bean *MATE- VuMATE* in tomato (Yang et al., 2011); *Brachypodium distachyon- BdMATE* in setaria (Ribeiro et al., 2017); barley *AACT-HvAACT1* in tobacco (Furukawa et al., 2007), wheat and barley (Zhou et al., 2013). Thus, there are many reports on improving Al tolerance of plants by overexpressing genes involved in organic acid transport. However, to our knowledge there is only one report showing improved Pi uptake by overexpression of a transporter. A root-specific *ALMT* gene, *GmALMT5* was overexpressed in hairy roots of soybean which increased malate exudation in these transgenic plants and also enhanced their capacity to utilize sparingly soluble Ca-P sources compared to the control (Peng et al., 2018).

Thus, a lot of information is available regarding the manipulation of enzymes involved in organic acid biosynthesis (mainly CS, MDH, and NADP-ICDH) and transport (ALMT and MATE) to enhance Al tolerance, but reports on similar approaches to improve Pi acquisition are still limited in number.

1.9 Manipulation of PPC/PPCK pathway

Although many correlative data suggest the contribution of PPCs for the generation of organic acids via the anaplerotic pathway to confer Al tolerance and improve Pi acquisition, little is known regarding the effects of manipulation of these enzymes in this context. A large body of information is available regarding manipulation of PPC levels by overexpressing C4-PPC or non-regulated PPC from bacterial sources in C3 plants like tobacco (Hudspeth et al., 1992; Kogami et al., 1994), rice (Agarie et al., 2002; Bandyopadhyay et al., 2007; Demao et al., 2001; Ding et al., 2013; Fukayama et al., 2003; Jiao et al., 2002; Ku et al., 1999; Suzuki et al., 2006; Taniguchi et al., 2008), potato (Beaujean et al., 2001; Gehlen et al., 1996; Häusler et al., 1999; Rademacher et al., 2002), and Arabidopsis (Chen et al., 2004; Kandoi et al., 2016; Wang et al., 2012) with the main aim of improving photosynthetic efficiency of C3 plants.

However, the effects of over-expression of *PPC*s on the rate of photosynthesis are controversial. There are some reports on the photosynthetic improvement of transgenic plants (Bandyopadhyay et al., 2007; Demao et al., 2001; Ding et al., 2013; Jiao et al., 2002; Kandoi et al., 2016; Ku et al., 1999; Wang et al., 2012). However, in some studies the rate of photosynthesis was either unaltered (Beaujean et al., 2001; Fukayama et al., 2003; Gehlen et al., 1996; Hudspeth et al., 1992; Kogami et al., 1994; Rademacher et al., 2002) or decreased with increasing activity of PPC (Agarie et al., 2002; Taniguchi et al., 2008). Effect of overexpression of *PPC*s on endogenous malate and citrate content in these studies were not consistently investigated. Only in few of these studies malate content was determined in leaves, but not in roots and exudates, and was found to be significantly higher compared to the levels in control (Agarie et al., 2002; Gehlen et al., 1996; Häusler et al., 1999; Hudspeth et al., 1992; Kogami et al., 1994; Rademacher et al., 2002).

To our knowledge, there is only one report where C3 transgenic lines overexpressing a C4 *PPC* were tested in terms of their organic acid biosynthesis and exudation capacity under Pi-deficient condition (Begum et al., 2005). In their study, transgenic rice lines carrying the maize *PPC* gene increased the allocation of fixed carbon to the organic acid pool and also increased low Pi-enhanced oxalate exudation, however, P concentration in these lines were not different from the untransformed plants. There was one more report where the effect of PPC manipulation on Al tolerance of plants was determined (Tesfaye et al., 2001). Only one out of nine transgenic alfalfa lines overexpressing *PPC* showed significantly higher enzyme activity compared to untransformed alfalfa lines. This line showed higher root malate content, but no change in citrate and oxalate content compared to control plants. Nevertheless, changes in malate and citrate exudation were not observed in this line.

Until now, the PPC regulator, PPCK was overexpressed and tested only in response to alkali-stress and was suggested to confer enhanced tolerance against such stress in plants (Sun et al., 2014; Zhengwei et al., 2013). Transgenic alfalfa lines overexpressing *PPCK3* gene from soybean exhibited increased citrate content in response to alkali stress compared to control plants (Sun et al., 2014). However, so far nothing is known regarding the response of plants overexpressing *PPCK*s to low Pi stress.

1.10 Hypothesis and objectives

Many correlative data suggest the contribution of PPC/PPCK pathway to anaplerotic feeding of the TCA cycle during low Pi-stress. However, recently it was shown that the carbon flux through PPC pathway during Pi-starvation was only slightly stimulated compared to the changes observed in other parts of carbon metabolism (Masakapalli et al., 2014). In fact, the flux through PK during low Pi-stress was very strong, suggesting a very minor contribution of PPC/PPCK pathway in feeding the TCA cycle. The traditional view that this pathway in plants is just there to feed the TCA cycle was also considered as an oversimplification of the contribution of this pathway to primary metabolism (O'Leary et al., 2011). Thus, the precise role of this pathway during Pi-starvation is still not very clear in plants.

Moreover, although transcriptomic studies on Arabidopsis revealed increase in expression of *PPC* and *PPCK* isoforms in Arabidopsis upon Pi-starvation, there were differences in their expression between roots and shoots. In the study by Gregory et al. (2009) and Feria et al. (2016), similar results were obtained for shoots, however, conflicting results were obtained for roots. In shoots, Pi-starvation induced the expression of *PPC1*, *PPC2*, *PPCK1*, and *PPCK2*, but not *PPC3* (Feria et al., 2016; Gregory et al., 2009). In roots, Gregory et al. (2009) reported increased expression of all *PPC* and *PPCK* isoforms. Whereas induction in expression of only *PPC3* and *PPCK2* was reported by Feria et al. (2016) in roots. Although the results are not very clear for roots, these two studies suggest distinct contributions of individual PPCs and PPCKs in roots and shoots during Pi-starvation. Feria et al. (2016) also analyzed T-DNA insertion lines with aberrant expression of *PPC*s and *PPCK*s and showed that PPC activity was affected only in roots and shoots of *ppc2* and *ppc3* plants, respectively, and lack of PPC phosphorylation was only observed in roots of *ppc3* and *ppck2* plants (Feria et al., 2016). However, the T-DNA insertion lines for *ppc3* (SALK_031519C) and *ppck2* (SALK_102132), they used for their analysis, which are named as *ppc3-1* and *ppck2-1*, respectively in this study showed similar *PPC3* transcripts levels and around 10 fold higher *PPCK2* transcript levels compared to the levels in wild-type (WT), respectively in this study. This suggests that the effects observed in their study were probably not due to loss of *PPC3* and *PPCK2*. Moreover, malate and citrate levels were also not determined in the T-DNA insertion lines of *PPC*s and *PPCK*s upon Pi-starvation in Arabidopsis. Thus, the precise role or contribution of individual PPC and PPCK isoforms during low Pi-stress is not yet assigned. Moreover, until now there is no information on effects of overexpression of the PPC/PPCK pathway genes with respect to Pi-starvation in Arabidopsis. Therefore, a number of questions arise from the current knowledge on the PPC pathway, which is the main focus of this study:

- What is the role or contribution of individual PPC and PPCK isoforms during Pi-deficiency induced malate and citrate generation and exudation in Arabidopsis?

- Is it possible to engineer the PPC/PPCK pathway by overexpression of *PPCK*s in Arabidopsis?
- What is the effect of overexpression of *PPCK*s during low Pi-stress in Arabidopsis?
- Can overexpression of *PPCK*s alter malate or citrate exudation in Arabidopsis?
- Can the Pi-status of transgenic plants overexpressing *PPCK*s be modified?

In order to answer these questions, the following goals were pursued in this doctoral thesis:

- Elucidation of the contribution of PPC pathway genes in Pi-deficiency-induced malate and citrate generation by analyzing Arabidopsis T-DNA insertion lines with impaired expression of *PPC1*, *PPC2*, *PPC3*, *PPCK1*, and *PPCK2*.
- Transcript profiling of PPC pathway genes together with a more detailed study on *PPCKs* with respect to their tissue-specific expression and subcellular localization.
- Characterization of transgenic lines overexpressing *PPCK*s with respect to their endogenous organic acid content and exudation capacity.
- Determination of Pi content and amino acid content in plants with altered *PPCK* expression to elucidate if there is any effect on the metabolism of these plants other than on organic acid metabolism.

2 RESULTS

2.1 Influence of Pi-starvation on PPC/PPCK pathway in Arabidopsis

As initial experiments, malate and citrate levels as well as the expression profiles of genes, which contribute to their generation and exudation, were investigated with a major focus on genes of the PPC/PPCK pathway, such as *PPC*s, *PPCKs*, and *MDH*s. The analysis was performed separately for roots and shoots. Additionally, promoter GUS and GFP reporter-lines were analyzed in order to obtain a more detailed impression about the expression domains of *PPCK1* and *PPCK2*.

2.1.1 Malate and citrate content after Pi-starvation in Arabidopsis

Accumulation of malate and citrate after Pi-starvation has already been reported in two independent studies in Arabidopsis (Morcuende et al., 2007; Pant et al., 2015). To confirm whether after Pi-starvation similar increase in endogenous malate and citrate levels can also be observed in seedlings growing under our experimental system, their levels were determined in this study.

The contents of malate and citrate were similar in 11 days old Arabidopsis seedlings grown under control (+Pi) condition. Between individual experiments, the average content in roots and shoots varied between 3-11 and 4-16 nmol per mg fresh weight for malate and citrate, respectively. Malate content was consistently and significantly induced after Pi-starvation by around 1.4 ($p=2.6\ e^{-12}$) and 2-fold ($p=1.1\ e^{-31}$) in roots and shoots, respectively [Figure 2-1(A) and Figure 2-1(C)]. Pi-deficiency also triggered citrate accumulation in shoots by around 2-fold ($p=2.64\ e^{-36}$) [Figure 2-1(D)]. In roots, Pi starvation-induced citrate accumulation was less pronounced (1.2 fold) [Figure 2-1(B)]. However, this increase was not consistently observed in all experiments, which is indicated by the comparably low statistical significance of p=0.0003 (n=76).

2.1.2 Malate and citrate exudation after Pi-starvation in Arabidopsis

Within the 2 h incubation period, roots of seedlings grown under Pi-sufficient condition exuded on average 230-1100 and 290-1580 pmol per mg root fresh weight of malate and citrate, respectively. Amount of citrate in root exudates was always higher than malate in all the independent experiments under Pi-sufficient conditions. Malate exudation was increased after Pi-starvation by 1.7-fold ($p=5.2\ e^{-08}$) [Figure 2-2(A)]. Similar increase in malate exudation after Pi-starvation was also detected recently in Arabidopsis by Maruyama et al. (2019). Changes in citrate content in root exudates of Pi-starved seedlings were not consistently detected in all the independent experiments [Figure 2-2(B)].

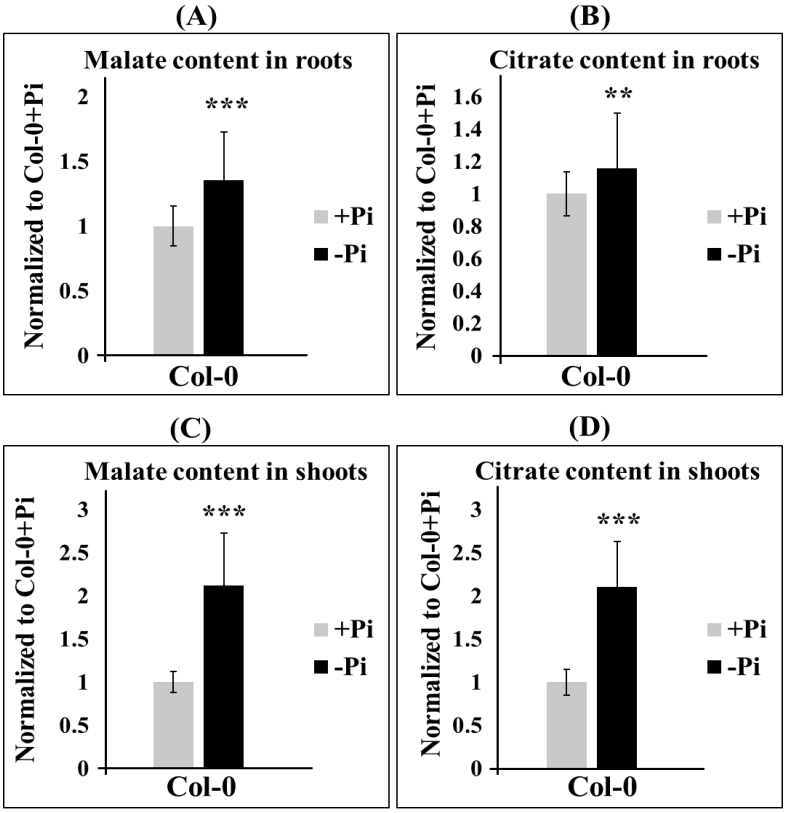

Figure 2-1: Normalized malate and citrate content after Pi-starvation in WT seedlings

Normalized content of (A) malate (B) citrate in roots (C) malate and (D) citrate in shoots after Pi starvation in WT (Col-0) seedlings. Seedlings were germinated for 6 days on +Pi agar plates, transferred to +Pi (500 µM) or –Pi (5 µM) conditions, and allowed to grow for additional 5 days before harvest. Data are normalized to the levels observed in +Pi. Shown are the cumulative data of 19 independent germination experiments. For each experiment, four biological replicates (two pooled seedlings per replicate) were analyzed. Error bars denote SD (n=76 total biological replicates). Asterisks above the error bars indicate the p values of Student's *t*-test (two-tailed, equal variances): **p ≤ 0.01 and ***p ≤ 0.0001.

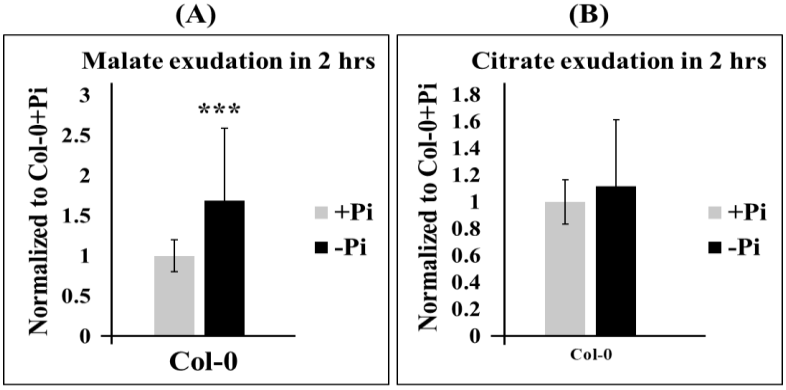

Figure 2-2: Normalized malate and citrate content in root exudates after Pi-starvation in WT seedlings

Normalized content of (A) malate and (B) citrate in exudates of WT (Col-0) after Pi-starvation. Seedlings were germinated for 6 days on +Pi agar plates, transferred to +Pi (500 µM) or –Pi (5 µM) conditions, and allowed to grow for additional 4 days. Subsequently, the root systems of three intact seedlings were incubated in 300 µl water, and exudates were collected after 2 h. Data are normalized to the levels observed in +Pi. Shown are the cumulative data of 19 independent germination experiments. For each experiment, four biological replicates (the exudates of three pooled root systems per replicate) were analyzed. Error bars denote SD (n=76). Asterisks above the bars indicate the p values of Student's *t*-test (two-tailed, equal variances): ***p ≤ 0.0001.

2.1.3 Expression analysis of *PPC*s and *PPCK*s by RT-qPCR

The steady-state mRNA levels of different isoforms of *PPC*s and *PPCK*s were determined in roots and shoots separately via RT-qPCR analysis.

In roots, the mRNA abundances of three *PPC* isoforms- *PPC1*, *PPC2*, and *PPC3* were different under Pi-sufficient condition. *PPC1* was the most abundant form of *PPC* followed by *PPC3* and *PPC2*. Transcript levels of *PPC3* were higher than *PPC2* by around 1.5 fold. After Pi-starvation, mRNA levels of all three *PPC* isoforms were increased. Transcript levels of *PPC1*, *PPC2*, and *PPC3* were induced by 4.5, 4.5, and 3-fold, respectively [Figure 2-3(A): (a)]. The induction in expression of *PPC1* was different from both *PPC2* and *PPC3* (two way ANOVA: $p=1.82e^{-09}$ between *PPC1* and *PPC2*; $p=6.36e^{-11}$ between *PPC1* and *PPC3*), whereas it was not different between *PPC2* and *PPC3* (two way ANOVA: p=0.381). *PPC1* transcript levels were higher than both *PPC2* and *PPC3* after Pi-starvation, whereas *PPC2* and *PPC3* transcript levels were similar. Transcript levels of *PPCK1* were higher than *PPCK2* both under Pi-sufficient and Pi-deficient condition by around 28 fold and 13 fold, respectively [Figure 2-3(A): (b)]. The induction in mRNA abundance of *PPCK2* after Pi-starvation was 6-fold compared to 2.5 fold induction detected for *PPCK1*. The induction in gene expression was stronger for *PPCK2* compared to *PPCK1* (two way ANOVA: $p=2.3e^{-05}$).

In shoots, the steady-state mRNA levels of *PPC1, PPC2, and PPC3* were different under Pi-sufficient condition. Unlike in roots, *PPC2* was the predominant *PPC* isoform expressed in shoots followed by *PPC1* and *PPC3.* Pi-starvation triggered induction in the expression of all three *PPC* isoforms but the extent of their increase was different [Figure 2-3(B): (a)]. In contrast to roots, induction was strongest for *PPC3* (15-fold). *PPC1* transcripts were elevated by 8-fold, whereas the induction of *PPC2* was the lowest among all three *PPC*s (2.4-fold). The induction in expression of *PPC3* was stronger than both *PPC1* and *PPC2* (two way ANOVA: $p=7.57e^{-08}$ between *PPC1* and *PPC3*; $p=1.35e^{-06}$ between *PPC2* and *PPC3*) and *PPC1* induction was stronger than *PPC2* (two way ANOVA: p=0.002). Transcript levels of *PPC1* and *PPC2* were similar after Pi-starvation and were higher than *PPC3* transcript levels. *PPCK1* transcripts were more abundant than *PPCK2* transcripts both under Pi-replete and Pi-depleted condition by around 48-fold and 1.5-fold, respectively [Figure 2-3(B): (b)]. After Pi-deficiency treatment, expression of both *PPCK1* and *PPCK2* was significantly induced by 9-fold and 280-fold, respectively. The induction in expression of *PPCK2* after Pi-starvation was stronger than that observed for *PPCK1* (two way ANOVA: p= 0.002).

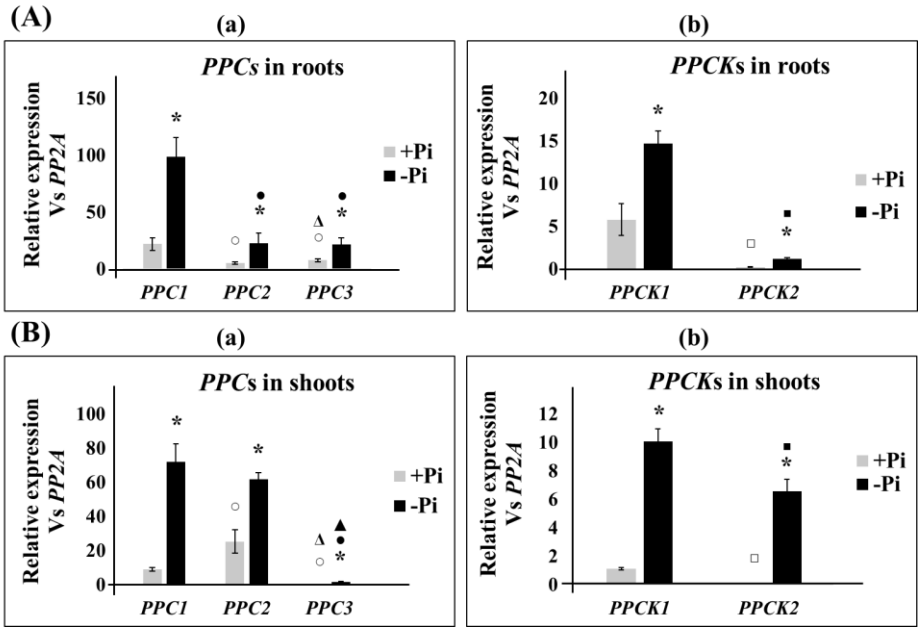

Figure 2-3: Expression analysis of *PPCs* and *PPCKs* in WT seedlings by RT-qPCR

Transcript levels of *PPC*s and *PPCK*s in (A) roots and (B) shoots of WT seedlings grown under Pi-sufficient and Pi-deficient conditions (a: *PPCs* and b: *PPCKs*). Seedlings were germinated for 6 days on +Pi agar plates, transferred to +Pi (500 µM) or –Pi (5 µM) conditions, and allowed to grow for additional 5 days before harvest. Error bars denote SD (n=4 biological replicates). Data from one representative out of three independent experiments are shown. Significance analyses were performed by Student's *t*-test (two-tailed, equal variances): *p ≤ 0.05, °p ≤ 0.05, •p ≤ 0.05, ᐞp ≤ 0.05, ▲p ≤ 0.05, □p ≤ 0.05, ▪p≤ 0.05 compared to +Pi condition, *PPC1*+Pi, *PPC1*-Pi, *PPC2*+Pi, *PPC2*-Pi, *PPCK1*+Pi, and *PPCK1*-Pi, respectively.

2.1.4 Expression analysis of *PPC*s and *PPCK*s in *phr1phl1* mutant by RT-qPCR

PHR1 and PHL1 regulate about 60% of the transcriptional changes after Pi deficiency (Bustos et al., 2010). In order to investigate the regulation of *PPC*s and *PPCK*s by these two MYB transcription factors, qRT-PCR analysis for all *PPC* and *PPCK* isoforms were performed in the *phr1phl1* seedlings [Supplementary Figure 7-1(A-E)]. Under Pi-sufficient condition, transcript levels of only *PPC2* and *PPCK1* were affected, showing 2-fold lower mRNA levels for both in *phr1phl1* compared to WT roots. PHR1PHL1 dependent Pi-starvation triggered induction was different for different *PPC* and *PPCK* isoforms. Unlike in WT roots, there was no increase in transcript levels of *PPC1*, *PPC3*, and *PPCK1* upon Pi-starvation in *phr1phl1* roots. Induction in expression of *PPC2* (p=0.041) and *PPCK2* was still present, although at a lower extent compared to WT (two way ANOVA: $p=3.13e^{-06}$ between WT and *PPC2*; $p=7.23e^{-08}$ between WT and *PPCK2*).

2.1.5 Tissue-specific expression analysis of *PPCK1* and *PPCK2*

Promoters of *PPCK1* and *PPCK2* were fused to *GFP* and *GUS* reporter genes and introduced into Arabidopsis through Agrobacterium-mediated gene transfer to investigate their expression domains. Transgenic lines with both long (approx. 2.5 kb upstream of the translational start site) and short (approx. 1 kb upstream of the translational start site) promoter variants of *PPCK1* and *PPCK2* fused to the reporter genes were generated. Since both promoter variants for each gene showed similar

expression patterns at the T_2 generation, transgenic lines with long promoter variants were propagated for further generation of T_3 seeds for which the results are shown.

2.1.5.1 Expression analysis of *PPCKs* by promoter GUS reporter lines

Histochemical GUS analysis was performed with six independent transgenic lines transformed with each of the *pPPCK1$_{long}$::GFP-GUS* and *pPPCK2$_{long}$::GFP-GUS* construct. As independent lines generated by transformation with the same construct showed similar GUS expression patterns, only one representative line for each construct is shown [Figure 2-4].

GUS reporter activity driven by the *PPCK1* promoter in plants growing under Pi-sufficient condition was detected in newly emerging young leaves and at the apex and margins of cotyledonary and older leaves. *PPCK1* promoter activity was not detected in roots of Pi-sufficient seedlings [Figure 2-4(A): (a-c)], which contradicts the RT-qPCR data showing *PPCK1* transcript abundance also in roots. However, strong GUS activity was detected after Pi-starvation throughout mature part of the entire root. Induction of *PPCK1* promoter activity was also detected in root-tips of both primary and lateral roots. All the leaves displayed an increase in GUS-staining after Pi-starvation [Figure 2-4(A): (d-f)].

In contrast to *PPCK1, PPCK2* promoter activity was detected both in roots and shoots under Pi-sufficient condition, corroborating the RT-qPCR data [Figure 2-4(B): (a-c)]. Leaves at all developing stages displayed GUS activity in their apex and margins. *PPCK2* promoter activity was detected in the entire length of primary and lateral roots, but not in their root tips. Under Pi-deficient condition, the expression domains of *PPCK2* and *PPCK1* were similar in roots and shoots. Induction in *GUS*-staining was also detected in root-tips and the entire length of primary and lateral roots. Similar to *PPCK1,* all the leaves after Pi-starvation displayed an increase in *PPCK2* promoter activity [Figure 2-4(B): (d-f)].

2.1.5.2 Expression analysis of *PPCKs* by promoter GFP reporter lines

Expression domains of *PPCK1* and *PPCK2* were also determined in seedlings growing under Pi-sufficient and Pi-deficient conditions using GFP as a reporter. GFP-fluorescence was determined in two independent transgenic lines transformed with each of the *pPPCK1$_{long}$::GFP-GUS* and *pPPCK2$_{long}$::GFP-GUS* constructs [Supplementary figure 7-2 and Supplementary figure 7-3]. For PPCK1, unlike our GUS expression analysis, GFP-fluorescence was detected in mature regions of the roots under untreated condition. Induction in GFP-fluorescence was also detected in roots and root-tips of Pi-starved seedlings [Supplementary figure 7-2(A)], similar to the results observed with the GUS reporter. *PPCK1* promoter activity was not detected in leaves of transgenic lines transformed with *pPPCK1$_{long}$::GFP-GUS* under Pi-sufficient condition. This is in contrast to our RT-qPCR and GUS expression analysis. After Pi-starvation, very weak GFP fluorescence was detected in leaves of only one out of two independent transgenic lines [Supplementary figure 7-2(B)].

GFP fluorescence driven by the *PPCK2* promoter was detected in roots but not in root tips of untreated seedlings. Increase in GFP-fluorescence was detected in roots under Pi-deficient condition [Supplementary figure 7-3(A)]. Under this condition, GFP fluorescence was detectable also in root-tips, which is consistent with our GUS expression analysis. In contrast to the results obtained using GUS as a reporter, GFP-fluorescence in shoots could only be detected after Pi-deficiency, but not under Pi-sufficient condition [Supplementary figure 7-3(B)].

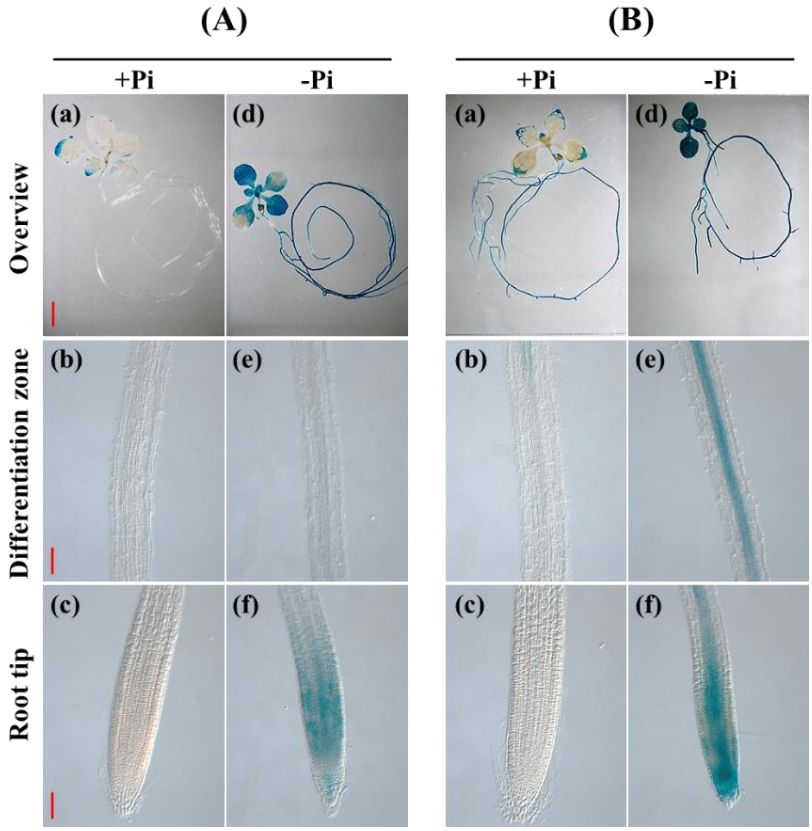

Figure 2-4: Tissue-specific expression analysis of *PPCK1* and *PPCK2* by GUS staining

Histochemical GUS staining of (A) *pPPCK1$_{long}$::GFP-GUS* and (B) *pPPCK2$_{long}$::GFP-GUS* reporter lines when grown under Pi-sufficient [(a): entire seedling; (b): differentiation zone; and (c): primary root tip] and Pi-deficient condition [(d): in the entire seedling; (e): differentiation zone; and (f): primary root tip]. Scale bars represent 2 mm in the upper panel and 100 µm in the center and bottom panels. Seedlings were germinated for 6 days on +Pi agar plates, transferred to +Pi (500 µM) or –Pi (5 µM) conditions, and allowed to grow for additional 5 days before staining. Seedlings were stained for 7 h.

2.1.6 Expression analysis of *PPCK1* and *PPCK2* in root-tips after different time points of Pi-deficiency treatment

GUS activities driven by *PPCK1* and *PPCK2* promoter were monitored in root-tips of transgenic lines after day 1, 3, and 6 of Pi-deficiency treatment [Figure 2-5(A) and (B)]. Induction in *PPCK1* promoter activity was detected at day 3 and 6, whereas induction in *PPCK2* promoter activity was detected in root-tips only after day 6. GUS staining was not detected in root-tips of Pi-sufficient seedlings at day 1, 3, and 6 for either construct.

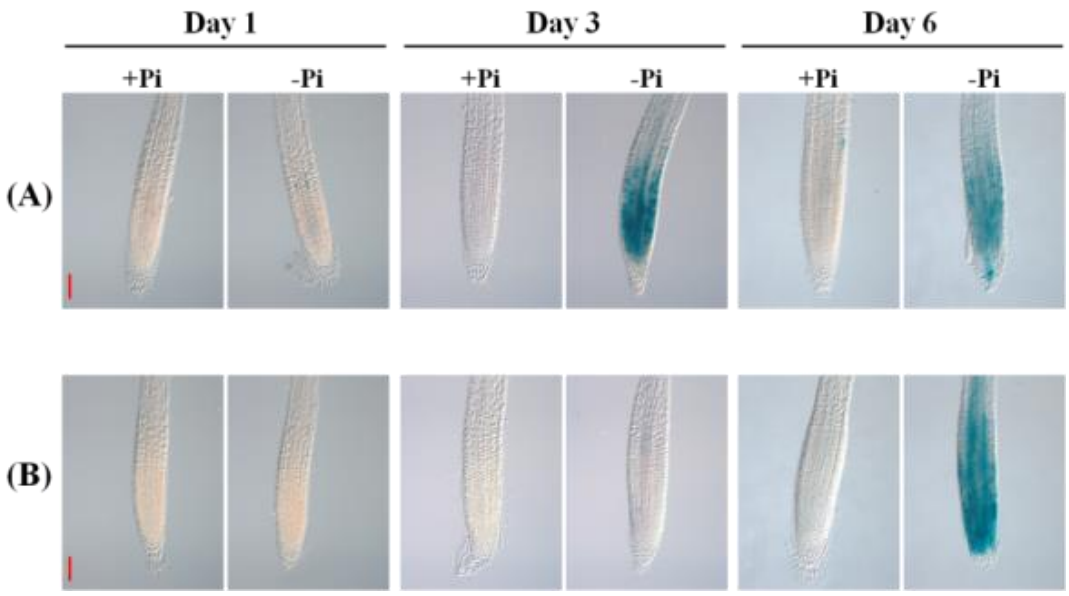

Figure 2-5: Expression analysis of *PPCK1* and *PPCK2* in root-tips after Pi-deficiency treatment

Histochemical GUS staining of (A) *pPPCK1$_{long}$::GFP-GUS* and (B) *pPPCK2$_{long}$::GFP-GUS* reporter lines in primary root tips. Seedlings were germinated for 6 days on +Pi agar plates, transferred to +Pi (500 µM) or –Pi (5 µM) conditions, and stained for 7 h in the GUS staining solution after day 1, 3, and 6 of transfer. Scale bars represent 100 µm.

2.1.7 Expression analysis of *PPCKs* in root-tips of plants growing on split plates

Split plate assays were performed to determine whether induction in the expression of *PPCKs* in root-tips is regulated by local or systemic Pi-starvation signaling [Figure 2-6(A) and (B)]. The analysis revealed that the entire seedling had to be in contact with Pi-depleted medium to induce *PPCK1* and *PPCK2* expression in root and root-tip; if shoot and the upper part of the root are exposed to Pi-sufficient condition, induction in promoter activity was not detected in root tip exposed to Pi-deficient condition. This indicates that both *PPCK* isoforms are regulated in the context of systemic Pi-sensing.

2.1.8 Characterization of transgenic lines having translational fusion construct of PPCK1 under its native promoter

A fusion protein construct with a fluorescent tag was generated in order to determine whether PPCK1 is regulated at the protein level. GFP was fused to the C-terminus of PPCK1 within a genomic fragment containing the native *PPCK1$_{long}$* promoter (*pPPCK1$_{long}$::gDNA-GFP*). In order to test the functionality of this construct, it was introduced in *ppck1-1* line by the Agrobacterium-mediated floral dip method (*PPCK1$_{long}$::gDNA-GFP/ppck1-1*). The *ppck1-1* plants exhibit strongly reduced *PPCK1* transcripts and are described in more detail later in section 2.2.2. Six independent transgenic lines (*PPCK1$_{long}$::gDNA-GFP/ppck1-1*) were analyzed in this study and were named D1.2, D6.9, D7.3, D9.3, D14.4, and D19.4. The *PPCK1* mRNA abundance was between 1.4 and 6-fold higher and between 17 and 70-fold higher in these lines compared to WT and *ppck1-1* plants, respectively [Supplementary figure 7-4].

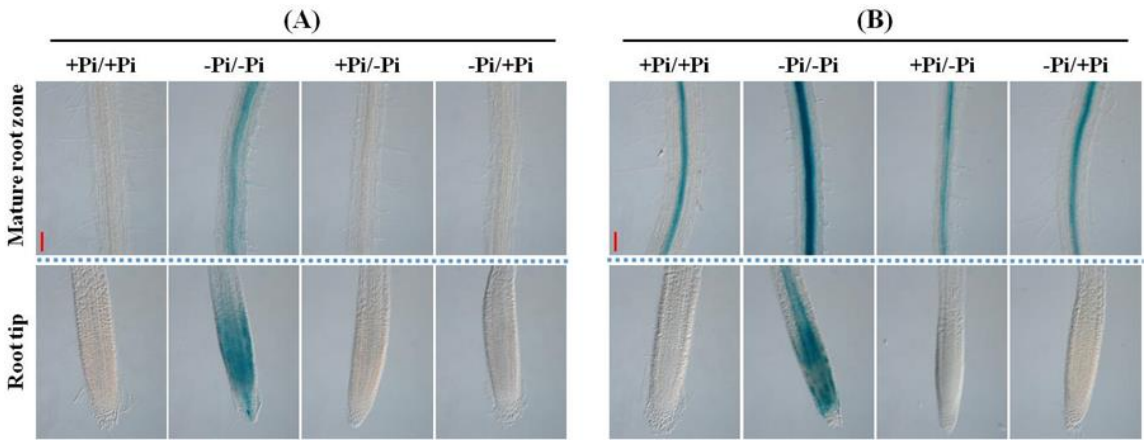

Figure 2-6: Expression analysis of *PPCK1* and *PPCK2* in roots of seedlings growing on split plates

Histochemical GUS staining in roots of (A) pPPCK1$_{long}$::GFP-GUS and (B) pPPCK2$_{long}$::GFP-GUS reporter lines when grown on split plates. Seedlings were germinated for 6 days on +Pi agar plates, and transferred to split plates with four different conditions: containing agar medium with Pi on both sides (+Pi/+Pi); without Pi on both sides (-Pi/-Pi); with Pi on top half and without Pi on bottom half (+Pi/-Pi); and without Pi on top half and with Pi on bottom half (-Pi/+Pi), and allowed to grow for additional 5 days before staining. Mature root-zone shown in the images were growing on top halves of split-plates. +Pi: 500 µM and -Pi: 5 µM. Scale bars represent 100 µm.

2.1.8.1 Malate content in transgenic lines having translational fusion construct of PPCK1 under its native promoter

Although higher *PPCK1* transcript levels were detected in D-lines, it was important to determine whether the introduced construct is also functional. In roots and shoots of *ppck1-1* seedling, lower malate levels were detected both under +Pi and -Pi condition compared to WT (section 2.2.2.1). If the GFP tagged PPCK1 proteins in D-lines are functional, malate levels should be restored to WT levels.

In roots [Figure 2-7(A)], malate levels in D-lines were either partially (D6.9, D7.3, D14.4, and D19.4) or completely restored (D1.2 and D9.3) to WT levels under Pi-replete condition. Malate levels were 1.8-fold lower in *ppck1-1*, whereas in D-lines only between 1.2 and 1.4-fold reduced levels were detected compared to WT under Pi-sufficient condition. In Pi-depleted D-lines, malate levels were even between 1.2 and 1.7-fold higher compared WT. When compared to *ppck1-1* plants, all the D-lines exhibited between 1.3 and 1.8-fold higher malate levels under Pi-sufficient condition. In Pi-deficient D-lines, between 2 and 2.7-fold higher malate levels were detected compared to *ppck1-1*.

In shoots [Figure 2-7(B)], malate levels were completely restored to WT levels in four out of six lines (D1.2, D6.9, D7.3, and D9.3) both under Pi-replete and Pi-deplete condition. Compared to *ppck1-1* seedlings, these four lines exhibited around 1.2-fold and between 1.2 and 1.6-fold higher malate content under Pi-sufficient and Pi-deficient condition, respectively. In contrast, the other two lines- D14.4 and D19.4 showed malate levels similar to *ppck1-1* both under +Pi and -Pi condition [Figure 2-7(B)]. Thus, in shoots malate levels were complemented only for lines- D1.2, D6.9, D7.3, and D9.3.

2.1.9 Western blot analysis to detect PPCK1 protein levels after Pi-starvation

After having confirmed the functionality of GFP tagged PPCK1 in D-lines, PPCK1 protein abundance was analyzed by immunoblotting using a GFP antibody [Figure 2-8]. Three independent D lines- D1.2, D6.9, and D9.3 were used for this assay. A band around 60 kDa was expected for GFP fused to PPCK1 (MW of PPCK1 and GFP is 32 kDa and 28 kDa, respectively). In all three D-lines, a band around 60 kDa was detected in both +Pi and -Pi samples. The signal intensity of this band was much stronger in protein extracts obtained from Pi-depleted seedings compared to that in Pi-replete seedlings. Results from this analysis suggest that *PPCK1* is also regulated at the protein level during low Pi-stress.

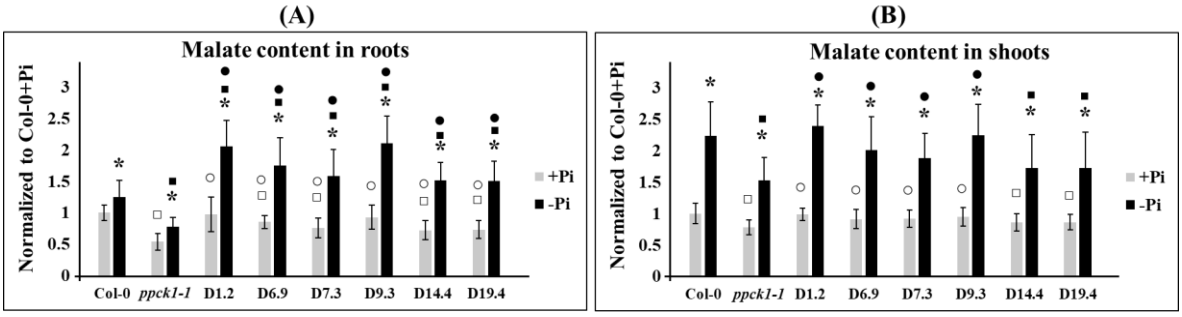

Figure 2-7: Normalized content of malate in *pPPCK1$_{long}$::gDNA-GFP/ppck1-1* lines

Normalized malate content in (A) roots and (B) shoots of *pPPCK1$_{long}$::gDNA-GFP/ppck1-1* lines (D-lines) grown under Pi-sufficient and Pi-deficient conditions. Seedlings were germinated for 6 days on +Pi agar plates, transferred to +Pi (500 µM) or –Pi (5 µM) conditions, and allowed to grow for additional 5 days before harvest. Data are normalized to the levels observed in Col-0+Pi. Shown are the cumulative data of 3 independent germination experiments. For each experiment, four biological replicates (two pooled seedlings per replicate) were analyzed. Error bars denote SD (n=12 total biological replicates). Significance analyses were performed by Student's *t*-test (two-tailed, equal variances): $^{*}p \le 0.05$, $^{\square}p \le 0.05$, $^{\blacksquare}p \le 0.05$, $^{\circ}p \le 0.05$; and $^{\bullet}p \le 0.05$ compared to +Pi, Col-0+Pi, Col-0-Pi, *ppck1-1*+Pi, and *ppck1-1*-Pi, respectively.

2.1.9.1 Detection of PPCK1 protein in *pPPCK1$_{long}$::gDNA-GFP/ppck1-1* lines

Western-blot analysis had revealed an accumulation of GFP-tagged PPCK1 after Pi-starvation in D lines. These lines were also used to analyze PPCK1 protein abundance in tissues using LSM and representative results for two lines (D6.9 and D9.3) are shown in [Figure 2-9]. In roots and leaves of Pi-sufficient seedlings, very weak GFP-signal was detected. In Pi-depleted seedlings, the signal intensity was higher in roots and also in the root-tips [Figure 2-9(A)]. Induction in GFP-fluorescence was also detected in leaves [Figure 2-9(B)].

Subcellular localization of PPCK1 was analyzed in Pi-depleted seedlings because of higher signal intensities [Supplementary figure 7-5(A)]. Cytosolic localization of PPCK1 was confirmed, which was also shown previously by other researchers using biochemical approaches. Since a faint band of around 28 kDa, which indicated free GFP, could also be detected in these lines by western blot assays after longer exposure time (2 min instead of 50 s) in Pi-depleted samples (results not shown), the nuclear localization visualized in these lines could be due to free GFP. Additionally, it was also found to be localized in some small randomly moving dot-like structures [Supplementary figure 7-5(B)]. Since

PPC/PPCK mediated reaction is involved in anaplerotic feeding of the TCA cycle, these dot-like structures were hypothesized to be mitochondria. However, preliminary co-localization study using mitotracker red dye revealed that these dot-like structures are not mitochondria [Supplementary figure 7-5(C)]. These moving bodies could not be associated with any organelles, such as peroxisome, mitochondria, and golgi bodies so far. It is also possible that these moving bodies are just aggregates of degraded proteins. However, since this construct was shown to be functional based on complementation of *ppck1-1*, it suggests that PPCK1 proteins are attached to these structures and are not just protein aggregates. Further investigations are needed to identify these dot-like structures.

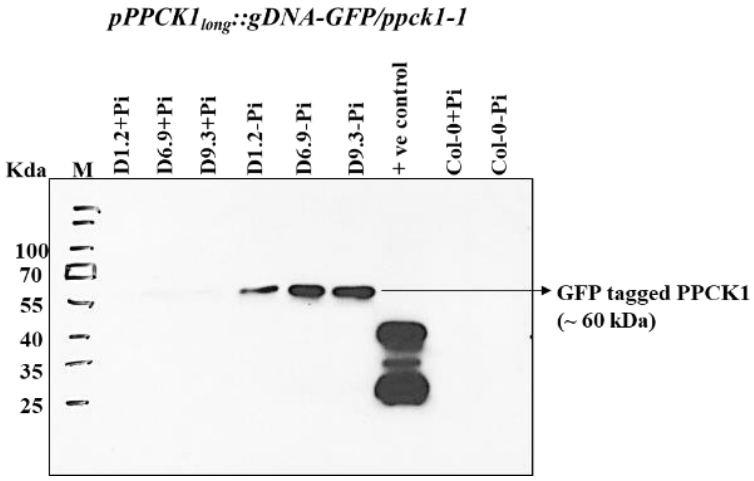

Figure 2-8: Detection of PPCK1 protein in *pPPCK1$_{long}$::gDNA-GFP/ppck1-1* lines grown under Pi-sufficient and Pi-deficient conditions

Seedlings were germinated for 6 days on +Pi agar plates, transferred to +Pi (500 µM) or –Pi (5 µM) conditions, and allowed to grow for additional 5 days before harvest. 50 µg of total protein extract from seedlings was loaded on to the SDS/PAGE gel and after transfer to the membrane was probed with anti-GFP antibody. GFP-ATG8 and WT (Col-0) samples were used as positive and negative control for GFP, respectively.

2.1.10 Expression analysis of *MDH*s by RT-qPCR

Since the generation of malate by PPC/PPCK pathway requires the action of MDHs, transcript levels of seven out of nine Arabidopsis *MDH*s- namely cytosolic malate dehydrogenases (*cMDH1*, *cMDH2*, and *cMDH3*), mitochondrial malate dehydrogenases (*mMDH1* and *mMDH2*), plastidic NAD-dependent malate dehydrogenase (*pNAD-MDH*) and NADP- dependent malate dehydrogenase (*NADP-MDH*) were determined in roots and shoots of Arabidopsis by RT-qPCR [Supplementary figure 7-6].

In roots of seedlings growing under Pi-sufficient and Pi-deficient conditions, expression of six out of seven isoforms of *MDHs* was similar. Only transcript levels of *NADP-MDH* were changed, exhibiting 3-fold reduced levels in Pi-starved roots compared to Pi-replete roots [Supplementary figure 7-6(A): (a-c)]. Transcript levels of *cMDH2* and *mMDH2* were significantly higher by around 2-fold in shoots of Pi-depleted seedlings compared to the levels in Pi-replete shoots. Expression of other *MDH*s was unaltered in shoots after Pi-starvation [Supplementary figure 7-6(B): (a-c)].

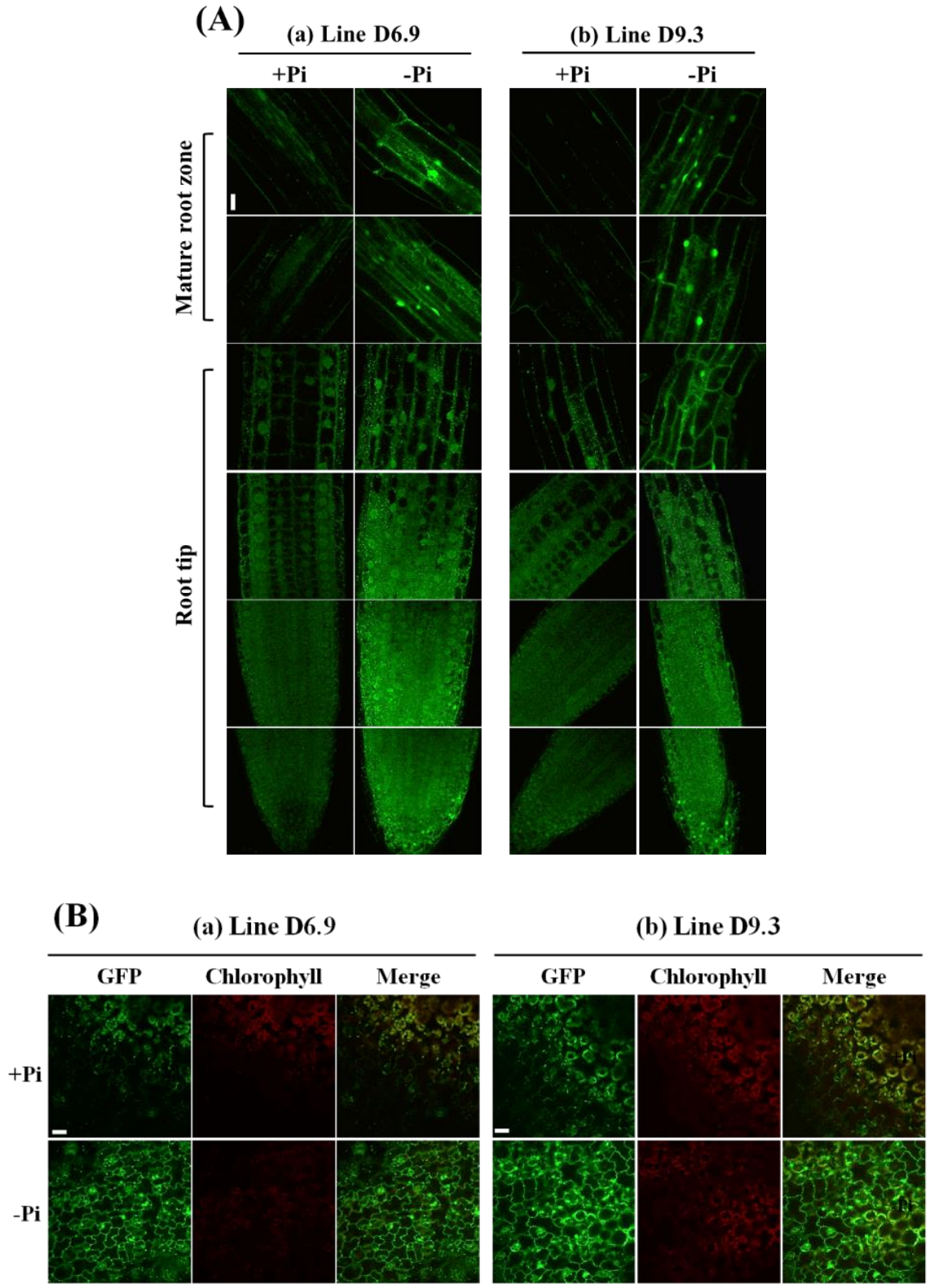

Figure 2-9: Detection of PPCK1 in *pPPCK1$_{long}$::gDNA-GFP/ppck1-1* lines grown under Pi-sufficient and Pi-deficient condition in Arabidopsis

PPCK1-GFP derived fluorescence in two representative *pPPCK1$_{long}$::gDNA-GFP/ppck1-1* lines [(a): Line D6.9 and (b): Line D9.3]. Images of single optical section of seedlings from (A) different regions of root-tip and mature root and (B) leaves. Representative merged images for leaves are presented as overlay images of the GFP channel (displayed in green) and the chlorophyll channel (displayed in red). Scale bars represent 20 µm. Data from one representative out of three independent experiments are shown. Seedlings were germinated for 6 days on +Pi agar plates, transferred to +Pi (500 µM) or –Pi (5 µM) conditions, and allowed to grow for additional 5 days before imaging.

2.1.11 Characterization of plants deficient in PPCs

Root and shoot of Arabidopsis exhibited differences in expression of individual *PPC*s as revealed by our RT-qPCR analysis. Also, individual *PPC*s were induced by Pi-starvation to different extents. Therefore, malate and citrate content of T-DNA insertion lines exhibiting aberrant expression of *PPCs* were analyzed to determine the contribution of individual *PPC* isoforms for malate and citrate generation in roots and shoots.

The T-DNA insertion line- SALK_088836 (Shi et al., 2015) was used for *PPC1*. Two independent T-DNA insertion lines- SALK_128516 (Feria et al., 2016) and SALK_025005 (Shi et al., 2015) were used for *PPC2*. These alleles were denoted as *ppc2-1* and *ppc2-2,* respectively. The T-DNA insertion lines used for *PPC3* were SALK_031519C (Feria et al., 2016) and SALK_143289.54.75X which were named as *ppc3-1* and *ppc3-2*, respectively. RT-qPCR analysis revealed no measurable *PPC1* transcripts in *ppc1* seedlings [Supplementary figure 7-7(A)]. The T-DNA insertion lines *ppc2-1* and *ppc2-2* exhibited around 380- and 23-fold lower *PPC2* transcript levels compared to WT seedlings, respectively [Supplementary figure 7-7(B)]. Expression of *PPC3* in *ppc3-1* seedlings was similar to WT, whereas *ppc3-2* exhibited 1000-fold reduced *PPC3* mRNA levels compared to WT seedlings [Supplementary figure 7-7(C)]. Therefore, the *ppc3-1* allele was omitted from analysis.

2.1.11.1 Malate and citrate content in plants deficient in *PPC*s

In roots, malate content was affected in all *ppc* mutants under Pi-replete condition [Supplementary figure 7-8(A)]. *Ppc1* roots exhibited 1.3-fold lower malate levels compared to WT roots. Similarly, 1.3- and 1.6-fold lower malate levels were detected in *ppc2-1* and *ppc2-2*, respectively. *Ppc3* exhibited 1.2-fold lower malate content in roots compared to WT roots. After Pi starvation, reduced malate (around 1.3-fold) content was detected only in *ppc1* roots compared to WT roots. Pi-starvation triggered induction in root malate content was detected in all these mutants and the response was similar to WT roots except for *ppc2-2* roots. *Ppc2-2* showed 2.28-fold induction in root malate content compared to 1.4-fold induction detected in WT root (two way ANOVA: p= 0.03) [Supplementary figure 7-8(A): (a-d)]. In shoots [Supplementary figure 7-8(B)], malate content was reduced in both *ppc2* alleles by around 1.4-fold compared to WT levels under Pi-sufficient condition, however, it was not affected in shoots of Pi-replete *ppc1* and *ppc3* plants. However, after Pi-starvation, malate content was reduced in all lines with reduced *PPC1*, *PPC2*, and *PPC3* expression [Supplementary figure 7-8(B): (a-d)]. Malate levels were reduced by 1.5, 1.6, 1.4, and 1.2-fold in Pi-deficient *ppc1-1*, *ppc2-1*, *ppc2-2*, and *ppc3-1* shoots, respectively compared to WT shoots. Pi-deficiency induced elevation in shoot malate content was present in all *ppc* mutants but the response was weaker compared to that in WT plants (two way ANOVA: p= $6.52e^{-04}$, 0.03, 0.001, and 0.002 for *ppc1, ppc2-1*, *ppc2-2*, and *ppc3-2*, respectively).

In roots, citrate content was not affected in any of the *ppc* mutants compared to WT, independent of the growing conditions, except for *ppc2-2* roots where it was reduced by 1.5-fold under Pi-replete condition [Supplementary figure 7-8(C): (a-d)]. Pi-deficiency triggered induction in root citrate content was detected in all *ppc* mutants and the response was also similar to WT roots, except in *ppc2-2* roots which exhibited 3-fold induction in root citrate content compared to 1.7-fold induction detected in WT plants (two way ANOVA: p=0.004). In shoots [Supplementary figure 7-8(D): (a-d)], increased levels of citrate were detected in Pi-sufficient *ppc2* seedlings. Around 1.3-fold elevated citrate levels were detected both in *ppc2-1* and *ppc2-2* shoots compared to the levels detected in WT shoots. However, citrate levels were unaffected in Pi-depleted *ppc2-1* and *ppc2-2* shoots compared to WT shoots. In shoots of *ppc1* and *ppc3-2*, citrate levels were similar to WT shoots both under Pi-replete and Pi-deplete condition. Pi-deficiency triggered induction in shoot citrate content was detected in all *ppc* mutants and the response was also similar to WT shoots.

2.1.12 Characterization of transgenic lines having GFP tagged PPCKs

PPCK1 and PPCK2 are assumed to be cytosolic proteins because they are soluble and lack any target signals. So far no *in vivo* studies are reported showing their subcellular localization using GFP tagged PPCK1 and PPCK2. To gain better insights into the subcellular localization of PPCK1 and PPCK2, fusion constructs were generated in which GFP was fused to the C- or N- terminus of the coding sequence of PPCK1 and PPCK2. These constructs were placed both under the control of the *CaMV* (*Cauliflower Mosaic Virus*) *35S* promoter and the *UBQ10* (*Ubiquitin 10*) promoter. Stably transformed Arabidopsis plants were generated by transforming these constructs into WT (Col-0) plants (*35S::PPCK1-GFP*, *35S::GFP-PPCK1*, *35S::PPCK2-GFP*, and *35S::GFP-PPCK2; UBQ10::PPCK1-GFP, UBQ10::GFP-PPCK1, UBQ10::PPCK2-GFP,* and *UBQ10::GFP-PPCK2*). Here results from fusion constructs only under *35S* promoter are mentioned, since under *UBQ10* promoter similar results were obtained.

The transgenic lines with N and C-terminally tagged PPCK1 under control of the *35S* promoter were denoted as J and R lines, respectively. *PPCK1* mRNA abundance in seedlings of J and R lines were between 38-190 fold and 8-238 fold higher than in WT seedlings, respectively [Supplementary figure 7-9(A-B)]. The transgenic lines with N and C-terminally tagged PPCK2 under 35S promoter were named as N and T lines, respectively. *PPCK2* transcript levels in N and T lines were between 2500-7300 fold and 1800-10,000 fold higher than in WT seedlings [Supplementary figure 7-9(C-D)].

2.1.12.1 Western blot analysis of transgenic lines having GFP-tagged PPCKs

The presence of full-length PPCK1 and PPCK2 fused to GFP in all generated transgenic lines were analyzed by western blots using an anti-GFP antibody [Figure 2-10(A-B)]. A band of the expected size of around 60 kDa for both fusion proteins (MW of PPCK1, PPCK2, and GFP are 31.82 kDa, 31.198 kDa,

and 28 kDa, respectively) could be detected. The intensity of this band in independent lines transformed with the same construct was different and did not correspond to the transcript levels detected in these lines. An additional band corresponding to free GFP at around 28 kDa, which was weaker in comparison to fused protein band was also detected in most of the lines. This band was not detected in J6.4, J7.6, and J9.4 lines. This could be due to the lower amount of overexpressed proteins in these lines and therefore the proportion of free GFP was not detected. Signals were not detected in WT plants which confirm the specificity of anti-GFP antibody used in this study.

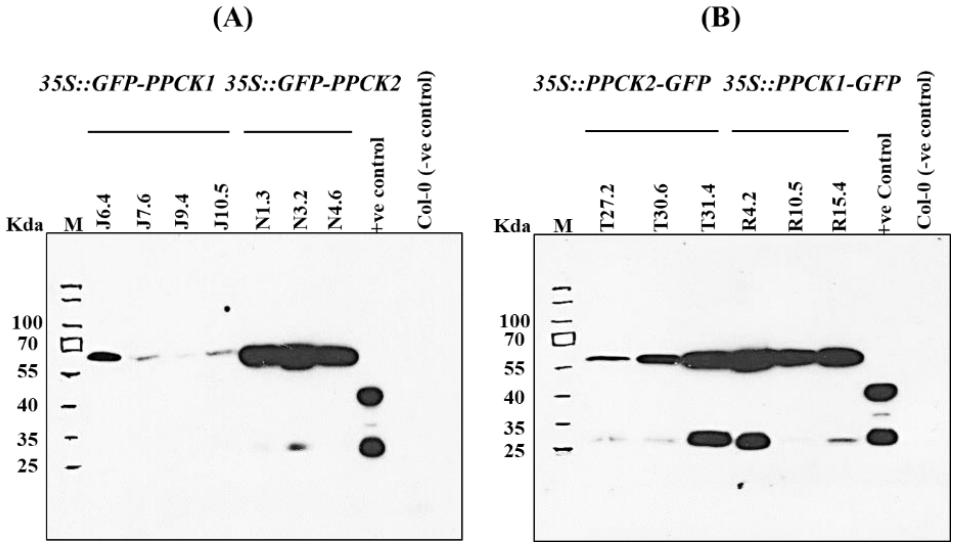

Figure 2-10: Detection of GFP-tagged PPCK1 and PPCK2 in stably transformed Arabidopsis by immunoblot analysis

Western blot assays to detect (A) N-terminally and (B) C-terminally tagged PPCKs in stably transformed Arabidopsis seedlings. Total protein was extracted from 11 days old Arabidopsis seedlings. 50 µg of total protein extract was loaded on to the SDS/PAGE gel and after transfer to the membrane was probed with anti-GFP antibody. GFP-ATG8 and WT (Col-0) samples were used as positive and negative control for GFP, respectively.

2.1.12.2 Malate content in transgenic lines having GFP-tagged PPCKs

Although the overexpressed GFP fused PPCKs were detected in transgenic lines, it was imperative to determine the functionality of these constructs *in vivo*. If the translational fusion constructs of PPCKs under *35S* promoter are functional, higher malate levels should be detected in all the generated transgenic lines, because phosphorylated PPCs are less sensitive to feedback inhibition by malate. Therefore in transgenic plants with higher levels of PPCKs, more PPCs should be phosphorylated and ultimately more malate should be generated compared to untransformed WT plants.

Root malate content was determined in two independent transgenic lines generated by transforming each of the N and C-terminally fused PPCK1 (J6.4, J9.4, R10.5, and R15.4) and PPCK2 (N2.10, N3.2, T27.2, and T30.6) constructs. Malate content in roots of all these transgenic lines was between 1.3-1.6-fold higher compared to the levels in WT roots [Supplementary figure 7-10]. This result confirmed the functionality of these translational fusion constructs, hence they are suitable for analysis of the subcellular localization of PPCK1 and PPCK2.

2.1.12.3 Subcellular localization of PPCK1 and PPCK2

The localization pattern of PPCK1 with GFP-tag either on N or C-terminal were similar and the same is also true for PPCK2 [Figure 2-11(A-B)]. The GFP signal was diffused in the entire cell suggesting cytosolic localization of PPCK1 and PPCK2, which confirms the earlier biochemical reports. This is the first study showing subcellular localization of PPCK1 and PPCK2 using fluorescently labeled protein. GFP signals were also detected in some small randomly moving dot-like structures. Since these dot-like structures were also detected in D-lines (*pPPCK1$_{long}$::gDNA-GFP/ppck1-1*) [Supplementary figure 7-5(B)], it suggests that these structures are not simply artifacts of protein aggregates due to high expression. Since the PPC/PPCK pathway is known to replenish the TCA-cycle intermediates, it was hypothesized that these dot-like structures could be mitochondria. However, colocalization studies performed using the MitoTracker red dye did not identify these dot-like structures as mitochondria. Moreover, our preliminary study could not associate these structures with any organelles like peroxisomes, mitochondria, and golgi-bodies so far. The GFP-signal in nucleus could be due to the presence of free GFP in these lines, as detected by our western blot analysis.

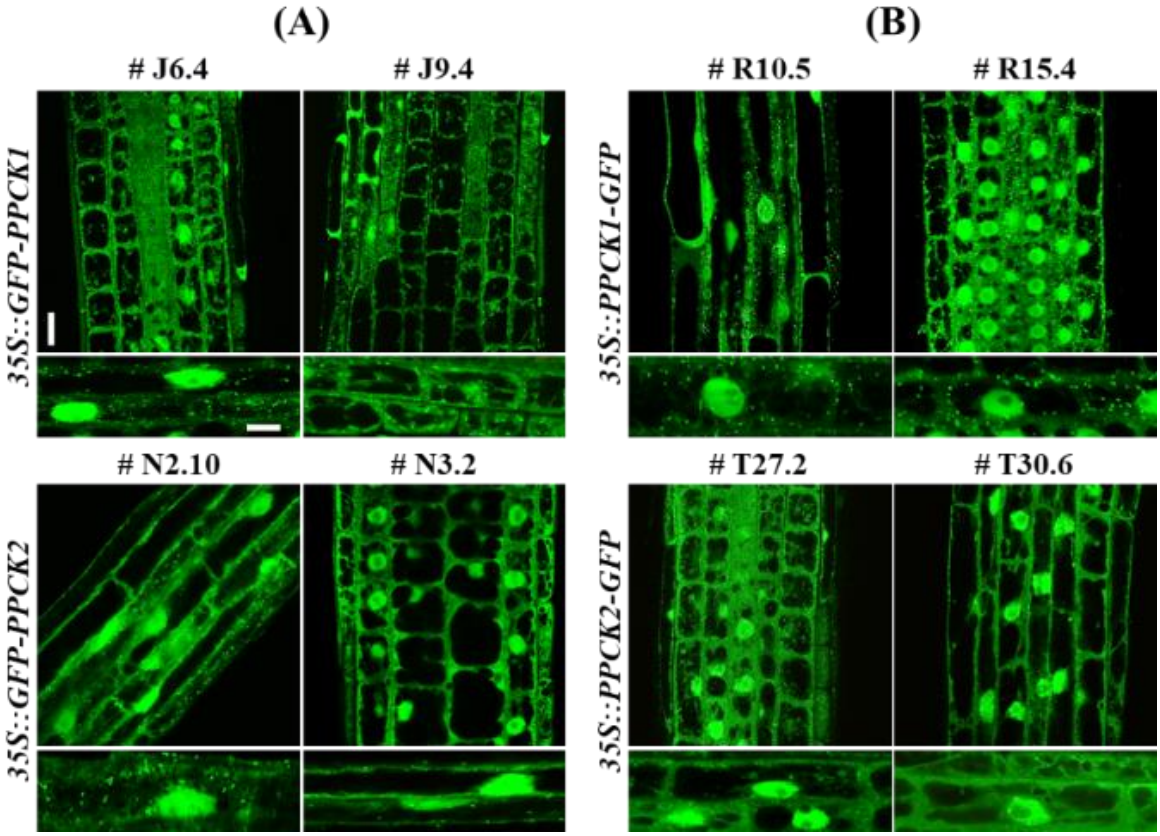

Figure 2-11: Subcellular localization of PPCK1 and PPCK2

Single optical section of roots showing localization of (A) N-terminally fused GFP and (B) C-terminally fused GFP to PPCK1 and PPCK2 in two independent transgenic lines. Lower panel for each transgenic line display an enlarged view of cells showing localization of PPCK1 and PPCK2 in cytoplasm, nucleus, and small moving dot-like structures. Images of 7 days old seedlings were taken. Scale bars represent 20 µm for overview and 10 µm for enlarged view.

2.2 Manipulation of PPC/PPCK pathway by misexpression of *PPCK*s

2.2.1 Modification of PPC/PPCK pathway by overexpression of *PPCK*s

The main objective of this research work was to determine whether the PPC/PPCK pathway could be manipulated in Arabidopsis and whether this manipulation can also lead to alteration in malate biosynthesis and exudation. In the present study, overexpression of *PPCK*s was considered rather than *PPC*s, because it has been suggested that overexpression of *PPC*s alone might not yield maximum malate levels since PPCs are strongly inhibited by malate unless they are phosphorylated. Therefore, it might be possible, that PPCKs can become rate limiting in *PPC* overexpressing plants, and that *PPCK* overexpression might further boost malate generation in *PPC* overexpressing plants. Since until now, no information is available on overexpression of *PPCK*s in Arabidopsis so far, it is not known to what extent altered *PPCK* levels per se actually modulates malate levels, i.e. whether or not PPCKs are rate-limiting at all. This the first report where efforts were made to manipulate malate biosynthesis by overexpression of *PPCK*s in Arabidopsis.

2.2.1.1 Characterization of transgenic lines overexpressing *PPCKs*

Stably transformed transgenic lines in the WT background were generated by introducing the coding sequence of PPCK1 and PPCK2 expressed under control of the *CaMV 35S* and of the *UBQ10* promoter. Plants transformed with *35S::PPCK1* and *UBQ10::PPCK1* construct were named as K and L-lines respectively. *PPCK1* mRNA abundance in K and L-lines was between 6-50 fold and 11-14 fold higher compared to WT seedlings, respectively [Supplementary Figure 7-11(A-B)]. Plants transformed with *35S::PPCK2* and *UBQ10::PPCK2* were denoted as O and P lines, respectively. There, *PPCK2* transcript levels were between 500-5500 fold and 5-700 fold higher compared to WT seedlings, respectively [Supplementary Figure 7-11(C-D)]. Since *PPCK1* and *PPCK2* overexpression worked both under *35S* and *UBQ10* promoter, only K and O-lines where coding sequence was expressed under the control of *35S* were taken for further characterization.

To elucidate whether Pi-starvation triggered induction in *PPCK1* and *PPCK2* transcript levels in roots could also be detected in K and O-lines, respectively, RT-qPCR analysis was performed [Figure 2-12]. The roots of Pi-sufficient K-lines exhibited between 6-22 fold higher *PPCK1* transcripts compared to WT roots. Increase in mRNA abundance after Pi-starvation was not detected in roots of K-lines [Figure 2-12(A)]. The transcript levels of *PPCK2* in roots of Pi-sufficient O-lines were between 170-1500 fold higher compared to the levels in WT roots. Pi-starvation triggered induction in *PPCK2* expression was detected in roots of only one (O2.1) out of three independent O-lines [Figure 2-12(B)].

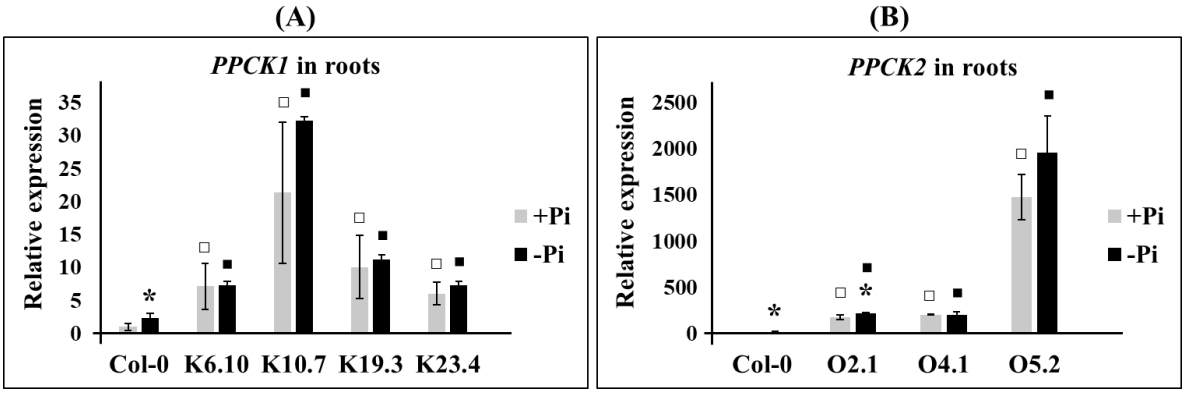

Figure 2-12: Expression analysis of *PPCK1* and *PPCK2* in roots of untagged overexpression lines grown under Pi-sufficient and Pi-deficient conditions by RT-qPCR

Transcript levels of (A) *PPCK1* in roots of *35S::PPCK1* lines (K-lines) and (B) *PPCK2* in roots of *35S::PPCK2* (O-lines). Seedlings were germinated for 6 days on +Pi agar plates, transferred to +Pi (500 µM) or –Pi (5 µM) conditions, and allowed to grow for additional 5 days before harvest. Error bars denote SD (n=3). Data from one representative out of two independent experiments are shown. Significance analyses were performed by Student's *t*-test (two-tailed, equal variances): *p ≤ 0.05, □p ≤ 0.05, and *p≤ 0.05 compared to +Pi condition, Col-0+Pi, and Col-0-Pi, respectively.

2.2.1.2 Growth analysis of transgenic lines overexpressing *PPCK1* and *PPCK2*

On agar plates, the seedling, shoot, and root fresh weight of 11-day old seedlings were determined to examine the effect of overexpression of *PPCK1* and *PPCK2* on the growth of K and O-lines, respectively, both under Pi-replete and Pi-depleted conditions [Supplementary Figure 7-12]. Under Pi-sufficient condition, three out of four independent K-lines (*PPCK1* overexpressor) exhibited between 1.2-1.4 fold higher seedling, shoot, and root fresh weight compared to fresh weight detected in WT. However, after Pi-starvation, seedling, shoot, and root fresh weight were similar to fresh weight in WT [Supplementary Figure 7-12(A): (a-c)]. All the three independent O-lines (*PPCK2* overexpressor) showed between 1.3-1.6 fold higher seedling and shoot fresh weight and between 1.2-1.4 fold higher root fresh weight compared to fresh weight detected in WT under Pi-sufficient conditions. However, no difference in fresh weight compared to WT seedlings was observed for two lines (O4.1 and O5.2) after Pi starvation. Only line O2.1 displayed an increase in seedling, shoot, and root fresh weight by 1.3, 1.2, and 1.4-fold, respectively, compared to WT after Pi-starvation [Supplementary Figure 7-12(B): (a-c)]. These results indicate that seedlings overexpressing *PPCK1* and *PPCK2* performed better with respect to seedling, shoot, and root fresh weight compared to WT on Pi-sufficient agar medium.

In order to elucidate whether K- (*PPCK1* overexpressor) and O-lines (*PPCK2* overexpressor) could also perform better when they are older and grown in soil, growth of these transgenic plants were monitored in the greenhouse. No obvious differences with respect to rosette appearance, number of leaves, flowering time, seed count, etc. were noticed in these plants compared to WT when grown in the greenhouse (results not shown). Plant growth was also monitored in phytochambers under more controlled growing conditions compared to the greenhouse. Rosette fresh weights of one-month old

plants were determined after separating the root system from it [Supplementary Figure 7-13]. Two out of four independent K-lines, K6.10 and K23.4 exhibited higher rosette fresh weight by around 1.4-fold compared to WT. Whereas in the other two K-lines (K10.7 and K19.3), the rosette fresh weight was similar to the WT plants. In only one out of three O-lines, O2.1 the rosette fresh weight was higher compared to WT plants by 1.3-fold. Interestingly, this is the same O-line which showed elevated fresh weights compared to WT plants under Pi-deficient condition on agar plates.

2.2.1.3 Malate and citrate content in transgenic lines overexpressing *PPCKs*

Transgenic lines overexpressing *PPCKs* should be able to phosphorylate their PPC targets more efficiently than untransformed plants [Figure 2-13]. Since phosphorylated PPCs are less sensitive to feedback inhibition by malate, more oxaloacetate should be produced in these lines. Oxaloacetate can be converted to malate in the cytosol by cytosolic MDH, or in the mitochondria by mitochondrial MDH. Oxaloacetate and/or malate in the mitochondria can enter the TCA cycle and can be converted to, among other TCA cycle intermediates to citrate. Therefore, both malate and citrate content were determined in the roots and shoots of transgenic plants overexpressing *PPCKs* [Figure 2-14].

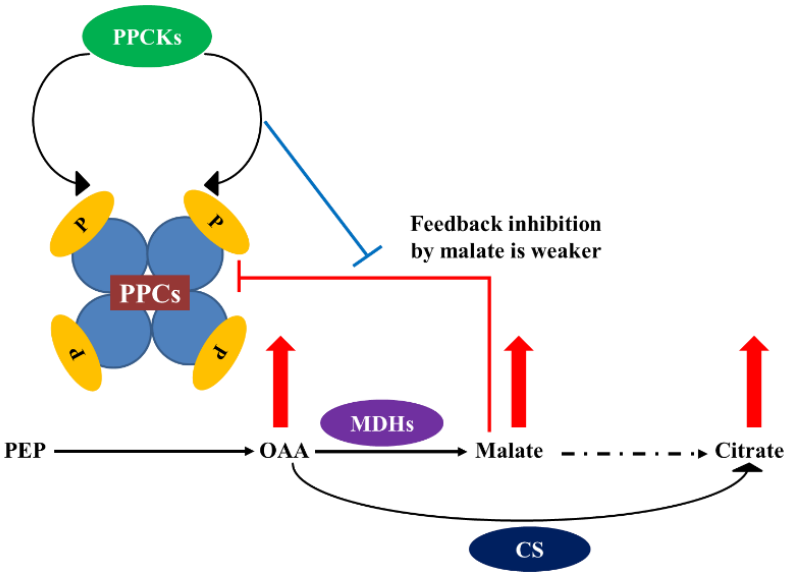

Figure 2-13: Model showing elevated generation of malate and citrate by overexpression of *PPCKs*

Overexpression of *PPCK*s should lead to more phosphorylation of PPCs. Phosphorylated PPCs are less sensitive to feedback inhibition by malate, as a result, more PEP should be converted to OAA which could subsequently lead to more malate and citrate generation. Red arrows indicate increased OAA, malate, and citrate levels. Blocked blue arrow indicates that phosphorylation of PPCs by PPCKs inhibit the feedback inhibition of PPCs by malate. Blocked red arrow indicates feedback inhibition by malate. The four blue spheres represent the subunits of plant-type PPCs.

Malate content in roots of all the four independent K-lines (*PPCK1* overexpressors; K6.10, K10.7, K19.3, and K23.4) were between 1.4 and 1.5-fold higher compared to untransformed WT plants under Pi-sufficient condition. Similarly, all the Pi-replete O-lines (*PPCK2* overexpressors; O2.1, O4.1, and O5.2) also exhibited between 1.2 and 1.7-fold higher malate content in roots compared to WT roots. In Pi

deprived conditions, however, root malate content was indistinguishable between the overexpression lines and WT plants except for O5.2 which showed 1.5-fold higher malate content [Figure 2-14(A-B)]. Although Pi-starvation triggered induction of root malate content was detected only in K10.7 (p=0.01) and K23.4 (p=0.04), this response (+Pi/-Pi in K-lines *Vs* +Pi/-Pi in WT) in all the K-lines was similar to WT response (two way ANOVA: p≥0.05). Similarly, although in two independent O-lines- O2.1 and O5.2, Pi-deficiency triggered induction in root malate content was present (p=0.003 for O2.1 and p=0.03 for O5.2), this response was similar to WT response in all these O-lines (two way ANOVA: p≥0.05). Malate content in shoots of K and O-lines was similar to untransformed WT both under Pi-replete and Pi-deplete conditions [Figure 2-14(C-D)]. Pi-starvation triggered induction in shoot malate content was detected in both K and O-lines as detected in WT shoots (two way ANOVA: p≥ 0.05).

Citrate content in Pi-sufficient roots of all the independent K-lines (*PPCK1* overexpressors) were between 1.4 and 1.6-fold higher compared to the levels detected in WT roots. However, citrate content was unaltered in roots of Pi-sufficient O-lines (*PPCK2* overexpressors). Pi-deficiency triggered slight induction in root citrate content observed in WT (p=0.03), was not detected in K and O-lines. Citrate content in roots of Pi-deficient K and O-lines was not statistically different from WT roots [Figure 2-14(E-F)]. In shoots under Pi-sufficient condition, citrate content was unaltered in all the K-lines and two independent O-lines (O2.1 and O4.1). Only line O5.2 exhibited reduced shoot citrate levels compared to WT levels. Around 1.4-fold increase in shoot citrate content was detected in Pi-depleted K-lines compared to WT shoots, whereas the citrate content in shoots of O-lines, was similar to WT. As seen for WT, Pi-deficiency triggered induction in shoot citrate content was also detected in both K and O-lines [Figure 2-14(G-H)]. However, this response was stronger in K-lines (two way ANOVA: p≤ 0.005) due to their increased citrate content after Pi-starvation and was similar to WT response in O-lines (two way ANOVA: p≥0.05).

2.2.1.4 Malate and citrate exudation in transgenic lines overexpressing *PPCKs*

In order to investigate whether overexpression of *PPCK*s can also lead to alteration in malate and citrate exudation, root exudation analysis was performed [Figure 2-15]. When grown in Pi-sufficient conditions, malate exudation was between 2 and 3-fold higher in all the independent K-lines, and O-lines compared to WT. Upon Pi-deficiency, K-lines (except K19.3) exhibited between 1.4 and 1.7-fold higher malate content in root exudates compared to WT [Figure 2-15(A)]. Similarly, malate content in root exudates of Pi-deficient O-lines was between 1.8 and 2.3-fold higher than WT [Figure 2-15(B)]. Pi-deficiency triggered induction in malate exudation was present in both K (except K19.3) and O-lines (except O5.2), and this response was similar to WT response in all the lines (two way ANOVA: p≥0.05), except O2.1 (two way ANOVA: p=0.04).

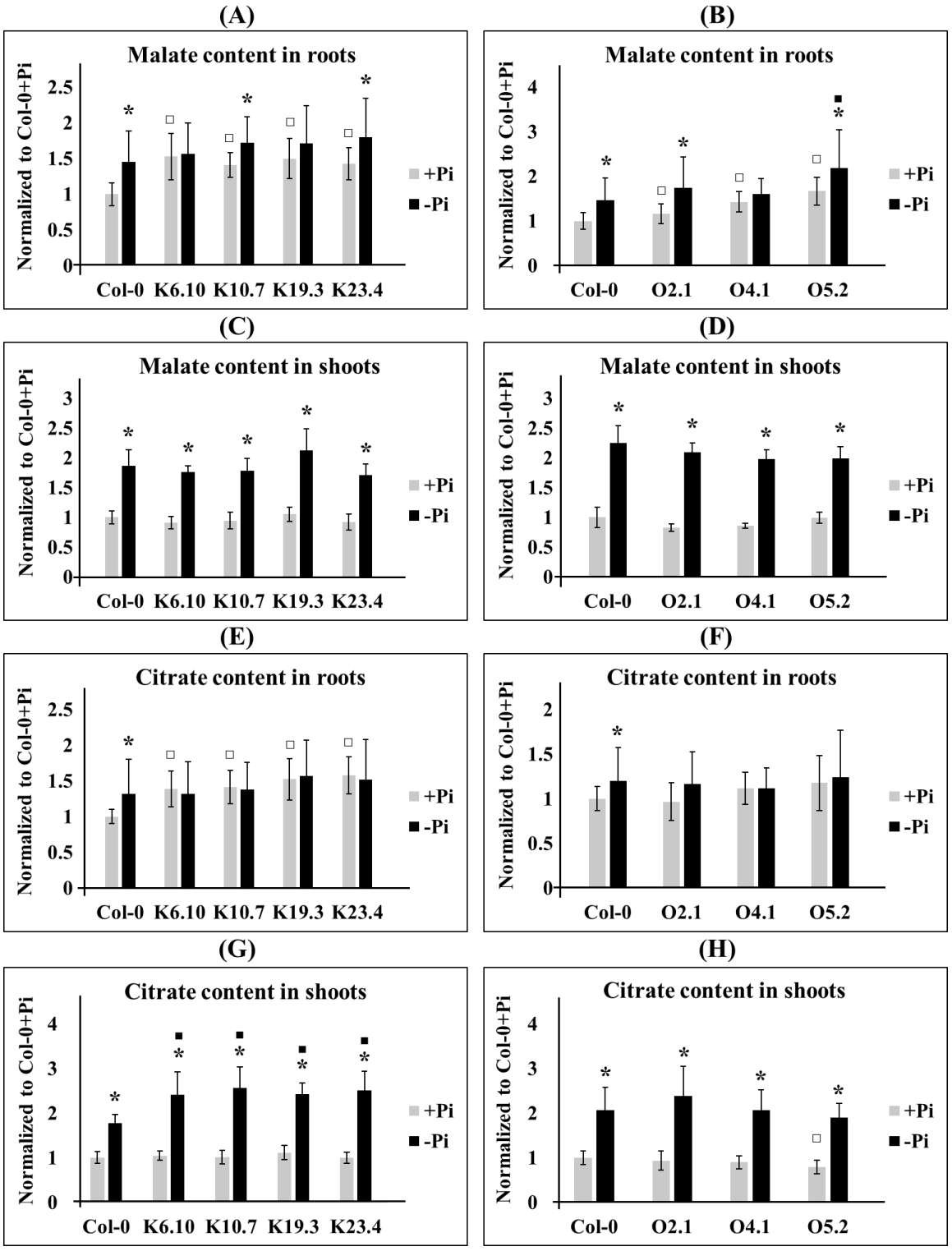

Figure 2-14: Normalized content of malate and citrate in transgenic lines overexpressing *PPCK1* and *PPCK2*

Normalized (A) root malate content in *35S::PPCK1*, (B) root malate content in *35S::PPCK2*, (C) shoot malate content in *35S::PPCK1*, (D) shoot malate content in *35S::PPCK2*, (E) root citrate content in *35S::PPCK1*, (F) root citrate content in *35S::PPCK2*, (G) shoot citrate content in *35S::PPCK1*, and (H) shoot citrate content in *35S::PPCK2* lines grown under Pi-sufficient and Pi-deficient conditions. Seedlings were germinated for 6 days on +Pi agar plates, transferred to +Pi (500 µM) or –Pi (5 µM) conditions, and allowed to grow for additional 5 days before harvest. Data are normalized to the levels detected in Col-0+Pi. Shown are the cumulative data of four independent germination experiments. For each experiment, four biological replicates (two pooled seedlings per replicate) were analyzed. Error bars denote SD (n=16 total biological replicates). Significance analyses were performed by Student's *t*-test (two-tailed, equal variances): *p ≤ 0.05; □p ≤ 0.05; and ▪p ≤ 0.05 compared to +Pi, Col-0+Pi, and Col-0-Pi, respectively.

The data regarding citrate exudation of K-lines growing under Pi-sufficient condition were inconsistent between the lines. Two K-lines (K10.7 and K23.4) exhibited around 1.65-fold higher citrate content in root exudates, and the other two lines (K6.10 and K19.3) showed citrate levels similar to that detected in WT [Figure 2-15(C)]. Citrate content in root exudates of all Pi-replete O-lines was between 1.4 and 1.7-fold higher than WT. In root exudates of Pi-depleted K (except K10.7) and O-lines, citrate content was similar to WT [Figure 2-15(D)]. There was no difference between +Pi and –Pi treatment with respect to citrate exudation in K and O-lines.

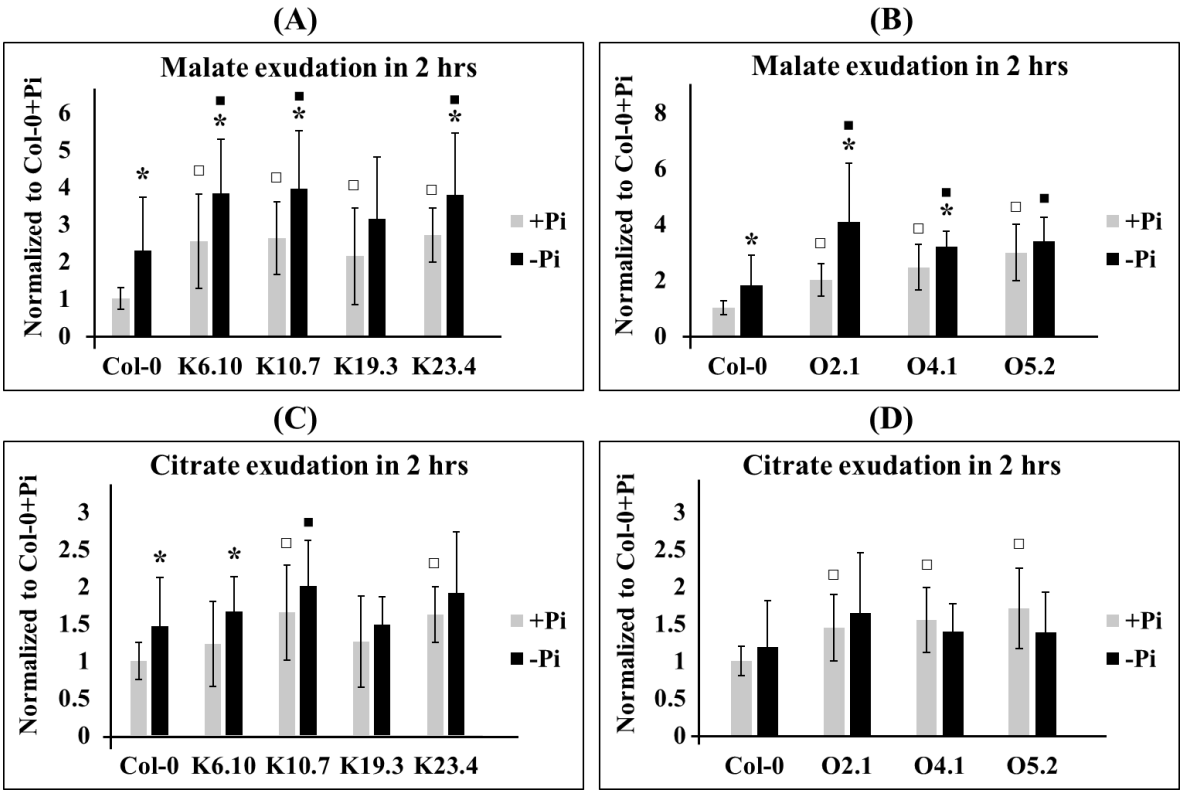

Figure 2-15: Normalized content of malate and citrate in root exudates of plants overexpressing *PPCK*s

Normalized content of malate in exudates of (A) *35S::PPCK1* and B) *35S::PPCK2* lines and citrate in exudates of C) *35S::PPCK1* and D) *35S::PPCK2* lines grown under Pi-sufficient and Pi-deficient conditions. Seedlings were germinated for 6 days on +Pi agar plates, transferred to +Pi (500 µM) or –Pi (5 µM) conditions, and allowed to grow for additional 4 days. Subsequently, the root systems of three intact seedlings were incubated in 300 µl water, and exudates were collected after 2 h. Data are normalized to the levels observed in Col-0+Pi. Shown are the cumulative data of four independent germination experiments. For each experiment, four biological replicates (the exudates of three pooled root systems per replicate) were analyzed. Error bars denote SD (n=16). Significance analyses were performed by Student's *t*-test (two-tailed, equal variances): *p ≤ 0.05; □p ≤ 0.05; and ▪p ≤ 0.05 compared to +Pi, Col-0+Pi, and Col-0-Pi, respectively.

2.2.2 Modification of PPC/PPCK pathway by downregulation of *PPCK1*

Alteration in biosynthesis and exudation of malate and citrate were achieved by generating plants overexpressing *PPCKs*. In order to substantiate that these effects are specific to *PPCK1* and *PPCK2* overexpression, respective mutants with aberrant expression of *PPCK1* and *PPCK2* were analyzed. Three independent T-DNA insertion lines GK_614F02_021894, SAIL_30_D02, and SALK_116510 (Feria

et al., 2016) for *PPCK1* were available at the beginning of this project and are referred to as *ppck1-1*, *ppck1-2*, and *ppck1-3,* respectively. The position of the T-DNA insertion in *ppck1-1*, *ppck1-2*, and *ppck1-3* is in the intron, second exon, and 3'-UTR of *PPCK1*, respectively [Figure 2-16(A)]. Semiquantitative RT-PCR analysis of *ppck1-1* with primers flanking the T-DNA insertion site revealed complete absence of *PPCK1* transcripts when compared to WT, revealing that the T-DNA insertion line is a null mutant allele [Figure 2-16(B)], whereas RT-qPCR analysis with primers binding at the 3'-UTR revealed 45-fold reduced *PPCK1* transcripts in *ppck1-1* [Figure 2-16(C)]. The *ppck1-2* line is in the Col-3 background, which could not be genotyped even after repeated attempts. The RT-qPCR analysis revealed similar transcript levels in *ppck1-3* and WT seedlings [Figure 2-16(D)]. Therefore, *ppck1-1* line (GK_614F02_021894) was analyzed in further experiments.

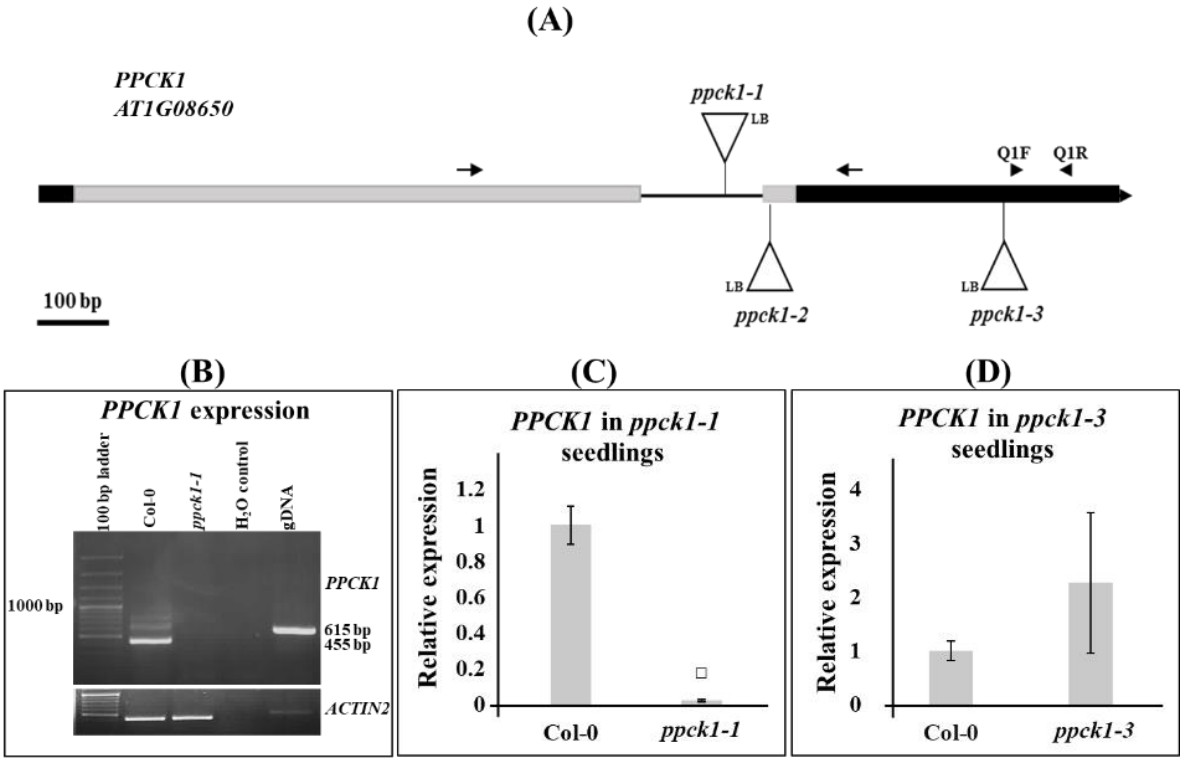

Figure 2-16: Characterization of T-DNA insertion mutants of *PPCK1*

(A) Gene model and position of T-DNA insertions in three independent lines, *ppck1-1*, *ppck1-2*, and *ppck1-3.* Black boxes indicate the 5'-UTR and 3'-UTR and light grey boxes indicate the exons. Intron is represented by the black line. The positions of the T-DNA insertion are indicated with triangles. Larger and smaller arrows indicate the position of primers used for amplification of *PPCK1* transcripts for semi-quantitative RT-PCR and RT-qPCR analysis, respectively. (B) Semi quantitative RT-PCR analysis revealed complete absence of *PPCK1* transcripts in *ppck1-1* seedlings. *ACTIN2* was included as a control for cDNA integrity. Genomic DNA (gDNA) was used for checking DNA contamination in cDNA samples. (C, D) *PPCK1* transcript levels in *ppck1-1 and ppck1-3* lines compared with the WT (Col-0) levels by RT-qPCR analysis. Total RNA was extracted from 7 days old seedlings. *PP2A* was used as a reference gene and relative expression levels were normalized to the levels in WT (Col-0). Error bars denote SD (n=3 total biological replicates). Data from one representative out of three independent experiments are shown. Significance analyses were performed by Student's *t*-test (two-tailed, equal variances): □p ≤ 0.05 compared to WT (Col-0).

Four independent T-DNA insertion lines SALK_102132 (Feria et al., 2016), SALK_023356, GK_196F01_014717, and SAILseq_210_F08 obtained for *PPCK2* are referred to as *ppck2-1*, *ppck2-2*, *ppck2-3*, and *ppck2-4*, respectively. The position of the T-DNA insertion in all these lines, except *ppck2-4*, is in the 5'-UTR, whereas for *ppck2-4*, it is in the second exon [Figure 2-17(A)]. Out of these four, only two lines- *ppck2-1*, and *ppck2-3* could be successfully genotyped. RT-qPCR analysis of *ppck2-1* and *ppck2-3* revealed 10 and 35-fold higher *PPCK2* transcript levels, respectively, compared to the levels in WT seedlings [Figure 2-17(B-C)]. Thus, T-DNA insertion lines for *PPCK2* having either knock-down or knock-out effect could not be obtained.

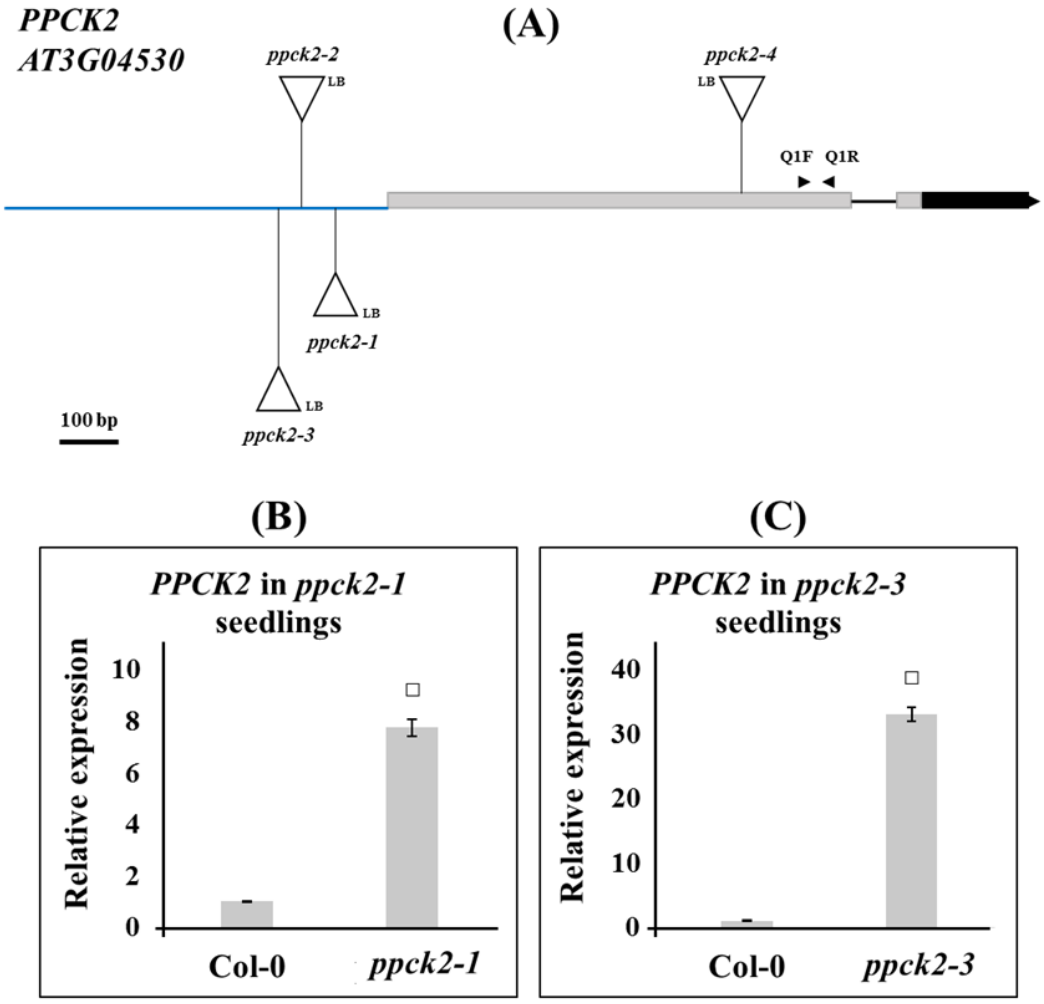

Figure 2-17: Characterization of T-DNA insertion mutants of *PPCK2*

(A) Gene model and position of T-DNA insertion in four independent lines, *ppck2-1*, *ppck2-2*, *ppck2-3,* and *ppck2-4.* Grey boxes indicate the exons and black box indicates the 3'-UTR. Intron is represented by the black line and the region above the first exon is indicated by a blue line. Position of the T-DNA insertion is indicated with triangles. Arrows indicate the position of primers used for amplification of *PPCK2* transcripts for RT-qPCR analysis. (B, C)) *PPCK2* transcript levels in *ppck2-1 and ppck2-3* lines compared with the WT (Col-0) levels by RT-qPCR analysis. Total RNA was extracted from 7 days old seedlings. *PP2A* was used as a reference gene and relative expression levels were normalized to the levels in WT (Col-0). Error bars denote SD (n=3 biological replicates). Data from one representative out of three independent experiments are shown. Significance analyses were performed by Student's *t*-test (two-tailed, equal variances): □p ≤ 0.05.

2.2.2.1 Malate and citrate content in *ppck1-1* line

Due to the absence of functional PPCK1 in *ppck1-1* plants, its PPC targets should be less phosphorylated. Since PPCs in their de-phosphorylated forms are more strongly inhibited by malate, biosynthesis of oxaloacetate, and also malate or citrate by PPC/PPCK mediated pathway should be reduced in *ppck1-1* plants [Figure 2-18].

Malate content in roots of Pi-sufficient and Pi-deficient *ppck1-1* seedlings were around 2-fold lower when compared to WT roots. Pi-deficiency triggered induction in root malate content was detected in *ppck1-1* and the response was weaker than WT response (two-way ANOVA: $p=4.96e^{-06}$) [Figure 2-19(A)]. In shoots of *ppck1-1* seedlings around 1.3-fold reduced malate content was detected both under Pi-replete and Pi-depleted condition compared to WT shoots. Although Pi-deficiency induced malate accumulation was detected in shoots of *ppck1-1* seedlings, the response was significantly lower from that detected in WT shoots (two-way ANOVA: p=0.002) [Figure 2-19(B)].

Citrate content in roots of Pi-sufficient and Pi-deficient *ppck1-1* seedlings was reduced by 1.5-fold and 1.9-fold, respectively when compared to WT roots. Induction in citrate levels could not be detected in *ppck1-1* roots after Pi-starvation unlike in WT roots (two-way ANOVA: $p=3.48e^{-04}$) [Figure 2-19(C)]. Citrate content was reduced in *ppck1-1* shoots only under Pi-replete condition by 1.2-fold, but not under Pi-deplete condition compared to WT shoots. Pi-starvation triggered induction in citrate content was detected in shoots of *ppck1-1* seedlings and the response was similar to WT shoots (two-way ANOVA: p=0.3) [Figure 2-19(D)].

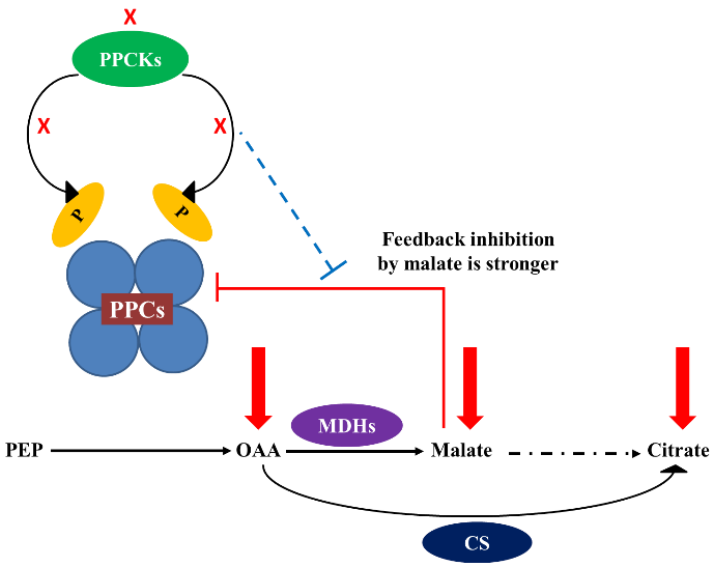

Figure 2-18: Model showing reduced generation of malate and citrate in plants due to absence of *PPCK1*
In *ppck1-1* plants, PPCs should be less phosphorylated. Since de-phosphorylated PPCs are strongly inhibited by malate, conversion of PEP to OAA should be reduced. Subsequently, conversion of OAA by MDHs to malate or to citrate by CS should also be reduced. Red arrows indicate reduced OAA, malate, and citrate levels. Blocked red arrow indicates feedback inhibition by malate which is blocked if PPCs are phosphorylated by PPCKs indicated by dashed blue arrows. Red cross marks indicate absence of PPC phosphorylation by PPCKs. The four blue spheres represent the subunits of PPCs.

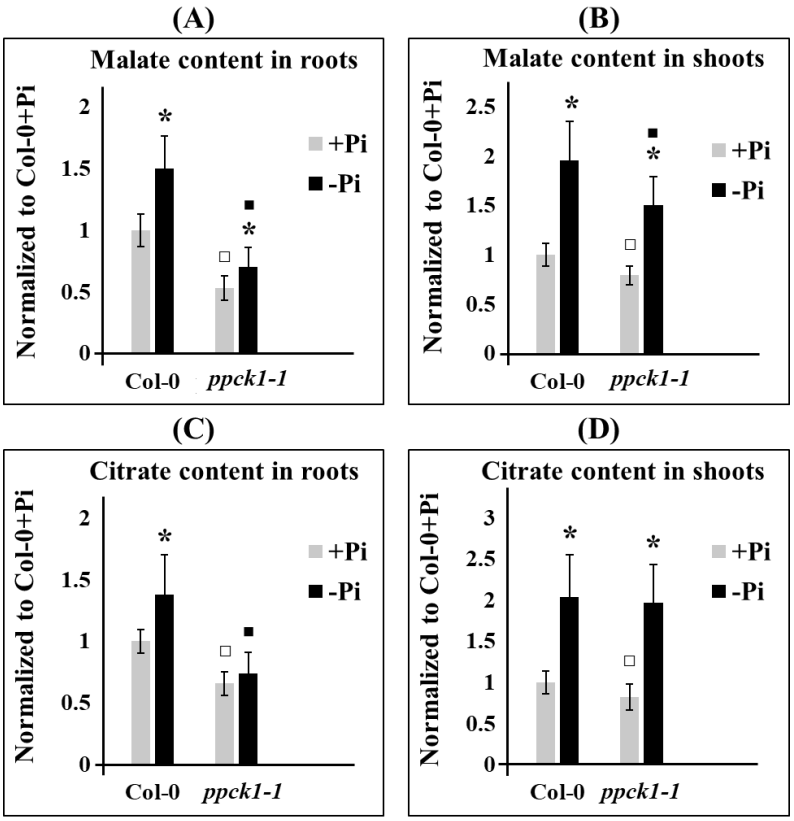

Figure 2-19: Normalized content of malate and citrate in *ppck1-1* compared to WT seedlings

Normalized content of (A) malate in roots, (B) malate in shoots, (C) citrate in roots, and (D) citrate in shoots of *ppck1-1* seedlings grown under Pi-sufficient and Pi-deficient conditions. Seedlings were germinated for 6 days on +Pi agar plates, transferred to +Pi (500 µM) or –Pi (5 µM) conditions, and allowed to grow for additional 5 days before harvest. Data are normalized to the levels detected in Col-0+Pi. Shown are the cumulative data of 7 independent germination experiments. For each experiment, four biological replicates (two pooled seedlings per replicate) were analyzed. Error bars denote SD (n=28 total biological replicates). Significance analyses were performed by Student's *t*-test (two-tailed, equal variances): *p ≤ 0.05, □p ≤ 0.05, and ▪p≤ 0.05 compared to +Pi condition, Col-0+Pi, and Col-0-Pi, respectively.

2.2.2.2 Phenotypic analysis of *ppck1-1* line

Fresh weight analysis

Seedling, shoot, and root fresh weights were analyzed for *ppck1-1* plants to examine the effect of the absence of functional *PPCK1* in Arabidopsis both under Pi-replete and Pi-depleted condition [Supplementary Figure 7-14]. The Pi-sufficient *ppck1-1* seedlings exhibited a slight but significant decrease in seedling, shoot, and root fresh weight by 1.1, 1.1, and 1.2-fold, respectively, compared to WT. In Pi-starved *ppck1-1* seedlings, around 1.5, 1.3, and 1.9-fold reduction in seedling, shoot, and root fresh weights were observed compared to WT seedlings, respectively [Supplementary Figure 7-14(A-C)]. The Pi-deficiency response with respect to reduction in seedling, and shoot fresh weight was similar between *ppck1-1* and WT (two way ANOVA: p≥0.05), whereas reduction in root fresh weight was stronger in *ppck1-1* than in WT plants (two way ANOVA: $p=1.36e^{-04}$). Growth of *ppck1-1* plants was also monitored in the greenhouse and phytochamber to analyze whether the slight decreases observed in fresh weight of *ppck1-1* seedlings on agar plates could also be detected when

they are older and grown in soil. No obvious morphological differences could be detected in *ppck1-1* plants when grown in the greenhouse (results not shown).The rosette fresh weight of one-month old *ppck1-1* plants grown in phytochambers was similar to WT plants [Supplementary Figure 7-15]. Thus, although *ppck1-1* seedlings showed slightly reduced growth on agar plates, no differences to WT plants could be detected when they were older and grown in soil.

Root length analysis

Malate was shown to be crucial for mediating Pi-deficiency induced primary root growth inhibition (local response) in Arabidopsis (Balzergue et al., 2017). To determine whether decreased malate content in *ppck1-1* plants also has an effect on the local response, root lengths of *ppck1-1* seedlings were recorded [Figure 2-20]. There was no difference in primary root length between Pi-sufficient *ppck1-1* and WT. However, *ppck1-1* line exhibited shorter primary roots compared to WT after Pi-starvation by around 2-fold. The Pi-deficiency induced primary root length inhibition response was stronger in *ppck1-1* line than WT (two-way ANOVA: $p=2.56e^{-11}$). Root-tip morphology of Pi-starved *ppck1-1* line was also found to be severely affected compared to WT seedlings [Figure 2-21].

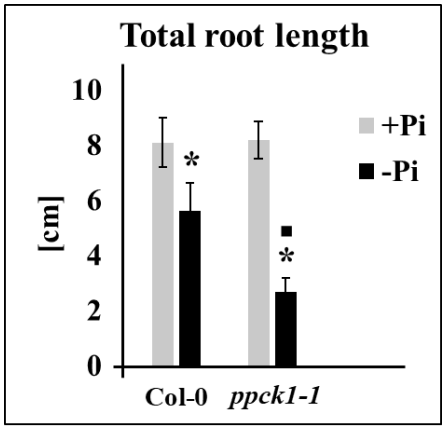

Figure 2-20: Comparison of total root length between *ppck1-1* and WT seedlings

Seedlings were germinated for 6 days on +Pi agar plates, transferred to +Pi (500 µM) or –Pi (5 µM) conditions, and allowed to grow for additional 9 days before root length measurement. Data from one representative out of three independent experiments are shown. Error bars denote SD (n=25). Significance analyses were performed by Student's *t*-test (two-tailed, equal variances): *p≤0.05, □p≤0.05, and ▪p≤0.05 compared to +Pi condition, Col-0+Pi, and Col-0-Pi, respectively.

Iron and Callose staining

Hypersensitive root growth response after Pi-starvation is correlated with increased iron accumulation and callose deposition in Arabidopsis roots (Müller et al., 2015). In order to determine whether *ppck1-1* seedlings also accumulate more iron and callose after Pi-deficiency treatment, iron and callose stainings were performed. Elevated apoplastic iron was detected in the mature regions of *ppck1-1* roots compared to WT [Supplementary Figure 7-16(A)]. Accumulation of callose was also higher in the transition zone, elongation zone, and mature regions of *ppck1-1* roots compared to WT

[Supplementary Figure 7-16(B)]. Thus, *ppck1-1* showed all signs of hypersensitivity with respect to the local Pi deficiency response. Considering that *PPCK1* expression is under control of the systemic Pi starvation response, it was surprising that downregulation of this gene exhibited such a strong effect on Pi-deficiency induced root growth inhibition in Arabidopsis.

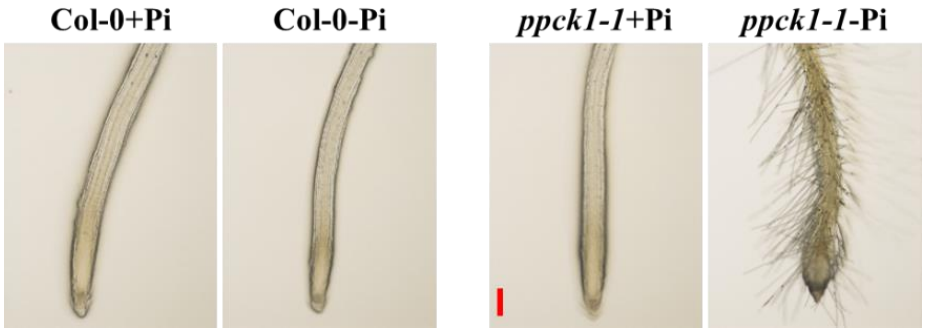

Figure 2-21: Comparison of root-tip morphology between Pi-starved *ppck1-1* and WT seedlings

Seedlings were germinated for 6 days on +Pi agar plates, transferred to +Pi (500 µM) or –Pi (5 µM) conditions, and allowed to grow for additional 4 days before imaging. Images were taken with Nikon SMZ1270 microscope. Representative image from one out of three independent experiments are shown. Scale bars represent 0.2 mm.

2.2.2.3 Malate and citrate exudation in *ppck1-1* line

Inhibition of primary root growth during Pi-starvation is linked to increased malate exudation in Arabidopsis (Balzergue et al., 2017). Since *ppck1-1* seedlings exhibited lower endogenous malate content, reduced malate exudation was expected. Therefore, it was unexpected to observe hypersensitive root growth response in *ppck1-1* seedlings after Pi-starvation. To identify the reason for this observed discrepancy, malate content in root exudates of *ppck1-1* plants was determined [Figure 2-22(A)]. Malate content in root exudates of Pi-replete *ppck1-1* seedlings was similar to that detected in WT. Surprisingly, about 2 fold increased malate exudation was detected from roots of Pi-starved *ppck1-1* seedlings compared to WT. Also, Pi-deficiency triggered induction in malate exudation was stronger in *ppck1-1* than in WT seedlings (two-way ANOVA: $p=7.31e^{-09}$).

To investigate whether the observed hypersensitivity in *ppck1-1* seedlings is specific to increased malate content in exudates and not to citrate, citrate content was also analyzed in root exudates of *ppck1-1* seedlings [Figure 2-22(B)]. Unlike malate, the citrate content in root exudates of *ppck1-1* seedlings was significantly reduced by 1.9-fold and 1.2-fold under Pi-sufficient and Pi-deficient conditions compared to WT, respectively. This corroborates the lower endogenous citrate content in *ppck1-1* seedlings. Thus, hypersensitivity in Pi starvation induced root growth inhibition can be correlated with higher malate exudation in *ppck1-1* seedlings. However, higher malate exudation of *ppck1-1* lines was surprising considering that they are expected to be impaired in malate generation and consequently also showed reduced endogenous malate content.

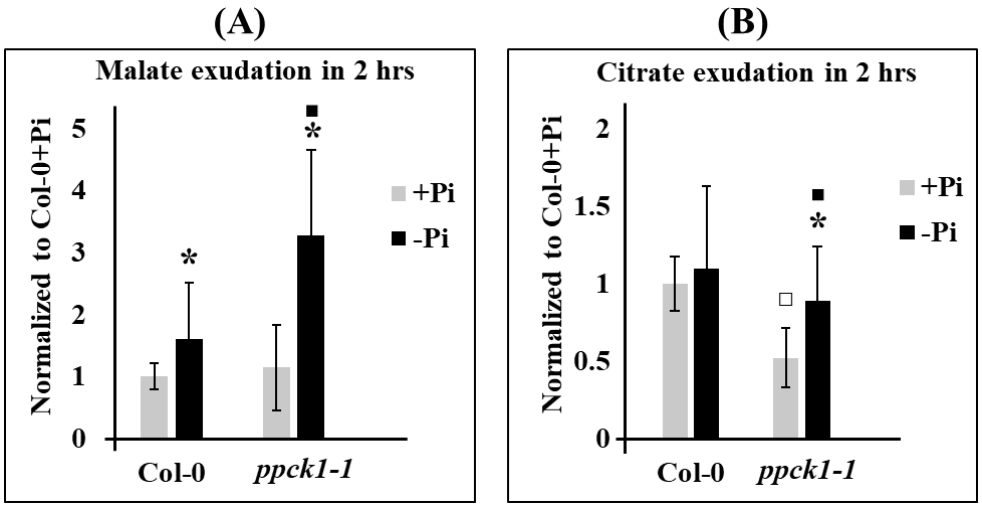

Figure 2-22: Normalized content of malate and citrate in root exudates of *ppck1-1* line compared to WT

Normalized content of (A) malate and (B) citrate in root exudates of *ppck1-1* seedlings grown under Pi-sufficient and Pi-deficient conditions. Seedlings were germinated for 6 days on +Pi agar plates, transferred to +Pi (500 µM) or –Pi (5 µM) conditions, and allowed to grow for additional 4 days. Subsequently, the root systems of three intact seedlings were incubated in 300 µl water, and exudates were collected after 2 h. Data are normalized to the levels detected in Col-0+Pi. Shown are the cumulative data of 15 independent germination experiments. For each experiment, four biological replicates (the exudates of three pooled root systems per replicate) were analyzed. Error bars denote SD (n=60 biological replicates). Significance analyses were performed by Student's *t*-test (two-tailed, equal variances): *p ≤ 0.05, □p ≤ 0.05, and •p≤ 0.05 compared to +Pi condition, Col-0+Pi, and Col-0-Pi, respectively.

2.2.2.4 Hypersensitive root growth response of *ppck1-1* line and *ALMT1* overexpressor after Pi-starvation

Hypersensitive root growth response of *ppck1-1* plants after Pi-starvation as revealed by their reduced primary root growth and severely affected primary root-tips are reminiscent of *ALMT1* overexpression. Knock-out and overexpression lines of *ALMT1* (named as *almt1* and *ALMT1^{OE}*, respectively) in Arabidopsis have been reported to show insensitive and hypersensitive root growth response during Pi-starvation, respectively (Balzergue et al., 2017; unpublished data from our group). Although, *almt1* and *ALMT1^{OE}* lines were analyzed phenotypically after Pi-starvation, malate exudation was not determined in these lines. To identify whether effects on root length are also reflected by differences in malate exudation during Pi-starvation, malate content in root exudates of *almt1* (SALK_009629) and *ALMT1^{OE}* (*35S::ALMT1*; obtained from Kobayashi et al., 2013) was determined [Figure 2-23(A)].

No difference in malate exudation was detected between *almt1* and WT seedlings either in Pi-sufficient or Pi-deficient condition. This could be due to the functional redundancy of ALMT1 with other members of ALMT protein family. Therefore, the ALMT1 mediated malate exudation could easily be masked by other malate transporters or channels distributed over the entire root system. In contrast, malate exudation was elevated by 1.5-fold and 2-fold in *ALMT1^{OE}* compared to WT seedlings under Pi-replete and Pi-depleted conditions, respectively [Figure 2-23(A)]. Pi-starvation triggered

induction in malate exudation was stronger in *ALMT1*^{OE} compared to WT (Two-way ANOVA: p=0.002). These effects were specific for malate since citrate content in root exudates of Pi-starved *almt1* and *ALMT1*^{OE} were similar to WT seedlings. Citrate content in root exudates of *almt1* and *ALMT1*^{OE} was 1.2-fold lower and similar to WT seedlings, respectively under Pi-sufficient condition. [Figure 2-23(B)]. Thus, hypersensitive root growth response in *ALMT1* overexpressor can be correlated to its elevated malate exudation during Pi-starvation. These effects are similar to the observed effects in *ppck1-1* which also shows increased malate exudation and hypersensitive root growth during low Pi stress.

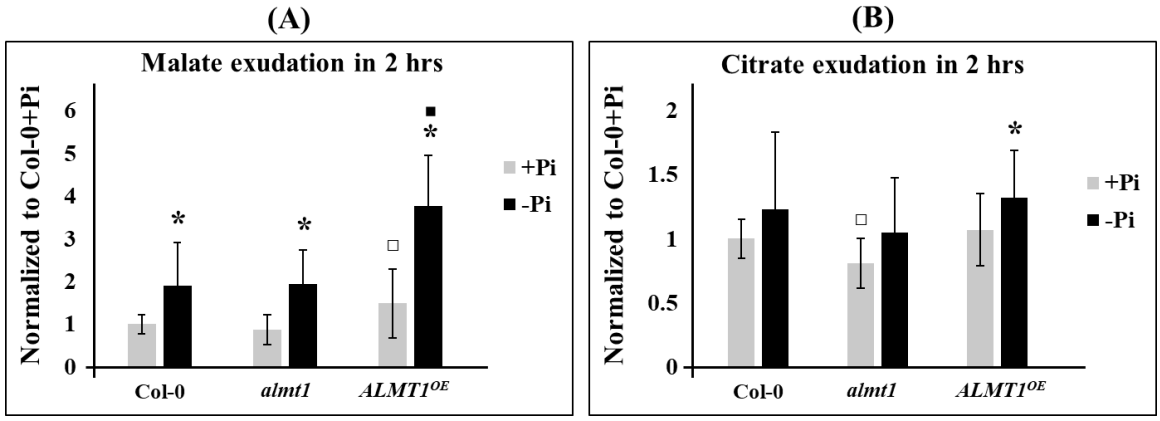

Figure 2-23: Normalized malate and citrate content in root exudates of *almt1* and *ALMT1*^{OE} compared to WT

Normalized content of (A) malate and (B) citrate in root exudates of *almt1* and *ALMT1*^{OE} compared to WT (Col-0) when grown under Pi-sufficient and Pi-deficient conditions. Seedlings were germinated for 6 days on +Pi agar plates, transferred to +Pi (500 µM) or –Pi (5 µM) conditions, and allowed to grow for additional 4 days. Subsequently, the root systems of three intact seedlings were incubated in 300 µl water, and exudates were collected after 2 h. Data are normalized to the levels detected in Col-0+Pi. Shown are the cumulative data of 5 independent germination experiments. For each experiment, four biological replicates (the exudates of three pooled root systems per replicate) were analyzed. Error bars denote SD (n=20 total biological replicates). Significance analyses were performed by Student's *t*-test (two-tailed, equal variances): *p ≤ 0.05, □p ≤ 0.05, and ▪p≤ 0.05 compared to +Pi condition, Col-0+Pi, and Col-0-Pi, respectively.

2.2.2.5 Malate and citrate content in *almt1* and *ALMT1*^{OE}

In order to elucidate the effect of altered malate exudation in *ALMT1*^{OE} and the absence of functional *ALMT1* in *almt1* plants on endogenous metabolite levels, malate and citrate content were determined in roots and shoots of these plants [Supplementary Figure 7-17].

Malate content in roots of *almt1* and *ALMT1*^{OE} was similar to WT roots both under Pi-sufficient and Pi-deficient condition [Supplementary Figure 7-17(A)]. However, in shoots, it was slightly but significantly reduced by 1.1-fold in both *almt1* and *ALMT1*^{OE}. This reduction was only detectable when plants were grown in Pi-sufficient condition, whereas growth in Pi-depleted condition resulted in unchanged or even 1.3-fold higher malate content compared to WT in shoots of *almt1* and *ALMT1*^{OE}, respectively. Additionally, Pi-deficiency triggered stronger malate accumulation in shoots of *ALMT1*^{OE} compared to WT shoots (two way ANOVA: p=0.002) [Supplementary Figure 7-17(B)].

Compared to WT, root citrate content was only affected in *ALMT1*^{OE} grown in Pi-deficient condition (1.4 fold reduction) [Supplementary Figure 7-17(C)]. In Pi replete shoots, citrate content was slightly but significantly reduced by 1.2-fold in both *almt1* and *ALMT1*^{OE} compared to WT shoots. The *almt1* seedlings exhibited similar shoot citrate content, but *ALMT1*^{OE} showed reduced citrate content by 1.2-fold compared to WT shoots under Pi-deficient condition. However, the Pi-deficiency triggered citrate accumulation response in shoots of *almt1* and *ALMT1*^{OE} line was similar to WT response (two way ANOVA: p≥0.05) [Supplementary Figure 7-17(D)].

2.2.2.6 Expression analysis of *ALMT1* in roots of *ppck1-1* line

The similarity between *ppck1-1* seedlings and *ALMT1*^{OE} with respect to Pi deficiency-induced hypersensitive root growth inhibition and increased malate exudation suggested to analyze *ALMT1* expression in *ppck1-1* roots [Figure 2-24(A)]. *ALMT1* mRNA levels in roots of Pi-sufficient and Pi-deficient *ppck1-1* seedlings were 2.3-fold and 4.5-fold higher compared to WT seedlings. Moreover, Pi-deficiency triggered stronger accumulation of *ALMT1* transcript levels in roots of *ppck1-1* compared to WT roots (two-way ANOVA: p=3.1e^{-06}).

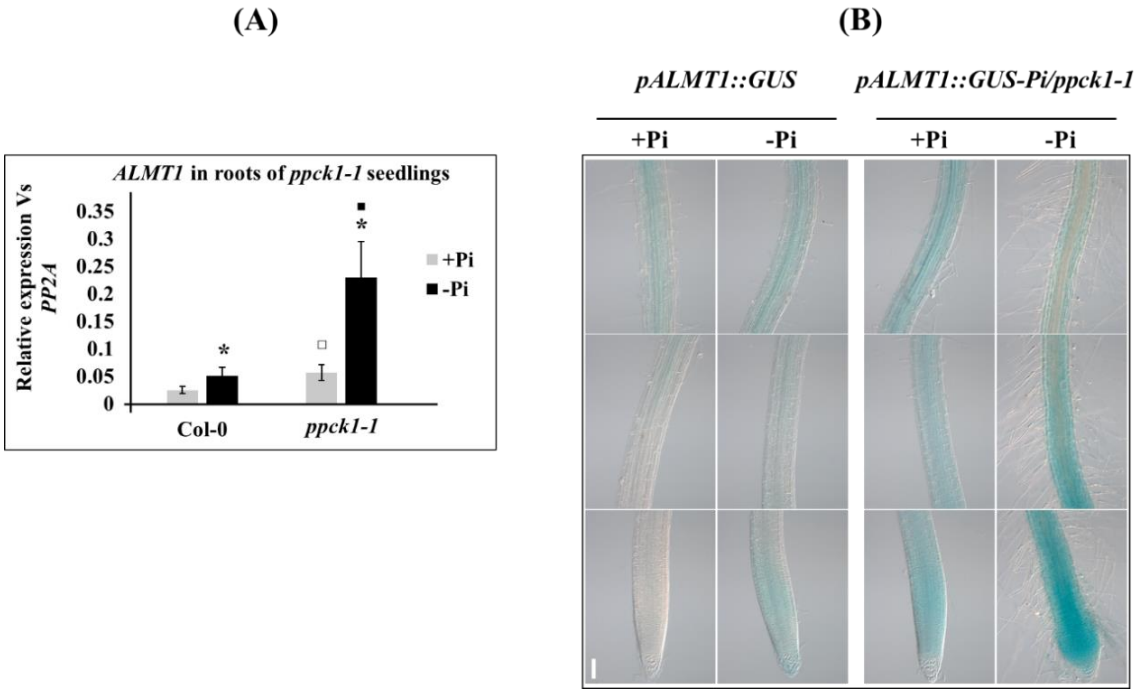

Figure 2-24: Expression analysis of *ALMT1* in roots of *ppck1-1* seedlings

(A) Comparison of *ALMT1* transcript levels in roots of *ppck1-1* and WT (Col-0) seedlings grown under Pi-sufficient and Pi-deficient conditions by RT-qPCR (B) GUS staining in roots of *pALMT1::GUS/Col-0* and *pALMT1::GUS/ppck1-1* reporter lines growing under Pi-sufficient and Pi-deficient conditions. Seedlings were germinated for 6 days on +Pi agar plates, transferred to +Pi (500 µM) or –Pi (5 µM) conditions, and allowed to grow for additional 5 days before harvest for total RNA extraction or GUS-staining. Data from one representative out of three independent experiments are shown. For (A) *PP2A* was used as a reference gene. Error bars denote SD (n=4 biological replicates). Significance analyses were performed by Student's *t*-test (two-tailed, equal variances): *p ≤ 0.05, □p ≤ 0.05, and •p≤ 0.05 compared to +Pi condition, Col-0+Pi, and Col-0-Pi, respectively. For (B) the top, center, and bottom panels depict the mature root zone, early differentiation zone, and root apical region, respectively. Roots were stained for 20 min in GUS-solution. Scale bars represent 100 µm.

In order to confirm increased expression of *ALMT1* in *ppck1-1* seedlings, a GUS reporter line to monitor *ALMT1* expression (*pALMT1::GUS*) was introduced into *ppck1-1* plants by crossing the *ppck1-1* plant with a transgenic line transformed with a *pALMT1::GUS* construct (obtained from Kobayashi et al., 2007). Histochemical GUS analysis was performed after confirming the homozygosity of the T-DNA insertion for *ppck1-1* and of the *pALMT1::GUS* insertion in the T_3 generation [Figure 2-24(B)]. In transgenic plants transformed with the *pALMT1::GUS* construct, the GUS reporter activity was detected in root-tips of only Pi-starved but not in root tips of Pi-sufficient seedlings after 20 min of staining. In contrast, GUS reporter activity was detected in root-tips of both Pi-replete and Pi-depleted seedlings in the *ppck1-1* background. Additionally, *ALMT1* promoter activity was stronger in root-tips of Pi-deficient *ppck1-1* compared to Pi-deficient WT plants transformed with *pALMT1::GUS* construct.

2.2.2.7 Characterization of transgenic lines generated to complement *ppck1-1*

In order to confirm whether the effects observed in *ppck1-1* plants are specific to *PPCK1* misexpression, the mutant was transformed with a complementation construct containing the genomic *PPCK1* sequence coding for the full-length protein under control of its native promoter (*pPPCK1$_{long}$::PPCK1*). Four independent transgenic lines transformed with this construct were analyzed in this study and were named as C-lines. The mRNA abundance of *PPCK1* in whole seedlings of three independent C-lines (C1.1, C2.2, and C6.8) was around 6-fold higher and in one line (C4.6) was 13-fold higher compared to WT seedlings. Moreover, when compared to *ppck1-1* seedlings, the *PPCK1* transcripts in C-lines were between 16 and 37-fold higher [Figure 2-25(A)].

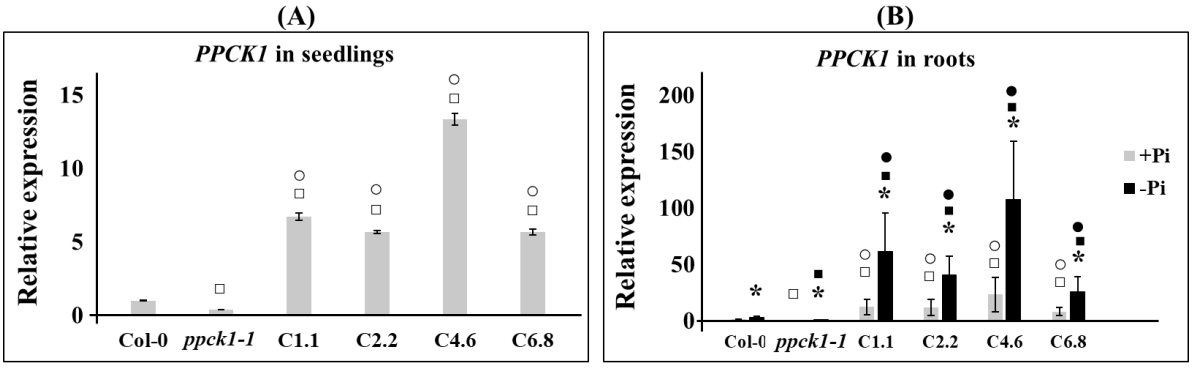

Figure 2-25: Expression analysis of *PPCK1* in *pPPCK1$_{long}$::gDNA/ppck1-1* lines by RT-qPCR

(A) *PPCK1* transcript levels in seedlings of C-lines (B) *PPCK1* transcript levels in roots of C-lines grown under Pi-sufficient and Pi-deficient conditions. For (A) Total RNA was extracted from 7 days old seedlings and for (B) seedlings were germinated for 6 days on +Pi agar plates, transferred to +Pi (500 µM) or –Pi (5 µM) conditions, and allowed to grow for additional 5 days before harvest for total RNA extraction. *PP2A* was used as a reference gene and relative expression levels were normalized to that of the Col-0+Pi levels. Error bars denote SD (n=4 biological replicates). Data from one representative out of three independent experiments are shown. Significance analyses were performed by Student's *t*-test (two-tailed, equal variances): *p ≤ 0.05, □p ≤ 0.05, ▪p≤ 0.05, ○p ≤ 0.05, and •p ≤ 0.05 compared to +Pi, Col-0+Pi, Col-0-Pi, *ppck1-1*+Pi, and *ppck1-1*-Pi, respectively.

C-lines exhibited increased *PPCK1* transcript levels compared to WT, although *PPCK1* in these lines was under the control of its own promoter and also segregation analysis suggested a single insertion of the transgene. This might be due to the insertion outside of the natural context. Therefore, it was interesting to determine whether Pi-starvation is still able to further increase *PPCK1* expression in roots of these lines. The C-lines exhibited between 8 and 23-fold and 9 and 38-fold higher *PPCK1* mRNA levels in roots compared to WT under Pi-sufficient and Pi-deficient conditions, respectively. Pi-deficiency also triggered stronger induction in *PPCK1* transcript levels in roots of C-lines compared to WT (two-way ANOVA response between WT and C-lines ≤ 0.05) [Figure 2-25(B)].

Malate and citrate content in complementation lines

Malate content in roots and shoots of C-lines should be restored if the introduced construct is functional and the loss of *PPCK1* is indeed responsible for observing lower malate levels in *ppck1-1* plants. Under Pi-replete condition, endogenous malate content in roots of C-lines was still between 1.3 and 1.4-fold lower compared to WT roots, but it was between 1.3 and 1.4-fold higher compared to *ppck1-1* roots. Thus, malate levels could be partially restored to WT levels in complementation lines (C-lines) under Pi-sufficient condition. After Pi-starvation, root malate content of C-lines was completely restored to WT levels and was between 1.9 and 2.1-fold higher compared to *ppck1-1* roots [Figure 2-26(A)]. Results for shoots showed a similar pattern [Figure 2-26(B)]. Malate levels were slightly lower in three independent C-lines (C1.1, C2.2, and C6.8) compared to WT shoots under Pi-sufficient condition, whereas it was completely restored in C4.6 shoots. Compared to *ppck1-1* shoots, malate content in C-lines were higher by 1.1 and 1.2 fold. After Pi starvation, malate content was completely restored in C-lines and was between 1.2 and 1.3-fold higher compared to *ppck1-1* shoots.

In contrast to malate, citrate content was not restored in roots and shoots of C-lines either under Pi-replete or Pi-depleted conditions [Figure 2-26(C-D)]. In fact, in shoots of three independent C-lines (C1.1, C2.2, and C4.6), citrate content was between 1.2 and 1.4-fold lower compared to *ppck1-1* shoots under Pi-sufficient condition. In Pi-depleted shoots of C2.2 and C4.6 also 1.3 and 1.4-fold lower citrate content was detected compared to *ppck1-1* shoots, respectively.

Phenotypic analysis of C-lines

Comparison of malate levels between *ppck1-1* and complementation lines indicated that the introduced *PPCK1* gene is translated to a functional enzyme. Therefore, the complementation lines were suitable to analyze whether the phenotypes of *ppck1-1* seedlings during low Pi-stress are solely due to the absence of *PPCK1.*

Fresh weight analysis

Seedling, shoot, and root fresh weight of all the independent C-lines was similar to *ppck1-1* when grown on agar plates with either Pi-sufficient or Pi-deficient media [Supplementary Figure 7-18(A-C)].

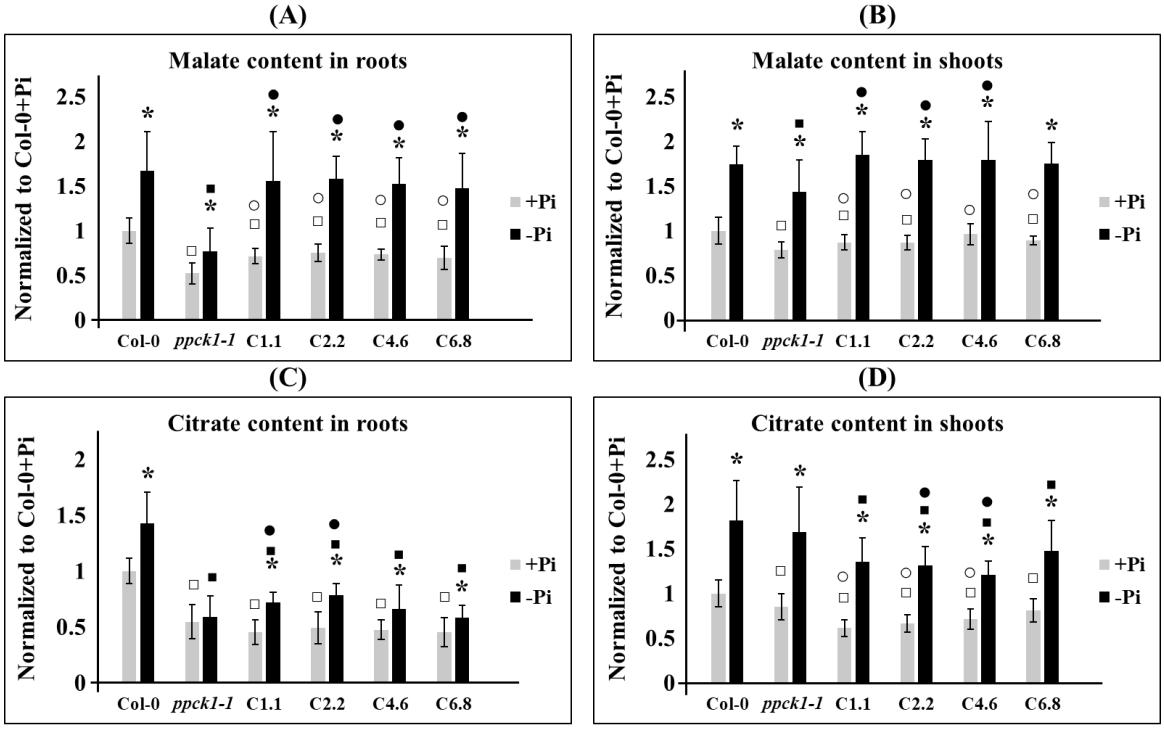

Figure 2-26: Normalized malate and citrate content in *pPPCK1$_{long}$::gDNA/ppck1-1* lines

Normalized content of (A) malate in roots, (B) malate in shoots, (C) citrate in roots, and (D) citrate in shoots of C-lines under Pi-sufficient and Pi-deficient conditions. Seedlings were germinated for 6 days on +Pi agar plates, transferred to +Pi (500 µM) or –Pi (5 µM) conditions, and allowed to grow for additional 5 days before harvest. Data are normalized to the levels detected in Col-0+Pi. Shown are the cumulative data of 3 independent germination experiments. For each experiment, four biological replicates (two pooled seedlings per replicate) were analyzed. Error bars denote SD (n=12). Significance analyses were performed by Student's *t*-test (two-tailed, equal variances): *p ≤ 0.05, □p ≤ 0.05, ▪p≤ 0.05, ○p ≤ 0.05, and •p≤ 0.05 compared to +Pi, Col-0+Pi, Col-0-Pi, *ppck1-1*+Pi, and *ppck1-1*-Pi, respectively.

Root phenotypes

Hypersensitive root growth inhibition observed in *ppck1-1* seedlings during low Pi stress was not restored to WT levels in three independent C-lines (C1.1, C2.2, and C4.6), and C6.8-line even exhibited reduced root length compared to *ppck1-1* seedlings under both Pi-sufficient and Pi-deficient conditions [Supplementary Figure 7-19]. Root-tip appearance was similar to *ppck1-1* seedlings [Supplementary Figure 7-20]. In addition, roots of C-lines also displayed a similar iron accumulation and callose deposition pattern like *ppck1-1* seedlings after Pi-starvation [Supplementary Figure 7-21 and Supplementary Figure 7-22]. Thus, it was quite evident from the analysis of C-lines that the observed phenotypic alterations in *ppck1-1* plants are independent of the absence of *PPCK1*.

Malate and citrate exudation in C-lines

Elevated malate exudation in Pi-starved *ppck1-1* despite having reduced endogenous malate content could be correlated to increased *ALMT1* expression. Since in Pi-depleted C-lines endogenous malate content was restored, it was interesting to determine malate exudation in C-lines [Figure 2-27(A)]. Malate content in exudates of Pi-sufficient C-lines was between 1.3 and 1.5-fold higher compared to WT, but not different from Pi-sufficient *ppck1-1* seedlings (p≥0.05). Pi-deficient C-lines exhibited between 3 and 4-fold higher malate exudation compared to WT. In addition, malate exudation of C-lines was also between 1.4 and 2.1-fold higher compared to *ppck1-1*. The Pi-deficiency triggered induction of malate exudation was stronger in C-lines compared to WT (two way ANOVA: $p=4.44e^{-16}$-$8.55e^{-10}$) and also compared to *ppck1-1* seedlings (two way ANOVA: $p=1.87e^{-07}$-0.02) [Figure 2-27(A)].

The exudation of citrate by C-lines was between 1.2 and 1.4-fold lower compared to WT seedlings and between 1.3 to 1.6-fold higher compared to *ppck1-1* seedlings under Pi-sufficient condition. In Pi-starved seedlings, citrate content in exudates was indistinguishable between C-lines and WT and also between C-lines and *ppck1-1*. [Figure 2-27(B)].

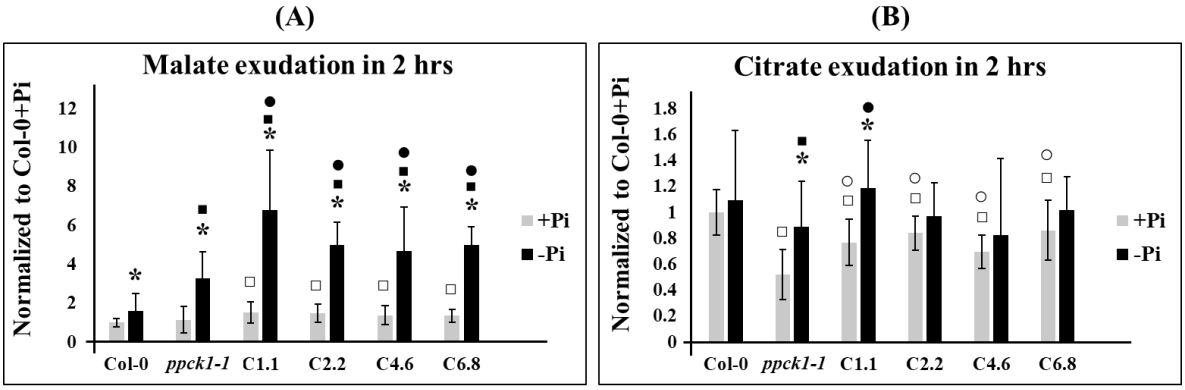

Figure 2-27: Normalized malate and citrate content in root exudates of *pPPCK1$_{long}$::gDNA/ppck1-1* lines

Normalized content of (A) malate and (B) citrate in root exudates of C-lines compared to untransformed WT (Col-0) and *ppck1-1* plants grown under Pi-sufficient and Pi-deficient conditions. Seedlings were germinated for 6 days on +Pi agar plates, transferred to +Pi (500 µM) or –Pi (5 µM) conditions, and allowed to grow for additional 4 days. Subsequently, the root systems of three intact seedlings were incubated in 300 µl water, and exudates were collected after 2 h. Data are normalized to the levels detected in Col-0+Pi. Shown are the cumulative data of 4 independent germination experiments. For each experiment, four biological replicates (the exudates of three pooled root systems per replicate) were analyzed. Error bars denote SD (n=16 total biological replicates). Significance analyses were performed by Student's *t*-test (two-tailed, equal variances): *p ≤ 0.05, □p ≤ 0.05, ▪p≤ 0.05, ○p ≤ 0.05; and •p ≤ 0.05 compared to +Pi, Col-0+Pi, Col-0-Pi, *ppck1-1*+Pi, and *ppck1-1*-Pi, respectively.

2.2.2.8 Detection of a second site insertion in *ppck1-1* line

Although the introduction of a functional *PPCK1* in *ppck1-1* seedlings (C-lines) restored the endogenous malate content under Pi-deficient condition, the phenotypic alterations could not be rescued. Rechecking the description of the T-DNA insertion line for *ppck1-1* on an updated Salk Institute Genomic Analysis Laboratory (SIGnAL) website revealed the presence of a second site

insertion in *ppck1-1* line apart from the T-DNA insertion in *PPCK1*. The second site insertion was located 1382 bp downstream of the stop codon of *ALMT1* (AT1G08430) and 616 bp upstream of the start codon of a gene annotated as *ALMT2* (AT1G08440) [Figure 2-28].

The position of the second site insertion could be the possible reason for the elevated expression of *ALMT1* in roots of *ppck1-1* seedlings, which was observed both under Pi-sufficient and Pi-deficient conditions [as shown in Figure 2-24], and which was probably responsible for the phenotypes of *ppck1-1* plants. However, the position of the second site insertion upstream of the gene annotated as *ALMT2* represents an additional option causing the elevated malate exudation and the phenotypes observed for *ppck1-1*.

ALMT2 is one of the members of the 14 membered ALMT protein family in Arabidopsis. It shares 80% similarity with ALMT1 on protein sequence level and 81% similarity on the nucleotide sequence level. Its high sequence similarity to ALMT1, suggests its involvement in malate transport, however, no physiological or biochemical function has yet been assigned to this protein. In order to determine whether the presence of the second site insertion also leads to alteration in *ALMT2* transcript levels in *ppck1-1* line similar to that observed for *ALMT1* transcripts, qRT-PCR analysis was performed [Figure 2-29]. Compared to WT, transcript levels of *ALMT2* in roots of *ppck1-1* seedlings were 48 and 103-fold higher in Pi-replete and Pi-depleted condition, respectively. After Pi-starvation, a 3-fold induction in *ALMT2* transcripts levels were detected in roots of *ppck1-1* seedlings compared to 1.5-fold induction detected in roots of WT seedlings. Thus, the Pi-deficiency triggered induction in *ALMT2* expression was stronger in *ppck1-1* line compared to that detected in WT (two-way ANOVA: $p=2.21e^{-05}$).

Figure 2-28: Position of the second site insertion in *ppck1-1* line

Organization of *ALMT1*, *ALMT2*, and *PPCK1* on the chromosome is represented in the model. The two T-DNA insertion sites in line *ppck1-1* are indicated with triangles on the model. The T-DNA insertion GK_614F02_021894 is located on the intron of *PPCK1* (AT1G08650). The second T-DNA insertion GK_614F02_021890 is located 1382 bp downstream of the stop codon of *ALMT1* (AT1G08430) and 616 bp upstream of the start codon of a gene annotated as *ALMT2* (AT1G08440).

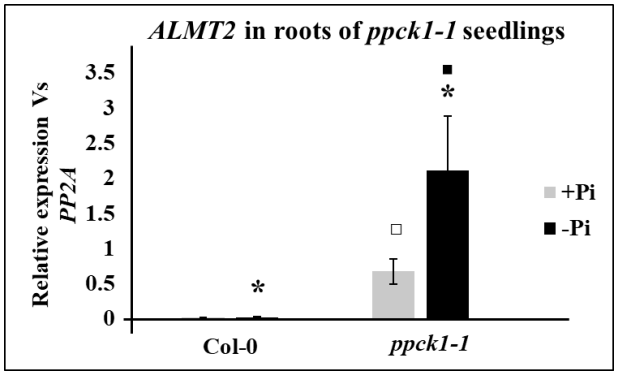

Figure 2-29: Expression analysis of *ALMT2* in roots of *ppck1-1* seedlings by RT-qPCR

Seedlings were germinated for 6 days on +Pi agar plates, transferred to +Pi (500 µM) or –Pi (5 µM) conditions, and allowed to grow for additional 5 days before harvest for total RNA extraction. Data from one representative out of three independent experiments are shown. Error bars denote SD (n=4 total biological replicates). Significance analyses were performed by Student's *t*-test (two-tailed, equal variances): *p ≤ 0.05, □p ≤ 0.05, and •p≤ 0.05 compared to +Pi condition, Col-0+Pi, and Col-0-Pi, respectively.

2.2.2.9 Characterization of T-DNA insertion lines of *ALMT2*

In order to determine whether ALMT2 mediates malate exudation and whether the observed hypersensitivity in *ppck1-1* is also due to increased *ALMT2* transcription, mutants deficient in *ALMT2* expression were analyzed. Three independent T-DNA insertion lines for *ALMT2,* SALK_108715C, SAIL_1285_G09, and SALK_010570C, were obtained and named *almt2-1*, *almt2-2*, and *almt2-3*, respectively. The position of the T-DNA insertion in *almt2-1*, *almt2-2*, and *almt2-3* is in the second exon, fifth intron, and in the promoter of *ALMT2*, respectively [Supplementary figure 7-23(A)]. RT-qPCR analysis revealed 11, 21, and 1.6-fold reduced *ALMT2* transcript levels in *almt2-1*, *almt2-2*, and *almt2-3,* respectively compared to WT seedlings [Supplementary figure 7-23(B)].

Malate and citrate content in tissues and root exudates of almt2 lines

Malate and citrate levels in roots and shoots [Supplementary Figure 7-24(A-D)], as well as in root exudates [Supplementary figure 7-25(A-B)] in all three *ALMT2* T-DNA insertion lines- *almt2-1*, *almt2-2*, and *almt2-3* were similar to WT seedlings, both under Pi-sufficient and Pi-deficient conditions.

2.2.2.10 Characterization of other T-DNA insertion lines of *PPCK1*

Alteration in malate and citrate levels detected in *ppck1-1* plants could be both due to the absence of functional *PPCK1* and overexpression of *ALMT1* and *ALMT2*. In order to determine the effect of the absence of *PPCK1* alone on the biosynthesis of malate and citrate, other *PPCK1* T-DNA insertion lines were considered. However, additional lines only became available in the later stage of this project. Two novel independent lines harboring insertion in the *PPCK1* gene (SALKseq_138855.1 and WiscDsLox477-480C13) were obtained and named as *ppck1-4* and *ppck1-5,* respectively. The position of the T-DNA insertion in *ppck1-4* (WT background) and *ppck1-5* (Col-2 background) is in the intron and first exon of *PPCK1*, respectively [Figure 2-30(A)].

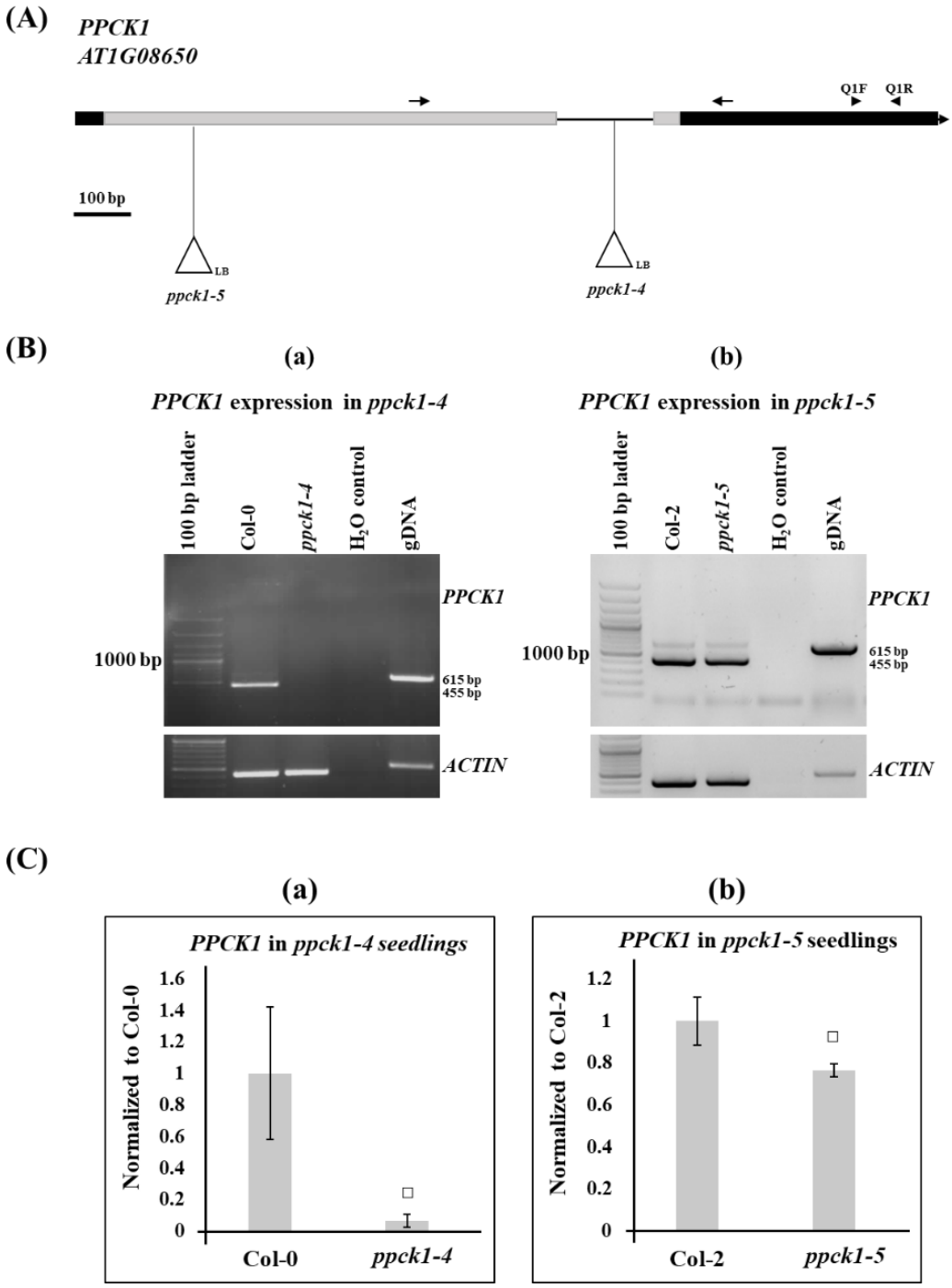

Figure 2-30: Characterization of *ppck1-4* and *ppck1-5* lines

(A) Gene model and position of T-DNA insertions in two independent lines, *ppck1-4* and *ppck1-5.* Black boxes indicate the 5'-UTR and 3'-UTR and light grey boxes indicate the exons. Intron is represented by the black line. Position of the T-DNA insertion is indicated with triangle. Larger and smaller arrows indicate the position of primers used for amplification of *PPCK1* transcripts for semi-quantitative RT-PCR and RT-qPCR analysis, respectively. (B) *PPCK1* transcript levels in (a) *ppck1-4* and (b) *ppck1-5* plants compared to the levels detected in their respective WT controls by RT-PCR analysis. *ACTIN2* was included as a control for cDNA integrity. Genomic DNA (gDNA) was used for checking DNA contamination in cDNA samples. (C) *PPCK1* expression in (a) *ppck1-4* and (b) *ppck1-5* seedlings compared to the expression levels in their respective WT controls by RT-qPCR analysis. Total RNA was extracted from 7 days old seedlings. *PP2A* was used as a reference gene and relative expression levels were normalized to that of the WT levels. Error bars denote SD (n=3 biological replicates). Data from one representative out of two independent experiments are shown. Significance analyses were performed by Student's *t*-test (two-tailed, equal variances): □p ≤ 0.05.

Semiquantitative RT-PCR analysis of *ppck1-4* seedlings revealed complete absence of *PPCK1* transcripts [Figure 2-30(B): (a)], whereas RT-qPCR with primers binding at the 3' end of the gene revealed 15-fold reduced *PPCK1* transcript levels in *ppck1-4* compared to WT (WT) seedlings [Figure 2-30(C): (a)]. *PPCK1* transcript levels between *ppck1-5* and Col-2 seedlings were indistinguishable as revealed by RT-PCR analysis [Figure 2-30(B): (b)], whereas around 1.3-fold reduced *PPCK1* transcript levels were detected in *ppck1-5* compared to Col-2 seedlings by RT-qPCR analysis [Figure 2-30(C): (b)].

Malate and citrate content in ppck1-4 and ppck1-5 lines

Ppck1-4 line exhibited 1.6 and 2-fold reduced malate content in roots under Pi-replete and Pi-depleted conditions, respectively. Pi-starvation induced malate accumulation was absent in roots of *ppck1-4* compared to WT roots (two way ANOVA: $p=9.06e^{-04}$) [Figure 2-31(A)]. Similarly, malate content in roots of *ppck1-5* line was reduced by 1.3-fold under Pi-replete and by 1.8-fold under Pi-depleted conditions compared to WT (Col-2). Unlike *ppck1-4*, Pi-deficiency triggered induction in malate content was detected in roots of *ppck1-5* (p=0.04), however, the response was weaker compared to the response detected in WT (Col-2) (two way ANOVA: $p=9.01e^{-04}$) [Figure 2-31(B)]. In shoots, malate content of *ppck1-4* was 1.2 and 1.5-fold lower under Pi-sufficient and Pi-deficient conditions, respectively, compared to the levels detected in WT. Pi-starvation triggered malate accumulation in shoots of *ppck1-4*, but the response was weaker compared to the response in WT (two way ANOVA: p=0.008) [Figure 2-31(C)]. *Ppck1-5* line exhibited similar malate content in Pi-replete and about 1.5-fold reduced content in Pi-depleted (p=0.04) shoots compared to WT (Col-2). Consequently, Pi-deficiency triggered induction of malate content in shoots of *ppck1-5* was less pronounced compared to the response in WT (Col-2) shoots (two way ANOVA: p=0.04) [Figure 2-31(D)].

Citrate content in roots of *ppck1-4* line was 1.2 and 1.3-fold lower under Pi-replete and Pi-depleted conditions, respectively, compared to WT. Although Pi-deficiency induced citrate accumulation was absent in *ppck1-4* roots, the response was similar to WT response (two way ANOVA: p=0.4) [Figure 2-31(E)]. The *ppck1-5* line exhibited similar and 1.3-fold reduced citrate content in roots under Pi-sufficient and Pi-deficient conditions, respectively, compared to WT (Col-2). Pi-deficiency triggered citrate accumulation was absent in *ppck1-5* roots but the response was similar to WT (Col-2) response (two way ANOVA: p=0.09) [Figure 2-31(F)]. In shoots, citrate content of *ppck1-4* and *ppck1-5* lines were unaffected under Pi-replete condition. However, under Pi-depleted condition, citrate content was 1.5 and 1.4-fold higher in *ppck1-4* and *ppck1-5* lines, respectively, compared to their respective WT. Pi-deficiency triggered citrate accumulation was detected in shoots of both *ppck1-4* and *ppck1-5* lines and the response was stronger in both mutants compared to the response detected in their respective WT (two way ANOVA: p=0.002 for *ppck1-4* and 0.01 for *ppck1-5*) [Figure 2-31(G) and (H)].

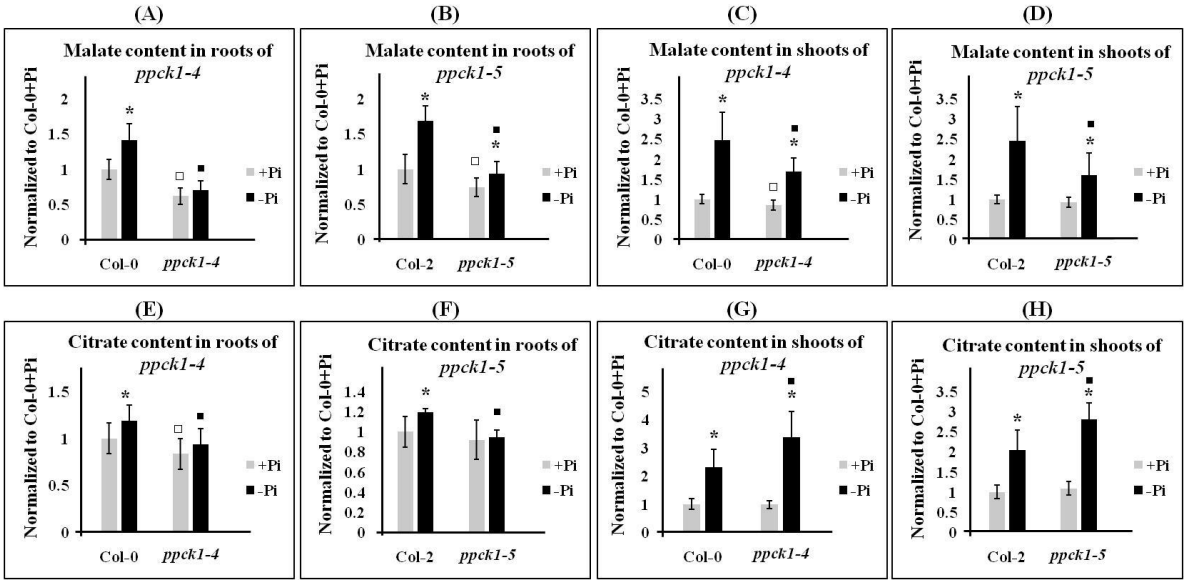

Figure 2-31: Normalized malate and citrate content in *ppck1-4* and *ppck1-5* lines compared to WT

Normalized content of malate (A) in roots of *ppck1-4,* (B) roots of *ppck1-5* plants, (C) shoots of *ppck1-4*, (D) shoots of *ppck1-5* and citrate in (E) roots of *ppck1-4*, (F) roots of *ppck1-5*, (G) shoots of *ppck1-4*, and (H) shoots of *ppck1-5* compared to the levels detected in WT (Col-0) plants grown under Pi-sufficient and Pi-deficient conditions. Seedlings were germinated for 6 days on +Pi agar plates, transferred to +Pi (500 µM) or –Pi (5 µM) conditions, and allowed to grow for additional 5 days before harvest. Data are normalized to the levels detected in WT+Pi. Shown are the cumulative data of 3 independent germination experiments. For each experiment, four biological replicates (two pooled seedlings per replicate) were analyzed. Error bars denote SD (n=12). Significance analyses were performed by Student's *t*-test (two-tailed, equal variances): *p ≤ 0.05, □p ≤ 0.05, and ▪p≤ 0.05 compared to +Pi condition, WT+Pi, and WT-Pi, respectively.

Malate and citrate exudation in ppck1-4 line

As already mentioned before, *ppck1-4* and *ppck1-5* lines became available in the later stage of this project. After propagation of *ppck1-5* seeds obtained from NASC, only one homozygous plant could be obtained. Therefore, for root exudation and other phenotypic analysis, sufficient amount of *ppck1-5* seeds were not available. Therefore, only *ppck1-4* line was analyzed for further experiments. Malate and citrate content was determined in root exudates of *ppck1-4* line to elucidate whether reduced biosynthesis of malate and citrate in roots can also affect their exudation [Figure 2-32]. Compared to WT, *ppck1-4* seedlings exhibited 1.7 and 1.8-fold reduced root malate exudation under Pi-sufficient and Pi-deficient conditions, respectively. Pi-deficiency triggered induction in malate exudation was also detected in *ppck1-4* seedlings and the response was weaker compared to the response detected in WT (two way ANOVA: p=0.04) [Figure 2-32(A)].

Citrate content in root exudates of Pi-sufficient *ppck1-4* seedlings was similar to WT seedlings, whereas it was reduced by 1.4-fold in root exudates of Pi-starved *ppck1-4* compared to WT seedlings (p=0.03). The Pi-starvation response between *ppck1-4* and WT seedlings were similar [Figure 2-32(B)].

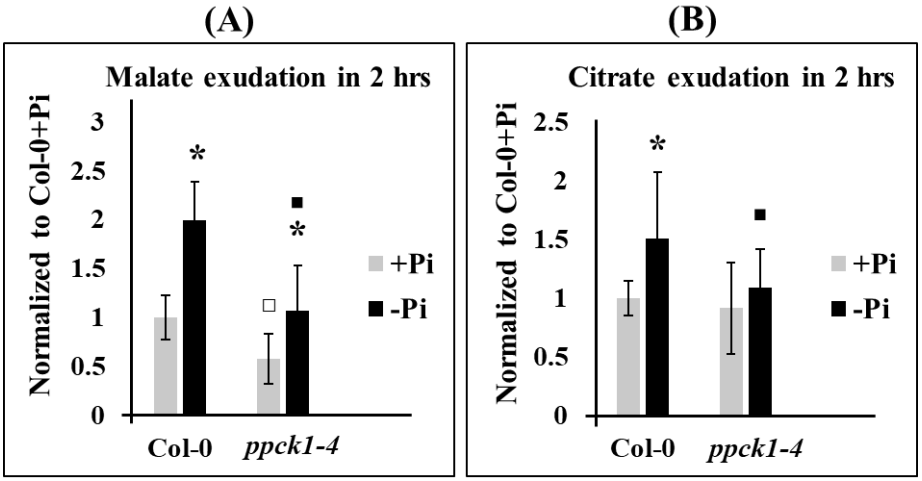

Figure 2-32: Normalized content of malate and citrate in root exudates of *ppck1-4* line compared to WT

Normalized content of (A) malate and (B) citrate in root exudates of *ppck1-4* plants grown under Pi-sufficient and Pi-deficient conditions compared to the levels detected in WT (Col-0). Seedlings were germinated for 6 days on +Pi agar plates, transferred to +Pi (500 µM) or –Pi (5 µM) conditions, and allowed to grow for additional 4 days. Subsequently, the root systems of three intact seedlings were incubated in 300 µl water, and exudates were collected after 2 h. Data are normalized to the levels detected in Col-0+Pi. Shown are the cumulative data of 3 independent germination experiments. For each experiment, four biological replicates (the exudates of three pooled root systems per replicate) were analyzed. Error bars denote SD (n=12 total biological replicates). Significance analyses were performed by Student's *t*-test (two-tailed, equal variances): *p ≤ 0.05, □p ≤ 0.05, and ▪p≤ 0.05 compared to +Pi condition, Col-0+Pi, and Col-0-Pi, respectively.

Phenotypic analysis of ppck1-4 line

Fresh weight analysis

In order to analyze the effect of absence of functional PPCK1 in seedling growth under Pi-sufficient and Pi-deficient conditions, seedling, shoot, and root fresh weights were determined for *ppck1-4* plants growing on agar plates. The *ppck1-4* plants displayed similar seedling, shoot, and root fresh weights both under Pi-sufficient and Pi-deficient condition compared to WT plants [Supplementary Figure 7-26(A-C)]. When grown in the greenhouse, no obvious morphological differences could be detected between *ppck1-4* and WT plants.

Root length analysis

Total root length of *ppck1-4* seedlings was similar to WT seedlings under Pi-sufficient condition. However, after transfer to low Pi, root lengths of *ppck1-4* plants were slightly longer (1.25 fold) compared to WT plants [Figure 2-33], suggesting insensitivity with respect to Pi deficiency-induced primary root growth inhibition. This corroborates with lower malate exudation of *ppck1-4* plants. Accordingly, the Pi-deficiency induced primary root growth inhibition response was weaker in *ppck1-4* compared to that in WT seedlings (two way ANOVA: p=0.01). Nevertheless, root-tip morphology of Pi-deficient *ppck1-4* was similar to Pi-deficient WT seedlings [Figure 2-34]. Similarly, *ppck1-4* seedlings exhibited no difference in Pi-deficiency induced iron accumulation and callose deposition in roots compared to WT seedlings [Supplementary figure 7-27(A) and (B)].

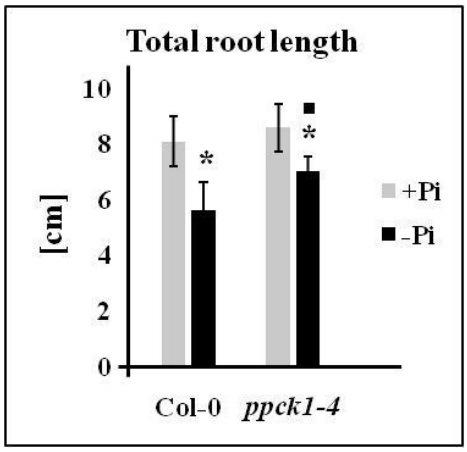

Figure 2-33: Comparison of total root length between *ppck1-4* and WT seedlings

Seedlings were germinated for 6 days on +Pi agar plates, transferred to +Pi (500 µM) or –Pi (5 µM) conditions, and allowed to grow for additional 9 days before root length measurement. Data from one representative out of three independent experiments are shown. Error bars denote SD (n=25). Significance analyses were performed by Student's *t*-test (two-tailed, equal variances): *p ≤ 0.05, □p ≤ 0.05, and •p≤ 0.05 compared to +Pi condition, Col-0+Pi, and Col-0-Pi respectively.

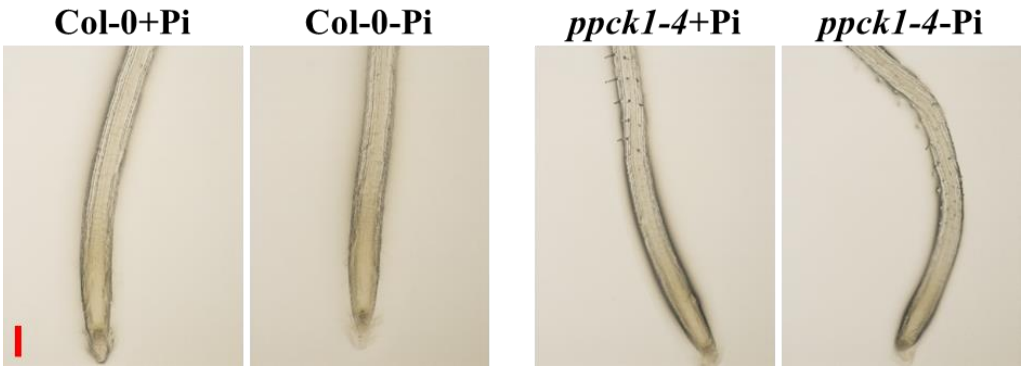

Figure 2-34: Comparison of root-tip morphology between Pi-starved *ppck1-4* and WT seedlings

Seedlings were germinated for 6 days on +Pi agar plates, transferred to +Pi (500 µM) or –Pi (5 µM) conditions, and allowed to grow for additional 4 days before imaging. Images were taken with Nikon SMZ1270 microscope. Representative image from one out of three independent experiments are shown. Scale bars represent 0.2 mm.

2.2.2.11 Expression analysis of *ALMT1* and *ALMT2* in *ppck1-4* line

The transcript levels of *ALMT1* and *ALMT2* in roots of Pi-replete and Pi-depleted *ppck1-4* seedlings were similar to the levels detected in WT seedlings [Supplementary figure 7-28(A) and (B)].

2.2.2.12 Expression analysis of *PPCK2* and *PPCs* in *ppck1-1 and ppck1-4* lines

RT-qPCR analysis was performed to analyze the effect of the loss of functional *PPCK1* together with overexpression of *ALMT1*/*ALMT2* in *ppck1-1* plants and absence of only *PPCK1* in *ppck1-4* plants on the expression of *PPCK2* and *PPC*s. The steady-state transcript levels of *PPCK2* and all three *PPC* isoforms in roots of both *ppck1-1* and *ppck1-4* lines were similar to WT roots under Pi-replete and Pi-depleted conditions [Supplementary figure 7-29(A-B) and Supplementary figure 7-30(A-B)].

In shoots, expression of *PPCK2* was 2-fold lower and 3.7-fold higher in Pi-sufficient *ppck1-1* and *ppck1-4,* respectively compared to the expression levels detected in WT shoots, whereas, when grown under Pi-deficient condition, it was 1.7 (p=0.04) and 2.4 (p=0.01) fold higher compared to WT in shoots of both *ppck1-1* and *ppck1-4* plants, respectively [Supplementary figure 7-29(C-D)]. Pi-starvation triggered induction in *PPCK2* transcript levels were stronger in *ppck1-1* and weaker in *ppck1-4* plants compared to the increase detected in WT shoots (two-way ANOVA: p=0.02 for *ppck1-1* and p=0.004 for *ppck1-4*). Shoot transcript levels of all three *PPC* isoforms in *ppck1-1* were similar to the levels in WT shoots under both Pi-sufficient and Pi-deficient conditions [Supplementary figure 7-30(C)]. However, the steady-state mRNA levels of *PPC1*, *PPC2*, and *PPC3* in shoots of *ppck1-4* were 2.4-fold higher compared to the levels in WT shoots under Pi-deficient condition, whereas no changes were detected under Pi-sufficient conditions [Supplementary figure 7-30(D)]. Consequently, Pi-deficiency triggered induction in transcript levels of all *PPC*s was stronger in shoots of *ppck1-4* compared to WT shoots (two way ANOVA: p=0.01 for *PPC1*, 0.04 for *PPC2*, and $7.44e^{-04}$ for *PPC3*).

2.3 Effect of malate exudation on Pi-solubilization capacity of plants

During this study, transgenic plants with altered exudation capacity for malate and citrate were generated by manipulation of enzymes involved in their biosynthesis (*PPCK1* and *PPCK2* overexpressors). RT-qPCR analysis confirmed that increased exudation detected in *PPCK1* and *PPCK2* overexpressors are not due to changes in *ALMT1* and *ALMT2* expression [Supplementary figure 7-31(A-D)]. By accident, transgenic plants, overexpressing enzymes involved in both malate biosynthesis (PPCK1) and transport (ALMT1/ALMT2) were also generated (C-lines). Data showing higher expression of *PPCK1* in C-lines compared to WT is already shown before [Figure 2-25]. Moreover, since C-lines were generated in the *ppck1-1* background which shows elevated *ALMT1/ALMT2* expression, both *ALMT1* and *ALMT2* expression should also be higher in C-lines under both Pi-sufficient and Pi-deficient condition, which was confirmed by our RT-qPCR analysis [Supplementary figure 7-32(A-B)]. Apart from *PPCK1* and *PPCK2* overexpressors and C-lines (overexpression of *PPCK1* and *ALMT1/ALMT2*), during this study we encountered with transgenic plants with different capacity to generate and exude malate like *ppck1-1* plants showing reduced biosynthesis but increased exudation capacity, *ppck1-4* plants showing both reduced biosynthesis and exudation capacity, and $ALMT1^{OE}$ with high exudation capacity but no alteration in malate generation. Since exudation of organic acids aids in Pi-solubilization to improve its uptake by plants, it was interesting to determine Pi content in all the above mentioned transgenic plants, showing different capacity to generate and exude malate.

2.3.1 Pi content in *PPCK1* and *PPCK2* overexpressors

Pi content in roots of both Pi-sufficient and Pi-deficient *PPCK1* and *PPCK2* overexpressors were similar to WT roots [Figure 2-35(A-B)]. However, in shoots, Pi content of all independent lines overexpressing *PPCK1* (K-lines) was between 1.2 and 1.5-fold lower compared to WT shoots under Pi-sufficient condition. Similarly, all four *PPCK1* overexpressors (K-lines) exhibited between 1.2 and 1.4-fold reduced Pi content in Pi-starved shoots compared to WT shoots [Figure 2-35(C)]. The *PPCK2* overexpressors (O-lines) also exhibited reduced Pi content between 1.3 and 1.5-fold under Pi-sufficient condition and between 1.2 and 1.4-fold under Pi-deficient condition when compared to WT shoots (except O4.1 under Pi-deficient condition; p=0.06) [Figure 2-35(D)].

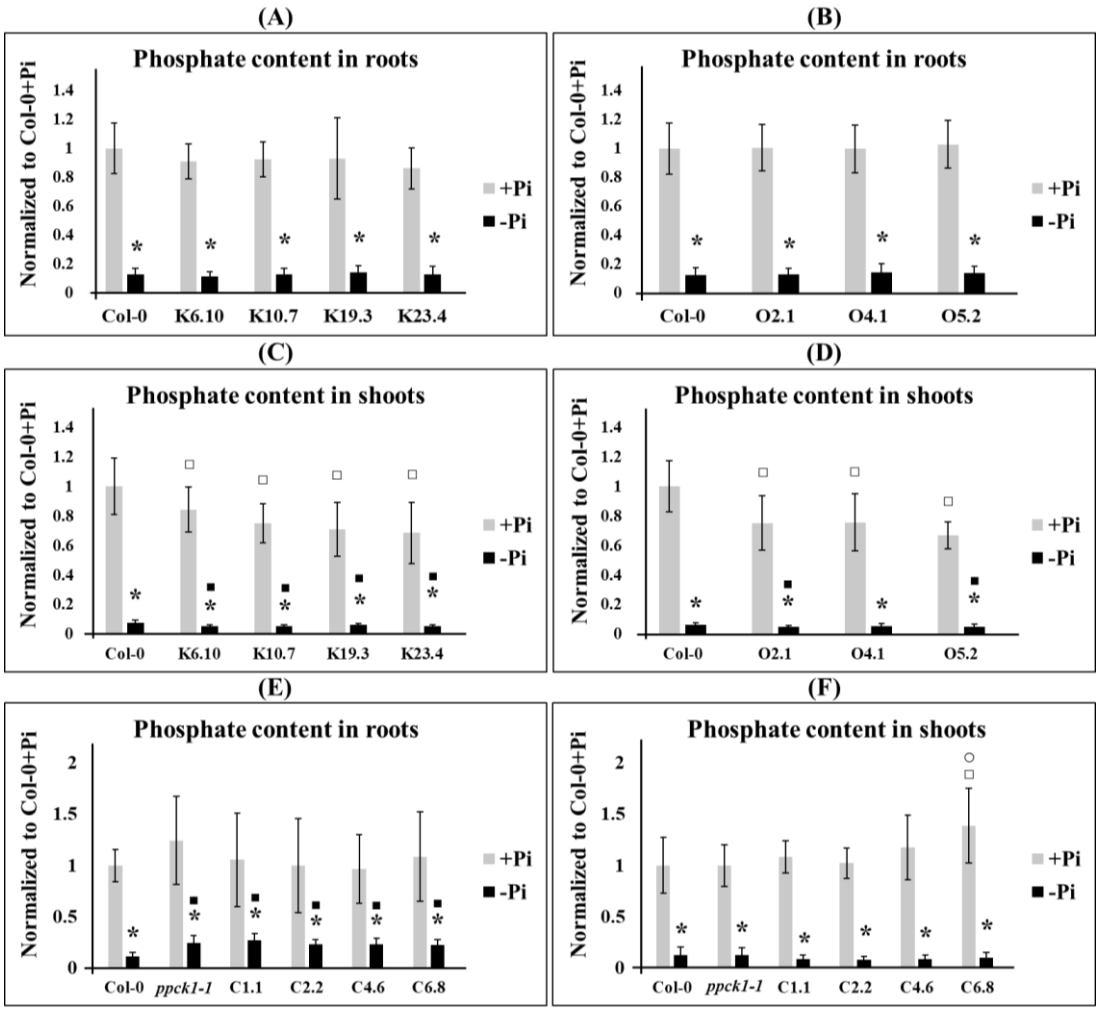

Figure 2-35: Normalized Pi content in transgenic lines overexpressing *PPCK1* and *PPCK2*, and in *ppck1-1* and *pPPCK1$_{long}$::gDNA/ppck1-1 lines* compared to WT

Normalized Pi content in (A) roots of *35S::PPCK1*, (B) roots of *35S::PPCK2*, (C) shoots of *35S::PPCK1*, (D) shoots of *35S::PPCK2*, (E) roots of *ppck1-1* and C-lines, and (D) shoots of *ppck1-1* and C-lines. Seedlings were germinated for 6 days on +Pi agar plates, transferred to +Pi (500 µM) or –Pi (5 µM) conditions, and allowed to grow for additional 5 days before harvest. Data are normalized to the levels detected in Col-0+Pi. Shown are the cumulative data of 4 independent germination experiments. For each experiment, four biological replicates (two pooled seedlings per replicate) were analyzed. Error bars denote SD (n=16 total biological replicates). Significance analyses were performed by Student's *t*-test (two-tailed, equal variances): *p≤ 0.05, □p≤ 0.05, and •p≤ 0.05, compared to +Pi, Col-0+Pi, and Col-0-Pi, respectively.

2.3.2 Pi content in *ppck1-1* and complementation lines

Pi content in roots of all the four C-lines, *ppck1-1* and WT seedlings were similar under Pi-sufficient condition. Upon Pi starvation, however, *ppck1-1* seedlings and C-lines exhibited 2.1-fold and between 2.1 and 2.4-fold elevated Pi content in roots, respectively, when compared to WT roots. Pi content was indistinguishable between *ppck1-1* and C-lines in either conditions [Figure 2-35(E)]. Pi content in shoots of Pi-sufficient and Pi-deficient *ppck1-1* and three independent C-lines were similar to WT shoots. Only line C6.8 line exhibited 1.3-fold higher Pi content compared to WT shoots under Pi-replete conditions. Pi content in shoots of three out of four C-lines was similar to *ppck1-1* shoots under either condition, whereas in C6.8 it was 1.3-fold higher under Pi-replete condition [Figure 2-35(F)].

2.3.3 Pi content in *ppck1-4*, *almt1*, and *ALMT1^{OE}*

Pi content in roots of both Pi-replete and Pi-depleted *ppck1-4* seedlings was comparable to WT roots [Figure 2-36(A)]. In shoots, Pi content was similar and reduced by 1.5-fold (p=0.035) under Pi-replete and Pi-deplete condition, respectively, when compared to WT shoots [Figure 2-36(B)]. In roots of Pi-sufficient *almt1* and *ALMT1^{OE}*, Pi content was similar to WT roots. *Almt1* exhibited similar Pi content in its roots as WT roots under Pi-starved condition, whereas *ALMT1^{OE}* displayed 2.7-fold higher Pi content [Figure 2-36(C)]. In shoots of Pi-sufficient *almt1* and *ALMT1^{OE}*, Pi content was similar to WT shoots. After Pi-starvation treatment, *ALMT1^{OE}* displayed similar Pi content in shoots when compared to WT shoots, whereas it was reduced by 1.3 fold (p=0.004) in *almt1* [Figure 2-36(D)].

2.3.4 Performance of K- and C-lines on media supplemented with insoluble Pi-source, calcium-phosphate

2.3.4.1 Pi content in K- and C-lines

The growth medium used for all the experiments performed so far in this study contained soluble Pi, which might not be an appropriate system to detect differences in endogenous Pi content in plants with different malate exuding, and probably different Pi-solubilization capacities. Therefore, the plants were grown in medium with insoluble Pi-sources such as calcium phosphate. In a first test experiment, MS medium with and without added KH_2PO_4 (KP) from Caissons lab was used. To the medium without KH_2PO_4, 1.25 mM of β-Calcium phosphate tribasic [$Ca_3(PO_4)_2$] (CaP) was added. Both media were used at a final pH of 7.6. Seeds were germinated on medium with either KH_2PO_4 and $Ca_3(PO_4)_2$ as Pi-source. Pi content was determined in seedlings after 11 days of growth [Figure 2-37].

Pi content in roots was reduced by 3.1-fold in CaP treated WT seedlings compared to KP treated seedlings, suggesting that WT plants can not efficiently solubilize Pi from CaP [Figure 2-37(A)]. Similarly, in all the lines except for C1.1, Pi content was diminished in CaP treated seedlings compared

to KP treated seedlings. In roots of C1.1, Pi content was similar under KP and CaP treated condition. Lines C1.1 and C4.6 showed reduced Pi content in roots compared to WT roots in KP treated condition by 2.4 and 1.9-fold, respectively, whereas no change was observed for lines K10.7 and K19.3. In roots of C1.1, C4.6, and K10.7 lines, Pi content was similar to WT roots under CaP treated condition, whereas line K19.3 showed 1.6-fold reduced Pi content [Figure 2-37(A)]. Thus, in all these transgenic lines increased root Pi content was not detected compared to the levels in WT roots when plants were grown on medium with CaP as the only Pi-source.

In shoots of CaP treated WT seedlings, 2.4-fold reduced Pi content was detected compared to KP treated seedlings [Figure 2-37(B)]. Similarly, all lines except line C4.6 exhibited between 1.4 and 1.6-fold reduced Pi content in shoots of CaP-treated seedlings compared to KP treated seedlings. Shoot Pi content of all these transgenic lines were indistinguishable to the levels in WT shoots under KP treated condition, however, these lines displayed between 1.5 and 2.5-fold higher Pi content in shoots under CaP treated condition compared to WT shoots [Figure 2-37(B)]. This increase was also evident when Pi content was determined for the entire seedling [Figure 2-37(C)]. Thus, increased Pi content was detected in shoots and seedlings of transgenic plants exuding higher levels of malate when grown on medium with CaP as the insoluble Pi-source compared to the levels detected in WT shoots.

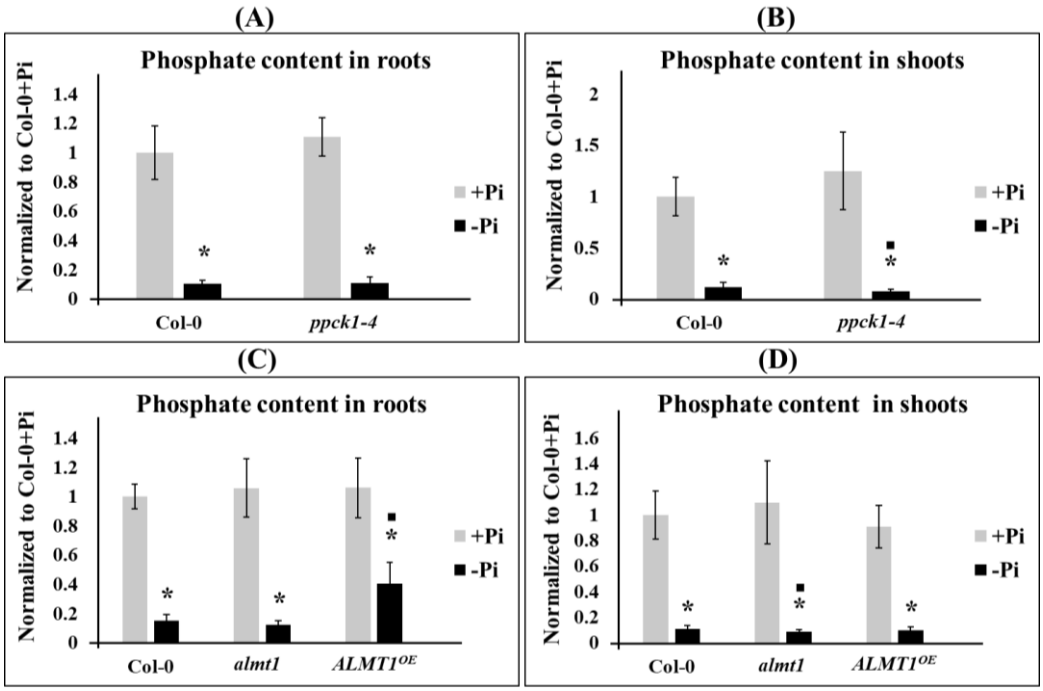

Figure 2-36: Normalized Pi content in *ppck1-4*, *almt1*, and *ALMT1^{OE}* compared to WT
Normalized Pi content in (A) roots and B) shoots of *ppck1-4*, (C) roots and (D) shoots of *almt1* and *ALMT1^{OE}* grown under Pi-sufficient and Pi-deficient conditions compared to the levels detected in WT (Col-0). Seedlings were germinated for 6 days on +Pi agar plates, transferred to +Pi (500 µM) or –Pi (5 µM) conditions, and allowed to grow for additional 5 days before harvest. Data are normalized to the levels detected in Co-0+Pi. Shown are the cumulative data of 3 independent germination experiments. For each experiment, four biological replicates (two pooled seedlings per replicate) were analyzed. Error bars denote SD (n=12 total biological replicates). Significance analyses were performed by Student's *t*-test (two-tailed, equal variances): *p ≤ 0.05, □p ≤ 0.05, and ▪p≤ 0.05, compared to +Pi, Col-0+Pi, and Col-0-Pi, respectively.

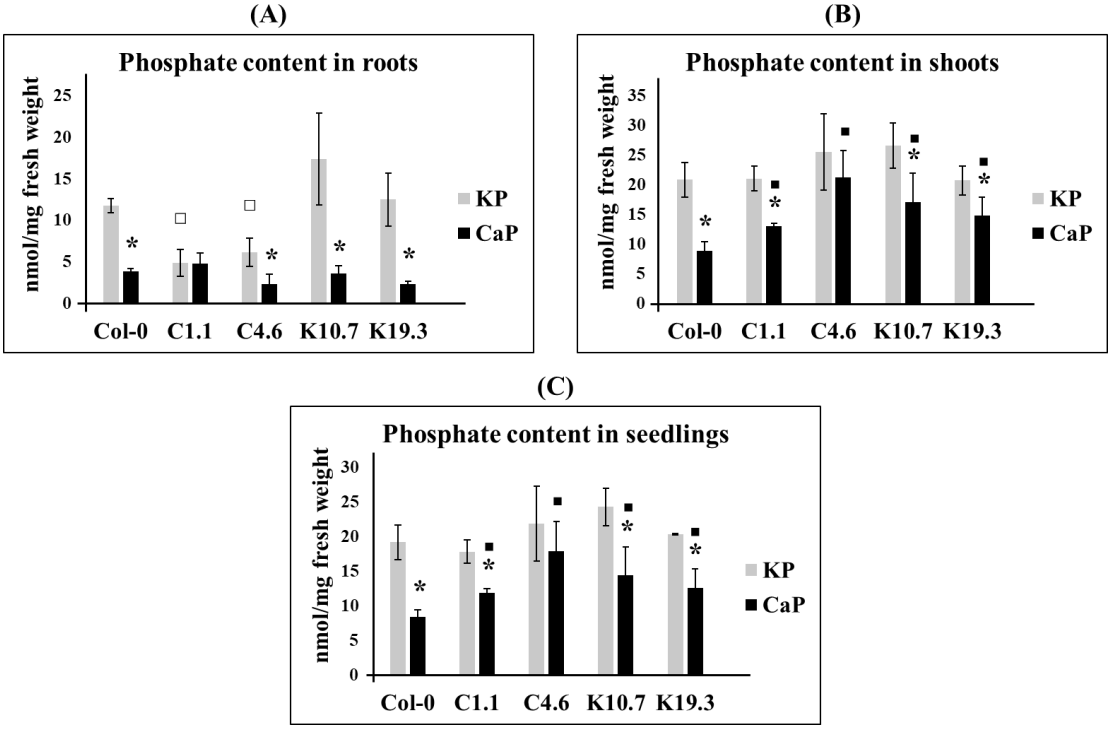

Figure 2-37: Pi content in *pPPCK1$_{long}$::gDNA/ppck1-1* and *35S::PPCK1* lines compared to WT when grown on insoluble Pi source, calcium phosphate

Pi content in (A) roots, (B) shoots, and (C) seedlings of C-lines (overexpression of *PPCK1* and *ALMT1*/*ALMT2*) and K-lines (overexpression of *PPCK1*), when grown on soluble Pi (potassium phosphate-KP) and insoluble Pi source (calcium phosphate-CaP). Seedlings were germinated on agar plates containing either 1.25 mM KH_2PO_4 or 1.25 mM $Ca_3(PO_4)_2$ as Pi-source and allowed to grow for 11 days before harvest. Both media were used at a final pH of 7.6. This experiment was performed only once with four biological replicates (two pooled seedlings per replicate). Error bars denote SD (n=04 total biological replicates). Significance analyses were performed by Student's *t*-test (two-tailed, equal variances): *p ≤ 0.05, □p ≤ 0.05, and •p≤ 0.05, compared to KP, Col-0-KP, and Col-0-CaP, respectively.

2.3.4.2 Malate content in K- and C-lines

In roots, malate content was 3-fold higher in CaP treated WT compared to the levels in KP treated WT. Since malate content is known to increase after Pi-starvation in Arabidopsis (Morcuende et al., 2007; Pant et al., 2015; Ziegler et al., 2016; and also in this study), increase in root malate content of CaP treated seedlings indicate that in CaP treated condition, WT is suffering from low Pi-stress [Supplementary figure 7-33(A)]. Root malate content was also higher in lines C4.6 and K10.7 by 2-fold and 1.5-fold, respectively under CaP treated condition compared to the levels in KP treated condition. Whereas in line C1.1 and K19.3 no such difference could be detected. In KP treated K10.7 and K19.3, higher malate content by 3-fold and 3.6-fold, respectively was detected compared to the levels in KP-treated WT roots. Roots of lines C1.1 and C4.6 exhibited similar malate content like WT roots under KP treated condition. Except for line K10.7 which showed higher malate content (1.5-fold), no other lines showed any difference compared to the levels in WT roots under CaP treated condition [Supplementary figure 7-33(A)]. Unlike in roots, malate content in shoots of CaP treated WT seedlings were indistinguishable to the levels in WT shoots growing under KP treated condition [Supplementary

figure 7-33(B)]. Similarly, all other lines showed no difference in shoot malate content under CaP and KP treated conditions, except line C1.1 which exhibited 1.3-fold reduced malate content under CaP treated condition. None of these lines growing under KP treated condition showed any difference in shoot malate content compared to the levels in WT shoots. Similarly, shoot malate content in these lines were indistinguishable to WT growing under CaP treated condition, except line K19.3 which exhibited 1.6-fold higher malate content under CaP treated condition [Supplementary figure 7-33(B)].

When entire seedling was considered, there was no difference in malate content between seedlings growing under CaP and KP-treated conditions. Lines K10.7 and K19.3 exhibited 1.4-fold elevated malate levels based on entire seedling compared to WT under KP-treated condition. Similarly, these two lines also exhibited higher malate content by 1.7-fold and 1.8-fold, respectively compared to WT seedlings under CaP treated condition. Line C4.6 also exhibited 1.6-fold (p=0.04) elevated malate content compared to WT seedlings under CaP treated condition [Supplementary figure 7-33(C)].

2.4 Analysis of other metabolites in all the generated transgenic lines

The PPC/PPCK pathway is a very central metabolic pathway and its modulation has already been reported to affect many metabolites like TCA cycle intermediates and amino acids (Chen et al., 2004; Meimoun et al., 2009; Rademacher et al., 2002; Shi et al., 2015). Considering this, changes in organic acids and amino acids were investigated in transgenic lines overexpressing *PPCK1* (K-lines) and *PPCK2* (O-lines), *ppck1-1*, *ppck1-4*, *ALMT1*^{OE}, and complementation lines for *ppck1-1* line (C-lines). Metabolites, which were consistently altered either in all the independent lines or at least in three out of four (K and C-lines) or two out of three independent lines (O-lines), are considered as different.

2.4.1 Metabolites altered in transgenic plants overexpressing *PPCKs*

In roots, Ala and Phe content in Pi-sufficient K-lines (*PPCK1* overxpressors) were around 1.4-fold and between 1.2 and 1.3-fold lower compared to WT, respectively. Asp content was elevated between 1.2 and 1.5-fold compared to WT in Pi-sufficient K-lines. Similarly, α-ketoglutarate and succinate contents were also increased in K-lines by around 1.4 and 1.2-fold [Supplementary table 7-1(A)]. Although in Pi-starved K-lines, some metabolites were altered, these metabolites were not consistent between all the lines [Supplementary table 7-1(B)]. Many metabolites were altered in Pi-sufficient O-lines (*PPCK2* overexpressors) compared to K-lines. The amino acids Ala, Asp, Lys, Arg, and Tyr, were significantly elevated between 1.2 and 1.6-fold in Pi-sufficient O-lines compared to WT. The only amino acid exhibiting reduced levels was Phe, for which the content was reduced by around 1.2-fold in O-lines compared to WT [Supplementary table 7-2(A)]. In Pi-starved O-lines, His and Pro contents were increased between 4.5 and 6.5-fold and 1.7 and 1.9-fold, respectively compared to the levels in WT [Supplementary table 7-2(B)].

In shoots, Asp and Gly content in Pi-replete K-lines was higher by around 1.2 and lower by 1.6-fold compared to WT, respectively, while between 1.2 and 1.4-fold higher and between 1.2 and 1.3-fold lower fumarate and α-ketoglutarate levels, respectively, were detected in K-lines compared to WT levels [Supplementary table 7-3(A)]. In Pi-deficient K-lines, Trp content was between 1.6 and 2-fold higher than in WT [Supplementary table 7-3(B)]. Similar to roots, the number of metabolites exhibiting altered levels in O-lines were also larger than in K-lines in shoots. O-lines exhibited 1.2-fold, between 1.4 and 1.8-fold, and between 1.2 and 1.8-fold reduced levels of Ala, Gly, and α-ketoglutarate, respectively compared to WT under Pi-sufficient condition. In contrast, Asp, Asn, Arg, and fumarate contents were elevated between 1.2 and 1.3, 1.3, 1.4 and 2.2, and 1.6-fold, respectively, compared to WT [Supplementary table 7-4(A)]. After Pi starvation, Pro, Trp, and fumarate content was between 1.4 and 2.4-fold, 1.4 and 1.8-fold, and 1.3 and 1.5-fold higher, respectively compared to WT whereas Ala content was reduced by 1.2-fold [Supplementary table 7-4(B)].

2.4.2 Metabolites altered in *ppck1-1* line

In roots, the levels of almost all analyzed metabolites were altered in *ppck1-1* both under Pi-sufficient and Pi-deficient condition [Supplementary table 7-5(A)]. The amino acids displaying significantly different levels between Pi-sufficient *ppck1-1* and WT were Ala, His, Iso, Lys, Met, Gln, Arg, Ser, Thr, Tyr, Ornithine, and Citrulline ($p \leq 0.01$) as well as Glu, Phe, Gly, and Asn ($p < 0.05$), of which their content was increased between 1.1 to 1.7-fold. In contrast, the levels of organic acids fumarate, α-ketoglutarate, and succinate were reduced by 1.4, 1.5, and 1.3-fold, respectively, compared to the levels in WT. After Pi starvation, the content of all analyzed proteinogenic amino acids as well as of ornithine, and citrulline was significantly higher in *ppck1-1* compared to WT, with Phe, Iso, Lys, Leu, Trp, and Tyr showing more than a two-fold difference. The Student's *t*-test p-value was below 0.001 for most amino acids except for Asp, Glu, Pro, and Arg. The α-ketoglutarate and succinate content was reduced by 2.4-fold and elevated by 1.4-fold, respectively in Pi-starved *ppck1-1* compared to WT.

In shoots, compared to the situation in roots, fewer metabolites were altered in *ppck1-1* line [Supplementary table 7-5(B)]. In Pi-replete *ppck1-1* line, significantly increased (around 1.2-fold) levels were observed for Asp, Glu ($p=0.04$), Asn, Ser, and citrulline, whereas around 1.1-fold reduced content of Phe and Trp was detected compared to WT. Levels of fumarate, alpha-ketoglutarate, and succinate were reduced by 1.1, 1.3, and 1.2-fold, respectively in *ppck1-1* shoots compared to WT. Between 1.1 to 1.5-fold increased levels of Ala, Cys, Glu, His, Lys, Met ($p=0.04$), Asn, Gln, Ser, Thr, and Tyr ($p=0.04$) were detected in Pi-depleted *ppck1-1* line compared to WT. Gly content was elevated by 2.3-fold in Pi-starved *ppck1-1*. Fumarate content was reduced by 1.2-fold and interestingly succinate content was elevated by 1.2-fold in Pi-starved *ppck1-1* compared to WT.

2.4.3 Metabolites altered in complementation lines

In roots, elevated levels (1.2 to 2.3 fold) of Asp, Lys, Pro, Gln, Ser, Trp, and Ile were detected in Pi-sufficient C-lines compared to WT. Fumarate content was reduced by 1.4-fold in C-lines compared to WT [Supplementary table 7-6(A)]. However, compared to *ppck1-1*, only the levels of Asp (between 1.3 and 1.5-fold higher) were significantly different in C-lines [Supplementary table 7-6(B)]. In Pi-starved C-lines, the content of 14 out of 20 proteinogenic amino acids (Ala, Cys, Phe, Iso, Lys, Leu, Met, Pro, Gln, Arg, Thr, Val, Trp, and Tyr) were significantly higher compared to the levels in WT. These amino acids were between 1.2 and 3-fold higher. Orn content was also between 1.7 and 3.2-fold higher compared to the levels in WT [Supplementary table 7-7(A)]. When compared to Pi-starved *ppck1-1*, the contents of Ala, Cys, His, Asn, and Ser were significantly reduced (1.2-2.6-fold) in C-lines. Pro levels were between 1.5 and 2-fold higher compared to *ppck1-1* [Supplementary table 7-7(B)]. Regarding the organic acids, fumarate and α-ketoglutarate content were elevated between 1.2 and 1.4-fold and diminished between 1.3 and 1.7-fold, respectively, in Pi-starved C-lines compared to WT.

In shoots, Asp, Glu, Asn, Pro, Lys, and Gln content of Pi-replete C-lines was higher compared to WT (between 1.2 and 1.6-fold). Gly content was reduced between 1.4 and 1.8-fold [Supplementary table 7-8(A)]. Compared to *ppck1-1*, Pi-replete C-lines exhibited lower levels of Gly, Ser, and Citrulline (between 1.2-1.5-fold), whereas Asp levels were between 1.2 and 1.5-fold higher [Supplementary table 7-8(B)]. After Pi-deficiency, Glu, Gln, and Orn content were significantly elevated in shoots of C-lines between 1.2-fold, 1.4 and 1.7-fold, and 1.7 and 2.1-fold, respectively, compared to WT [Supplementary table 7-9(A)]. Compared to *ppck1-1* seedlings, reduced levels of Ala, Cys, His, Ser, and Thr were detected in Pi depleted C-lines. The contents of these amino acids were reduced between 1.2 and 1.9-fold. The strongest decrease compared to *ppck1-1* was observed for Gly, for which the levels were reduced between 2.8 and 5-fold. Elevated levels of Asp and Pro (around 2-fold) were detected in Pi-starved C-lines compared to *ppck1-1* [Supplementary table 7-9(B)].

2.4.4 Metabolites altered in *ppck1-4* line

In roots of *ppck1-4* line, proteinogenic amino acids were not altered either under Pi-replete or Pi-depleted conditions compared to WT. However, Orn content was higher in Pi-replete *ppck1-4* compared to WT by 2.4-fold. Levels of organic acids- fumarate and succinate were reduced by around 1.3-fold under Pi-sufficient condition compared to the levels detected in WT. In Pi-depleted condition, fumarate, α-ketoglutarate, and succinate levels were reduced by 1.4, 2.1, and 1.3-fold, respectively, compared to WT [Supplementary table 7-10(A)].

In shoots, levels of Cys, Thr, and succinate were reduced by around 1.2-fold in Pi-sufficient *ppck1-4* compared to WT. However, in Pi-depleted *ppck1-4*, elevated levels of Ala, Cys, Asn, Thr were detected compared to WT. The α-ketoglutarate content was reduced by 2.1 fold in *ppck1-4* compared to WT [Supplementary table 7-10(B)]. Amino acid analysis in *ppck1-4* plants was performed only once due to time reason and need to be repeated again for confirmation.

2.4.5 Metabolites altered in *ALMT1^{OE}*

In roots [Supplementary table 7-11(A)], fewer metabolites were altered in Pi-sufficient *ALMT1^{OE}* compared to WT. Levels of amino acids, Lys and Orn were elevated by 1.5-fold, whereas Phe levels were reduced by 1.3 (p=0.04). Fumarate and α-ketoglutarate contents were reduced and elevated by 1.2-fold, respectively in *ALMT1^{OE}* compared to WT. Levels of 18 out of 20 proteinogenic amino acids, except Glu and Arg, were elevated in Pi-starved *ALMT1^{OE}* compared to WT. These amino acids were elevated between 1.7 and 3-fold, except Iso which was elevated by around 4-fold. Ornithine, and citrulline contents were elevated by around 3-fold in Pi-starved *ALMT1^{OE} c*ompared to WT. Among organic acids, levels of fumarate and succinate were elevated by 1.5-fold and 1.3-fold, respectively, whereas α-ketoglutarate content was reduced by around 3-fold in *ALMT1^{OE}* compared to WT.

In shoots [Supplementary table 7-11(B)], levels of Asp, Lys, and Val were elevated by around 1.2-fold in Pi-replete *ALMT1^{OE}* compared to WT. Succinate and α-ketoglutarate contents were reduced by 1.2 and 1.4-fold, respectively. Compared to Pi-starved roots of *ALMT1^{OE}*, fewer amino acids were altered in Pi-starved shoots. These amino acids were Lys, Met, Pro, Arg, Trp, Tyr, and Orn, which were elevated between 1.5 and 3-fold in *ALMT1^{OE}* compared to WT. Slight but significant reduction in Ser content by 1.1-fold was also detected. *ALMT1^{OE}* exhibited elevated content of succinate by 1.3-fold compared to Pi-depleted WT. Similar to *ppck1-4* plants, amino acid analyses in *ALMT^{OE}* lines were also performed only once due to time reason and need to be repeated again for confirmation.

3 DISCUSSION

3.1 Role of individual PPC isoforms in Arabidopsis

The expression analysis by RT-qPCR revealed that all the three plant-type *PPC*s (*PPC1*, *PPC2*, and *PPC3*) were expressed in roots and shoots with differences in their relative abundance, suggesting different functions for each isoform in the respective tissues. In shoots, PPC2 seems to be the predominant isoform based on its higher transcript levels compared to PPC1 or PPC3. This is in agreement with published data (Feria et al., 2016; Gousset-Dupont et al., 2005; Sánchez et al., 2006; Shi et al., 2015). Furthermore, it was reported that the total extracted PPC activity was reduced only in shoots of *ppc2* plants (Feria et al., 2016), but not in *ppc1* or *ppc3* plants. This is corroborated by reduced malate content, which was detected only in shoots of *ppc2* plants in the present study. Interestingly, citrate content was elevated in shoots of *ppc2* plants only. The increase in citrate content observed in *ppc2* plants could be due to the higher availability of PEP for the PK reaction because of its restricted conversion to OAA as a consequence of loss of *PPC2*. This could shift the metabolic flux towards the TCA cycle for citrate generation. However, such a hypothesis need to be tested by metabolic flux analysis. Nevertheless, the changes in malate and citrate levels only in *ppc2* underscores the predominant role of PPC2 in shoots. However, Shi et al. (2015) did not observe any alteration in malate and citrate levels in the same T-DNA insertion line of *PPC2* (SALK_025005; *ppc2*-2) analyzed in this study. The reasons for such contradiction could be that they analyzed the metabolites in entire seedlings rather than in roots and shoots separately as done in this study or because of the differences in growth conditions of the seedlings. Plants in their experiment were grown on ½ MS medium for 10 days in incubators with a photon flux density of 60 to 80 µmol m^{-2} s^{-1} at 22° C which is different from the growth conditions used in this study.

Based on transcript abundance, *PPC2* seems to play a minor role in roots because the expression of *PPC1* and *PPC3* was higher than *PPC2*. This is in agreement with published data (Shi et al., 2015). However, the present study showed that *PPC1* mRNA levels are most abundant in roots contradicting other studies showing *PPC3* as the predominant PPC isoform in roots (Feria et al., 2016; Sánchez et al., 2006). One explanation for such discrepancy might be due to the differences in plant age used for analysis since they analyzed relatively older plants. This also suggests that individual PPC isoforms might exhibit distinct roles during root growth and development since plant roots at different growing stages showed differences in expression of individual PPCs. In this study, reduced malate content in roots of all the *ppc* mutants suggested an important role of individual PPC isoforms. This contradicts a report showing reduced total PPC activity only in root extracts of *ppc3* plants, which suggested a predominant role of PPC3 in roots (Feria et al., 2016). However, in the present study analysis of *PPC3*

transcript levels in the same T-DNA insertion line of *PPC3* (SALK_031519C; *ppc3-1*) used by Feria et al. revealed similar transcript levels between the mutant and WT. Thus, reduced total PPC activity observed in their study was probably not due to loss of *PPC3*. Therefore, results from our study might represent a more accurate picture of the role of individual PPC isoforms in roots, since all *ppc* mutants analyzed in this study showed reduced transcript levels including the novel T-DNA insertion line of *PPC3* (SALK_143289.54.75X; *ppc3-2*). Citrate content was not altered in roots of any *ppc* mutants in contrary to changes observed in shoots. This finding suggests that under unstressed conditions, the PPC pathway in roots is more involved towards malate biosynthesis in the cytosol than towards anaplerotic feeding of the TCA cycle to support citrate biosynthesis. However, this is speculative and requires confirmation by metabolic flux analysis.

Pi-starvation induced the expression of all three plant type *PPC*s in roots and shoots of Arabidopsis. However, the extent of increase in their transcript abundances was different for each of these genes. The fold inductions in transcript levels of *PPC3* were highest followed by *PPC1* and *PPC2* in shoots*,* but transcript abundance was still higher for both *PPC1* and *PPC2* than *PPC3.* This finding together with the results that mutants with impaired expression of all three *PPC* genes exhibited lower malate levels when grown under Pi deficient conditions indicate that all PPC isoforms contribute to Pi deficiency-induced malate accumulation in shoots. Increase in transcript abundance of *PPC1* and *PPC2*, but not of *PPC3* was also detected after Pi-starvation in shoots of Arabidopsis in two other studies (Feria et al., 2016; Gregory et al., 2009). Inductions in *PPC3* transcripts were not observed in their studies probably due to the differences in age and growth condition of the seedlings used for their analysis. Gregory et al. cultured Arabidopsis seedlings in ½ MS medium supplemented with 200 µM Pi at 24°C under a 16/8-h light/dark cycle; the medium was replaced with fresh medium containing 3 mM or 20 µM Pi on 7th day; on day 14 the medium was replaced again and on the 21st day, roots and shoots were harvested for analysis. Feria et al. used hydroponics system where seeds were germinated on ½ MS medium in tubes placed in Araponics systems and cultivated them for a total of 5 weeks on medium with or without Pi under short-day conditions before harvest. Whereas in the present study, seedlings were germinated on medium supplemented with 500 µM Pi for 6 days in a growth chamber at 22° C under illumination for 16 h daily (170 µmol s^{-1} m^{-2}); transferred to medium with Pi (500 µM) and without Pi (5 µM) and allowed to grow for additional 5 days before harvesting. Possibly, the role of individual PPC isoforms during Pi starvation might be dependent on plant age and development, however, until and unless it is known to what extent changes in transcript abundances of *PPC1*, *PPC2*, and *PPC3* are translated into their respective protein abundances, it is hard to estimate the contribution of individual PPC isoform to malate accumulation under these conditions in Arabidopsis.

In roots of Pi-depleted seedlings, fold induction in the expression of *PPC1* and *PPC2* were similar and slightly higher than for *PPC3*. However, transcript abundance was much higher for *PPC1* than for *PPC2* and *PPC3*, suggesting a predominant role of PPC1 in roots of Pi-starved seedlings. This was also supported by a strong decline in root malate content of only *ppc1*, but not of *ppc2* and *ppc3* plants. The present expression analysis is in agreement with the study of Gregory et al., (2009), who reported increased expression of all the three *PPC* isoforms in roots after Pi-starvation. However, only *PPC3* transcript levels were reported to be elevated in roots after Pi-starvation by Feria et al., (2016). This discrepancy in result could again be due to the differences in age and growth condition of the analyzed seedlings and could indicate that the Pi deficiency response in roots with respect to the induction of *PPC*s might depend on their developmental stage.

Induction in the expression of *PPC1*, *PPC2*, and *PPC3* after Pi-starvation in roots was lower in *phr1/phl1* plants indicating that the activation of *PPC* genes is under control of PHR1 and PHL1, the major regulators of systemic Pi deficiency responses. This is further supported by the presence of PHR1 binding site (P1BS sequence GAATATTC) in the promoters of both *PPC1* and *PPC3* (Feria et al., 2016). *PPC2* is also regulated by PHR1 and PHL1 according to the present study, although it was reported to lack these P1BS binding sequences (Feria et al., 2016). Probably *PPC2* belongs to the few Pi starvation-induced genes, which are controlled by PHR1 and/or PHL1 independent of the presence of the P1BS sequences in their promoter (Bustos et al., 2010). It has not yet been established how the regulation of these genes is mediated by PHR1/PHL1, but the differences in these conserved promoter elements between the *PPC* genes also suggest distinct functions of the PPC isoforms.

Citrate content was not affected in roots and shoots of any *ppc* mutant under Pi-depleted condition, which is contrary to the results obtained under Pi sufficient condition. This suggests that when Arabidopsis seedlings are exposed to Pi-deficient conditions, the PPC pathway might contribute more towards malate than towards citrate biosynthesis in roots. Again, considering increased malate exudation after Pi-starvation in WT seedlings, it can be assumed that the PPC pathway together with cMDHs predominantly generates malate in the cytosol for exudation instead of shuttling the PPC pathway products into the mitochondria to replenish the TCA cycle for citrate generation in Arabidopsis. Metabolic flux analysis performed in Arabidopsis suspension cells pointed to a similar direction, showing only a minor contribution of the PPC pathway to anaplerotic replenishment of the TCA cycle intermediates in Pi-depleted growth conditions (Masakapalli et al., 2014). However, similar experiments need to be performed with seedlings to determine whether such a scenario also applies to roots and shoots of Pi-depleted Arabidopsis.

3.2 Role of PPCK isoforms in Arabidopsis

PPCK1 represents the predominant isoform of both kinases in roots as well as in shoots under Pi-sufficient condition based on transcript levels. This is corroborated by the analysis of plants deficient in *PPCK1*, which showed strongly reduced malate levels, indicating that the functional PPCK2 isoform in the *ppck1* mutants cannot compensate for the loss of *PPCK1*. Several studies claim predominant expression of *PPCK1* and *PPCK2* in shoots and roots, respectively (Feria et al., 2016; Fontaine et al., 2002). However, in the study by Fontaine et al., the relative expression of these two genes in each organ could not be compared due to different RT-PCR conditions used for the analysis of these two genes. The possible reason for detecting higher *PPCK2* expression in roots compared to *PPCK1* in the study by Feria et al. might be due to the differences in age and growth condition of the seedlings analyzed, which were similar as described above for *PPC* expression analysis in section 3.1. This indicates that PPCK isoforms could also exhibit distinct roles during root growth and development.

Induction in the expression of *PPCK1* and *PPCK2* was detected both in roots and shoots after Pi-starvation by RT-qPCR and promoter-reporter analysis, which is in agreement with published data (Chen et al., 2007; Gregory et al., 2009; Morcuende et al., 2007; Müller et al., 2007). However, Feria et al. (2016), reported induction of only *PPCK2* but not *PPCK1* in roots, suggesting that *PPCK2* represents the predominant isoform in Pi-starved roots. The reason for not observing *PPCK1* induction in roots in their study could be due to differences in the age and growth condition of the seedlings analyzed and could indicate that the Pi deficiency response with respect to the induction of *PPCK*s depends on the developmental stage of the roots. The fold induction in transcript levels of *PPCK2* was stronger than *PPCK1* in both roots and shoots of Arabidopsis. Similar results were also reported in Arabidopsis suspension cells showing a less pronounced change in *PPCK1* expression compared to *PPCK2* after Pi-deficiency treatment (Chen et al., 2007). These results suggest that the PPCK2 isoform is more important during Pi-starvation in Arabidopsis. However, it was revealed in the present study that *PPCK1* transcript levels are higher than *PPCK2* transcript levels both in roots and shoots of Pi-depleted Arabidopsis seedlings, indicating a predominant role for PPCK1 during Pi-starvation. And, similar to Pi-sufficient condition, functional PPCK2 in *ppck1* mutants could not compensate for the loss of *PPCK1* with respect to malate content under Pi-deficient condition. This further supports the predominant role of *PPCK1* during Pi-starvation and also suggests different function of both kinases in roots and shoots of Arabidopsis. However, analysis of *PPCK2* knock-out plants is required in order to understand the contribution of each kinase during Pi-starvation in Arabidopsis. Additionally, it needs to be determined to what extent the transcript abundances of both kinases are translated into their respective protein abundances after Pi-starvation.

Induction in *PPCK1* transcripts was completely under the control of the systemic response regulator PHR1 and its close homolog PHL1, which is consistent with the presence of the sequence homologous to the cis-element of phosphate starvation responsive genes in the 5' region of *PPCK1* (Feria et al., 2016). However, the present study showed that induction in *PPCK2* expression was only partially regulated by PHR1 and PHL1, although the PHR1 binding sequence is also present in the promoter of *PPCK2* (Feria et al., 2016). This suggests that *PPCK2* might also be regulated by additional mechanisms and there might be different roles for PPCK1 and PPCK2 during Pi starvation in Arabidopsis.

There is one inconsistency between the expression data obtained by RT-qPCR and promoter-reporter analysis in this study. GUS activity or GFP fluorescence could only be detected in roots of Pi-replete *pPPCK2$_{long}$::GFP-GUS* lines and not in *pPPCK1$_{long}$::GFP-GUS* lines, although *PPCK1* transcript levels were higher than *PPCK2* in roots. This might be due to the higher stability of *PPCK1* transcripts compared to *PPCK2* transcripts because of the presence of additional regulatory elements in the intron or in the 3'-UTR region of the *PPCK1* gene which is absent in the reporter construct. With GUS reporter assays, induction in promoter activity of both *PPCK1* and *PPCK2* was detected in shoots, roots, as well as in root-tips. However, analysis of GFP-fluorescence after Pi-starvation revealed a difference between *PPCK1* and *PPCK2* promoter activity. GFP fluorescence driven by *PPCK1* promoter was only detected in roots and root tips but not in shoots, unlike GFP fluorescence driven by *PPCK2* promoter. The absence of *PPCK1* promoter-driven GFP fluorescence in shoots could be due to the autofluorescence of chlorophyll masking the low expression of *PPCK1*. However, this result indicates that *PPCK1* promoter activity is lower than the *PPCK2* promoter activity in shoots which also contradicts the RT-qPCR data. Detection of GUS activity but not GFP fluorescence in shoots of *pPPCK1::GUS-GFP* lines could be due to the high stability of GUS, which can accumulate over time.

ALMT1 mediated malate exudation in the transition zone together with the LPR1 catalyzed Fe-redox cycling is important for root growth inhibition (local response) during low Pi-stress in Arabidopsis. (Abel, 2017; Balzergue et al., 2017; Mora-Macías et al., 2017). Induction in the expression of *PPCK1* and *PPCK2* in root-tips overlapped with the expression domains of *ALMT1* and *LPR1* suggesting that the required malate for ALMT1 mediated malate exudation in the root-tips for triggering low Pi-induced root shortening might be generated by the PPC pathway. Induction in the expression of *PPCK1* and *PPCK2* in roots tips is also systemically regulated as revealed by the split plate assays. This suggests the contribution of systemically generated malate by PPC pathway in mediating local response during Pi-starvation in Arabidopsis. Moreover, a predominant role of *PPCK1* for malate generation in root-tips during Pi-starvation is suggested because the induction in GUS reporter activity driven by *PPCK1* was faster compared to *PPCK2*, preceding the first visible signs of alteration in root morphology (after day 6 of transfer). Also, slight insensitivity of *ppck1-4* plants with respect to Pi deficiency-induced

primary root growth shortening which correlated with their reduced malate exudation further supports the importance of PPCK1 to regulate malate generation for exudation in the context of local Pi starvation response. Complementation of *ppck1-4* line needs to be performed and/or other *ppck1* knock-out lines need to be analyzed in order to substantiate this finding. The contradicting hypersensitive root growth phenotype of *ppck1-1* line was due to increased malate exudation, probably due to a second site insertion disrupting the expression of *ALMT1* and *ALMT2*, discussed later in more detail in section 3.9. Analysis of plants deficient in *PPCK2* would be needed to further elucidate the contribution of both kinases to malate exudation during the local Pi-starvation response.

3.3 Subcellular localization of PPCKs in Arabidopsis

This is the first report showing cytosolic localization of PPCKs *in vivo* using C and N-terminally tagged PPCK1 and PPCK2 under control of the *CaMV 35S* promoter, confirming the previous biochemical data. C-terminally tagged PPCK1 under control of its own promoter also showed cytosolic localization. Both PPCK1 and PPCK2 were also detected in moving bodies randomly distributed in the cytosol. It has been reported that PTPC in developing COS endosperm and cotyledons are attached to the surface of mitochondria (Park et al., 2012). Since PPCKs must interact with PPCs in order to phosphorylate them, the moving bodies observed in the present study were hypothesized to be mitochondria. However, attempts to associate the GFP labeled bodies to any organelles were not successful so far and therefore the identification of these moving bodies need further investigation in future. However, it is possible that these moving bodies do not represent any organelles but are rather aggregates of degraded proteins. Aggregates are commonly observed because of the higher amounts of overexpressed proteins especially when they are expressed under the control of strong constitutive promoters (Khachatoorian et al., 2015; Zhang et al., 2004).

PPCK1 was also localized to these moving bodies when expressed under its own promoter showing lower *PPCK1* expression compared to when expressed under the control of *UBQ10* and *35S* promoter. However, *PPCK1* transcript levels when expressed under its native promoter were still higher compared to untransformed plants. It is known that the transgene expression among independent transformants can differ greatly, depending on the copy number of insertions, on the insertion site of the transgene into the genome or because of silencing effects (Głowacka et al., 2016). Although, segregation analysis suggested the single insertion of *pPPCK1::PPCK1-GFP* construct in the genome of *ppck1-1* line*,* one cannot exclude multiple insertions occurring at a single locus which remains undetected by segregation analysis (Głowacka et al., 2016). Therefore, the formation of protein aggregates because of higher protein levels is possible despite the use of native promoter. Unless these moving bodies are identified as organelles using appropriate organellar markers (e.g.

mitochondria, peroxisomes, and golgi bodies), the possibility that these moving bodies are simply protein aggregates can not be ruled out. Additionally, the localization studies should be performed in the *ppck1-4* background instead of *ppck1-1* containing a second site insertion.

3.4 Contribution of PPCK1 and PPCK2 to malate and citrate generation

Loss of *PPCK1* led to the expected chemotypes with respect to organic acid content suggesting that decreased phosphorylation of PPCs lead to stronger feedback inhibition by malate and lower activity of the PPC pathway. However, there seem to be differences between roots and shoots in the contribution of *PPCK1* and *PPCK2* to malate and citrate generation. The decrease in malate and citrate content in roots of both *PPCK1* knock-out lines (*ppck1-1* and *ppck1-4*) suggests that *PPCK1* is mainly responsible for the biosynthesis of both organic acids in roots. Unaltered expression of *PPCK2* in roots of both these lines indicates that PPCK2 cannot compensate for the loss of PPCK1 in these lines.

In shoots, malate content was affected in both lines but citrate levels were reduced only in *ppck1-1* line. Considering that *PPCK2* transcript levels in Pi-sufficient shoots of *ppck1-1* and *ppck1-4* plants were lower and higher respectively, it might be assumed that PPCK2 contributes to citrate biosynthesis whereas PPCK1 is more important for malate biosynthesis in shoots. As such, lower *PPCK1* and *PPCK2* transcript levels in *ppck1-1* results in lower malate and citrate levels, whereas lower transcript levels of only *PPCK1* results in lower malate levels in *ppck1-4* plants. However, an effect of the second site insertion in the *ppck1-1* line leading to unspecific disturbance in metabolism cannot be ruled out. Therefore, more investigations using plants deficient in *PPCK2*, or complementation lines of *ppck1-4* are necessary to substantiate the assumption of the different role of both kinases to malate or citrate generation in Arabidopsis. Additionally, it needs to be confirmed whether the altered *PPCK2* transcript levels in shoots of *ppck1-1* and *ppck1-4* also lead to altered PPCK2 protein levels. Pi-sufficient *ppck1-5* plants exhibited different chemotypes compared to *ppck1-1* and *ppck1-4* plants. They only showed reduced root malate content but no differences in root citrate content, or shoot malate and citrate content possibly because it exhibited only a very slight reduction in *PPCK1* transcript levels (around 1.3 fold). The data from this study contradicts the report where no difference in malate and citrate content compared to the WT plants was detected in other *ppck1* lines, *dln1* and *csi8*, isolated from the Versailles T-DNA mutant library (INRA Versailles, France) (Meimoun et al., 2009). Possible reasons for observing such differences could be the age and growth condition of the plants as well as the tissue analyzed. In the study of Meimoun et al., 2009, metabolites were measured from rosette leaves, unlike in our study where metabolites were measured from root and shoot separately. Moreover, the mutants analyzed in their study were in the Arabidopsis Wassilevskija ecotype background compared to mutants in this study, which were in the Col-0 background.

After Pi-starvation in all three *ppck1* lines (*ppck1-1*, *ppck1-4*, and *ppck1-5*), root malate and citrate content, but only shoot malate content was diminished. This suggests that phosphorylation of PPCs by PPCK1 contributes to Pi deficiency-induced malate and citrate generation in roots, but only to malate generation in the shoots. Based on these results, it might be assumed that citrate generation in shoots depends on PPCK2 activity. Indeed, shoot citrate content in Pi-starved *ppck1-4* (and also *ppck1-5*) seedlings were higher compared to WT plants which could be correlated to elevated *PPCK2* transcript levels which might have different PPC targets in shoots. However, shoot citrate content after Pi-starvation was not altered in plants overexpressing *PPCK2*. Therefore, the higher availability of PEP for the PK reaction providing more precursors for the TCA cycle because of the absence of functional *PPCK1* in *ppck1-4* (and also *ppck1-5*) line could be a more likely explanation for detecting an increase in shoot citrate content in these lines. This is supported by a preliminary data showing a slight increase in pyruvate content in *ppck1-4* plants further strengthening the assumption that the increased citrate content observed in *ppck1-4* plants after Pi-starvation could be due to the higher availability of PEP for the PK reaction. It is still surprising that the increase in citrate content occurred only in shoots, whereas it was reduced in roots. It is reported that Pi-starvation triggers induction in the expression of *PK* in shoots of Arabidopsis, whereas it is unaltered or only slightly increased in roots (Wu et al., 2003). Thus, in shoots of *ppck1-4* and *ppck1-5* plants increased availability of PEP together with elevated expression of PK might have led to elevated citrate biosynthesis after Pi-starvation.

Analysis of plants deficient in *PPCK2* and also more experiments such as determination of the specific activity of PPCs, and their phosphorylation status in roots and shoots of *ppck1* and *ppck2* mutants are required in future to elucidate the contribution of PPCK1 and PPCK2 to malate and citrate generation both under Pi-sufficient and Pi-deficient conditions. It was shown already that PPC activity was not affected in Pi-replete and Pi-depleted roots and shoots of *ppck1* and *ppck2* mutants (Feria et al., 2016). Curiously, Pi-starvation induced PPC phosphorylation was affected only in roots of *ppck2* plants in their study suggesting a predominant role of PPCK2 to phosphorylate PPCs in roots after Pi-starvation. However, the T-DNA insertion line in which they observed the effect is *ppck2-1* line (SALK_102132) tested in this study, for which RT-qPCR analysis revealed higher *PPCK2* transcript levels compared to WT. Therefore, the observed reduction in phosphorylation of PPCs in *ppck2* lines in the study by Feria et al. was not due to the absence of *PPCK2* but was rather due to some other reasons. The results obtained by Feria et al., are hardly comparable to the results presented here.

3.5 Effect of *PPCK* overexpression on malate content under Pi-sufficient conditions

The major objective of the present study was to explore the possibility of modifying PPC pathway activity and to increase malate levels by overexpression of *PPCK*s. Transgenic lines having increased expression of *PPCK1* and *PPCK2* exhibited elevated malate content in roots when grown under Pi-sufficient conditions. This indicates higher PPC activity based on lower malate feedback inhibition as a consequence of stronger phosphorylation by overexpression of the kinases. However, in shoots of these lines, malate levels were indistinguishable from WT. It was reported that the phosphorylation state of PPCs in shoots is higher than that in roots, although PPC and PPCK activity is higher in roots than in shoots (Willick et al., 2019). Therefore, the probable reason for detecting unaltered malate content in shoots of *PPCK* overexpressors might be that PPCs in shoots are already highly phosphorylated so that additional PPCKs might have a very marginal effect. PPC phosphorylation state in roots and shoots of plants overexpressing *PPCK*s need to be determined in order to further substantiate this assumption. The lack of malate accumulation in shoots of *PPCK* overexpression lines might also indicate that the abundance of PPCs as PPCK targets are rate-limiting in shoots. This result is also corroborated by a study on transgenic alfalfa plants overexpressing *PPCK3* from soybean (Sun et al., 2014), where it was shown that PPC activity which is a measure of PPC phosphorylation was not altered in leaves under control conditions. Whereas the data on PPC phosphorylation or PPC activity in roots was not provided in their study.

Nevertheless, results from this study showed that the PPC pathway can be successfully engineered for modified malate generation by overexpression of *PPCK*s at least in roots. Moreover, the elevated malate content detected in these transgenic lines is probably not due to a general effect on the metabolism of these lines but are rather specific effects of elevated PPC phosphorylation, since only a few out of many analyzed metabolites were altered in these lines. Furthermore, these changes were observed only for metabolites which are directly linked to the PPC/PPCK pathway, like Asp and Phe. Elevation in levels of Asp which is derived from OAA, and reduction in levels of Phe which is derived from PEP, suggested that PEP is utilized more towards OAA generation for malate biosynthesis than towards its conversion to Phe via the shikimate pathway, by overexpression of *PPCK*s.

In this study, malate levels were elevated between 1.2 and 1.7 fold and a further increase in malate levels were not detected in any of these transgenic lines. Moreover, no correlation could be established between malate content and *PPCK* transcript levels in these lines. Although it is unknown whether the elevated *PPCK* transcripts in these lines are also reflected in the PPCK protein levels, our analysis suggests that there is a certain capacity of plants beyond which further increase in malate content is not possible by overexpression of *PPCK*s. So far, there is no information available on the effect of overexpression of *PPCK*s on the endogenous malate content. Most of the information is

available only from studies on overexpression of *PPC*s from C4 plants or from bacterial sources in C_3 plants (Agarie et al., 2002; Bandyopadhyay et al., 2007; Demao et al., 2001; Ding et al., 2013; Fukayama et al., 2003; Hudspeth et al., 1992; Jiao et al., 2002; Kogami et al., 1994; Ku et al., 1999; Suzuki et al., 2006; Taniguchi et al., 2008). Therefore, one to one comparison of these studies with the present study is not possible. Also, malate levels were not consistently determined in most of these studies since their major emphasis was only to improve the photosynthetic efficiency of C3 plants. In those studies where malate levels were analyzed, it was reported to be higher with increased PPC activity (Agarie et al., 2002; Begum et al., 2005; Häusler et al., 1999; Hudspeth et al., 1992; Kogami et al., 1994; Rademacher et al., 2002). Thus, endogenous malate levels can also be elevated by overexpression of *PPC*s. Interestingly, although extracted PPC activities were much higher in some of the transgenic lines, a similar increase in malate content was detected compared to the lines with relatively lower PPC activities (Begum et al., 2005). This indicates that by overexpression of *PPC*s also elevation in malate content beyond a certain limit is not possible. However, the *in vitro* PPC activity measurements of the extracted PPCs are not indicative of *in vivo* PPC activity, since in this kind of assays distinction between phosphorylated and non-phosphorylated PPCs is not possible, and thus the feedback inhibition by malate could not be established. Therefore, in transgenic plants overexpressing *PPC*s, *in vivo* PPC activities can be completely different from the *in vitro* condition. Nevertheless, both approaches showed, that modulation of malate content beyond a certain limit was not possible by overexpression of either *PPC*s or *PPCK*s alone. Possible reasons leading to the observed saturation in root malate content in transgenic plants overexpressing *PPCK*s could be as followed:

1) PPCs might be rate-limiting in these transgenic lines, and therefore further phosphorylation of PPCs by overexpression of *PPCK*s alone might not be sufficient for further increase in malate content. Thus, overexpression of *PPC*s and *PPCK*s together might aid in achieving a further increase in malate content.

2) In addition to PPCs, MDHs which are known to work in conjunction with PPCs to generate malate from PEP (Maurino and Engqvist, 2015) can also be rate-limiting. Plants overexpressing *cMDH* from Arabidopsis and *MDH* from Escherichia have also been shown to accumulate more malate in both leaves and roots of tobacco plants (Wang et al., 2010). Therefore, transgenic plants overexpressing *MDH*s with *PPC*s and *PPCK*s could also be generated to investigate if these plants exhibit more malate levels than plants overexpressing these genes alone.

3) The substrate of the PPC reaction, PEP, might also become rate-limiting in *PPCK* overexpressors. PEP is the substrate for three more metabolic routes in plants: for mitochondrial respiration associated with PK, for the biosynthesis of isoprenoids in chloroplast through the methylerythritol-4-phosphate (MEP) pathway, and for the shikimate pathway (Dizengremel et al., 2012). Therefore, PEP

availability might become limiting for the PPC reaction in transgenic plants overexpressing *PPCK*s. Although reductions in endogenous PEP content was not observed in our preliminary experiments, a decrease in Phe content in *PPCK* overexpression lines suggests that PEP might become rate-limiting.

4) Malate generated in these transgenic lines might act as a negative regulator of PPCKs itself. PPCK from developing castor oil seeds and banana were shown to be inhibited by 10 mM malate (Law and Plaxton, 1997; Murmu and Plaxton, 2007). However, whether malate can also act as a negative regulator of PPCKs from Arabidopsis needs further verification.

5) PPC is allosterically regulated by Asp, which acts as its negative regulator (Gregory et al., 2009). Therefore, feedback inhibition of PPCs due to increased levels of Asp generated in *PPCK* overexpressors could also be a possible reason for observing saturation in the malate levels.

6) Due to the increased conversion of PEP to OAA in *PPCK* overexpressors, levels of glucose-6-phosphate, an allosteric activator of PPC (Gregory et al., 2009), might be reduced due to its increased conversion through other glycolytic intermediates to PEP, thereby reducing the PPC activity. In order to substantiate this, glucose-6-phosphate levels should be determined in *PPCK* overexpressors.

7) Elevated malate exudation in transgenic plants overexpressing *PPCK*s suggests that excess malate generated can be exuded from the roots. In fact, exudation of organic anions was suggested primarily as a means to prevent cytoplasmic acidosis, which could result from their excessive accumulation in roots (Neumann et al., 2000). It is possible that after reaching a certain limit in endogenous malate content, the excess malate might be exuded by the plant roots and therefore further elevation in endogenous malate content is not possible.

3.6 Effect of *PPCK* overexpression on citrate content under Pi-sufficient conditions

One role of the PPC/PPCK pathway is to replenish the TCA cycle, from which carbon intermediates are withdrawn to support anabolism (O'Leary et al., 2011). Increased levels of citrate were detected in roots of transgenic plants overexpressing *PPCK1* under Pi-sufficient condition. CS is responsible for catalyzing the production of citrate as the first committed step of the TCA cycle and, unlike other TCA cycle enzymes, it is exclusively localized in mitochondria. Therefore, in transgenic lines overexpressing *PPCK1*, elevated citrate must have been generated in mitochondria, suggesting that elevated OAA or malate generated in the cytosol by overexpression of *PPCK*s entered the TCA cycle. There are four possible routes for elevated citrate generation in mitochondria of transgenic plants overexpressing *PPCK1* [Figure 3-1]. 1) OAA generated in the cytosol by the PPC/PPCK pathway can enter the mitochondria where it can be condensed with acetyl-CoA to generate citrate by CS, 2) OAA can first be converted to malate by cMDHs in the cytosol, which can then be transported to mitochondria

where it can be converted back to OAA by mMDHs and finally OAA can condense with acetyl-CoA by the action of CS to generate citrate, 3) Malate, either imported from the cytosol or generated in the mitochondria can be converted by mitochondrial NAD-ME to pyruvate and further to OAA by pyruvate carboxylase (PC) (Yakunin and Hallenbeck, 1997) or to acetyl-CoA by the pyruvate dehydrogenase complex (PDC) (Tovar-Mendez et al., 2003). Both OAA and acetyl-CoA can finally be utilized to generate citrate in the mitochondria, and 4) Cytosolic malate can be decarboxylated by cytosolic NADP-ME to pyruvate (Gerrard Wheeler et al., 2008), which is then transported to mitochondria where it can be converted to OAA or to acetyl-CoA by the action of PC and PDC, respectively. OAA or acetyl-CoA can finally be converted to citrate by CS.

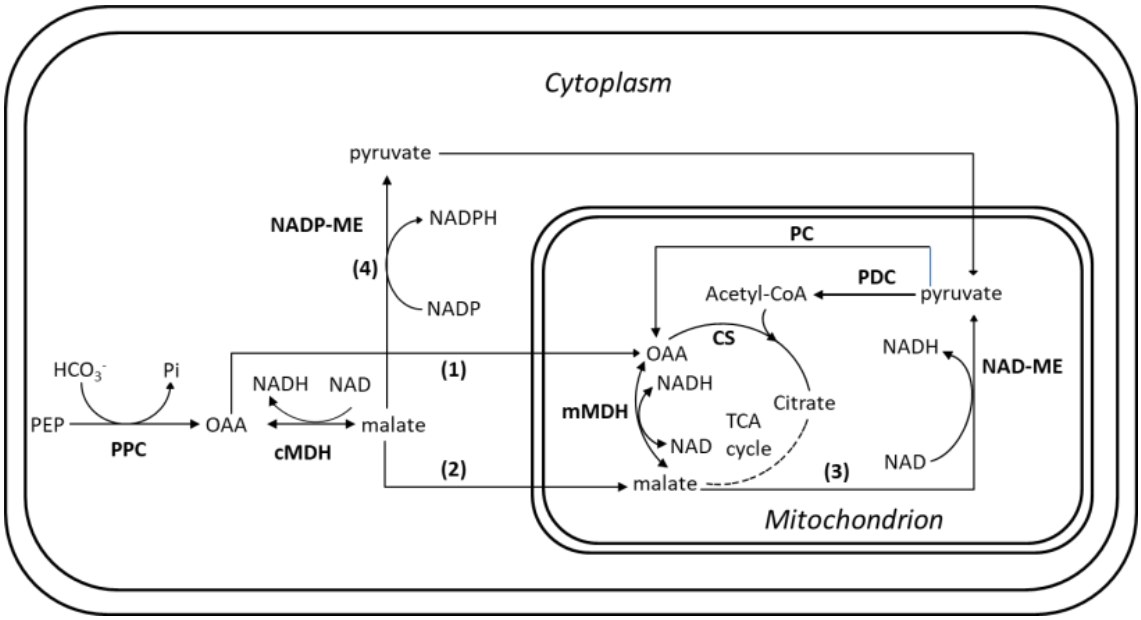

Figure 3-1: Possible routes of citrate generation in plants overexpressing *PPCK1* under Pi-sufficient condition

The four routes are indicated with numbers in parenthesis and are explained in detail in the text.

In preliminary experiment, which require confirmation by repetition, it was found that pyruvate content is not altered in seedlings of *PPCK1* overexpressors, suggesting that elevation of citrate content in these lines is not due to conversion of malate either by cytosolic or mitochondrial ME to pyruvate but rather due to the direct incorporation of OAA and/or malate into the TCA cycle. However, tracer studies are needed to elucidate this further. But even with tracer studies, which could distinguish between direct or indirect incorporation of OAA or malate into the TCA cycle, it would be very challenging to distinguish between routes (1) and (2). This is because malate and OAA can easily be transported between the mitochondria and cytosol through carriers with broad substrate specificity: the dicarboxylate carrier (DIC) and the dicarboxylate-tricarboxylate carrier (DTC) (Maurino and Engqvist, 2015).

Interestingly, elevated endogenous citrate content could only be observed after overexpression of *PPCK1*, but not of *PPCK2*, suggesting that the PPC isoforms responsible for feeding the TCA cycle are specifically activated by PPCK1. On the other hand, citrate exudation was increased in *PPCK2* overexpressors, suggesting that in these plants the biosynthesis of citrate was also higher. Whether this is a specific effect of *PPCK2* overexpression requires further investigations, since elevated citrate exudation was also detected in two out of four independent transgenic lines overexpressing *PPCK1*, which might be due to the positional effect of transgene. Therefore, increased citrate exudation might also be due to positional effects in *PPCK2* overexpressors. Analysis of citrate transporters like MATE in roots might further give information on whether overexpression of *PPCK1* and *PPCK2* have different influence on citrate transporters. It is also possible that high internal citrate levels might trigger citrate exudation, but more investigations are needed in order to confirm this. This seems to be the case for malate in *PPCK1* and *PPCK2* overexpressors, since increase in malate biosynthesis also led to increased malate exudation in these lines, suggesting that internal malate levels could indeed determine malate exudation. However, expression of *ALMT1* was unaltered in these lines questioning the relevance of this hypothesis, but an effect of elevated malate biosynthesis on other malate channels or transporters cannot be excluded.

3.7 Effect of *PPCK* overexpression on malate and citrate content under Pi-deficient conditions

Overexpression of both *PPCK*s had similar effects after Pi-starvation, showing no influence on endogenous malate content compared to WT. Possibly, the strong induction of *PPCK*s together with *PPC*s under Pi depleted conditions results in strong and perhaps saturated PPC phosphorylation already in the WT, so that additional PPCKs might only have a marginal effect. However, considering the stronger malate exudation in these lines, generation of malate must have also been higher. As such, and as emphasized above, it is reasonable to assume that overexpression of *PPCK*s results in excess malate generation, which is then exuded by plants. However, it is difficult to calculate the amount of produced malate in these plants because exudation was determined during 2 h of incubation. Interpolation of malate exudation during this 2 h to 6 days of growth on Pi-depleted condition might not be accurate since this would postulate constant malate exudation for the entire 6 days, which is not applicable, as it is known that root exudation follows diurnal rhythms, with exudation increasing during light periods (Badri and Vivanco, 2009; Watt and Evans, 1999). Under Pi-depleted condition, only shoot citrate, but not shoot malate content was increased in *PPCK1* overexpressors compared to WT, indicating increased conversion of PEP to OAA, which is preferentially utilized for citrate generation via CS reaction than for malate generation via MDH reaction in shoots. However, the activities of both CS and MDH are reported to be higher during Pi-

starvation (Johnson et al., 1996; Li et al., 2008; Uhde-Stone et al., 2003), therefore both malate and citrate content should be elevated in *PPCK1* overexpressors. Additionally, higher expression of *cMDH2* and *mMDH2* in shoots of Pi-depleted seedlings also suggests that more malate should be generated in shoots, provided that the elevated transcripts of *cMDH2* and *mMDH2* are also reflected in higher protein levels. However, it should be considered that the accumulation of a metabolite depends not only on its increased biosynthesis but also on its reduced catabolism. Interestingly, activity of aconitase, which catalyzes the conversion of citrate to isocitrate is reduced in plants during Pi-deficiency (Neumann and Römheld, 1999), whereas activity of NAD-ME, involved in the catabolism of malate to pyruvate is induced upon Pi-starvation (Juszczuk and Rychter, 2002). Thus, higher availability of OAA together with increased activity of CS and reduced activity of aconitase in Pi-depleted *PPCK1* overexpressors might have led to more utilization of OAA towards citrate biosynthesis compared to malate [Figure 3-2]. However, it is possible that generation of malate might also be higher in *PPCK1* overexpressors, but to sustain malate exudation, it was transported from shoot to root in these lines.

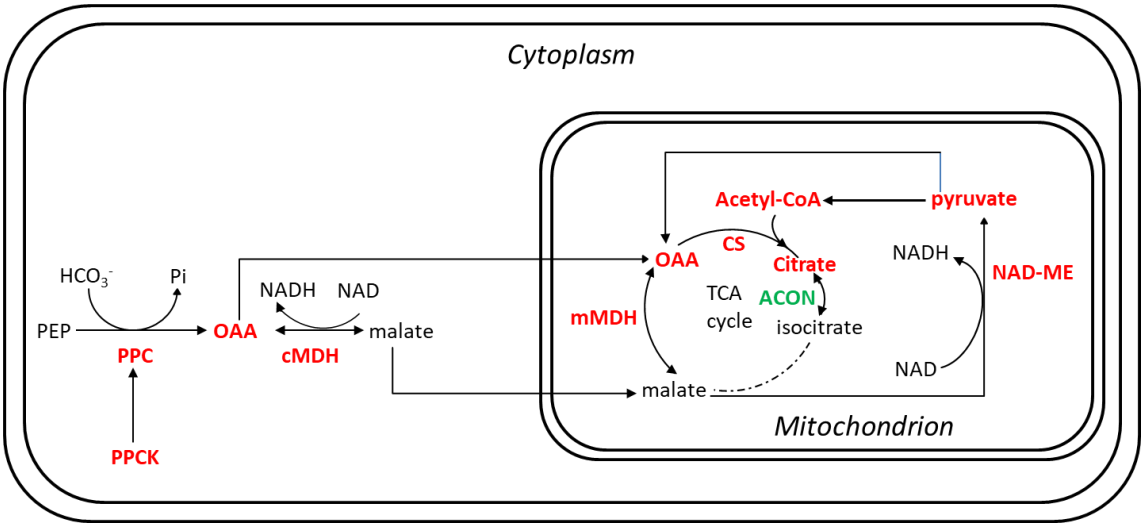

Figure 3-2: Possible route of elevated citrate generation in shoots of Pi-depleted *PPCK1* overexpressors

Enzymes marked as red and green are reported to show elevated and reduced enzyme activities, respectively under P-deficient condition (Johnson et al., 1996; Li et al., 2008; Neumann and Römheld, 1999; Uhde-Stone et al., 2003). Increased activities of enzymes involved in citrate biosynthesis-PPCs, CS, NAD-ME together with reduced activity of citrate degrading enzyme- Acon (Aconitase) could possibly lead to more utilization of OAA for citrate than to malate biosynthesis.

Interestingly, elevation in citrate content was detected only in shoots of plants overexpressing *PPCK1* and not *PPCK2* under Pi-depleted condition. This suggests a specific role for PPCK1 in phosphorylating PPCs which are predominantly active in shoots and that PPCK1 and PPCK2 might have different PPC targets. However, *ppck1* plants also showed elevated citrate content under Pi-depleted condition as discussed in section 3.4. The probable reasons for this contradiction were explained in section 3.4. However, this needs further investigations, e.g. the analysis of *ppck2* plants, or by directly analyzing phosphorylation specificity of PPCKs. Nevertheless, our analysis revealed that with overexpression of *PPCK1* during Pi-starvation, the PPC pathway supports citrate generation in shoots, that is, towards

anaplerotic feeding of the TCA cycle. If it is considered that malate exudation is mainly determined by malate content in root and not by its content in shoot from where it might be transported to roots for exudation, it can be suggested that by overexpression of *PPCK*s, the PPC pathway supports malate biosynthesis in roots under Pi-depleted condition.

3.8 Effect of altered *PPCK* expression on the morphology of plants

Transgenic plants overexpressing *PPCK1* and *PPCK2* exhibited elevated shoot and root fresh weights compared to WT when grown on agar plates under controlled conditions. This suggests that overexpression of *PPCK*s might improve plant performance due to increased exudation of malate in these plants, which could improve solubilization and acquisition of Pi, which could then be utilized by plants for their growth. Elevation in rosette fresh weight was also detected in some of these lines when grown on soil. It is possible that due to higher variability of growth on soil compared to that on agar plates, small differences in rosette fresh weight between transgenic lines and WT might remain undetected and, therefore, was only visible in some of these transgenic lines. No other morphological differences were detected between *PPCK* overexpressors and WT which is also corroborated by a study on transgenic alfalfa plants overexpressing *PPCK3* from soybean (Sun et al., 2014). Even the *PPCK1* knock-out lines (*ppck1-1* and *ppck1-4*) exhibited no differences in morphology compared to WT when grown on soil. This result contradicts the previous report (Meimoun et al., 2009), showing slower growth with reduced rosette diameter in *PPCK1*-deficient plants. Possible reasons for not observing similar results could be due to the differences in ecotype background and in the conditions used for plant growth. The *ppck1* mutant lines (*dln1* and *csi8*) used in their study were in Arabidopsis Wassilevskija ecotype background, whereas the *ppck1* mutant lines (*ppck1-1* and *ppck1-4*) used in the present study were in Col-0 background. Moreover, they watered their plants daily with a standard nutrient solution: Hydrokani C2 (5 ml/L of water: Hydro Agri France) which was not done in our study. Another reason could also be due to differences in soil types used in these two studies, which can also have a strong influence on plant growth.

The reduction in root and shoot fresh weights of *ppck1-1* line both under Pi-sufficient and Pi-deficient conditions on agar plates were not due to loss of *PPCK1* since *ppck1-4* line exhibited unaltered root and shoot fresh weight compared to WT. Moreover, transgenic lines generated in the *ppck1-1* background by introducing functional *PPCK1* (C-lines) displayed similar root and shoot fresh weights compared to *ppck1-1*. It further confirms that the reduced fresh weights detected in *ppck1-1* line is not due to loss of *PPCK1*, but might rather be due to the effect of the second site insertion detected in *ppck1-1* line. Since T-DNA insertion lines did not show reduced expression or complete absence of *PPCK2*, the effect of loss of *PPCK2* on the morphology or fresh weight of plants could not be determined in the present investigation.

3.9 Effect of malate exudation on primary root length during low Pi stress

Pi-deficiency-induced malate exudation is crucial in regulating primary root growth in Arabidopsis, which was shown by two independent reports, published during the course of this study (Balzergue et al., 2017; Mora-Macías et al., 2017; unpublished data from our group). It has been reported that ALMT1 mediated malate exudation is especially important in root-tips, where it was suggested to form complexes with Fe^{3+} for reduction by ascorbate (Grillet et al., 2014), and subsequently Fe^{2+} re-oxidation by LPR1, initiating Fe-redox cycling which ultimately leads to ROS generation and callose deposition during Pi-starvation (Abel, 2017; Balzergue et al., 2017). Hypersensitive root growth response of *ALMT1*^{OE} during low Pi correlates with elevated malate exudation [Figure 2-23]. However, it was not reduced in *almt1* line although it showed insensitive root growth response after Pi-deficiency treatment. As described above, malate exudation at the root tip is crucial for Pi deficiency-induced root growth inhibition, although GUS reporter activity driven by *ALMT1* promoter was induced after Pi-starvation in the entire root including root-tips (Figure 2-24(B); Balzergue et al., 2017). It is possible that other malate channels or transporters share their expression domain with *ALMT1* in the root, except in the transition zone of the root-tips which might be exclusive for ALMT1; and that it is this localized *ALMT1* expression and malate exudation which regulates primary root growth inhibition during Pi-starvation. This might be the possible reason for insensitive primary root growth response of *almt1* during Pi-starvation, even though malate exudation was similar compared to WT. Unfortunately, it is practically not possible to incubate only root-tips in order to determine malate exudation, and therefore differences in malate exudation between WT and *almt1* are masked by other malate transporter or channels, which might be active throughout the entire root.

Indirect evidence in support of highly localized ALMT1 mediated malate exudation as a trigger for the local Pi deficiency response was also provided by analysis of malate exudation in lines overexpressing *PPCK1* and *PPCK2*. Although root malate exudation was higher after Pi-starvation in these lines compared to WT, primary root length was similar to WT. Since expression of *ALMT1* was similar between *PPCK* overexpressors and WT, ALMT1 mediated malate exudation might also be similar especially in root-tip, and higher exudation of malate detected in these lines might be contributed by other malate channels.

The T-DNA insertion lines, *ppck1-1* and *ppck1-4* displayed opposite root phenotypes when exposed to Pi-depleted conditions. *Ppck1-4* line displayed slightly insensitive root growth which correlated with their reduced malate exudation compared to WT plants. Although mutants like *lpr1* and *almt1* showing insensitive primary root growth response during low Pi displayed reduced iron and callose deposition (Balzergue et al., 2017; Müller et al., 2015), slightly insensitive *ppck1-4* plants displayed no

such difference compared to WT. This might probably be due to the limitation in sensitivity of iron and callose staining techniques which might not be sufficient to detect the small differences between *ppck1-4* and WT. Additionally, the effect of *PPCK1* knock-out on root growth in line *ppck1-4* needs to be confirmed by complementation. Unfortunately, line *ppck1-4* became available during the later stage of this project, so that complementation was not feasible based on time reasons. The hypersensitive root growth response and increased iron and callose staining detected in *ppck1-1* correlated well with elevated malate exudation displayed by these plants. When *PPCK1* was introduced into *ppck1-1* line (C-lines), it still exhibited hypersensitive primary root growth under Pi-depleted condition and malate exudation was even higher compared to *ppck1-1*, suggesting that hypersensitivity in *ppck1-1* is not due to the absence of *PPCK1* but due to enhanced malate exudation in these lines. This result again underscores the importance of malate exudation during the local Pi deficiency response. The complementation lines showed enhanced malate exudation compared to WT and even higher than *ppck1-1* line, most likely because the *PPCK1* levels in the mutant were restored in the complementation lines, leading to higher malate production. As discussed above, increased *PPCK1* transcript levels in C-lines compared to WT, although controlled by its native promoter, might be due to positional effects but it might also be due to transcriptional activation by increased malate exudation. Although activation of malate biosynthesis because of increased malate exudation has not been reported yet, it was quite surprising to detect elevated expression of *PPC*s, *PPCK*s, and *MDH*s in *ALMT1*^{OE} lines. However, these preliminary data need to be substantiated by additional experiments. Additionally, if malate exudation activates malate biosynthesis, one should also see increased expression of malate biosynthesis genes in *ppck1-1* and C-lines. Transcript levels of *PPC*s in *ppck1-1* lines, however, were unaltered both in roots and shoots and was higher in shoots of *ppck1-4* plants which exudates lower malate compared to WT. This result does not support the hypothesis that increased malate exudation might activate malate biosynthesis. However, expression of *MDH*s in *ppck1-1* line and *PPC*s, *PPCK*s, and *MDH*s in C-lines should be determined in order to confirm this hypothesis. Interestingly, citrate levels were not restored by the introduction of *PPCK1* in *ppck1-1* line indicating that PPCK1 mediated generation of OAA or malate is destined for malate exudation rather than for citrate generation in C-lines.

Hypersensitive root growth response of *ppck1-1* plants during low Pi-stress was unexpected because reduced *PPCK1* levels should lead to reduced malate biosynthesis and exudation due to stronger feedback inhibition of PPCs by malate. However, malate exudation was higher in *ppck1-1* compared to *ppck1-4* line, most likely due to the presence of a second site insertion affecting the expression of *ALMT1* and *ALMT2* simultaneously. Since the second site insertion was detected downstream of the annotated 3'-UTR of *ALMT1*, it might lead to stabilization of *ALMT1* transcripts. This might be the

probable reason for detecting moderate elevation in *ALMT1* transcripts compared to WT both under Pi-sufficient and Pi-deficient conditions. Stability of *ALMT1* transcripts in *ppck1-1* plants needs to be determined in order to confirm this hypothesis. However, increased constitutive GUS reporter activity driven by *ALMT1* promoter in *ppck1-1* plants indicated that increase in *ALMT1* expression in *ppck1-1* plants is not due to second site insertion alone. This is because the integration of *pALMT1::GUS* construct in the *ppck1-1* genome should be located at different positions than the second site insertion in this transgenic line. At present, it was not possible to determine the reason for the activation of *ALMT1* promoter in *ppck1-1* line, but possibly there might be a positive feedback loop due to excess malate exudation which might trigger *ALMT1* expression. The strongly increased *ALMT2* transcript levels in *ppck1-1* are probably due to the presence of the second site insertion in the promoter of *ALMT2*. *Ppck1-1* is a GABI-KAT line and the vector used for generating most of the GABI-KAT T-DNA insertion lines (pAC106 in this case) were originally designed for activation tagging and contains the *35S* promoter at its right border (RB) (Rosso et al., 2003; Ülker et al., 2008). It is reported that if the T-DNA integrates close to and upstream of the 5'-end of the gene in the 5'-LB-T-DNA-RB-3' direction, as is the case for *ALMT2* in *ppck1-1* line, it can activate the downstream gene, leading to gain of function or overexpression (Ülker et al., 2008).

Because of high sequence similarity between ALMT2 and ALMT1, ALMT2 has been suggested to be involved in malate transport. However, experimental proof showing *ALMT2* as malate transporter is still missing. Our results showing strongly increased *ALMT2* expression and elevated malate exudation suggests that ALMT2 is a functional malate transporter. However, *almt2* lines did not show reduced malate exudation, perhaps, as with *almt1*, the effect might be masked by additional transporter. Therefore, transgenic lines overexpressing *ALMT2* should be generated and analyzed for malate exudation in order to substantiate the function of ALMT2 as malate transporter. Despite the similarities between ALMT1 and ALMT2, *almt2* lines did not show insensitive root growth response, suggesting that it does not play a role during the local Pi deficiency response.

Constitutive expression of *ALMT1* and *ALMT2* in *ppck1-1* line not only altered malate exudation but also affected the metabolism of this line. This is indicated by the elevated levels of amino acids in *ppck1-1* line both under Pi-sufficient and Pi-deficient conditions which was only partially restored when *PPCK1* was introduced in *ppck1-1* line. However, in *PPCK1* knock-out mutant *ppck1-4*, alteration in amino acids was not detected suggesting that altered amino acid levels in *ppck1-1* line might be due to the increased malate exudation. This was also confirmed by elevated levels of amino acids detected in *ALMT1*^{OE} line. The observed increase in amino acid content in *ppck1-1*, C-lines, and *ALMT1*^{OE} suggest that malate exudation leads to strong metabolic disturbances in plants.

3.10 Pi-solubilization capacity of transgenic lines

Higher exudation of malate is assumed to increase the Pi-solubilization capacity of plants (Jones, 1998; Schulze et al., 2002), however, there are only a few reports showing elevated P content in transgenic plants exhibiting higher malate exudation capacities (Lü et al., 2012; Peng et al., 2018; Wang et al., 2015). In this study, detection of elevated Pi content in roots of *ppck1-1*, *ALMT1*^{OE}, and C-lines showing increased malate exudation under Pi-depleted condition suggests that increased malate exudation could indeed improve Pi acquisition. Further evidence in support of this was provided by the *ppck1-4* line exhibiting reduced Pi content in shoots which correlated with their reduced malate exudation capacity. However, there was no strict correlation between malate exudation and Pi content, since malate exudation of C-lines was stronger compared to *ppck1-1* and *ALMT1*^{OE} lines, but Pi content was similar in roots of all these lines. Alternatively, altered free Pi content could also be due to changes in Pi metabolism which could explain the reduced Pi content detected in roots and shoots of *PPCK* overexpressors, although they exude more malate. Evidence in support of altered Pi levels in plants with modulated PPC/PPCK pathway genes was provided by a study on rice overexpressing maize *PPC.* It was shown in that study that with enhanced PPC activity in the leaves of transgenic plant, availability of Pi in the chloroplast decreases via reduction in the activities of two key enzymes- SUCROSE PHOSPHATE SYNTHASE (SPS) and FRUCTOSE 1,6-BISPHOSPHATASE (FBPase) responsible for Pi-recycling (Agarie et al., 2002). It is possible that in *PPCK* overexpressors similar reduction in the activities of SPS and FBPase might have led to reduced Pi content due to enhanced PPC activity. If this is true then plants deficient in *PPCK*s should show increased Pi content in shoots which was not the case for the *PPCK1* knock-out mutant, *ppck1-4*, showing reduced Pi content in shoots. However, one to one correlation between knock-outs and overexpressors especially for genes like *PPC*s and *PPCK*s which are involved in such a central metabolic pathway is difficult to draw. Therefore, activities of SPS and FBPase should be determined in both *ppck1-4* and *PPCK* overexpressors in order to validate their effect on Pi content. As such, more work is required to elucidate whether or not higher free Pi levels in plant generated for increased malate exudation is due to increased Pi-solubilization and uptake or due to changes in Pi metabolism.

Since the growth media in this study contained 5 µM KH_2PO_4 (KP) which can be easily solubilized, provided it does not form complexes with other constituents in the growth medium, it might not be an appropriate system to analyze the full potential of plants with different malate exudation capacity in solubilizing Pi. Therefore, a preliminary investigation was performed on media supplemented with the insoluble Pi-source calcium phosphate (CaP). Since Pi content was reduced in roots, shoots, and seedlings of CaP treated WT compared to KP treated WT, it suggests that the plants were indeed suffering due to low Pi availability after CaP treatment. Initial results suggested increased ability of

transgenic plants having elevated malate exudation capacity in solubilizing Pi from insoluble Pi-metal complexes. This is because *PPCK1* overexpressors and C-lines (overexpression of *PPCK1* and *ALMT1/ALMT2*) exhibited higher Pi content in their shoots compared to WT when grown on media containing CaP as Pi-source. Moreover, overexpression of *PPCK1* alone was sufficient to improve Pi-solubilization capacity of plants, since similar increase in Pi content was detected in *PPCK1* overexpressors and C-lines. Probably after CaP treatment, which was performed at a pH of 7.6, malate exudation capacity might be similar between K and C-lines, which might have resulted in similar Pi content in these lines. In order to confirm this, malate exudation should be determined for both C and K-lines after CaP treatment. It is reported that at an alkaline pH of 7.1, *ALMT1* expression is not detectable in Arabidopsis (Balzergue et al., 2017). Therefore, it is unlikely that ALMT1 is responsible for malate exudation after CaP treatment in C-lines. On the contrary, since *PPCK1* expression is induced at high pH (Chen et al., 2008), malate exudation might possibly be contributed solely by elevated malate generation due to higher *PPCK1* expression in C-lines. Whether ALMT2 can act as a malate transporter and can also exert its function at alkaline pH needs further verifications. Moreover, in order to confirm whether the elevated Pi content detected in these lines was due to increased solubilization of Pi from insoluble metal-complexes because of higher malate exudation capacity, Pi uptake experiments with labeled Pi sources should be performed in future. It should also be considered that the Pi content determined in this study is free Pi which might not give a true indication about the total P-content in these lines. Therefore, total P-content should be determined in order to study whether transgenic plants having higher malate exudation can improve Pi-solubilization and acquisition capacity of these lines.

Nevertheless, during the course of this study, transgenic plants with different malate generation and exudation capacities were generated like *ppck1-1*, *ppck1-4*, *PPCK* overexpressors, and C-lines (overexpression of *PPCK1* and *ALMT1*/*ALMT2*). All these lines can be used as tools in future to perform Pi-solubilization and Pi-uptake experiments.

4 SUMMARY AND OUTLOOK

Malate biosynthesis and exudation play an important role during Pi-deficiency induced systemic and local responses in *Arabidopsis thaliana*. Malate generation in plants can proceed by carboxylation of phosphoenolpyruvate (PEP) to oxaloacetate (OAA) by phosphoenolpyruvate carboxylases (PPCs), and subsequent reduction of OAA to malate by malate dehydrogenases (MDHs). PPCs are subject to feedback inhibition by malate, which can be relieved by phosphorylation of PPCs by phosphoenolpyruvate carboxylase kinases (PPCKs). Induction in malate biosynthesis and exudation has always been correlated to activation of PPC/PPCK pathway during low Pi-stress.

This study revealed that Pi-starvation differentially induces the expression of *PPCs and PPCKs*. However, there is no exclusive occurrence and inducibility of distinct isoforms in roots and shoots. Analysis of promoter-reporter lines revealed that *PPCK1* and *PPCK2* exhibit indistinguishable expression domains after Pi-starvation. Inductions in expression of *PPCK1* and *PPCK2* in root-tips overlap with the expression domains of *LOW PHOSPHATE RESPONSE 1* (*LPR1*) and *ALUMINUM ACTIVATED MALATE TRANSPORTER 1* (*ALMT1*). This suggests that the required malate for ALMT1 mediated malate exudation in the root-tips for triggering low Pi-induced root shortening might be generated by PPC/PPCK pathway. This was also supported by the observed insensitive root growth-response of *ppck1-4* line which exhibits reduced malate exudation after Pi-starvation. Complementation of *ppck1-4* line is needed in future to confirm its insensitive root growth phenotype. This is the first report which confirmed cytosolic localization of PPCKs *in vivo* using fluorescent reporter protein. PPCKs were also localized to some moving dot-like structures. The nature of these structures could not be determined yet and needs further investigation. Moreover, metabolite profiling data of T-DNA insertion lines having aberrant expression of PPC and PPCK genes suggested distinct functions of different isoforms.

The major focus of this study was to investigate whether PPC/PPCK pathway could be manipulated by overexpression of *PPCK*s. The present study revealed that this pathway can be successfully engineered for modified malate generation and exudation by overexpression of *PPCK*s in Arabidopsis. However, there seems to be a certain limit beyond which further increase in malate levels could not be obtained by overexpression of *PPCK*s alone, possibly due to the limitation of PPCs availability. Metabolic analysis of these lines suggested that there is specificity of PPCKs in phosphorylating distinct PPC isoforms. Moreover, there were also some hints suggesting that the produced malate by PPC/PPCK pathway during Pi-starvation in Arabidopsis roots is destined for exudation. Initial investigation of transgenic lines with different malate exudation capacity revealed a positive correlation between malate exudation and Pi content of seedlings when grown on media with insoluble Pi-metal complexes.

The transgenic lines generated during the course of this study can be used as tools in future to perform several experiments which are proposed below.

To elucidate the effect of elevated malate exudation on Pi-solubilization

- Transgenic lines showing different malate exudation capacities could be cultivated on media supplemented with insoluble Pi-complexes like calcium, aluminum, and iron phosphate. The Pi content could then be measured and compared between WT plants and these transgenic lines in order to observe the effect of elevated malate exudation on Pi-solubilization.
- Pi-uptake experiments with labeled Pi-sources could be performed with these lines to determine whether the elevated Pi levels in these lines are indeed due to higher Pi uptake.
- Performance of transgenic lines with different malate exudation capacity could be determined by growing them on soil which reflects real *in planta* condition.

To elucidate the origin of malate exuded from plants

- The biosynthetic origin of exuded malate could be analyzed in the transgenic lines having altered expression of PPC and *PPCKs* by $^{13}CO_2$ feeding studies. This will be followed by the analysis of the label distribution in the exuded malate by GC-MS/MS, which differs between malate generated by PPCs and malate generated by the TCA cycle. For instance, based on theoretical assumptions, fourth carbon position of malate in *PPCK* overexpressors would be more isotope-enriched compared to WT in $^{13}CO_2$ feeding studies, in case the generated malate for exudation is synthesized by the PPC pathway.

To elucidate the specific PPC phosphorylation targets of PPCK1 and PPCK2

- Phosphoproteomics could be performed with transgenic plants overexpressing *PPCK*s and also with *PPCK1* knock-out lines. The analysis of the phosphorylation status of the PPC isoforms in *PPCK* overexpressors or knock-out lines will help in elucidating whether there is specificity of PPCKs in phosphorylation of specific PPC isoforms.
- In additions, transgenic lines with GFP tagged PPCK fusion proteins are an appropriate tool to perform pull down assays to identify their PPC phosphorylation targets.

To elucidate the effect of PPCK overexpression on phosphorylated metabolites

- Phosphorylated metabolites could be analyzed in transgenic lines in order to gain a comprehensive overview of misexpression of PPC/PPCK genes on central carbon metabolism.

To elucidate the effect of PPCK overexpression on other stresses

- There are reports on upregulation of PPC/PPCK genes in response to different kinds of environmental stresses like pH, alkaline, salt, and cadmium (Chen et al., 2008; Feria et al., 2016; Sun et al., 2014; Willick et al., 2019). The performance of transgenic plants generated during this study could be tested in response to all these stresses.

The existing collection of transgenic plants with altered expression of PPC pathway genes should be extended by the generation of *PPCK2 knock-out* plants by CRISPR/Cas approach, in order to analyze the contribution of PPCK2 for malate generation in Arabidopsis. In addition, transgenic plants overexpressing *PPC* genes could be generated and analyzed for malate and Pi contents, as well as for their response to Pi-starvation, in order to substantiate the assumptions suggested by the results obtained from the *PPC* knock-out lines. Transgenic plants overexpressing *ALMT2* could be generated to further verify the role of this gene as a malate transporter and to elucidate whether ALMT2 can contribute to Pi-starvation induced malate exudation.

5 MATERIALS AND METHODS

5.1 Materials

5.1.1 Chemicals, Reagents, and standards

All chemicals, media constituents, and solvents used were of reagent or HPLC grade and were obtained from the following suppliers: Carl Roth (Karlsruhe, Germany), Merck (Darmstadt, Germany), Macherey-Nagel (Düren, Germany), Sigma-Aldrich (St Louis, MO, USA), J.T. Baker (Deventer, The Netherlands), Duchefa Biochemie (Haarlem, The Netherlands), CDN isotopes (Point Claire, QC, Canada), and Caissons Laboratories (East Smithfield, USA). Molecular Biology supplies and kits were obtained from Life Technologies and Thermo Fischer Scientific (California, USA), and New England Biolabs (Massachusetts, USA). Sequencing and primer synthesis was performed by Eurofins Genomics (Ebersberg, Germany).

5.1.2 Bacterial strains and plasmid vectors

The bacterial strain *Escherichia coli* One Shot® TOP10 chemically competent cells provided with the pENTR™ Directional TOPO® Cloning kit from Invitrogen was used for propagation of the Gateway entry cassette. Whereas self-made chemically competent cells of bacterial strain Escherichia coli TOP10 was used for propagation of the Gateway expression cassette. The *Agrobacterium tumefaciens* strain *GV3101::pMP90RK* (Koncz and Schell, 1986) was used for plant transformation via the floral dip method. The plasmid vectors used during the course of this work for molecular cloning and recombinant expression are listed in Table 5-1.

5.2 Media

Media used for culturing *E. coli* and Agrobacterium, and for growing Arabidopsis are listed with their composition and additional supplements in Table 5-2. All media were sterilized at 121° C and 2 bar for 20 min. Supplements like basta and antibiotics were added after filter sterilization to autoclaved growth media.

To remove residual phosphate which is important for performing P treatments, agar (Duchefa, Haarlem, The Netherlands) was routinely purified by repeated washings in deionized water and subsequent dialysis using Dowex 1X8 anion exchanger (Sigma-Aldrich, St Louis, MO, USA). The agar was then air dried at 60° C for 2 – 3 days.

Table 5-1: Plasmid vectors used in this study and their purpose and feature

Plasmid	Purpose	Feature	Reference
pENTR/D-TOPO	Entry vector for Gateway cloning	*rrn*B T1 and T2, M13 forward and reverse priming site, *att*L1 and *att*L2, TOPO cloning site (directional), T7 promoter/priming site, Kan^r, pUC ori	Thermo Fischer Scientific
pB7WG	Binary plant expression vector	attR1and attR2, ccdB, LB and RB site, Sm/SpR, T35S, Bar	(Karimi et al., 2005, 2002)
pB7FWG	Binary plant expression vector	attR1and attR2, ccdB gene, LB and RB site, Sm/SpR, T35S, Bar, Egfp	(Karimi et al., 2005, 2002)
pB7WG2	Binary plant expression vector	attR1 and attR2, p35S, T35S, CmR, ccdB, Sm/SpR, Bar	(Karimi et al., 2005, 2002)
pB7FWG2	Binary plant expression vector	attR1, attR2, p35S, T35S, ccdB, Sm/SpR, Bar, Egfp	(Karimi et al., 2005, 2002)
pB7WGF2	Binary plant expression vector	attR1, attR2, p35S, T35S, ccdB, Sm/SpR, Bar, Egfp	(Karimi et al., 2005, 2002)
pBGWFS7	Binary plant expression vector	attR1, attR2, p35S, T35S, ccdB, Sm/SpR, Bar, Egfp and Gus	(Karimi et al., 2005, 2002)
pUB-Dest	Binary plant expression vector	pUBQ10, attR1, Bar, LB,RB, SmR, pBR322, pVS1attR2, CmR, ccdB, T35S	(Grefen et al., 2010)
pUB-C-GFP-Dest	Binary plant expression vector	pUBQ10, attR1, Bar, LB,RB, SmR, pBR322, pVS1attR2, CmR, ccdB, T35S	(Grefen et al., 2010)
pUB-N-GFP-Dest	Binary plant expression vector	pUBQ10, attR1, Bar, LB,RB, SmR, pBR322, pVS1attR2,CmR,ccdB,T35S	(Grefen et al., 2010)

Table 5-2: Media composition

Medium	Composition	Reference
Modified ATS medium (*A. thaliana*)	0.5% D-Sucrose, 5mM KNO_3, 0.5 mM (+Pi) or 0.005mM (-Pi) KH_2PO_4, 2 mM $MgSO_4$, 2 mM $Ca(NO_3)_2$, 0.05 mM Fe^{3+}-EDTA, 0.07 mM, H_3BO_3, 0.014 mM $MnCl_2$, 0.005 mM $CuSO_4$, 0.001 mM $ZnSO_4$, 0.0002 mM Na_2MoO_4, 0.010 mM $CoCl_2$, 1% Washed Agar, pH 5.6	(Wilson et al., 1990)
0.5x Murashige and Skoog medium (MS) (*A. thaliana*)	2.203 g/L MS with vitamins (Duchefa), 10 g/L MES, 1% (w/v) sucrose, 0.8 g/L Plant Agar, 10 µg/ml Basta (200 g/L Glufosinate-ammonium; Bayer), pH 5.6	(Murashige and Skoog, 1962)
Luria Bertani medium (*E. coli*, *A. tumefaciens*)	10 g/L Bacto tryptone, 10 g/L NaCl, 5 g/L Yeast extract, pH 7.5 10 g/L Agar-agar 50 µg/ml Kanamycin or 75 µg/ml Spectinomycin or 100 µg/ml Rifampicin	(Bertani, 1951)
Super Optimal Broth with Catabolite repression medium (SOC) (bacterial transformation)	20 g/L Tryptone, 5 g/L Yeast Extract, 10 mM NaCl, 2.5 mM KCl, 10 mM $MgCl_2$, 10 mM $MgSO_4$, 20 mM Glucose	(Hanahan, 1983)

5.3 Plant material and cultivation

5.3.1 Plant lines

Arabidopsis thaliana accession Col-0 was used as WT throughout the study. All T-DNA insertion lines (Col-0 background) were obtained from the Nottingham Arabidopsis Stock Centre (NASC). The T-DNA insertion lines analyzed in this study are listed in the Supplementary table 7-12. Homozygous plants were generated by selfing heterozygous plants, and homozygosity was confirmed by PCR with the primers listed in the Supplementary table 7-13.

5.3.2 Plant cultivation on soil

Plants for propagation, transformation, and selection purposes were grown in the greenhouse under long-day conditions at 18-20° C and 55-65% relative humidity. The substrate used was "Einheitserde Typ GS 90" mixed with vermiculite (1-2 mm) in a 4:3 ratio.

5.3.3 Plant cultivation under aseptic conditions

For sterile cultivation of plants, seeds were surface sterilized with chlorine gas and individually placed with a toothpick on sterile agar plates containing modified ATS medium. Plates were incubated for two days at 4° C in the dark to synchronize seed germination and thereafter the plates were kept vertically in a growth chamber at 22° C under illumination for 16 h daily (170 µmol s^{-1} m^{-2}; Osram LumiluxDeLuxe Cool Daylight L58W/965, Osram, Augsberg, Germany). After 6 days of growth, seedlings were transferred to fresh plates containing +Pi (0.5 M KH_2PO_4) or -Pi (5 µM KH_2PO_4) and allowed to grow for 5 more days. Thereafter, the roots were separated from their shoots, their fresh weights were recorded, and the samples are frozen in liquid nitrogen until further processing. One biological replicate consisted of roots or shoots from two plants.

For determination of rosette fresh weight, after 10 days of germination on agar plates, according to the condition as mentioned above, seedlings were transferred to pots containing "Einheitserde Typ GS 90" mixed with vermiculite (1-2 mm) in a 4:3 ratio as a substrate. Seedlings were allowed to grow for additional 21 days before harvest in phytochamber under long-day conditions (16 h day, 8 h night) with ca. 130 µmol s^{-1} m^{-2} light fluency at 24° C and 60 % relative humidity. Rosette fresh weights were recorded after separation of roots from the rosette.

5.3.4 Transformation of Arabidopsis

Arabidopsis plants were transformed by *A. tumefaciens* mediated transfection using the floral dip method as described by Clough and Bent, 1998. Agrobacteria harboring the gene of interest on a binary vector were cultivated on LB plates with appropriate antibiotics for 2 days at 28° C. The cells were resuspended in liquid LB medium and diluted to an OD_{600} of 2.0. A freshly prepared 5 % (w/v)

sucrose solution was added to the bacterial suspension in a 4:1 ratio. Before dipping, Silwet-L77 at a concentration of 0.03% (v/v) was added to the suspension. Arabidopsis plants which had just bolted and begun to flower were dipped upside down into the suspension solution and gently agitated for nearly 10-15 s. The plants were then kept horizontally on a tray and were kept moist by wrapping the tray with plastic foil. The plastic foil was removed after two days. Plants were kept vertically and cultivated in the greenhouse to set seeds under the conditions described in section 5.3.2.

5.3.5 Selection of transformed Arabidopsis plants

T1 seeds were harvested from transformed plants and sown densely on soil in large trays, stratified for 2 days, and grown in the greenhouse. After 7 days of germination, the seedlings were sprayed with Basta solution (80 mg/L) every three days until Basta resistant seedlings were visible. Twenty four independent lines per construct (T1 lines) were cultivated further for seed setting. Several transgenic lines were selected segregating in a 3:1 ratio in the T2 generation for resistance to Basta (10 µg/ml). Such T2 seedlings were then further propagated until the setting of T3 seeds. T3 seeds were again sown on Basta containing medium on plates to select for homozygous lines. These lines were used for all our experiments. For analysis of GFP fluorescence and GUS expression, three to six T3 lines were selected showing representative GFP fluorescence and GUS expression patterns.

5.4 Bacterial culture and transformation

5.4.1 *Escherichia coli* and *Agrobacterium tumefaciens* cultivation

E. coli cells were cultured in LB liquid medium or on LB plates containing appropriate antibiotics for 24 h at 37° C. The Agrobacteria were also cultured in LB liquid or solid medium with appropriate antibiotics and cultivated for 48 h at 28° C. The liquid cultures were incubated on a rotary shaker which was set at 150 rpm.

For long-term storage of bacterial clones, glycerol stocks were prepared by mixing bacterial cultures with glycerol to reach a final concentration of 20 %. Stocks were flash-frozen in liquid nitrogen and stored at -80° C.

5.4.2 *Escherichia coli* and *Agrobacterium tumefaciens* transformation

Chemically competent *E. coli* Top10 and One-Shot cells were transformed through heat shock method as described in the Invitrogen pENTR™ Directional TOPO® Cloning Kit. Transformed cells were cultivated overnight (16 h) at 37° C on LB plates containing appropriate antibiotics for selection of the transformed plasmid.

For transformation of *A. tumefaciens* strain *GV3101::pMP90RK*, 100 ng of purified plasmids were mixed carefully with 50 µl of competent cells and incubated on ice for 30 min. The cells were then frozen in liquid nitrogen for 5 min, followed by incubation at 37° C for 5 min. 250 µl of SOC medium was added to this mixture and incubated horizontally at 28° C in a shaker at 150 rpm for 2 h. For the selection of transformed plasmids, the cells were plated on an LB plate with the respective antibiotics and cultured for 48 h at 30° C.

5.5 Molecular Biology methods

5.5.1 Isolation of genomic DNA

All the centrifugation steps during DNA extraction were carried out at 4° C. Approximately 1.25 g of plant material was collected in a 2 ml Eppendorf tubes and a 5 mm steel bead was added for grinding the sample. The samples were ground using a Tissue Lyser II (QIAGEN) bead mill at 25 s^{-1} for 50 s. 850 µl of DNA extraction buffer (consisting of 50 mM Tris, pH-8, 10 mM EDTA, pH-8, 100 mM NaCl, 1% w/v SDS, 0.07% β-mercaptoethanol) was added to the tube, followed by vortexing for 1-2 min. After centrifuging for 3 min, 750 µl of supernatant was transferred to a 1.5 ml Eppendorf tube. The tubes were then incubated at 65° C in a Thermo block (Eppendorf Thermo Stat Plus) for 15 min. After addition of 150 µl of Bio101 solution III (consisting of 3 M potassium acetate, and 11.5% glacial acetic acid) the samples were vortexed for 1 min. The samples were incubated on ice for 1 hr, followed by centrifugation at 14000 rpm for 5 min. The supernatant was transferred to a new 1.5 ml Eppendorf tube containing 750 µl of isopropanol. The tubes were inverted 6-7 times before centrifugation at 14000 rpm for 10 min. The supernatant was discarded and the DNA pellet was washed with 500 µl of 70% ethanol. Ethanol was carefully discarded after centrifuging for 3 min. The pellet was air-dried in an evaporator and resuspended in 45 µl of sterile Millipore water. The extracted DNA was stored at -20° C till further use. The DNA extraction buffer was stored at room temperature after autoclaving. The Bio101 Solution III was filter sterilized and stored at 4° C.

5.5.2 Isolation of plasmid DNA from *E. coli*

Plasmid DNA was extracted with the GeneJET Plasmid Mini Prep Kit (Thermo Fisher Scientific) according to manufacturer's guidelines and instructions. The concentration of isolated plasmid DNA was determined spectrophotometrically using Infinite® 200 NanoQuant (Tecan) device.

5.5.3 Polymerase chain reaction (PCR)

All PCR reactions were carried out in a Veriti™ 96-Well Thermal Cycler (Applied Biosystems).

5.5.3.1 Standard PCRs

Colony PCRs and PCRs for genotyping were performed using 10x DreamTaq Polymerase Green buffer and DreamTaq polymerase (Thermo Fischer Scientific). A reaction volume of 20 µl was generally used and the concentration of other components included is mentioned in Table 5-3.

Table 5-3: Components of standard PCR and colony PCR reaction

Components	Stock concentration	Final concentration	Volume
Dream Taq Polymerase Green buffer	10 x	1x	2 µl
dNTPs	10 mM	500 µM	1 µl
Forward primer	10 µM	0.5 µM	1 µl
Reverse primer	10 µM	0.5 µM	1 µl
Template	-	˜100 ng or one bacterial colony	1 µl
DreamTaq polymerase	5U/ µl	0.0625 U/ µl	0.25 µl
Millipore water	-	-	13.75 µl

The annealing temperature was typically set to 5° C lower than the melting temperature (Tm) of primers used. The thermal profile used is shown in Table 5-4.

Table 5-4: Thermal profile for DreamTaq PCR

Phase	Temperature	Duration	No. of cycles
Initial denaturation	95° C	2 min	1
Denaturation	95° C	1 min	35
Annealing	˜Tm-5° C	50 s	35
Extension	72° C	1 min/kb	35
Final extension	72°C	10 min	1

5.5.3.2 High fidelity PCR for molecular cloning

For the generation of Gateway entry clone with pENTR/D-Topo vector, PCR products were amplified from genomic DNA or cDNA using gene-specific primers. A 50 µl reaction was performed using Phusion Green High Fidelity DNA Polymerase and 5x Phusion Green HF buffer (Thermo Fisher Scientific). The concentration of PCR components included is mentioned in the Table 5-5.

Table 5-5: Components of high fidelity PCR

Components	Stock concentration	Final concentration	Volume
5x Phusion Green HF buffer	5x	1x	10 µl
dNTPs	10 mM	300 µM	1.5 µl
Forward primer	10 µM	0.4 µM	2 µl
Reverse primer	10 µM	0.4 µM	2 µl
Template	-	˜200 ng DNA or cDNA	2 µl
Phusion polymerase	2U/ µl	0.02 U/µl	0.5 µl
Millipore water	-	-	32 µl

The annealing temperature was typically set to 5° C lower than the melting temperature (Tm) of primers used. The thermal profile used is shown in Table 5-6.

Table 5-6: Thermal profile Phusion High-Fidelity PCR

Phase	Temperature	Duration	No. of cycles
Initial denaturation	98° C	30 s	1
Denaturation	98° C	10 s	35
Annealing	˜Tm-5° C	30 s	35
Extension	72° C	15-30 s/kb	35
Final extension	72° C	10 min	1

5.5.4 Agarose gel electrophoresis

PCR products were analyzed through electrophoretic separation in a 1% Agarose Gel which was prepared by dissolving Agarose (Roth, Karlsruhe, Germany) in 1x TAE buffer (40 mM Tris-HCl pH-7.6, 20 mM acetic acid, and 1 mM EDTA), followed by brief boiling. Before casting the gel, Serva DNA stain G at 0.003% (v/v) was added. Electrophoretic separation was performed at 100 V for 10-20 min depending on the size of the product. A Gene Genius UV transilluminator (Syngene) was used to visualize the DNA fragments on the gel.

5.5.5 Extraction of DNA fragments from agarose gel

PCR products from Agarose gel were purified using GeneJET Gel Extraction Kit (Thermo Fisher Scientific) following the manufacturer's instructions. The extracted products were stored at -20° C until further processing.

5.5.6 Gateway cloning

For this study, a number of stably transformed transgenic Arabidopsis plants were generated using the Gateway system (Thermo Fisher Scientific). A complete list of transgenic plants generated along with their utility is mentioned in Supplementary table 7-14. Entry clones were generated via the topoisomerase-assisted pENTR/D-TOPO vector system (pENTR™ Directional TOPO® Cloning Kit, Thermo Fisher Scientific).

5.5.6.1 Directional cloning in pENTR/D-TOPO vector system

The short and long promoter variants of *PPCK1* and *PPCK2* were obtained by amplifying 2,468 bp (*pPPCK1*$_{long}$) and 1029 bp (*pPPCK1*$_{short}$) for *PPCK1* and 2,699 bp (*pPPCK2*$_{long}$) and 1235 bp (*pPPCK2*$_{short}$) for *PPCK2*, respectively from genomic DNA. For generation of overexpression lines for *PPCK1* and *PPCK2* with C/N terminal tag or no tag, coding sequences for Gateway cloning were amplified from WT cDNA with gene specific primers. Genomic *pPPCK1*$_{long}$*::PPCK1(w/-stop codon)* and *pPPCK1*$_{short}$*::PPCK1(w/-stop codon)* were amplified with gene specific primers to generate

complementation lines for *ppck1-1.* Primers listed in Supplementary table 7-15 were used for entry clone generation with pENTR/D-TOPO vector system. To meet the requirements of cloning into pENTR/D-TOPO vector, CACC extensions were added at the 5' end of the forward primers. After extracting the amplified product from the gel, the TOPO cloning reaction was performed according to the manufacturer's protocol. The reaction products were then transformed into the chemically competent TOP10 *E. coli* cells. Positive clones were identified by performing colony PCR using primer pairs listed in Supplementary table 7-16. Plasmids from positive colonies were isolated and sequenced with the M13 uni (-21) primer provided by the eurofins sequencing service.

5.5.6.2 Generation of expression clones via the Gateway system

The entry clones and destination vectors were combined via LR reaction with Gateway® LR Clonase™ II Enzyme mix (Thermo Fisher Scientific) according to the manufacturer's protocol to create expression clones . 1 µl of reaction products were used to transform 50 µl of chemically competent TOP10 *E. coli* cells. Positive transformants were confirmed by colony PCR and were sent for sequencing at Eurofins. Primers used for sequencing the positive clones are listed in Supplementary table 7-17.

5.5.7 Restriction enzyme digestion

Restriction enzyme digestion was performed to check whether our gene of interest has ligated in a correct orientation in entry and destination vectors. The restriction enzymes used to digest the entry and destination cassettes are listed in Supplementary table 7-18. A 15 µl double digest reaction was performed using appropriate restriction enzymes with suitable buffers from Fermentas, New England Biolabs and Thermo Fisher Scientific. A typical 15 µl reaction consists of 1.5 µl plasmid DNA (˜150 ng), 1.5 µl Buffer (1X), 0.1 µl Enzyme 1 (1U), 0.1 µl Enzyme 2 (1U), and 11.8 µl millipore water. The reaction mixture was incubated at 37° C for atleast 1 h. The digested DNA was viewed on a 1% agarose gel.

5.5.8 Analysis of transcript levels from Arabidopsis seedlings

5.5.8.1 Isolation of RNA

In order to determine the transcript levels in T-DNA insertion lines and overexpression lines, a pool of seedlings growing on agar plates was collected in triplicates. Whereas, for analysis of transcript levels for specific genes under +Pi and -Pi conditions, roots and shoots were harvested separately in triplicates. Around 100 mg of tissue was collected in 2 ml Eppendorf tubes with 5 mm steel bead inside, frozen in liquid nitrogen, and stored at -80° C until further processing. Total RNA was extracted with the RNeasy Plant Mini Kit (Qiagen) following the manufacturer's protocol. The concentration of RNA was determined spectrophotometrically using Infinite® 200 NanoQuant (Tecan) device. The isolated RNA was stored at -80° C until processing for cDNA synthesis.

5.5.8.2 Processing of RNA samples to prevent contamination by genomic DNA

An endonuclease, dsDNase (Thermo Fisher Scientific), having high specific activity towards double-stranded DNA was used for genomic DNA elimination from RNA samples prior to reverse transcription. A total reaction volume of 10 µl was used for digesting. A typical 10 µl reaction consisted of 1µl 10x dsDNase buffer, 1 µl dsDNase, 8 µl template RNA and the volume was made upto 10 µl with nuclease-free water. After mixing and spinning down the samples, the reaction tubes were incubated at 37° C for 5 min in a Thermo block (Eppendorf Thermo Stat Plus). The samples were ready directly for cDNA synthesis after this processing step.

5.5.8.3 cDNA synthesis

A total reaction volume of 20 µl was used to synthesize cDNA using RevertAid Reverse Transcriptase (Thermo Fisher Scientific). 12 µl of dsDNase digested RNA was mixed with 1 µl of 100 µM oligodT18VN (5'-TTTTTTTTTTTTTTTTTTVN-3') and 2 µl of 40 mM dNTPs (10 mM each) and incubated at 65° C for 5 min. After 1 min of incubation on ice, the following components were added in the indicated order: 4 µl of 5x Reaction buffer (final concentration: 1x), 0.5 µl of 40 U/ µl RiboLock RNase Inhibitor **(**final concentration: 1 U/µl), and 0.5 µl of 200 U/ µl Reverse Transcriptase (final concentration: 5 U/µl). The samples were incubated at 42° C for 1 hr, followed by the termination of reaction by heating at 70° C for 15 min. The samples were stored at -20° C until further use.

5.5.8.4 Semi-quantitative PCR (RT-PCR)

2 µl of undiluted cDNA was used for RT-PCR. As an endogenous control, *ACTIN2* was amplified from 2 µl of 1:10 diluted cDNA. RT-PCR primers used during this work are listed in the Supplementary table 7-19. The concentration of other PCR components and the thermal profile used were similar to that discussed under section 5.5.3.1.

5.5.8.5 Quantitative Real-Time-PCR (RT-qPCR)

RT-qPCR was performed on a QuantStudio 5 Real-Time PCR System (Applied Biosystems) using PowerUp™ SYBR® Green Master Mix (Thermo Fisher Scientific). To test for contamination with genomic DNA, dsDNase digested RNA preparations were used as no template control, diluted corresponding to the cDNA dilutions finally used in RT-qPCR. According to the manufacturer's instructions, a 10 µl reaction was set up with the components mentioned in Table 5-7.

Primers for RT-qPCR were designed manually to generate product size of 60-120 bp and the quality of the primers were checked through Primer Blast tool of the National Centre for Biotechnology Information (NCBI). Primers for amplification were selected only after calculating their efficiencies from the standard curves. RT-qPCR primers used during this work are listed in the Supplementary table

7-19. The thermal profile used for RT-qPCR is mentioned in Table 5-8. For relative quantification of transcripts, the constitutively expressed gene *PROTEIN PHOSPHATASE 2A* (*PP2A*) was always detected in parallel in every RT-qPCR sample and used as a reference gene.

Table 5-7: Components of RT-qPCR reaction

Components	Final concentration	Volume (10 µl/well)
PowerUp™ SYBR Green Master Mix (2x)	1x	5 µl
Forward primer (10 µM)	0.4 µM	0.4 µl
Reverse primer (10 µM)	0.4 µM	0.4 µl
cDNA or no template control	-	2 µl (from 1:10 dilution)
Millipore water	-	2.2 µl

Table 5-8: Thermal cycling conditions for RT-qPCR

Step	Temperature	Duration	Cycles
UDG activation	50° C	2 min	Hold
Dual-Lock™ DNA polymerase	95° C	2 min	Hold
Denature	95° C	3 s	40
Anneal/extend	60° C	30 s	
Melt Curve Stage			
Step1	95° C	15 s	
Step2	60° C	1 min	
Step3	95° C	15 s	
Step4	60° C	15 s	

5.6 Biochemical Methods

5.6.1 Analysis of metabolites from plant tissues and exudates

5.6.1.1 Extraction of samples for targeted metabolite profiling

Two tissues per replicate (1-15 mg) were ground using a 5 mm steel ball in a Tissue Lyser II (QIAGEN) bead mill at 25 s^{-1} for 50 s. The resulting powder was extracted by vigorous shaking for 20 min with 200 µl of 70 % (v/v) methanol containing 2 nmol L-norvaline as internal standard for quantification of amino acids as well as 5 nmol each of [2,2,4,4-^{2}H] citric acid, [2,3,3-^{2}H] malic acid, and [2,2,3,3-^{2}H] succinic acid as internal standards for quantification of organic acids. After two centrifugations at 10000×g for 5 min each, the resulting supernatant was stored at -80° C until further processing.

5.6.1.2 Analysis of amino acids

Amino acids were analyzed as described by Ziegler and Abel, (2014). In order to record the calibration curve, the standard stock solution containing 500 pmol of each amino acid was diluted. For derivatization, 50 µl of 0.5 M sodium borate buffer pH 7.9 and 100 µl of a 3 mM Fmoc-Cl solution in acetone was added to 25 µl of samples. After 5 mins of incubation, the reaction was extracted three times with 0.5 ml of n-pentane. After removing the organic phase in the last extraction step, remaining organic acid was allowed to evaporate for 10 min. 500 µl of 5% (v/v) acetonitrile was added to the

aqueous phase before loading into the SPE resin. HR-X-resin (50mg/well) was distributed into the 96-well filtration plate. After this, the resin was conditioned by adding 1 ml of methanol followed by 1 ml of water. All the centrifugation steps to pass the liquid through the resin were performed in a JS5.3 swingout rotor in an Avanti J-26XP centrifuge (Beckman Coulter, Fullerton, CA, USA) at 250×g for 5 min. The resin was washed with 1 ml of water after loading the samples, followed by eluting with 1 ml of methanol into a 96-deep well plate (Roth, Karlsruhe, Germany). After putting the eluates into the 2 ml Eppendorf tubes, the solvent was evaporated in an Eppendorf Concentrator 5301 at 45° C (Eppendorf, Hamburg, Germany) under vacuum until 150-200 µl of eluate is left in the tubes. After centrifugation at 10000×g for 10 mins, the samples were transferred to autosampler vials for LC-MS/MS analysis.

A Nucleoshell RP18 column (50 × 3mm, particle size 2.7 µm; Macherey-Nagel, Düren, Germany) at 30° C was used to perform the separation using an Agilent 1100 series HPLC system. A and B eluents were 10 mM aqueous ammonium formate buffer pH 4.5 and acetonitrile, respectively. The percentage of B was increased to 50% over the first 6 min, further to 98% in 0.5 min, followed by an isocratic period of 0.5 min at 98% B from the initial starting condition of 25% B. Within the next 0.5 min, the starting conditions were restored, followed by column re-equilibration at 25% B for 5 min. The flow rate was set to 0.9 ml/min. The analytes were detected on-line by ESI-MS/MS using an API 3200 triple-quadrupole LC-MS/MS system equipped with an ESI Turbo Ion Spray interface, operated in the negative ion mode (AB Sciex, Darmstadt, Germany). The ion source parameters were set as follows: curtain gas: 30 psi, ion spray voltage: -4500 V, ion source temperature: 350° C, nebulizing and drying gas: 50 psi. Triple-quadrupole scans were acquired in the MRM mode with Q1 and Q3 set at 'unit' resolution. Scheduled MRM was performed with a window of 90 s and a target scan time of 0.5 s. The MRMs for each amino acids are used as mentioned in Ziegler and Abel, (2014). The IntelliQuant algorithm of the Analyst 1.6 software (AB Sciex, Darmstadt, Germany) was used to calculate the peak areas automatically and adjusted manually if necessary. Microsoft Excel was used to perform subsequent calculations.

5.6.1.3 Analysis of organic acids

Organic acids were analyzed as described by Ziegler et al. (2016). Ten microliters of root extracts were evaporated to dryness, methoxylated with 20 µl of 20 mg/ml of methoxyamine in pyridine for 1.5 h at room temperature, and silylated for 30 min at 37° C with 35 µl of Silyl 991. Gas chromatography (GC)-MS/MS analysis was performed using an Agilent 7890 GC system equipped with an Agilent 7000B triple quadrupole mass spectrometer operated in the positive chemical ionization mode (reagent gas: methane, gas flow: 20%, ion source temperature: 230° C). One microliter was injected [pulsed (25 psi)

splitless injection, 220° C] and separations were performed on a OPTIMA 5 column (10 m×0.25 mm, 0.25 µm, Macherey-Nagel, Düren, Germany) using Helium as a carrier gas (2.39 ml/min). The initial temperature of 70° C was held for 1 min, followed by increases at 9° C/min to 150° C and 30° C/min to 300° C. The final temperature of 300° C was held for 5 min. The transfer line was set to a temperature of 250° C, and N2 and He were used as collision and quench gases, respectively (1.5 and 2.25 ml/min). Data were acquired by multiple reaction monitoring using compound-specific parameters with Q1 and Q3 set to unit resolution. Peak areas were automatically integrated using the Agile algorithm of the MassHunter Quantitative Analysis software (version B.06.00) and manually adjusted if necessary. All subsequent calculations were performed with Excel, using the peak areas of the respective internal standards for quantification. MS parameters for MRM-transitions are mentioned in Supplementary table 7-20.

5.6.1.4 Water incubation experiment for root exudate analysis

Seedlings were grown aseptically on agar plates as described in the section 5.3.3. Root exudates were collected after 4 days of transfer of seedlings to +Pi or -Pi conditions. Each experiment consisted of 4 biological replicates per genotype and per treatment. Three seedlings for each biological replicate were carefully lifted with forceps from agar plates and washed with deionized water for 3-5 s. The roots of these three intact seedlings were incubated in 300 µl of deionized water which was filled in each well of 96 well microplate (Greiner Bio-one, Kremsmünster, Germany). After incubation of the roots in water for 2 hr, seedlings were harvested by separating roots and shoots and fresh weights were recorded. Exudates from each well were collected in a 2 ml Eppendorf tube and frozen in liquid nitrogen and stored at -80° C until further processing.

5.6.1.5 Preparation of exudates for organic acid analysis

20 µl of root exudate was mixed with 100 pmol each of [2,2,4,4-^{2}H] citric acid, [2,3,3-^{2}H] malic acid, and [2,2,3,3-^{2}H] succinic acid as internal standards. The samples were evaporated to dryness for 2 h and then the subsequent steps of derivatization and Gas chromatography (GC)-MS/MS analysis were performed as described before in section 5.6.1.3.

5.6.2 Treatment of plants with calcium phosphate as insoluble Pi-source

To determine whether increased malate exudation can improve Pi-solubilization capacity of transgenic plants from insoluble Pi sources, seedlings were germinated on medium containing α-tri-Calcium phosphate (Sigma-Aldrich). Ready to use Murashige and Skoog medium (MS) with and without KH_2PO_4 (KP) from Caissons lab was used for this experiment. The concentration of KP in MS medium was 1.25 mM. The pH of the media was adjusted to 7.6 with 1M KOH. $Ca_3(PO4)_2$ (CaP) was

added at a concentration of 1.25 mM to MS medium without phosphate. Surface sterilized seeds were individually placed with toothpicks on agar plates containing MS medium with KP and CaP as Pi-source. After stratification for 2 days at 4° C in the dark to synchronize seed germination, the plates were kept vertically in a growth chamber at 22° C under illumination for 16 h daily (170 µmol s^{-1} m^{-2}; Osram LumiluxDeLuxe Cool Daylight L58W/965, Osram, Augsberg, Germany). The seedlings were allowed to grow for 11 days and thereafter, the roots were separated from their shoots, their fresh weights were recorded and the samples were frozen in liquid nitrogen until further processing. One biological replicate consisted of roots or shoots from two plants.

5.6.3 Analysis of protein from plant tissues

5.6.3.1 Extraction of protein from plant material

Around 50-100 mg of Arabidopsis seedlings were harvested from agar plates and frozen in liquid nitrogen. The samples were ground using a 5 mm steel ball in a Tissue Lyser II (QIAGEN) bead mill at 25 s^{-1} for 50 s and total protein was extracted by adding 100-200 ul of protein extraction buffer. The protein extraction buffer consisted of Tris-Cl (25 mM, pH-7.6), $MgCl_2$ (15 mM), NaCl (85 mM), NaF (2.5 mM), EGTA (15 mM), DTT (5 mM), PMSF (1 mM), nonidet P40 (0.1% v/v), tween 20 (0.1% v/v), disodium nitrophenyl phosphate (15 mM), and disodium-β-glycerophosphate (60 mM). After vortexing the samples for 5-10 s, the samples were kept on a shaker in cold room for atleast 30 min. The sample tubes were centrifuged at 10,000 rpm for 5 min at 4° C and the supernatant was collected in a 1.5 ml eppendorf tube. The protein samples were stored at -80° C until further processing.

5.6.3.2 Protein quantification

The 2-D Quant Kit (GE Healthcare, Piscataway, USA) was used for determination of protein concentration in samples. A standard curve was prepared according to the manufacturer's instructions using 2 mg/ml Bovine Serum albumin (BSA) standard solution provided with the kit. The absorbance of each sample and standard was read at 480 nm using water as a reference with the Teccan Nanoquant Infinite M1000 (Männedorf, Switzerland).

5.6.3.3 Sodium dodecyl sulfate polyacrilamide gel electrophoresis (SDS-PAGE)

Protein samples were electrophoretically separated on a SDS-PAGE gel (Laemmli, 1970). The stacking gel and separating gel consisted of 4% and 12% polyacrylamide, respectively. The samples were mixed with 4x loading buffer (200 mM Tris-HCl, pH 6.8, 8% SDS, 0.4% Bromophenol blue, 50% glycerol, and 20% β-Mercaptoethanol) before loading on the gels. SDS-PAGE was performed at 100 V in a running buffer (25 mM Tris, pH 8.3, 192 mM glycine, and 0.1% SDS) until the dye front had reached the lower rim of the gel. The composition of stacking and separating gel is mentioned in Table 5-9.

Table 5-9: Composition of SDS-PAGE Gel

Components	Stacking gel (4%)	Separating gel (12%)
Millipore water	4.71 ml	5.75 ml
0.5 M Tris pH 6.8	1.88 ml	-
1.5 M Tris pH 8.8	-	3.75 ml
Glycerol	-	0.75 ml
40% Acrylamide	0.75 ml	4.5 ml
10% SDS	0.075 ml	0.15 ml
10% Ammonium persulphate	0.0225 ml	0.075 ml
TEMED	0.0225 ml	0.03 ml
Total Volume	7.5 ml	15 ml

5.6.3.4 Immunoblotting (Western Blot)

Proteins electrophoretically separated on a SDS-PAGE gel were transferred to a nitrocellulose membrane (Amersham Protran 0.45 µm) via semi-dry blotting with towbin transfer buffer [25 mM Tris-HCl, 192 mM Glycine, 20% methanol, 1.3 mM SDS, pH 8.3 (without adjustment)] at 20 V and 150 Watt for 1 h. After transfer, the membrane was blocked in 1x TBS (50 mM Tris-HCl, 150 mM NaCl, and 1mM $MgCl_2$, pH adjusted to 7.8 using HCl) with 2 % BSA and 2 % milk powder for 1 h with gentle shaking. After washing the membrane for 10 min with 1x TBS, primary antibody [GFP Antibody (B-2); mouse monoclonal IgG2a, Santa cruz biotechnology] was applied over the membrane at a dilution of 1:1000 with 2 % BSA and 2 % milk powder in 1x TBS and incubated overnight at 4° C with gentle shaking. The membrane was washed three times for 10 min with TBS and then the secondary antibody (Anti-mouse IgG-HRP, Sigma) was added at a dilution of 1:80,000 with 2 % BSA and 2 % milk powder in 1x TBS buffer and incubated for 1 h with gentle shaking. The membrane was rinsed with 1x TBS 3 times followed by incubation with 1x TBST (0.05% Tween 20 added to TBS buffer) for 1 h. The Horseradish peroxidase (HRP) detection was performed using Amersham ECL Prime Western Blotting Detection Reagent according to manufacturer's guidelines and chemoluminescent signal was detected with X-ray films.

5.6.4 Histochemical analysis

5.6.4.1 Iron staining

Accumulation and distribution of iron in roots were visualized by Perls staining as described in Müller et al. (2015). After clearing the roots in chloral hydrate (1 g/ml, 15% glycerol), imaging was performed with Zeiss Apotome 2 microscope using 10x DIC objective.

5.6.4.2 Callose staining

To stain callose, seedlings were incubated for 1.5 h with 0.1% (w/v) aniline blue (AppliChem) in 100 mM Na-phosphate buffer pH 7.2. Imaging was done by confocal microscopy on a Zeiss LSM 700 inverted microscope using 20x objective. Aniline blue was excited with a 405 nm laser, and emission was detected with a 490 nm short-pass filter.

5.6.4.3 GUS (β-glucuronidase) staining

For GUS staining, seedlings were incubated in GUS staining solution [50 mM Na-phosphate, pH 7.2, 0.5 mM 579 $K_3Fe(CN)_6$, 0.5 mM $K_4Fe(CN)_6$, 2 mM X-Gluc, 10 mM EDTA, 0,1% (v/v) Triton X-100] at 37° C for 10 min upto 8 h, depending on the intensity of staining. Imaging of GUS staining patterns was performed using a Zeiss Apotome 2 microscope with 10x DIC objective.

5.6.4.4 Confocal laser microscopy

Imaging for confocal microscopy was performed with a Zeiss LSM 710 inverted microscope using 40x water immersion objective. The excitation wavelength for Green Fluorescent Protein (GFP) was 488 nm, and emission was detected between 493 and 550 nm. For chlorophyll, excitation wavelength used was 639 nm and emission was detected between 644 and 800 nm.

5.6.5 Physiological assays

5.6.5.1 Root length measurement assay

Seeds were sown on modified ATS medium and stratified for 2 days at 4° C in the dark. The plates were kept vertically in a growth chamber at 22° C under illumination for 16 h daily (170 µmol s^{-1} m^{-2}; Osram LumiluxDeLuxe Cool Daylight L58W/965, Osram, Augsberg, Germany). After 6 days of growth, seedlings were transferred to fresh plates containing +Pi (0.5 M KH_2PO_4) or -Pi (5 µM KH_2PO_4) and allowed to grow for 9 more days. Images of seedlings growing on the plates were taken with a Nikon camera. Root measurements were performed using Fiji ImageJ (Schneider et al., 2012) with NeuronJ plugin (Meijering et al., 2004).

5.7 Data analysis

Data are normalized to the levels observed in Col-0+Pi for each experiment. The data from 3 or 4 independent germination experiments were combined to perform statistical analysis. Significance analysis was performed by Student's *t*-test (two-tailed, equal variances) in Microsoft excel. Two way ANOVA was performed using the MultiExperiment Viewer (MEV) software (Saeed et al., 2003).

6 REFERENCES

Abel, S., 2017. Phosphate scouting by root tips. Curr. Opin. Plant Biol. 39, 168–177.

Abel, S., 2011. Phosphate sensing in root development. Curr. Opin. Plant Biol. 14, 303–309.

Agarie, S., Miura, A., Sumikura, R., Tsukamoto, S., Nose, A., Arima, S., Matsuoka, M., Miyao-Tokutomi, M., 2002. Overexpression of C4 PEPC caused O_2-insensitive photosynthesis in transgenic rice plants. Plant Sci. 162, 257–265.

Ahmed, R., 2015. Molecular identification and characterization of the phosphate deficiency response related genes, PRT1 (ATP-Phosphoribosyl Transferase 1) and ALMT1 (Aluminium-activated Malate Transporter 1).

Anoop, V.M., Basu, U., McCammon, M.T., McAlister-Henn, L., Taylor, G.J., 2003. Modulation of citrate metabolism alters aluminum tolerance in yeast and transgenic canola overexpressing a mitochondrial citrate synthase. Plant Physiol. 132, 2205–2217.

Aono, T., Kanada, N., Ijima, A., Oyaizu, H., 2001. The response of the phosphate uptake system and the organic acid exudation system to phosphate starvation in Sesbania rostrata. Plant Cell Physiol. 42, 1253–1264.

Ap Rees, T., 1990. Carbon metabolism in mitochondria. Plant Physiol. Biochem. Mol. Biol. 106–123.

Asai, N., Nakajima, N., Tamaoki, M., Kamada, H., Kondo, N., 2000. Role of malate synthesis mediated by phosphoenolpyruvate carboxylase in guard cells in the regulation of stomatal movement. Plant Cell Physiol. 41, 10–15.

Badri, D.V., Vivanco, J.M., 2009. Regulation and function of root exudates. Plant Cell Environ. 32, 666–681.

Baker, A., Ceasar, S.A., Palmer, A.J., Paterson, J.B., Qi, W., Muench, S.P., Baldwin, S.A., 2015. Replace, reuse, recycle: improving the sustainable use of phosphorus by plants. J. Exp. Bot. 66, 3523–3540.

Bakrim, N., Echevarria, C., Cretin, C., Arrio-Dupont, M., Pierre, J.N., Vidal, J., Chollet, R., Gadal, P., 1992. Regulatory phosphorylation of Sorghum leaf phosphoenolpyruvate carboxylase. Eur. J. Biochem. 204, 821–830.

Balzergue, C., Dartevelle, T., Godon, C., Laugier, E., Meisrimler, C., Teulon, J.-M., Creff, A., Bissler, M., Brouchoud, C., Hagège, A., Müller, J., Chiarenza, S., Javot, H., Becuwe-Linka, N., David, P., Péret, B., Delannoy, E., Thibaud, M.-C., Armengaud, J., Abel, S., Pellequer, J.-L., Nussaume, L., Desnos, T., 2017. Low phosphate activates STOP1-ALMT1 to rapidly inhibit root cell elongation. Nat. Commun. 8, 15300.

Bandyopadhyay, A., Datta, K., Zhang, J., Yang, W., Raychaudhuri, S., Miyao, M., Datta, S.K., 2007. Enhanced photosynthesis rate in genetically engineered indica rice expressing pepc gene cloned from maize. Plant Sci. 172, 1204–1209.

Barone, P., Rosellini, D., LaFayette, P., Bouton, J., Veronesi, F., Parrott, W., 2008. Bacterial citrate synthase expression and soil aluminum tolerance in transgenic alfalfa. Plant Cell Rep. 27, 893–901.

Beaujean, A., Issakidis-Bourguet, E., Catterou, M., Dubois, F., Sangwan, R.S., Sangwan-Norreel, B.S., 2001. Integration and expression of Sorghum C4 phosphoenolpyruvate carboxylase and chloroplastic NADP+-malate dehydrogenase separately or together in C3 potato plants1.This paper is dedicated to the memory of our colleague Claude CRETIN.1. Plant Sci. 160, 1199–1210.

Begum, H.H., Osaki, M., Shinano, T., Miyatake, H., Wasaki, J., Yamamura, T., Watanabe, T., 2005. The function of a maize-derived phosphoenolpyruvate carboxylase (PEPC) in phosphorus-deficient transgenic rice. Soil Sci. Plant Nutr. 51, 497–506.

Bertani, G., 1951. Studies on lysogenesis. I. The mode of phage liberation by lysogenic Escherichia coli. J. Bacteriol. 62, 293–300.

Bläsing, O.E., Ernst, K., Streubel, M., Westhoff, P., Svensson, P., 2002. The non-photosynthetic phosphoenolpyruvate carboxylases of the C4 dicot Flaveria trinervia–implications for the evolution of C4 photosynthesis. Planta 215, 448–456.

Borland, A.M., Hartwell, J., Jenkins, G.I., Wilkins, M.B., Nimmo, H.G., 1999. Metabolite control overrides circadian regulation of phosphoenolpyruvate carboxylase kinase and CO_2 fixation in crassulacean acid metabolism. Plant Physiol. 121, 889–896.

Bustos, R., Castrillo, G., Linhares, F., Puga, M.I., Rubio, V., Pérez-Pérez, J., Solano, R., Leyva, A., Paz-Ares, J., 2010. A central regulatory system largely controls transcriptional activation and repression responses to phosphate starvation in Arabidopsis. PLoS Genet. 6, e1001102.

Cambraia, J., Galvani, F.R., Estevão, M.M., Sant'Anna, R., 1983. Effects of aluminum on organic acid, sugar and amino acid composition of the root system of sorghum (Sorghum bicolor L. Moench). J. Plant Nutr. 6, 313–322.

Carter, P.J., Fewson, C.A., Nimmo, G.A., Nimmo, H.G., Wilkins, M.B., 1996. Roles of circadian rhythms, light and temperature in the regulation of phosphoenolpyruvate carboxylase in crassulacean acid metabolism, in: Winter, K., Smith, J.A.C. (Eds.), Crassulacean Acid Metabolism: Biochemistry, Ecophysiology and Evolution, Ecological Studies. Springer Berlin Heidelberg, Berlin, Heidelberg, pp. 46–52.

Carter, P.J., Nimmo, H.G., Fewson, C.A., Wilkins, M.B., 1991. Circadian rhythms in the activity of a plant protein kinase. EMBO J. 10, 2063–2068.

Carter, P.J., Nimmo, H.G., Fewson, C.A., Wilkins, M.B., 1990. Bryophyllum fedtschenkoi protein phosphatase type 2A can dephosphorylate phosphoenolpyruvate carboxylase. FEBS Lett. 263, 233–236.

Chen, L.-M., Li, K.-Z., Miwa, T., Izui, K., 2004. Overexpression of a cyanobacterial phosphoenolpyruvate carboxylase with diminished sensitivity to feedback inhibition in Arabidopsis changes amino acid metabolism. Planta 219, 440–449.

Chen, Y.-T., Wang, Y., Yeh, K.-C., 2017. Role of root exudates in metal acquisition and tolerance. Curr. Opin. Plant Biol. 39, 66–72.

Chen, Z.-H., Jenkins, G.I., Nimmo, H.G., 2008. pH and carbon supply control the expression of phosphoenolpyruvate carboxylase kinase genes in Arabidopsis thaliana. Plant Cell Environ. 31, 1844–1850.

Chen, Z.-H., Nimmo, G.A., Jenkins, G.I., Nimmo, H.G., 2007. BHLH32 modulates several biochemical and morphological processes that respond to Pi starvation in Arabidopsis. Biochem. J. 405, 191–198.

Chiou, T.-J., Lin, S.-I., 2011. Signaling network in sensing phosphate availability in plants. Annu. Rev. Plant Biol. 62, 185–206.

Chollet, R., Vidal, J., O'Leary, M.H., 1996. PHOSPHOENOLPYRUVATE CARBOXYLASE: A ubiquitous, highly regulated enzyme in plants. Annu. Rev. Plant Physiol. Plant Mol. Biol. 47, 273–298.

Clough, S.J., Bent, A.F., 1998. Floral dip: a simplified method for Agrobacterium-mediated transformation of Arabidopsis thaliana. Plant J. Cell Mol. Biol. 16, 735–743.

Cook, R.M., Lindsay, J.G., Wilkins, M.B., Nimmo, H.G., 1995. Decarboxylation of malate in the crassulacean acid metabolism plant Bryophyllum (Kalanchoe) fedtschenkoi (Role of NAD-Malic enzyme). Plant Physiol. 109, 1301–1307.

Dakora, F.D., Phillips, D.A., 2002. Root exudates as mediators of mineral acquisition in low-nutrient environments, in: Adu-Gyamfi, J.J. (Ed.), Food Security in Nutrient-Stressed Environments: Exploiting Plants' Genetic Capabilities. Springer Netherlands, Dordrecht, pp. 201–213.

Dam, N., J. Bouwmeester, H., 2016. Metabolomics in the Rhizosphere: Tapping into Belowground Chemical Communication. Trends Plant Sci. 21(3), 256-265.

Delhaize, E., Hebb, D.M., Ryan, P.R., 2001. Expression of a Pseudomonas aeruginosa citrate synthase gene in tobacco is not associated with either enhanced citrate accumulation or efflux. Plant Physiol. 125, 2059–2067.

Delhaize, E., Ryan, P.R., Hebb, D.M., Yamamoto, Y., Sasaki, T., Matsumoto, H., 2004. Engineering high-level aluminum tolerance in barley with the ALMT1 gene. Proc. Natl. Acad. Sci. 101, 15249–15254.

Delhaize, E., Ryan, P.R., Hocking, P.J., Richardson, A.E., 2003. Effects of altered citrate synthase and isocitrate dehydrogenase expression on internal citrate concentrations and citrate efflux from tobacco (Nicotiana tabacum L.) roots. Plant Soil 248, 137–144.

Delhaize, E., Ryan, P.R., Randall, P.J., 1993. Aluminum tolerance in wheat (Triticum aestivum L.)(II. Aluminum-stimulated excretion of malic acid from root apices). Plant Physiol. 103, 695–702.

Delhaize, E., Taylor, P., Hocking, P.J., Simpson, R.J., Ryan, P.R., Richardson, A.E., 2009. Transgenic barley (Hordeum vulgare L.) expressing the wheat aluminium resistance gene (TaALMT1) shows enhanced phosphorus nutrition and grain production when grown on an acid soil. Plant Biotechnol. J. 7, 391–400.

Demao, J., Xia, L., Xueqing, H., Wei, C., Tingyun, K., Maurice, K.S.B., 2001. The characteristics of CO_2 assimilation of photosynthesis and chlorophyll fluorescence in transgenic PEPC rice. Chin. Sci. Bull. 46, 1080.

Deng, W., Luo, K., Li, Z., Yang, Y., Hu, N., Wu, Y., 2009. Overexpression of Citrus junos mitochondrial citrate synthase gene in Nicotiana benthamiana confers aluminum tolerance. Planta 230, 355–365.

Ding, Z.-S., Huang, S.-H., Zhou, B.-Y., Sun, X.-F., Zhao, M., 2013. Over-expression of phosphoenolpyruvate carboxylase cDNA from C4 millet (Seteria italica) increase rice photosynthesis and yield under upland condition but not in wetland fields. Plant Biotechnol. Rep. 7, 155–163.

Dinkelaker, B., Hengeler, C., Marschner, H., 1995. Distribution and function of proteoid roots and other root clusters. Bot. Acta 108, 183–200.

Dizengremel, P., Vaultier, M.-N., Le Thiec, D., Cabané, M., Bagard, M., Gérant, D., Gérard, J., Dghim, A.A., Richet, N., Afif, D., Pireaux, J.-C., Hasenfratz-Sauder, M.-P., Jolivet, Y., 2012. Phosphoenolpyruvate is at the crossroads of leaf metabolic responses to ozone stress. New Phytol. 195, 512–7.

Dong, D., Peng, X., Yan, X., 2004. Organic acid exudation induced by phosphorus deficiency and/or aluminium toxicity in two contrasting soybean genotypes. Physiol. Plant. 122, 190–199.

Dong, L.-Y., Masuda, T., Hata, S., Izui, K., 1998. Molecular evolution of C4-form PEPC in maize: comparison of primary sequences and kinetic properties with a newly cloned recombinant root-form PEPC, in: Garab, G. (Ed.), Photosynthesis: Mechanisms and Effects: Volume I–V: Proceedings of the XIth International Congress on Photosynthesis, Budapest, Hungary, August 17–22, 1998. Springer Netherlands, Dordrecht, pp. 3411–3414.

Duff, S., Chollet, R., 1995. In vivo regulation of wheat-leaf phosphoenolpyruvate carboxylase by reversible phosphorylation. Plant Physiol. 107, 775–782.

Duff, S.M.G., Moorhead, G.B.G., Lefebvre, D.D., Plaxton, W.C., 1989. Phosphate starvation inducible `bypasses' of adenylate and phosphate dependent glycolytic enzymes in Brassica nigra suspension cells. Plant Physiol. 90, 1275–1278.

Eastmond, P.J., Graham, I.A., 2001. Re-examining the role of the glyoxylate cycle in oilseeds. Trends Plant Sci. 6, 72–78.

Echevarria, C., Pacquit, V., Bakrim, N., Osuna, L., Delgado, B., Arriodupont, M., Vidal, J., 1994. The effect of pH on the covalent and metabolic control of C4 phosphoenolpyruvate carboxylase from Sorghum leaf. Arch. Biochem. Biophys. 315, 425–430.

Ernst, K., Westhoff, P., 1997. The phosphoenolpyruvate carboxylase (ppc) gene family of Flaveria trinervia (C4) and F. pringlei (C3): molecular characterization and expression analysis of the ppcB and ppcC genes. Plant Mol. Biol. 34, 427–443.

Feria, A.B., Bosch, N., Sánchez, A., Nieto-Ingelmo, A.I., de la Osa, C., Echevarría, C., García-Mauriño, S., Monreal, J.A., 2016. Phosphoenolpyruvate carboxylase (PEPC) and PEPC-kinase (PEPC-k) isoenzymes in Arabidopsis thaliana: role in control and abiotic stress conditions. Planta 244, 901–913.

Fernie, A.R., Carrari, F., Sweetlove, L.J., 2004. Respiratory metabolism: glycolysis, the TCA cycle and mitochondrial electron transport. Curr. Opin. Plant Biol. 7, 254–261.

Fontaine, V., Hartwell, J., Jenkins, G.I., Nimmo, H.G., 2002. Arabidopsis thaliana contains two phosphoenolpyruvate carboxylase kinase genes with different expression patterns. Plant Cell Environ. 25, 115–122.

Fontecha, G., Silva-Navas, J., Benito, C., Mestres, M.A., Espino, F.J., Hernández-Riquer, M.V., Gallego, F.J., 2006. Candidate gene identification of an aluminum-activated organic acid transporter gene at the Alt4 locus for aluminum tolerance in rye (Secale cereale L.). Theor. Appl. Genet. 114, 249–260.

Fuente, J.M. de la, Ramírez-Rodríguez, V., Cabrera-Ponce, J.L., Herrera-Estrella, L., 1997. Aluminum tolerance in transgenic plants by alteration of citrate synthesis. Science 276, 1566–1568.

Fukayama, H., Hatch, M.D., Tamai, T., Tsuchida, H., Sudoh, S., Furbank, R.T., Miyao, M., 2003. Activity regulation and physiological impacts of maize C4-specific phosphoenolpyruvate carboxylase overproduced in transgenic rice plants. Photosynth. Res. 77, 227–239.

Furukawa, J., Yamaji, N., Wang, H., Mitani, N., Murata, Y., Sato, K., Katsuhara, M., Takeda, K., Ma, J.F., 2007. An aluminum-activated citrate transporter in barley. Plant Cell Physiol. 48, 1081–1091.

Gardner, W.K., Barber, D.A., Parbery, D.G., 1983. The acquisition of phosphorus by Lupinus albus L. Plant Soil 70, 107–124.

Gardner, W K, Parbery, D.G., Barber, D.A., 1982. The acquisition of phosphorus by Lupinus albus L. I. Some characteristics of the soil/root interface. Plant Soil 68, 19–32.

Gardner, W. K., Parbery, D.G., Barber, D.A., 1982. The acquisition of phosphorus by Lupinus albus L. II. The effect of varying phosphorus supply and soil type on some characteristics of the soil/root interface. Plant Soil 68, 33–41.

Gehlen, J., Panstruga, R., Smets, H., Merkelbach, S., Kleines, M., Porsch, P., Fladung, M., Becker, I., Rademacher, T., Häusler, R.E., Hirsch, H.-J., 1996. Effects of altered phosphoenolpyruvate carboxylase activities on transgenic C3 plant Solanum tuberosum. Plant Mol. Biol. 32, 831–848.

Gennidakis, S., Rao, S., Greenham, K., Uhrig, R.G., O'Leary, B., Snedden, W.A., Lu, C., Plaxton, W.C., 2007. Bacterial-and plant-type phosphoenolpyruvate carboxylase polypeptides interact in the hetero-oligomeric Class-2 PEPC complex of developing castor oil seeds. Plant J. 52, 839–849.

Gerrard Wheeler, M.C., Arias, C.L., Tronconi, M.A., Maurino, V.G., Andreo, C.S., Drincovich, M.F., 2008. Arabidopsis thaliana NADP-malic enzyme isoforms: high degree of identity but clearly distinct properties. Plant Mol. Biol. 67, 231–242.

Gietl, C., 1992. Malate dehydrogenase isoenzymes: Cellular locations and role in the flow of metabolites between the cytoplasm and cell organelles. Biochim. Biophys. Acta BBA - Bioenerg. 1100, 217–234.

Głowacka, K., Kromdijk, J., Leonelli, L., Niyogi, K.K., Clemente, T.E., Long, S.P., 2016. An evaluation of new and established methods to determine T-DNA copy number and homozygosity in transgenic plants. Plant Cell Environ. 39, 908–917.

Gonçalves, J.F., Cambraia, J., Roberto Mosquim, P., Fernandes Araújo, E., 2005. Aluminum effect on organic acid production and accumulation in Sorghum. J. Plant Nutr. 28, 507–520.

Gousset-Dupont, A., Lebouteiller, B., Monreal, J., Echevarria, C., Pierre, J.N., Hodges, M., Vidal, J., 2005. Metabolite and post-translational control of phosphoenolpyruvate carboxylase from leaves and mesophyll cell protoplasts of Arabidopsis thaliana. Plant Sci. 169, 1096–1101.

Gowik, U., Westhoff, P., 2011. The Path from C3 to C4 Photosynthesis. Plant Physiol. 155, 56–63.

Grefen, C., Donald, N., Hashimoto, K., Kudla, J., Schumacher, K., Blatt, M.R., 2010. A ubiquitin-10 promoter-based vector set for fluorescent protein tagging facilitates temporal stability and native protein distribution in transient and stable expression studies. Plant J. Cell Mol. Biol. 64, 355–365.

Gregory, A.L., Hurley, B.A., Tran, H.T., Valentine, A.J., She, Y.-M., Knowles, V.L., Plaxton, W.C., 2009. In vivo regulatory phosphorylation of the phosphoenolpyruvate carboxylase AtPPC1 in phosphate-starved Arabidopsis thaliana. Biochem. J. 420, 57–65.

Grierson, P.F., 1992. Organic acids in the rhizosphere of Banksia integrifolia. Plant Soil. 144, 259–265.

Grillet, L., Ouerdane, L., Flis, P., Hoang, M.T.T., Isaure, M.-P., Lobinski, R., Curie, C., Mari, S., 2014. Ascorbate efflux as a new strategy for iron reduction and transport in plants. J. Biol. Chem. 289, 2515–2525.

Gruber, B.D., Delhaize, E., Richardson, A.E., Roessner, U., James, R.A., Howitt, S.M., Ryan, P.R., 2011. Characterisation of HvALMT1 function in transgenic barley plants. Funct. Plant Biol. 38, 163–175.

Guillet, C., Just, D., Bénard, N., Destrac-Irvine, A., Baldet, P., Hernould, M., Causse, M., Raymond, P., Rothan, C., 2002. A fruit-specific phosphoenolpyruvate carboxylase is related to rapid growth of tomato fruit. Planta 214, 717–726.

Han, Y., Zhang, W., Zhang, B., Zhang, S., Wang, W., Ming, F., 2009. One novel mitochondrial citrate synthase from Oryza sativa L. can enhance aluminum tolerance in transgenic tobacco. Mol. Biotechnol. 42, 299–305.

Hanahan, D., 1983. Studies on transformation of E. coli with plasmids. J. Mol. Biol. 166, 557–580.

Hartwell, J., Gill, A., Nimmo, G.A., Wilkins, M.B., Jenkins, G.I., Nimmo, H.G., 1999. Phosphoenolpyruvate carboxylase kinase is a novel protein kinase regulated at the level of expression. Plant J. Cell Mol. Biol. 20, 333–342.

Hartwell, J., Smith, L.H., Wilkins, M.B., Jenkins, G.I., Nimmo, H.G., 1996. Higher plant phosphoenolpyruvate carboxylase kinase is regulated at the level of translatable mRNA in response to light or a circadian rhythm. Plant J. 10, 1071–1078.

Häusler, R.E., Hirsch, H., Kreuzaler, F., Peterhänsel, C., 2002. Overexpression of C4-cycle enzymes in transgenic C3 plants: a biotechnological approach to improve C3-photosynthesis. J. Exp. Bot. 53, 591–607.

Häusler, R.E., Kleines, M., Uhrig, H., Hirsch, H.-J., Smets, H., 1999. Overexpression of phosphoenolpyruvate carboxylase from Corynebacterium glutamicum lowers the CO2 compensation point (Γ*) and enhances dark and light respiration in transgenic potato. J. Exp. Bot. 50, 1231–1242.

Heazlewood, J.L., 2004. AMPDB: the Arabidopsis Mitochondrial Protein Database. Nucleic Acids Res. 33, D605–D610.

Hocking, P.J., 2001. Organic acids exuded from roots in phosphorus uptake and aluminum tolerance of plants in acid soils, in: Advances in Agronomy. Academic Press, pp. 63–97.

Hoekenga, O.A., Maron, L.G., Pineros, M.A., Cancado, G.M.A., Shaff, J., Kobayashi, Y., Ryan, P.R., Dong, B., Delhaize, E., Sasaki, T., Matsumoto, H., Yamamoto, Y., Koyama, H., Kochian, L.V., 2006. AtALMT1, which encodes a malate transporter, is identified as one of several genes critical for aluminum tolerance in Arabidopsis. Proc. Natl. Acad. Sci. 103, 9738–9743.

Hoffland, E., Findenegg, G.R., Nelemans, J.A., 1989. Solubilization of rock phosphate by rape. Plant Soil 113, 155–160.

Hoffland, E., Van Den Boogaard, R., Nelemans, J., Findenegg, G., 1992. Biosynthesis and root exudation of citric and malic acids in phosphate-starved rape plants. New Phytol. 122, 675–680.

Hoffland, E., Wei, C., Wissuwa, M., 2006. Organic anion exudation by lowland rice (Oryza sativa L.) at zinc and phosphorus deficiency. Plant Soil. 283, 155–162.

Hudspeth, R.L., Grula, J.W., Dai, Z., Edwards, G.E., Ku, M.S., 1992. Expression of maize phosphoenolpyruvate carboxylase in transgenic tobacco : effects on biochemistry and physiology. Plant Physiol. 98, 458–464.

Igamberdiev, A.U., Eprintsev, A.T., 2016. Organic Acids: The pools of fixed carbon involved in redox regulation and energy balance in higher plants. Front. Plant Sci. 7, 1042.

Igawa, T., Fujiwara, M., Tanaka, I., Fukao, Y., Yanagawa, Y., 2010. Characterization of bacterial-type phosphoenolpyruvate carboxylase expressed in male gametophyte of higher plants. BMC Plant Biol. 10, 200.

Izui, K., Matsumura, H., Furumoto, T., Kai, Y., 2004. PHOSPHOENOLPYRUVATE CARBOXYLASE: A new era of structural biology. Annu. Rev. Plant Biol. 55, 69–84.

Jemo, M., Abaidoo, R.C., Nolte, C., Horst, W.J., 2007. Aluminum resistance of cowpea as affected by phosphorus-deficiency stress. J. Plant Physiol. 164, 442–451.

Jiao, D., Huang, X., Li, X., Chi, W., Kuang, T., Zhang, Q., Ku, M.S.B., Cho, D., 2002. Photosynthetic characteristics and tolerance to photo-oxidation of transgenic rice expressing C4 photosynthesis enzymes. Photosynth. Res. 72, 85–93.

Jiao, J., Echevarría, C., Vidal, J., Chollet, R., 1991. Protein turnover as a component in the light/dark regulation of phosphoenolpyruvate carboxylase protein-serine kinase activity in C4 plants. Proc. Natl. Acad. Sci. U. S. A. 88, 2712–2715.

Johnson, J.F., Allan, D.L., Vance, C.P., 1994. Phosphorus stress-induced proteoid roots show altered metabolism in Lupinus albus. Plant Physiol. 104, 657–665.

Johnson, L.N., Noble, M.E.M., Owen, D.J., 1996. Active and Inactive Protein Kinases: Structural Basis for Regulation. Cell 85, 149–158.

Jones, D.L., 1998. Organic acids in the rhizosphere – a critical review. Plant Soil 205, 25–44.

Jones, D.L., Darrah, P.R., 1994. Role of root derived organic acids in the mobilization of nutrients from the rhizosphere. Plant Soil 166, 247–257.

Jones, D.L., Dennis, P.G., Owen, A.G., Hees, P.A.W. van, 2003. Organic acid behavior in soils – misconceptions and knowledge gaps. Plant Soil 248, 31–41.

Juszczuk, I.M., Rychter, A.M., 2002. Pyruvate accumulation during phosphate deficiency stress of bean roots. Plant Physiol. Biochem. 40, 783–788.

Kai, Y., Matsumura, H., Izui, K., 2003. Phosphoenolpyruvate carboxylase: three-dimensional structure and molecular mechanisms. Arch. Biochem. Biophys. 414, 170–179.

Kandoi, D., Mohanty, S., Govindjee, Tripathy, B.C., 2016. Towards efficient photosynthesis: overexpression of Zea mays phosphoenolpyruvate carboxylase in Arabidopsis thaliana. Photosynth. Res. 130, 47–72.

Karimi, M., Inzé, D., Depicker, A., 2002. GATEWAY^{TM} vectors for Agrobacterium-mediated plant transformation. Trends Plant Sci. 7, 193–195.

Karimi, M., Meyer, B.D., Hilson, P., 2005. Modular cloning in plant cells. Trends Plant Sci. 10, 103–105.

Kawamura, T., Shigesada, K., Yanagisawa, S., Izui, K., 1990. Phosphoenolpyruvate carboxylase prevalent in maize roots: Isolation of a cDNA clone and its use for analyses of the gene and gene expression. J. Biochem. 107, 165-168.

Keerthisinghe, G., Hocking, P.J., Ryan, P.R., Delhaize, E., 1998. Effect of phosphorus supply on the formation and function of proteoid roots of white lupin (Lupinus albus L.). Plant Cell Environ. 21, 467–478.

Khachatoorian, C., Ramirez, R.A., Hernandez, F., Serna, R., Kwok, E.Y., 2015. Overexpressed Arabidopsis Annexin4 accumulates in inclusion body like structures. Acta Histochem. 117, 279–287.

Kitagawa, T., Morishita, T., Tachibana, Y., Namai, H., Ohta, Y., 1986. Differential aluminum resistance of wheat varieties and organic acid secretion. Jpn. J. Soil Sci. Plant Nutr. 57(4), 352-358.

Kobayashi, Y., Hoekenga, O.A., Itoh, H., Nakashima, M., Saito, S., Shaff, J.E., Maron, L.G., Piñeros, M.A., Kochian, L.V., Koyama, H., 2007. Characterization of AtALMT1 expression in aluminum-inducible malate release and its role for rhizotoxic stress tolerance in Arabidopsis. Plant Physiol. 145, 843–852.

Kobayashi, Yasufumi, Lakshmanan, V., Kobayashi, Yuriko, Asai, M., Iuchi, S., Kobayashi, M., Bais, H.P., Koyama, H., 2013. Overexpression of AtALMT1 in the Arabidopsis thaliana ecotype Columbia results in enhanced Al-activated malate excretion and beneficial bacterium recruitment. Plant Signal. Behav. 8(9), e25565.

Kochian, L.V., Hoekenga, O.A., Piñeros, M.A., 2004. How do crop plants tolerate acid soils? Mechanisms of aluminum tolerance and phosphorous efficiency. Annu. Rev. Plant Biol. 55, 459–493.

Kochian, L.V., Piñeros, M.A., Hoekenga, O.A., 2005. The physiology, genetics, and molecular biology of plant aluminum resistance and toxicity. Plant Soil 274, 175–195.

Kochian, L.V., Piñeros, M.A., Liu, J., Magalhaes, J.V., 2015. Plant adaptation to acid soils: The molecular basis for crop aluminum resistance. Annu. Rev. Plant Biol. 66, 571–598.

Kogami, H., Shono, M., Koike, T., Yanagisawa, S., Izui, K., Sentoku, N., Tanifuji, S., Uchimiya, H., Toki, S., 1994. Molecular and physiological evaluation of transgenic tobacco plants expressing a maize

phosphoenolpyruvate carboxylase gene under the control of the cauliflower mosaic virus 35S promoter. Transgenic Res. 3, 287–296.

Koncz, C., Schell, J., 1986. The promoter of TL-DNA gene 5 controls the tissue-specific expression of chimaeric genes carried by a novel type of Agrobacterium binary vector. Mol. Gen. Genet. MGG 204, 383–396.

Koyama, H., Takita, E., Kawamura, A., Hara, T., Shibata, D., 1999. Over expression of mitochondrial citrate synthase gene improves the growth of carrot cells in Al-phosphate medium. Plant Cell Physiol. 40, 482–488.

Ku, M.S., Agarie, S., Nomura, M., Fukayama, H., Tsuchida, H., Ono, K., Hirose, S., Toki, S., Miyao, M., Matsuoka, M., 1999. High-level expression of maize phosphoenolpyruvate carboxylase in transgenic rice plants. Nat. Biotechnol. 17, 76–80.

Laemmli, U.K., 1970. Cleavage of structural proteins during the assembly of the head of bacteriophage T4. Nature 227, 680–685.

Lambers, H., Cawthray, G.R., Giavalisco, P., Kuo, J., Laliberté, E., Pearse, S.J., Scheible, W.-R., Stitt, M., Teste, F., Turner, B.L., 2012. Proteaceae from severely phosphorus-impoverished soils extensively replace phospholipids with galactolipids and sulfolipids during leaf development to achieve a high photosynthetic phosphorus-use-efficiency. New Phytol. 196, 1098–1108.

Lambers, H., Martinoia, E., Renton, M., 2015. Plant adaptations to severely phosphorus-impoverished soils. Curr. Opin. Plant Biol. 25, 23–31.

Lambers, H., Shane, M.W., Cramer, M.D., Pearse, S.J., Veneklaas, E.J., 2006. Root structure and functioning for efficient acquisition of phosphorus: Matching morphological and physiological traits. Ann. Bot. 98, 693–713.

Lance, C., Rustin, P., 1984. The central role of malate in plant metabolism. Physiol Veg 22, 625–641.

Law, R.D., Plaxton, W.C., 1997. Regulatory phosphorylation of banana fruit phosphoenolpyruvate carboxylase by a copurifying phosphoenolpyruvate carboxylase-kinase. Eur. J. Biochem. 247, 642–651.

Le Van Quy, Foyer, C., Champigny, M.-L., 1991. Effect of light and NO_3^- on wheat leaf phosphoenolpyruvate carboxylase activity. Plant Physiol. 97, 1476–1482.

Lepiniec, L., Keryer, E., Philippe, H., Gadal, P., Crétin, C., 1993. Sorghum phosphoenolpyruvate carboxylase gene family: structure, function, and molecular evolution. Plant Mol. Biol. 21, 487–502.

Li, K., Xu, C., Li, Z., Zhang, K., Yang, A., Zhang, J., 2008. Comparative proteome analyses of phosphorus responses in maize (Zea mays L.) roots of wild-type and a low-P-tolerant mutant reveal root characteristics associated with phosphorus efficiency. Plant J. 55, 927–939.

Li, W., Lan, P., 2015. Genome-wide analysis of overlapping genes regulated by iron deficiency and phosphate starvation reveals new interactions in Arabidopsis roots. BMC Res. Notes 8, 555.

Liao, H., Wan, H., Shaff, J., Wang, X., Yan, X., Kochian, L.V., 2006. Phosphorus and aluminum interactions in soybean in relation to aluminum tolerance. Exudation of specific organic acids from different regions of the intact root system. Plant Physiol. 141, 674–684.

Ligaba, A., Katsuhara, M., Ryan, P.R., Shibasaka, M., Matsumoto, H., 2006. The BnALMT1 and BnALMT2 genes from rape encode aluminum-activated malate transporters that enhance the aluminum resistance of plant cells. Plant Physiol. 142, 1294–1303.

Lin, Z.-H., Chen, L.-S., Chen, R.-B., Zhang, F.-Z., Jiang, H.-X., Tang, N., Smith, B.R., 2011. Root release and metabolism of organic acids in tea plants in response to phosphorus supply. J. Plant Physiol. 168, 644–652.

Liu, J., Magalhaes, J.V., Shaff, J., Kochian, L.V., 2009. Aluminum-activated citrate and malate transporters from the MATE and ALMT families function independently to confer Arabidopsis aluminum tolerance. Plant J. 57, 389–399.

López-Arredondo, D.L., Leyva-González, M.A., González-Morales, S.I., López-Bucio, J., Herrera-Estrella, L., 2014. Phosphate Nutrition: Improving Low-Phosphate Tolerance in Crops. Annu. Rev. Plant Biol. 65, 95–123.

López-Bucio, J., de La Vega, O.M., Guevara-García, A., Herrera-Estrella, L., 2000. Enhanced phosphorus uptake in transgenic tobacco plants that overproduce citrate. Nat. Biotechnol. 18, 450–453.

Lü, J., Gao, X., Dong, Z., Yi, J., An, L., 2012. Improved phosphorus acquisition by tobacco through transgenic expression of mitochondrial malate dehydrogenase from Penicillium oxalicum. Plant Cell Rep. 31, 49–56.

Lynch, J.P., Brown, K.M., 2001. Topsoil foraging–an architectural adaptation of plants to low phosphorus availability. Plant Soil. 237, 225–237.

Ma, J.F., Ryan, P.R., Delhaize, E., 2001. Aluminium tolerance in plants and the complexing role of organic acids. Trends Plant Sci. 6, 273–278.

Ma, J.F., Taketa, S., Yang, Z.M., 2000. Aluminum tolerance genes on the short arm of chromosome 3R are linked to organic acid release in triticale. Plant Physiol. 122, 687–694.

Magalhaes, J.V., Liu, J., Guimarães, C.T., Lana, U.G.P., Alves, V.M.C., Wang, Y.-H., Schaffert, R.E., Hoekenga, O.A., Piñeros, M.A., Shaff, J.E., Klein, P.E., Carneiro, N.P., Coelho, C.M., Trick, H.N., Kochian, L.V., 2007. A gene in the multidrug and toxic compound extrusion (MATE) family confers aluminum tolerance in sorghum. Nat. Genet. 39, 1156–1161.

Maier, A., Zell, M.B., Maurino, V.G., 2011. Malate decarboxylases: evolution and roles of NAD(P)-ME isoforms in species performing C4 and C3 photosynthesis. J. Exp. Bot. 62, 3061–3069.

Mamedov, T.G., Moellering, E.R., Chollet, R., 2005. Identification and expression analysis of two inorganic C- and N-responsive genes encoding novel and distinct molecular forms of eukaryotic phosphoenolpyruvate carboxylase in the green microalga Chlamydomonas reinhardtii. Plant J. 42, 832–843.

Maron, L.G., Piñeros, M.A., Guimarães, C.T., Magalhaes, J.V., Pleiman, J.K., Mao, C., Shaff, J., Belicuas, S.N.J., Kochian, L.V., 2010. Two functionally distinct members of the MATE (multi-drug and toxic compound extrusion) family of transporters potentially underlie two major aluminum tolerance QTLs in maize. Plant J. 61, 728–740.

Marsh, J.T., Sullivan, S., Hartwell, J., Nimmo, H.G., 2003. Structure and expression of phosphoenolpyruvate carboxylase kinase genes in solanaceae. A novel gene exhibits alternative splicing. Plant Physiol. 133, 2021–2028.

Martin, B.C., George, S.J., Price, C.A., Ryan, M.H., Tibbett, M., 2014. The role of root exuded low molecular weight organic anions in facilitating petroleum hydrocarbon degradation: Current knowledge and future directions. Sci. Total Environ. 472, 642–653.

Martinoia, E., Rentsch, D., 1994. Malate compartmentation-responses to a complex metabolism. Annu. Rev. Plant Physiol. Plant Mol. Biol. 45, 447–467.

Maruyama, H., Sasaki, T., Yamamoto, Y., Wasaki, J., 2019. AtALMT3 is involved in malate efflux induced by phosphorus deficiency in Arabidopsis thaliana root hairs. Plant Cell Physiol. 60, 107–115.

Masakapalli, S.K., Bryant, F.M., Kruger, N.J., Ratcliffe, R.G., 2014. The metabolic flux phenotype of heterotrophic Arabidopsis cells reveals a flexible balance between the cytosolic and plastidic contributions to carbohydrate oxidation in response to phosphate limitation. Plant J. 78, 964–977.

Masumoto, C., Miyazawa, S.-I., Ohkawa, H., Fukuda, T., Taniguchi, Y., Murayama, S., Kusano, M., Saito, K., Fukayama, H., Miyao, M., 2010. Phosphoenolpyruvate carboxylase intrinsically located in the chloroplast of rice plays a crucial role in ammonium assimilation. Proc. Natl. Acad. Sci. 107, 5226–5231.

Maurino, V.G., Engqvist, M.K.M., 2015. 2-Hydroxy Acids in Plant Metabolism. Arab. Book 13, e0182.

Meijering, E., Jacob, M., Sarria, J.-C.F., Steiner, P., Hirling, H., Unser, M., 2004. Design and validation of a tool for neurite tracing and analysis in fluorescence microscopy images. Cytom. Part J. Int. Soc. Anal. Cytol. 58, 167–176.

Meimoun, P., Gousset-Dupont, A., Lebouteiller, B., Ambard-Bretteville, F., Besin, E., Lelarge, C., Mauve, C., Hodges, M., Vidal, J., 2009. The impact of PEPC phosphorylation on growth and development of Arabidopsis thaliana: molecular and physiological characterization of PEPC kinase mutants. FEBS Lett. 583, 1649–1652.

Meyer, S., De Angeli, A., Fernie, A.R., Martinoia, E., 2010. Intra- and extra-cellular excretion of carboxylates. Trends Plant Sci. 15, 40–47.

Meyer, S., Scholz-Starke, J., Angeli, A.D., Kovermann, P., Burla, B., Gambale, F., Martinoia, E., 2011. Malate transport by the vacuolar AtALMT6 channel in guard cells is subject to multiple regulation. Plant J. 67, 247–257.

Miller, S.S., Driscoll, B.T., Gregerson, R.G., Gantt, J.S., Vance, C.P., 1998. Alfalfa malate dehydrogenase (MDH): molecular cloning and characterization of five different forms reveals a unique nodule-enhanced MDH. Plant J. 15, 173–184.

Monreal, J.A., McLoughlin, F., Echevarría, C., García-Mauriño, S., Testerink, C., 2010. Phosphoenolpyruvate carboxylase from C4 Leaves is selectively targeted for inhibition by anionic phospholipids. Plant Physiol. 152, 634–638.

Mora-Macías, J., Ojeda-Rivera, J.O., Gutiérrez-Alanís, D., Yong-Villalobos, L., Oropeza-Aburto, A., Raya-González, J., Jiménez-Domínguez, G., Chávez-Calvillo, G., Rellán-Álvarez, R., Herrera-Estrella, L., 2017. Malate-dependent Fe accumulation is a critical checkpoint in the root developmental response to low phosphate. Proc. Natl. Acad. Sci. 114, E3563–E3572.

Morcuende, R., Bari, R., Gibon, Y., Zheng, W., Pant, B.D., Bläsing, O., Usadel, B., Czechowski, T., Udvardi, M.K., Stitt, M., Scheible, W.R., 2007. Genome-wide reprogramming of metabolism and regulatory networks of Arabidopsis in response to phosphorus. Plant Cell Environ. 30, 85–112.

Müller, J., Toev, T., Heisters, M., Teller, J., Moore, K.L., Hause, G., Dinesh, D.C., Bürstenbinder, K., Abel, S., 2015. Iron-dependent callose deposition adjusts root meristem maintenance to phosphate availability. Dev. Cell. 33, 216–230.

Müller, R., Morant, M., Jarmer, H., Nilsson, L., Nielsen, T.H., 2007. Genome-wide analysis of the Arabidopsis leaf transcriptome reveals interaction of phosphate and sugar metabolism. Plant Physiol. 143, 156–171.

Murashige, T., Skoog, F., 1962. A revised medium for rapid growth and bio assays with tobacco tissue cultures. Physiol. Plant. 15, 473–497.

Murmu, J., Plaxton, W.C., 2007. Phosphoenolpyruvate carboxylase protein kinase from developing castor oil seeds: partial purification, characterization, and reversible control by photosynthate supply. Planta 226, 1299–1310.

Murphy, A.S., Eisinger, W.R., Shaff, J.E., Kochian, L.V., Taiz, L., 1999. Early copper-induced leakage of K+ from Arabidopsis seedlings is mediated by ion channels and coupled to citrate efflux. Plant Physiol. 121, 1375–1382.

Nagano, M., Hachiya, A., Ashihara, H., 1994. Phosphate starvation and a glycolytic bypass catalyzed by phosphoenolpyruvate carboxylase in suspension-cultured Catharanthus roseus cells. Z. Naturforschung C J. Biosci. 49c, 742–750.

Narang, R.A., Bruene, A., Altmann, T., 2000. Analysis of phosphate acquisition efficiency in different Arabidopsis accessions. Plant Physiol. 124, 1786–1799.

Neumann, G., Massonneau, A., Langlade, N., Dinkelaker, B., Hengeler, C., Römheld, V., Martinoia, E., 2000. Physiological aspects of cluster root function and development in phosphorus-deficient White Lupin (Lupinus albus L.). Ann. Bot. 85, 909–919.

Neumann, G., Römheld, V., 1999. Root excretion of carboxylic acids and protons in phosphorus-deficient plants. Plant Soil. 211, 121–130.

Nhiri, M., Bakrim, Naïma, Bakrim, Nadia, El Hachimi-Messouak, Z., Echevarria, C., Vidal, J., 2000. Posttranslational regulation of phosphoenolpyruvate carboxylase during germination of Sorghum seeds: influence of NaCl and L-malate. Plant Sci. 151, 29–37.

Nimmo, G.A., Wilkins, M.B., Nimmo, H.G., 2001. Partial purification and characterization of a protein inhibitor of phosphoenolpyruvate carboxylase kinase. Planta. 213, 250–257.

Nimmo, H.G., 2003. Control of the phosphorylation of phosphoenolpyruvate carboxylase in higher plants. Arch. Biochem. Biophys. 414, 189–196.

Nimmo, H.G., 2000. The regulation of phosphoenolpyruvate carboxylase in CAM plants. Trends Plant Sci. 5, 75–80.

Nomura, M., Mai, H.T., Fujii, M., Hata, S., Izui, K., Tajima, S., 2006. Phosphoenolpyruvate carboxylase plays a crucial role in limiting nitrogen fixation in Lotus japonicus nodules. Plant Cell Physiol. 47, 613–621.

O'Leary, B., Park, J., Plaxton, W.C., 2011. The remarkable diversity of plant PEPC (phosphoenolpyruvate carboxylase): recent insights into the physiological functions and post-translational controls of non-photosynthetic PEPCs. Biochem. J. 436, 15–34.

Palmgren, M.G., Nissen, P., 2011. P-Type ATPases. Annu. Rev. Biophys. 40, 243–266.

Pant, B.-D., Pant, P., Erban, A., Huhman, D., Kopka, J., Scheible, W.-R., 2015. Identification of primary and secondary metabolites with phosphorus status-dependent abundance in Arabidopsis, and of the transcription factor PHR1 as a major regulator of metabolic changes during phosphorus limitation. Plant Cell Environ. 38, 172–187.

Park, J., Khuu, N., Howard, A.S.M., Mullen, R.T., Plaxton, W.C., 2012. Bacterial- and plant-type phosphoenolpyruvate carboxylase isozymes from developing castor oil seeds interact in vivo and associate with the surface of mitochondria. Plant J. 71, 251–262.

Pellet, DidierM., Grunes, DavidL., Kochian, LeonV., 1995. Organic acid exudation as an aluminum-tolerance mechanism in maize (Zea mays L.). Planta. 196(4), 788-795.

Peng, W., Wu, W., Peng, J., Li, J., Lin, Y., Wang, Y., Tian, J., Sun, L., Liang, C., Liao, H., 2018. Characterization of the soybean GmALMT family genes and the function of GmALMT5 in response to phosphate starvation. J. Integr. Plant Biol. 60, 216–231.

Pereira, J.F., Zhou, G., Delhaize, E., Richardson, T., Zhou, M., Ryan, P.R., 2010. Engineering greater aluminium resistance in wheat by over-expressing TaALMT1. Ann. Bot. 106, 205–214.

Péret, B., Clément, M., Nussaume, L., Desnos, T., 2011. Root developmental adaptation to phosphate starvation: better safe than sorry. Trends Plant Sci. 16, 442–450.

Petricka, J.J., Winter, C.M., Benfey, P.N., 2012. Control of Arabidopsis root development. Annu. Rev. Plant Biol. 63, 563–590.

Pilbeam, D.J., Cakmak, I., Marschner, H., Kirkby, E.A., 1993. Effect of withdrawal of phosphorus on nitrate assimilation and PEP carboxylase activity in tomato, in: Fragoso, M.A.C., Van Beusichem, M.L., Houwers, A. (Eds.), Optimization of Plant Nutrition: Refereed Papers from the Eighth International Colloquium for the Optimization of Plant Nutrition, 31 August – 8 September 1992, Lisbon, Portugal, Developments in Plant and Soil Sciences. Springer Netherlands, Dordrecht, pp. 555–561.

Plaxton, W., Lambers, H., 2015. Annual Plant Reviews, Phosphorus Metabolism in Plants. John Wiley & Sons. 48

Plaxton, W.C., Carswell, M.C., 1999. Metabolic aspects of the phosphate starvation response in plants. Plant Responses Environ. Stress. Phytohorm. Genome Reorganization Marcel Dekker N. Y. 349–372.

Plaxton, W.C., Podestá, F.E., 2006. The functional organization and control of plant respiration. Crit. Rev. Plant Sci. 25, 159–198.

Plaxton, W.C., Tran, H.T., 2011. Metabolic adaptations of phosphate-starved plants. Plant Physiol. 156, 1006–1015.

Pracharoenwattana, I., Zhou, W., Keech, O., Francisco, P.B., Udomchalothorn, T., Tschoep, H., Stitt, M., Gibon, Y., Smith, S.M., 2010. Arabidopsis has a cytosolic fumarase required for the massive allocation of photosynthate into fumaric acid and for rapid plant growth on high nitrogen. Plant J. 62, 785–795.

Rademacher, T., Häusler, R.E., Hirsch, H.-J., Zhang, L., Lipka, V., Weier, D., Kreuzaler, F., Peterhänsel, C., 2002. An engineered phosphoenolpyruvate carboxylase redirects carbon and nitrogen flow in transgenic potato plants. Plant J. Cell Mol. Biol. 32, 25–39.

Remy, E., Cabrito, T.R., Batista, R.A., Teixeira, M.C., Sá-Correia, I., Duque, P., 2012. The Pht1;9 and Pht1;8 transporters mediate inorganic phosphate acquisition by the Arabidopsis thaliana root during phosphorus starvation. New Phytol. 195, 356–371.

Ribeiro, A.P., de Souza, W.R., Martins, P.K., Vinecky, F., Duarte, K.E., Basso, M.F., da Cunha, B.A.D.B., Campanha, R.B., de Oliveira, P.A., Centeno, D.C., Cançado, G.M.A., de Magalhães, J.V., de Sousa, C.A.F., Andrade, A.C., Kobayashi, A.K., Molinari, H.B.C., 2017. Overexpression of BdMATE gene improves aluminum tolerance in Setaria viridis. Front. Plant Sci. 8.

Robinson, W.D., Park, J., Tran, H.T., Del Vecchio, H.A., Ying, S., Zins, J.L., Patel, K., McKnight, T.D., Plaxton, W.C., 2012. The secreted purple acid phosphatase isozymes AtPAP12 and AtPAP26 play a pivotal role in extracellular phosphate-scavenging by Arabidopsis thaliana. J. Exp. Bot. 63, 6531–6542.

Rosso, M.G., Li, Y., Strizhov, N., Reiss, B., Dekker, K., Weisshaar, B., 2003. An Arabidopsis thaliana T-DNA mutagenized population (GABI-Kat) for flanking sequence tag-based reverse genetics. Plant Mol. Biol. 53, 247–259.

Ruiz-Ballesta, I., Feria, A.-B., Ni, H., She, Y.-M., Plaxton, W.C., Echevarría, C., 2014. In vivo monoubiquitination of anaplerotic phosphoenolpyruvate carboxylase occurs at Lys624 in germinating sorghum seeds. J. Exp. Bot. 65, 443–451.

Ryan, P., Delhaize, E., Jones, D., 2001. Function and mechanism of organic anion exudation from plant roots. Annu Rev Plant Physiol Plant Mol Biol. 52, 527-560.

Ryan, P.R., Tyerman, S.D., Sasaki, T., Furuichi, T., Yamamoto, Y., Zhang, W.H., Delhaize, E., 2011. The identification of aluminium-resistance genes provides opportunities for enhancing crop production on acid soils. J. Exp. Bot. 62, 9–20.

Saeed, A.I., Sharov, V., White, J., Li, J., Liang, W., Bhagabati, N., Braisted, J., Klapa, M., Currier, T., Thiagarajan, M., Sturn, A., Snuffin, M., Rezantsev, A., Popov, D., Ryltsov, A., Kostukovich, E., Borisovsky, I., Liu, Z., Vinsavich, A., Trush, V., Quackenbush, J., 2003. TM4: a free, open-source system for microarray data management and analysis. BioTechniques 34, 374–378.

Sánchez, R., Cejudo, F.J., 2003. Identification and expression analysis of a gene encoding a bacterial-type phosphoenolpyruvate carboxylase from Arabidopsis and rice. Plant Physiol. 132, 949–957.

Sánchez, R., Flores, A., Cejudo, F.J., 2006. Arabidopsis phosphoenolpyruvate carboxylase genes encode immunologically unrelated polypeptides and are differentially expressed in response to drought and salt stress. Planta. 223, 901–909.

Sasaki, T., Yamamoto, Y., Ezaki, B., Katsuhara, M., Ahn, S.J., Ryan, P.R., Delhaize, E., Matsumoto, H., 2004. A wheat gene encoding an aluminum-activated malate transporter. Plant J. 37, 645–653.

Saze, H., Ueno, Y., Hisabori, T., Hayashi, H., Izui, K., 2001. Thioredoxin-mediated reductive activation of a protein kinase for the regulatory phosphorylation of C4-form phosphoenolpyruvate carboxylase from maize. Plant Cell Physiol. 42, 1295–1302.

Schmidtmann, E., König, A.-C., Orwat, A., Leister, D., Hartl, M., Finkemeier, I., 2014. Redox regulation of Arabidopsis mitochondrial citrate synthase. Mol. Plant. 7, 156–169.

Schneider, C.A., Rasband, W.S., Eliceiri, K.W., 2012. NIH Image to ImageJ: 25 years of image analysis. Nat. Methods 9, 671–675.

Schulze, J., Tesfaye, M., Litjens, R.H.M.G., Bucciarelli, B., Trepp, G., Miller, S., Samac, D., Allan, D., Vance, C.P., 2002. Malate plays a central role in plant nutrition. Plant Soil. 247, 133–139.

Selinski, J., Scheibe, R., 2014. Lack of malate valve capacities lead to improved N-assimilation and growth in transgenic A. thaliana plants. Plant Signal. Behav. 9, e29057.

Shane, M.W., Fedosejevs, E.T., Plaxton, W.C., 2013. Reciprocal control of anaplerotic phosphoenolpyruvate carboxylase by in vivo monoubiquitination and phosphorylation in developing proteoid roots of phosphate-deficient Harsh Hakea. Plant Physiol. 161, 1634–1644.

Shen, J., Yuan, L., Zhang, J., Li, H., Bai, Z., Chen, X., Zhang, W., Zhang, F., 2011. Phosphorus Dynamics: From Soil to Plant. Plant Physiol. 156, 997–1005.

Shenton, M., Fontaine, V., Hartwell, J., Marsh, J.T., Jenkins, G.I., Nimmo, H.G., 2006. Distinct patterns of control and expression amongst members of the PEP carboxylase kinase gene family in C4 plants. Plant J. 48, 45–53.

Shi, J., Yi, K., Liu, Y., Xie, L., Zhou, Z., Chen, Yue, Hu, Z., Zheng, T., Liu, R., Chen, Yunlong, Chen, J., 2015. Phosphoenolpyruvate carboxylase in Arabidopsis leaves plays a crucial role in carbon and nitrogen metabolism. Plant Physiol. 167, 671–681.

Shin, H., Shin, H.-S., Dewbre, G.R., Harrison, M.J., 2004. Phosphate transport in Arabidopsis: Pht1;1 and Pht1;4 play a major role in phosphate acquisition from both low- and high-phosphate environments. Plant J. 39, 629–642.

Sivaguru, M., Fujiwara, T., Šamaj, J., Baluška, F., Yang, Z., Osawa, H., Maeda, T., Mori, T., Volkmann, D., Matsumoto, H., 2000. Aluminum-induced 1→ 3-β-d-glucan inhibits cell-to-cell trafficking of molecules through plasmodesmata. A new mechanism of aluminum toxicity in plants. Plant Physiol. 124, 991–1006.

Sørensen, D.M., Holen, H.W., Holemans, T., Vangheluwe, P., Palmgren, M.G., 2015. Towards defining the substrate of orphan P5A-ATPases. Biochim. Biophys. Acta BBA - Gen. Subj., Structural biochemistry and biophysics of membrane proteins. 1850, 524–535.

Strobel, B.W., 2001. Influence of vegetation on low-molecular-weight carboxylic acids in soil solution—a review. Geoderma. 99, 169–198.

Ström, L., Owen, A.G., Godbold, D.L., Jones, D.L., 2005. Organic acid behaviour in a calcareous soil implications for rhizosphere nutrient cycling. Soil Biol. Biochem. 37, 2046–2054.

Sullivan, S., Jenkins, G.I., Nimmo, H.G., 2004. Roots, cycles and leaves. Expression of the phosphoenolpyruvate carboxylase kinase gene family in soybean. Plant Physiol. 135, 2078–2087.

Sun, M., Sun, X., Zhao, Y., Zhao, C., DuanMu, H., Yu, Y., Ji, W., Zhu, Y., 2014. Ectopic expression of GsPPCK3 and SCMRP in Medicago sativa enhances plant alkaline stress tolerance and methionine content. PLoS ONE. 9, e89578.

Sun, P., Tian, Q.-Y., Chen, J., Zhang, W.-H., 2010. Aluminium-induced inhibition of root elongation in Arabidopsis is mediated by ethylene and auxin. J. Exp. Bot. 61, 347–356.

Suzuki, S., Murai, N., Kasaoka, K., Hiyoshi, T., Imaseki, H., Burnell, J., Arai, M., 2006. Carbon metabolism in transgenic rice plants that express phosphoenolpyruvate carboxylase and/or phosphoenolpyruvate carboxykinase. Plant Sci. 170, 1010–1019.

Svensson, P., Bläsing, O.E., Westhoff, P., 2003. Evolution of C4 phosphoenolpyruvate carboxylase. Arch. Biochem. Biophys. 414, 180–188.

Svistoonoff, S., Creff, A., Reymond, M., Sigoillot-Claude, C., Ricaud, L., Blanchet, A., Nussaume, L., Desnos, T., 2007. Root tip contact with low-phosphate media reprograms plant root architecture. Nat. Genet. 39, 792–796.

Taniguchi, Y., Ohkawa, H., Masumoto, C., Fukuda, T., Tamai, T., Lee, K., Sudoh, S., Tsuchida, H., Sasaki, H., Fukayama, H., Miyao, M., 2008. Overproduction of C4 photosynthetic enzymes in transgenic rice plants: an approach to introduce the C4-like photosynthetic pathway into rice. J. Exp. Bot. 59, 1799–1809.

Taybi, T., Nimmo, H.G., Borland, A.M., 2004. Expression of phosphoenolpyruvate carboxylase and phosphoenolpyruvate carboxylase kinase genes. Implications for genotypic capacity and phenotypic plasticity in the expression of crassulacean acid metabolism. Plant Physiol. 135, 587–598.

Taybi, T., Patil, S., Chollet, R., Cushman, J.C., 2000. A minimal serine/threonine protein kinase circadianly regulates phosphoenolpyruvate carboxylase activity in crassulacean acid metabolism-induced leaves of the common Ice Plant. Plant Physiol. 123, 1471–1482.

Tesfaye, M., Temple, S.J., Allan, D.L., Vance, C.P., Samac, D.A., 2001. Overexpression of malate dehydrogenase in transgenic Alfalfa enhances organic acid synthesis and confers tolerance to aluminum. Plant Physiol. 127, 1836–1844.

Theodorou, M.E., Plaxton, W.C., 1993. Metabolic adaptations of plant respiration to nutritional phosphate deprivation. Plant Physiol. 101, 339–344.

Ticconi, C.A., Lucero, R.D., Sakhonwasee, S., Adamson, A.W., Creff, A., Nussaume, L., Desnos, T., Abel, S., 2009. ER-resident proteins PDR2 and LPR1 mediate the developmental response of root meristems to phosphate availability. Proc. Natl. Acad. Sci. 106, 14174–14179.

Ting, I.P., Osmond, C.B., 1973. Photosynthetic phosphoenolpyruvate carboxylases: Characteristics of alloenzymes from leaves of C3 and C1 plants. Plant Physiol. 51, 439–447.

Tovar-Mendez, A., Miernyk, J.A., Randall, D.D., 2003. Regulation of pyruvate dehydrogenase complex activity in plant cells. Eur. J. Biochem. 270, 1043–1049.

Toyota, K., Koizumi, N., Sato, F., 2003. Transcriptional activation of phosphoenolpyruvate carboxylase by phosphorus deficiency in tobacco. J. Exp. Bot. 54, 961–969.

Tsuchida, Y., Furumoto, T., Izumida, A., Hata, S., Izui, K., 2001. Phosphoenolpyruvate carboxylase kinase involved in C4 photosynthesis in Flaveria trinervia: cDNA cloning and characterization. FEBS Lett. 507, 318–322.

Ueno, O., 2001. Environmental regulation of C3 and C4 differentiation in the amphibious Sedge Eleocharis vivipara. Plant Physiol. 127, 1524–1532.

Ueno, Y., Imanari, E., Emura, J., Yoshizawa-Kumagaye, K., Nakajima, K., Inami, K., Shiba, T., Sakakibara, H., Sugiyama, T., Izui, K., 2000. Immunological analysis of the phosphorylation state of maize C4-form phosphoenolpyruvate carboxylase with specific antibodies raised against a synthetic phosphorylated peptide. Plant J. Cell Mol. Biol. 21, 17–26.

Uhde-Stone, C., Gilbert, G., Johnson, J.M.-F., Litjens, R., Zinn, K.E., Temple, S.J., Vance, C.P., Allan, D.L., 2003. Acclimation of white lupin to phosphorus deficiency involves enhanced expression of genes related to organic acid metabolism. Plant Soil. 248, 99–116.

Uhrig, R.G., She, Y.-M., Leach, C.A., Plaxton, W.C., 2008. Regulatory monoubiquitination of phosphoenolpyruvate carboxylase in germinating castor oil seeds. J. Biol. Chem. 283, 29650–29657.

Ülker, B., Peiter, E., Dixon, D.P., Moffat, C., Capper, R., Bouché, N., Edwards, R., Sanders, D., Knight, H., Knight, M.R., 2008. Getting the most out of publicly available T-DNA insertion lines. Plant J. 56, 665–677.

Vance, C.P., Uhde-Stone, C., Allan, D.L., 2003. Phosphorus acquisition and use: critical adaptations by plants for securing a nonrenewable resource. New Phytol. 157, 423–447.

Vidal, J., Chollet, R., 1997. Regulatory phosphorylation of C4 PEP carboxylase. Trends Plant Sci. 2, 230–237.

Wang, Q.-F., Zhao, Y., Yi, Q., Li, K.-Z., Yu, Y.-X., Chen, L.-M., 2010. Overexpression of malate dehydrogenase in transgenic tobacco leaves: enhanced malate synthesis and augmented Al-resistance. Acta Physiol. Plant. 32, 1209–1220.

Wang, Y.-M., Xu, W.-G., Hu, L., Zhang, L., Li, Y., Du, X.-H., 2012. Expression of maize gene encoding C4-pyruvate orthophosphate dikinase (PPDK) and C4-phosphoenolpyruvate carboxylase (PEPC) in transgenic Arabidopsis. Plant Mol. Biol. Report. 30, 1367–1374.

Wang, Z.-A., Li, Q., Ge, X.-Y., Yang, C.-L., Luo, X.-L., Zhang, A.-H., Xiao, J.-L., Tian, Y.-C., Xia, G.-X., Chen, X.-Y., 2015. The mitochondrial malate dehydrogenase 1 gene GhmMDH1 is involved in plant and root growth under phosphorus deficiency conditions in cotton. Sci. Rep. 5, 10343.

Ward, J.T., Lahner, B., Yakubova, E., Salt, D.E., Raghothama, K.G., 2008. The effect of iron on the primary root elongation of Arabidopsis during phosphate deficiency. Plant Physiol. 147, 1181–1191.

Watt, M., Evans, J.R., 1999. Linking development and determinacy with organic acid efflux from proteoid roots of white lupin grown with low phosphorus and ambient or elevated atmospheric CO_2 concentration. Plant Physiol. 120, 705–716.

White, J.C., Mattina, M.I., Lee, W.-Y., Eitzer, B.D., Iannucci-Berger, W., 2003. Role of organic acids in enhancing the desorption and uptake of weathered p,p'-DDE by Cucurbita pepo. Environ. Pollut. 124, 71–80.

Willick, I.R., Plaxton, W.C., Lolle, S.J., Macfie, S.M., 2019. Transcriptional and post-translational upregulation of phosphoenolpyruvate carboxylase in Arabidopsis thaliana (L. Heynh) under cadmium stress. Environ. Exp. Bot. 164, 29–39.

Wilson, A.K., Pickett, F.B., Turner, J.C., Estelle, M., 1990. A dominant mutation in Arabidopsis confers resistance to auxin, ethylene and abscisic acid. Mol. Gen. Genet. MGG 222, 377–383.

Wu, P., Ma, L., Hou, X., Wang, M., Wu, Y., Liu, F., Deng, X.W., 2003. Phosphate starvation triggers distinct alterations of genome expression in Arabidopsis roots and leaves. Plant Physiol. 132, 1260–1271.

Wu, X., Li, R., Shi, J., Wang, J., Sun, Q., Zhang, H., Xing, Y., Qi, Y., Zhang, N., Guo, Y.-D., 2014. Brassica oleracea MATE encodes a citrate transporter and enhances aluminum tolerance in Arabidopsis thaliana. Plant Cell Physiol. 55(8),1426-1436.

Yakunin, A.F., Hallenbeck, P.C., 1997. Regulation of synthesis of pyruvate carboxylase in the photosynthetic bacterium Rhodobacter capsulatus. J. Bacteriol. 179, 1460–1468.

Yang, L.-T., Qi, Y.-P., Jiang, H.-X., Chen, L.-S., 2013. Roles of organic acid anion secretion in aluminium tolerance of higher plants. BioMed Res. Int. 1–16.

Yang, X.Y., Yang, J.L., Zhou, Y., Piñeros, M.A., Kochian, L.V., Li, G.X., Zheng, S.J., 2011. A de novo synthesis citrate transporter, Vigna umbellata multidrug and toxic compound extrusion, implicates in Al-activated citrate efflux in rice bean (Vigna umbellata) root apex. Plant Cell Environ. 34, 2138–2148.

Yang, Y.-Y., Jung, J.-Y., Song, W.-Y., Suh, H.-S., Lee, Y., 2000. Identification of rice varieties with high tolerance or sensitivity to lead and characterization of the mechanism of tolerance. Plant Physiol. 124, 1019–1026.

Yokosho, K., Yamaji, N., Ma, J.F., 2011. An Al-inducible MATE gene is involved in external detoxification of Al in rice. Plant J. 68, 1061–1069.

Yokosho, K., Yamaji, N., Ma, J.F., 2010. Isolation and characterisation of two MATE genes in rye. Funct. Plant Biol. 37, 296.

Zhang, L., Wu, X.-X., Wang, J., Qi, C., Wang, X., Wang, G., Li, M., Li, X., Guo, Y.-D., 2018. BoALMT1, an Al-induced malate transporter in Cabbage, enhances aluminum tolerance in Arabidopsis thaliana. Front. Plant Sci. 8.

Zhang, Y.-B., Howitt, J., McCorkle, S., Lawrence, P., Springer, K., Freimuth, P., 2004. Protein aggregation during overexpression limited by peptide extensions with large net negative charge. Protein Expr. Purif. 36, 207–216.

Zhao, Z., Ma, J.F., Sato, K., Takeda, K., 2003. Differential Al resistance and citrate secretion in barley (Hordeum vulgare L.). Planta 217, 794–800.

Zheng, S.J., Ma, J.F., Matsumoto, H., 1998. High aluminum resistance in Buckwheat: I. Al-induced specific secretion of oxalic acid from root tips. Plant Physiol. 117, 745–751.

Zhengwei, W., Yan-ming, Z., Ye, H., Hua, C., Wei, J.H., Xi, B., Zhen-yu, W., Yidong, W., 2013. Transgenic alfalfa with GsPPCK1 and its alkaline tolerance analysis.

Zhou, G., Delhaize, E., Zhou, M., Ryan, P.R., 2013. The barley MATE gene, HvAACT1, increases citrate efflux and Al^{3+} tolerance when expressed in wheat and barley. Ann. Bot. 112, 603–612.

Zhou, G., Pereira, J.F., Delhaize, E., Zhou, M., Magalhaes, J.V., Ryan, P.R., 2014. Enhancing the aluminium tolerance of barley by expressing the citrate transporter genes SbMATE and FRD3. J. Exp. Bot. 65, 2381–2390.

Zhou, Y., Yang, Z., Xu, Y., Sun, H., Sun, Z., Lin, B., Sun, W., You, J., 2018. Soybean NADP-Malic enzyme functions in malate and citrate metabolism and contributes to their efflux under Al stress. Front. Plant Sci. 8.

Ziegler, J., Abel, S., 2014. Analysis of amino acids by HPLC/electrospray negative ion tandem mass spectrometry using 9-fluorenylmethoxycarbonyl chloride (Fmoc-Cl) derivatization. Amino Acids. 46, 2799–2808.

Ziegler, J., Schmidt, S., Chutia, R., Müller, J., Böttcher, C., Strehmel, N., Scheel, D., Abel, S., 2016. Non-targeted profiling of semi-polar metabolites in Arabidopsis root exudates uncovers a role for coumarin secretion and lignification during the local response to phosphate limitation. J. Exp. Bot. 67, 1421–1432.

7 APPENDIX

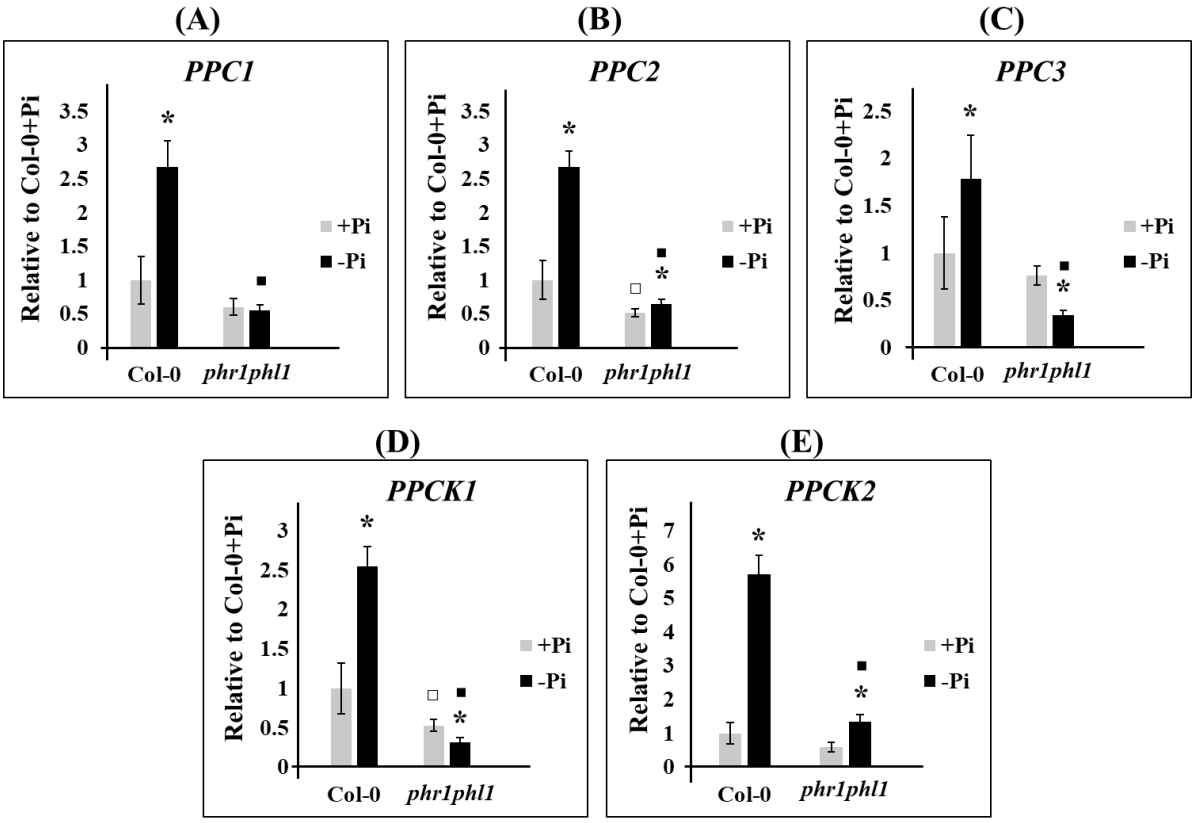

Supplementary Figure 7-1: Expression analysis of *PPC* and *PPCK* isoforms in roots of *phr1phl1* seedlings by RT-qPCR

Transcript levels of (A) *PPC1*, (B) *PPC2*, (C) *PPC3*, (D) *PPCK1*, and (E) *PPCK2* in roots of *phr1phl1* seedlings grown under Pi-sufficient and Pi-deficient conditions compared to the levels detected in WT (Col-0) roots. Seedlings were germinated for 6 days on +Pi agar plates, transferred to +Pi (500 µM) or –Pi (5 µM) conditions, and allowed to grow for additional 5 days before harvest. Data from one representative out of three independent experiments are shown. *PP2A* was used as a reference gene and relative expression levels were normalized to the levels detected in Col-0+Pi. Error bars denote SD (n=4 biological replicates). Significance analyses were performed by Student's *t*-test (two-tailed, equal variances): *p ≤ 0.05, □p ≤ 0.05, and ▪p≤ 0.05 compared to +Pi, Col-0+Pi, and Col-0-Pi, respectively.

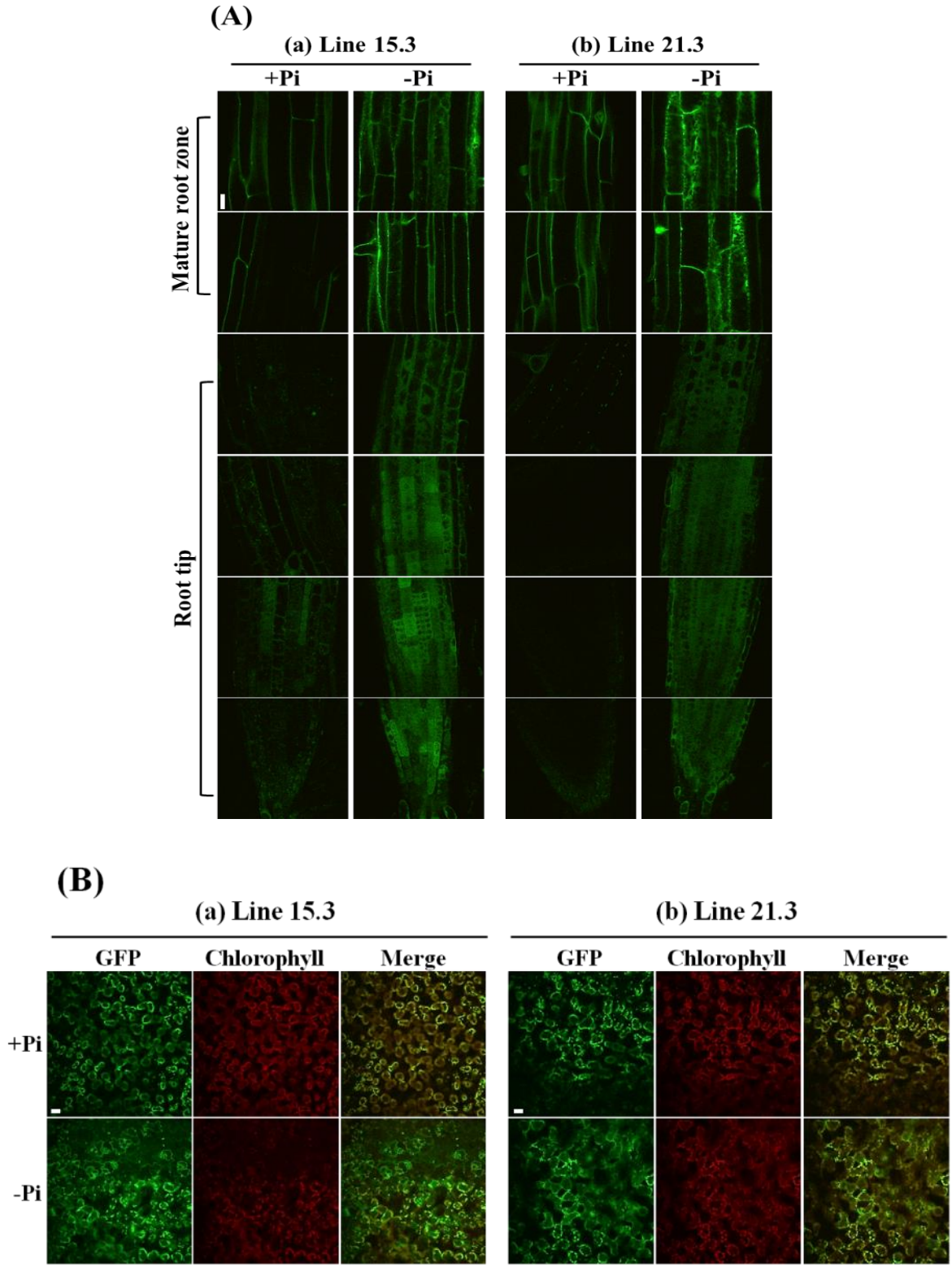

Supplementary figure 7-2: GFP-flourescence detected in roots and leaves of *pPPCK1$_{long}$::GFP-GUS* reporter lines grown under Pi-sufficient and Pi-deficient conditions

GFP-fluorescence detected in two representative *pPPCK1$_{long}$::GFP-GUS* reporter lines [(a): Line 15.3 and (b): Line 21.3)]. Images of single optical sections of seedlings from (A) different regions of root-tip and mature root and (B) leaves. Representative merged images for leaves are presented as overlay images of the GFP channel (displayed in green) and the chlorophyll channel (displayed in red). Scale bars represent 20 µm. Data from one representative out of three independent experiments are shown. Seedlings were germinated for 6 days on +Pi agar plates, transferred to +Pi (500 µM) or –Pi (5 µM) conditions, and allowed to grow for additional 5 days before imaging.

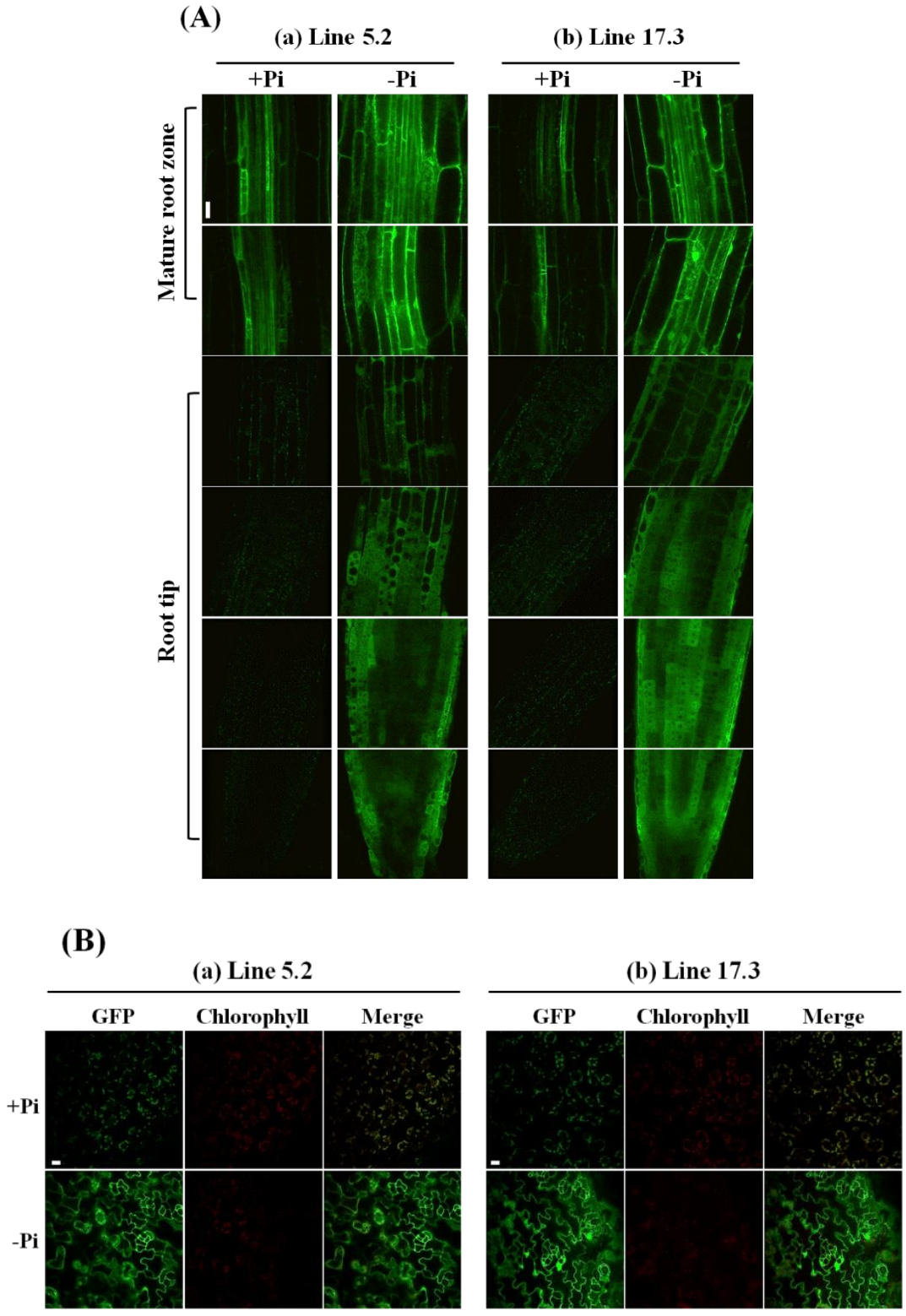

Supplementary figure 7-3: GFP-flourescence detected in roots and leaves of *pPPCK2$_{long}$::GFP-GUS* reporter lines grown under Pi-sufficient and Pi-deficient conditions

GFP-fluorescence detected in two representative *pPPCK2$_{long}$::GFP-GUS* reporter lines [(a): Line 5.2 and (b): Line 17.3)]. Images of single optical sections of seedlings from (A) different regions of root-tip and mature root and (B) leaves. Representative merged images for leaves are presented as overlay images of the GFP channel (displayed in green) and the chlorophyll channel (displayed in red). Scale bars represent 20 µM. Data from one representative out of three independent experiments are shown. Seedlings were germinated for 6 days on +Pi agar plates, transferred to +Pi (500 µM) or –Pi (5 µM) conditions, and allowed to grow for additional 5 days before imaging.

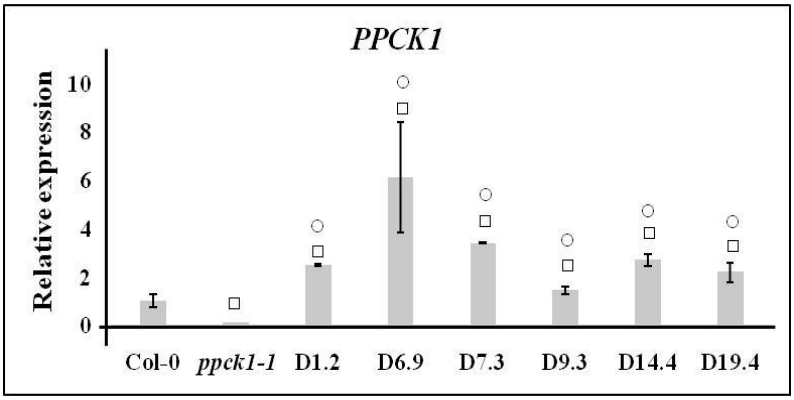

Supplementary figure 7-4: Expression analysis of *PPCK1* in *pPPCK1$_{long}$::gDNA-GFP* lines by RT-qPCR

Total RNA was extracted from 7 days old seedlings. *PP2A* was used as a reference gene and relative expression levels were normalized to the levels detected in WT (Col-0). Error bars denote SD (n=3). Data from one representative out of three independent experiments are shown. Significance analyses were performed by Student's *t*-test (two-tailed, equal variances): □p ≤ 0.05 and °p ≤ 0.05 compared to WT and *ppck1-1*, respectively.

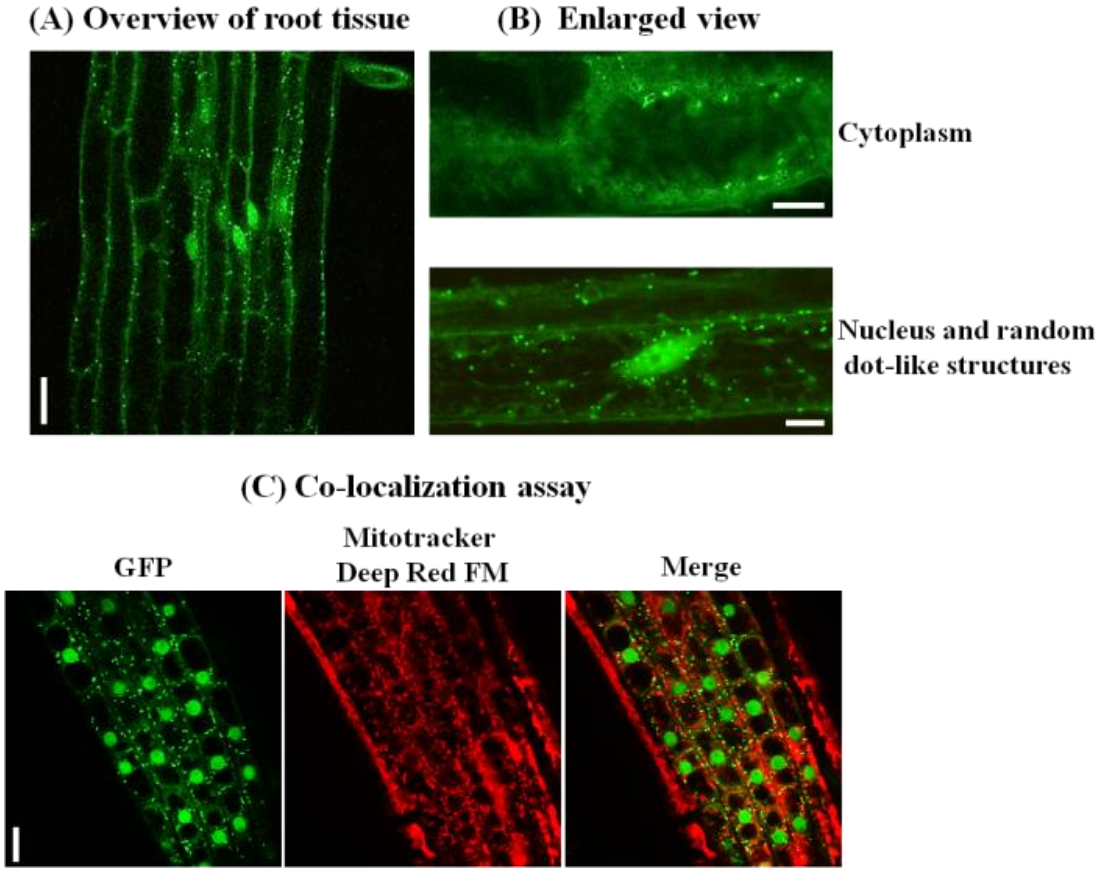

Supplementary figure 7-5: Subcellular localization of PPCK1 *in pPPCK1$_{long}$::gDNA-GFP/ppck1-1* lines

(A) Image of a single optical section of root tissue (B) a single cell resolution showing localization of PPCK1 to the cytoplasm (upper panel), nucleus, and some randomly moving dot-like structures (lower panel) and (C) PPCK1 does not localize to mitochondria, as demonstrated by co-localization assays performed using Mitotracker Deep Red FM dye which stains mitochondria (preliminary data). Scale bars represent 20 µm (for A) and 10 µm (for B and C). Seedlings were germinated for 6 days on +Pi agar plates and then transferred to –Pi (5 µM) condition, and allowed to grow for additional 5 days before imaging. For subcellular localization of PPCK1, seedlings growing under Pi-depleted medium were used since in Pi-sufficient seedlings, the signal intensity was very weak.

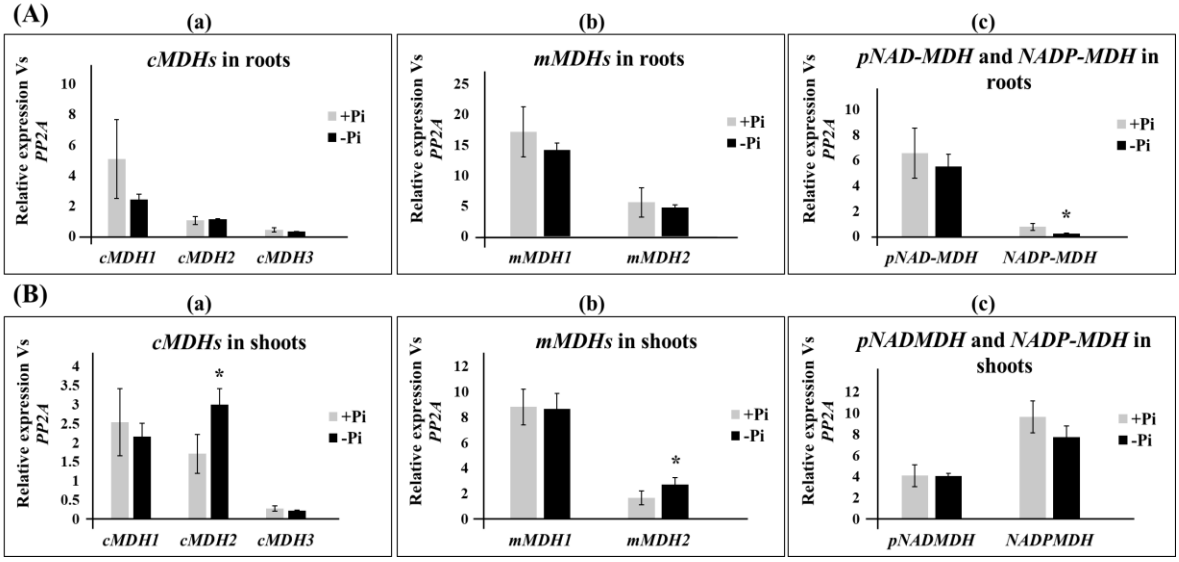

Supplementary figure 7-6: Expression analysis of *MDH*s in WT seedlings by RT-qPCR

Transcript levels of *MDH*s in (A) roots and (B) shoots of WT (Col-0) seedlings grown under Pi-sufficient and Pi-deficient conditions [(a): *cMDH*s, (b): *mMDH*s, and (c): *pNADMDH* and *NADPMDH*)]. Seedlings were germinated for 6 days on +Pi agar plates, transferred to +Pi (500 µM) or –Pi (5 µM) conditions, and allowed to grow for additional 5 days before harvest. Error bars denote SD (n=4). Data from one representative out of two independent experiments are shown. Significance analyses were performed by Student's *t*-test (two-tailed, equal variances): *p ≤ 0.05 compared to +Pi condition.

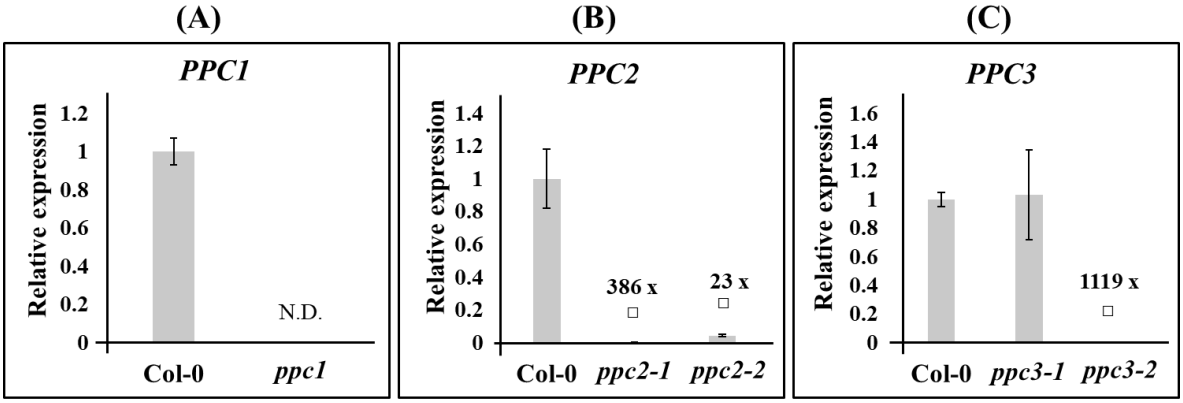

Supplementary figure 7-7: Expression analysis of *PPC*s in their respective T-DNA insertion lines by RT-qPCR

Transcript levels of (A) *PPC1* in *ppc1* (SALK_088836) (B) *PPC2* in *ppc2-1* (SALK_128516) and *ppc2-2* (SALK_025005) and (C) *PPC3* in *ppc3-1* (SALK_031519C) and *ppc3-2* (SALK_143289.54.75X) compared to the levels detected in WT (Col-0). Total RNA was extracted from 7 days old seedlings. *PP2A* was used as a reference gene and relative expression levels were normalized to the levels detected in WT (Col-0). Error bars denote SD (n=3 biological replicates). Data from one representative out of two independent experiments are shown. Significance analyses were performed by Student's *t*-test (two-tailed, equal variances): □p ≤ 0.05 compared to WT (Col-0). Numbers above the bars indicate fold reduction in transcript levels in the T-DNA insertion lines compared to the WT (Col-0). In *ppc1* seedlings, Ct values could not be detected during the 40 cycles PCR run, which is represented as N.D. (not detectable) above the bar.

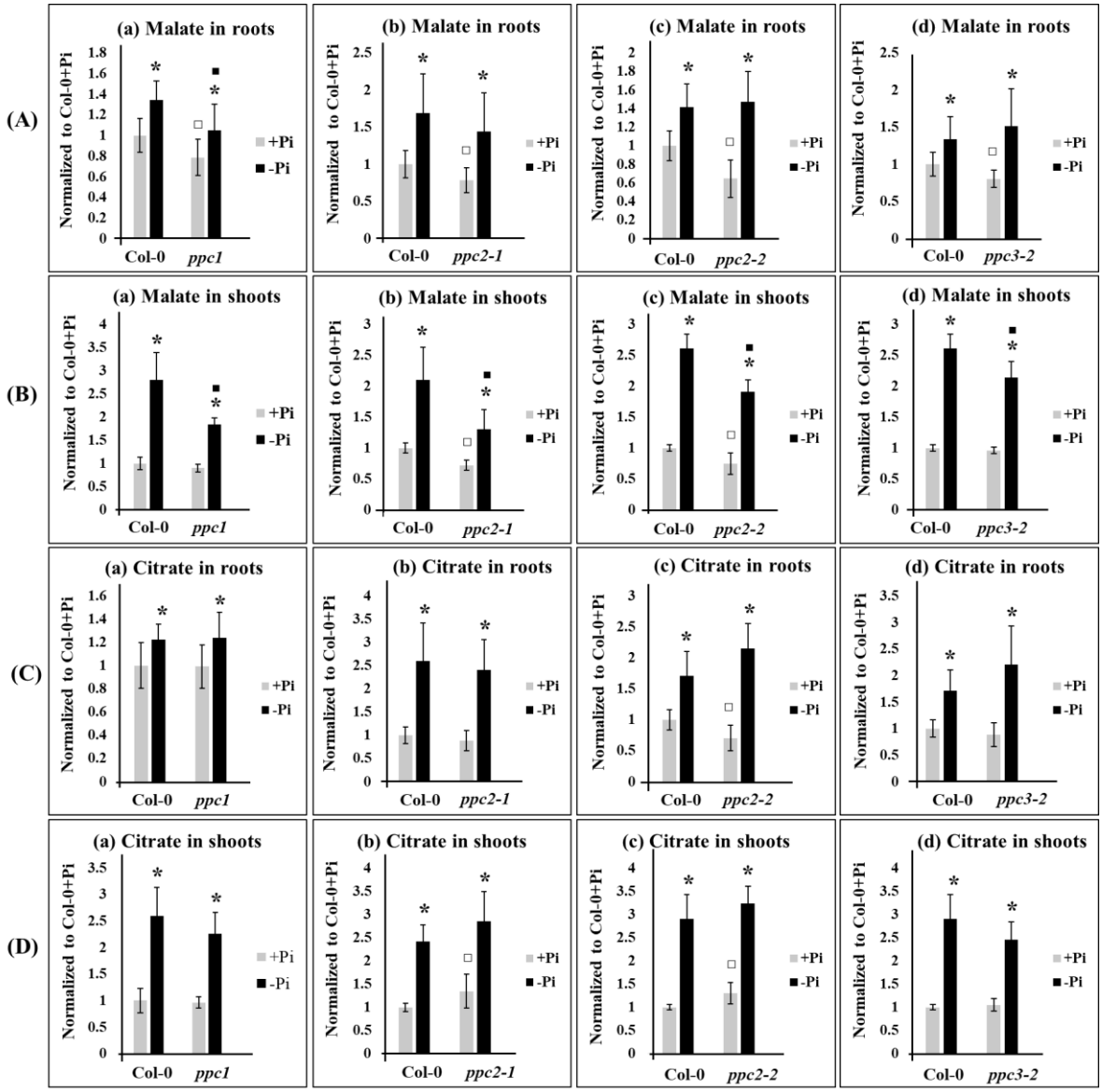

Supplementary figure 7-8: Normalized malate and citrate content in *ppc* mutants compared to WT

Normalized content of (A) malate in roots, (B) malate in shoots, (C) citrate in roots, and (D) citrate in shoots of T-DNA insertion lines showing aberrant expression of *PPC*s [(a) *ppc1,* (b) *ppc2-1,* (c) *ppc2-2*, and (d) *ppc3-2*], compared to WT (Col-0) when grown under Pi-sufficient and Pi-deficient conditions. Seedlings were germinated for 6 days on +Pi agar plates, transferred to +Pi (500 µM) or –Pi (5 µM) conditions, and allowed to grow for additional 5 days before harvest. Data are normalized to the levels detected in Col-0+Pi. Shown are the cumulative data of two independent germination experiments. For each experiment, four biological replicates (two pooled seedlings per replicate) were analyzed. Error bars denote SD (n=08 total biological replicates). Significance analyses were performed by Student's *t*-test (two-tailed, equal variances): *p ≤ 0.05; □p ≤ 0.05; and ▪p ≤ 0.05 compared to +Pi, Col-0+Pi, and Col-0-Pi respectively.

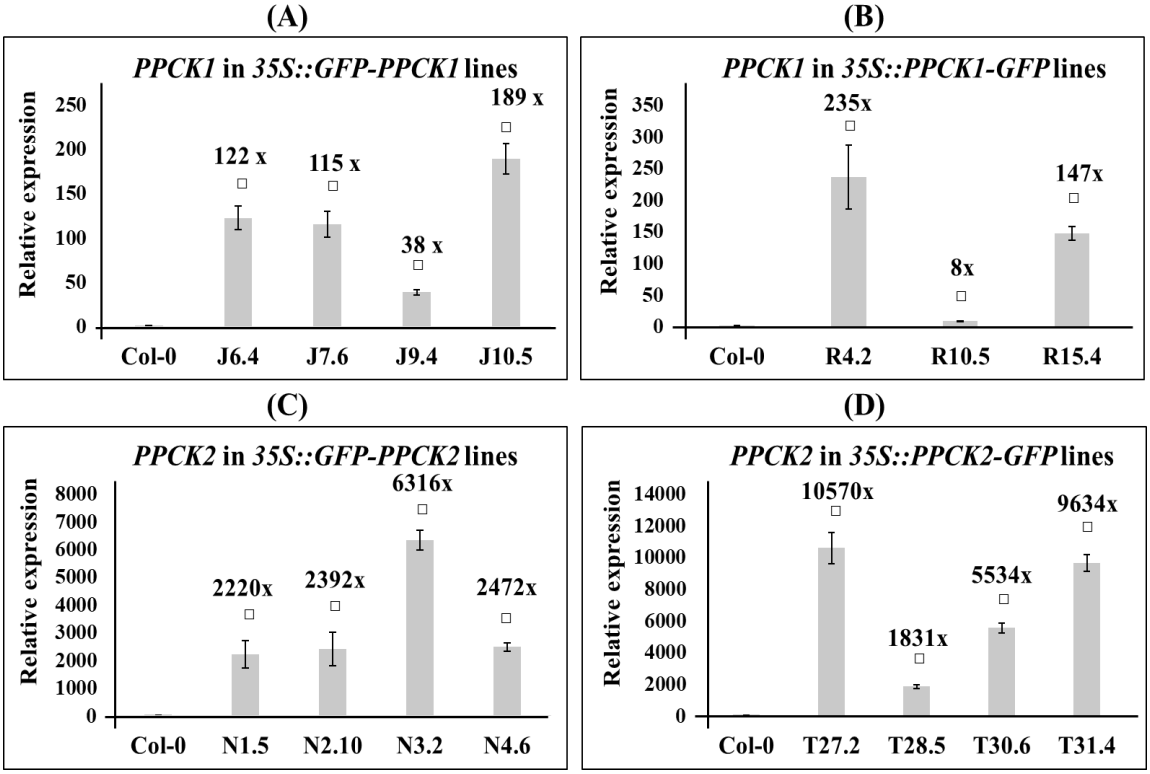

Supplementary figure 7-9: Expression analysis of *PPCK1* and *PPCK2* by RT-qPCR in transgenic lines transformed with N or C-terminally tagged GFP protein construct

PPCK1 transcript levels in (A) *35S::GFP-PPCK1* (J-lines) and (B) *35S::PPCK1-GFP* (R-lines) and *PPCK2* transcript levels in (C) *35S::GFP-PPCK2* (N-lines), and (D) *35S::PPCK2-GFP* (T-lines) compared to WT (Col-0). Total RNA was extracted from 7 days old seedlings. *PP2A* was used as a reference gene and relative expression levels were normalized to the levels detected in WT (Col-0). Error bars denote SD (n=3). Data from one representative out of two independent experiments are shown. Significance analyses were performed by Student's *t*-test (two-tailed, equal variances): □p ≤ 0.005 compared to WT (Col-0). Numbers above the bars indicate fold induction in transcript levels in the transgenic lines compared to WT.

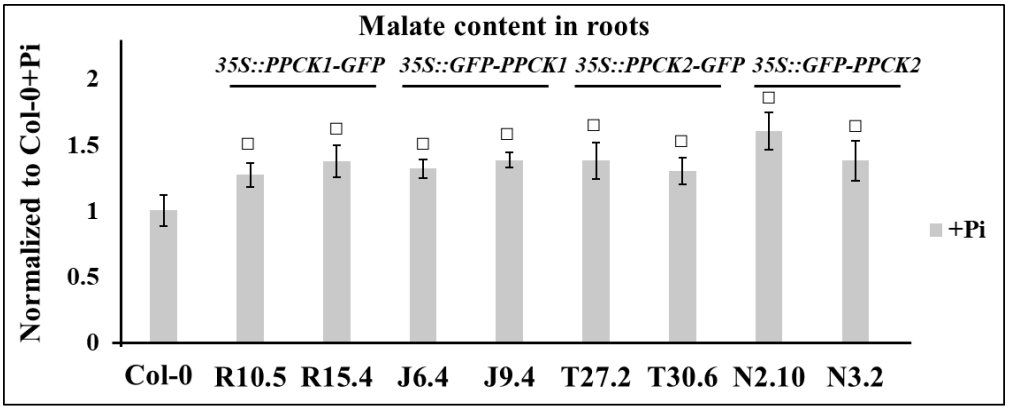

Supplementary figure 7-10: Normalized root malate content in transgenic lines overexpressing GFP-tagged PPCKs

Seedlings were germinated for 11 days on +Pi (500 µM) containing agar media before harvest. Data are normalized to the levels detected in WT (Col-0). Shown are the cumulative data of two independent germination experiments. For each experiment, four biological replicates (two pooled seedlings per replicate) were analyzed. Error bars denote SD (n=08 total biological replicates). Significance analyses were performed by Student's *t*-test (two-tailed, equal variances): □p≤ 0.005 compared to WT.

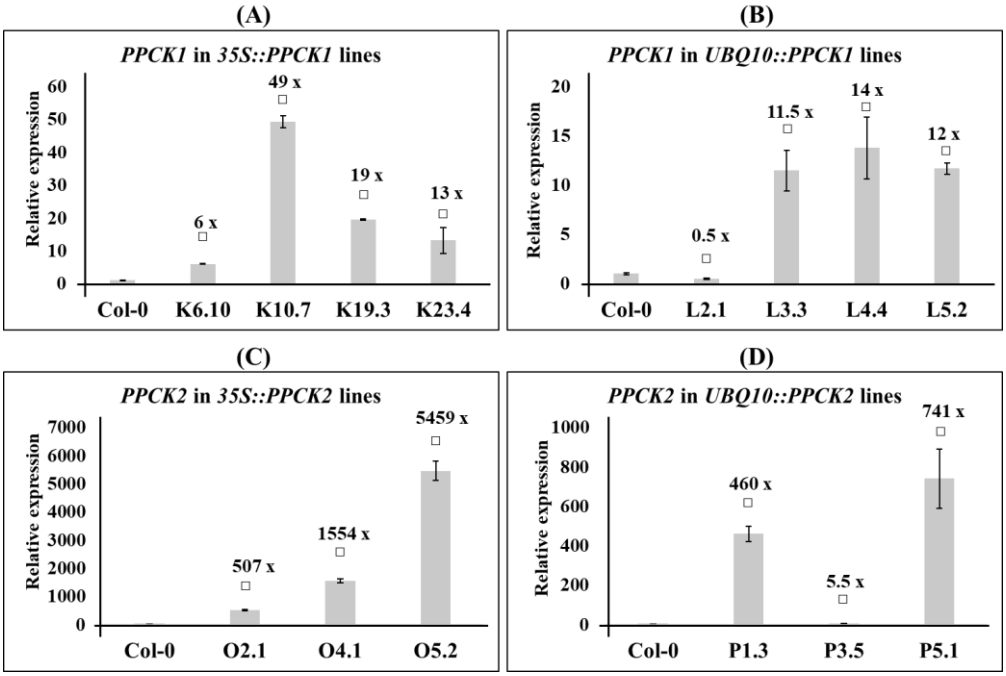

Supplementary Figure 7-11: Expression analysis of *PPCK1* and *PPCK2* by RT-qPCR in transgenic lines overexpressing *PPCK1* and *PPCK2*

Transcript levels of *PPCK1* in (A) *35S::PPCK1* (K-lines) (B) *UBQ10::PPCK1* (L-lines) and *PPCK2* in (C) *35S::PPCK2* (O-lines) (D) *UBQ10::PPCK2* (P-lines) compared to the levels detected in WT (Col-0). Total RNA was extracted from 7 days old seedlings. *PP2A* was used as a reference gene and the relative expression levels were normalized to the levels detected in WT. Error bars denote SD (n=3 biological replicates). Data from one representative out of two independent experiments are shown. Significance analyses were performed by Student's *t*-test (two-tailed, equal variances): □p ≤ 0.005 compared to WT (Col-0). Numbers above the bars indicate fold induction in transcript levels in the transgenic lines compared to the levels detected in WT.

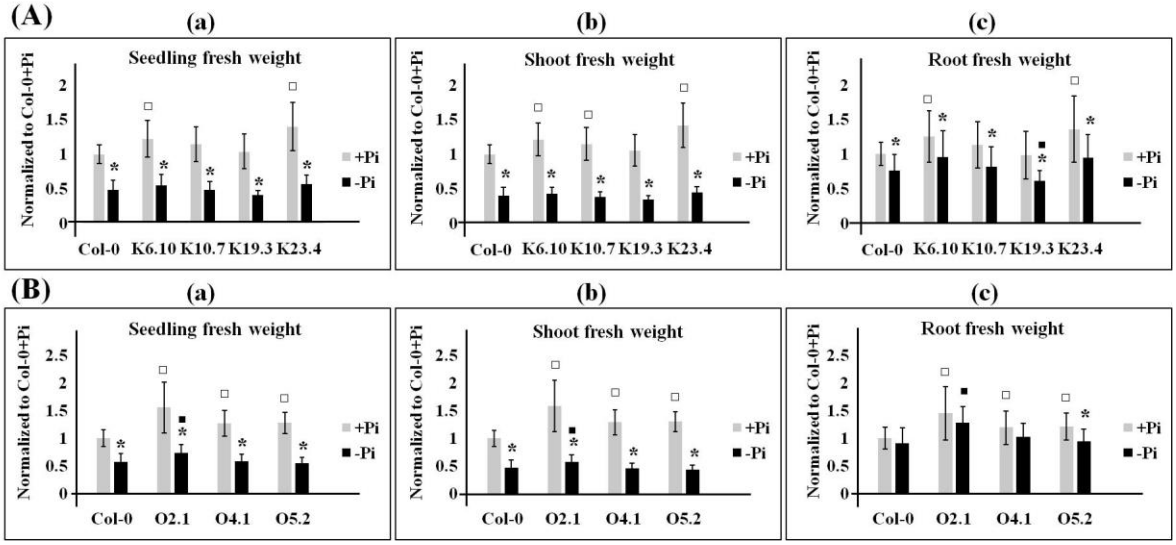

Supplementary Figure 7-12: Comparison of fresh weight of plants overexpressing *PPCK1* and *PPCK2* to WT

Normalized fresh weight of plants overexpressing (A) *PPCK1* (K-lines) and (B) *PPCK2* (O-lines) compared to untransformed WT (Col-0) plants [(a) seedling, (b) shoot, and (c) root fresh weight]. Seedlings were germinated for 6 days on +Pi agar plates, transferred to +Pi (500 µM) or –Pi (5 µM) conditions, and allowed to grow for additional 5 days before harvest. Data are normalized to Col-0+Pi. Shown are the cumulative data of four independent germination experiments. For each experiment, four biological replicates (two pooled seedlings per replicate) were analyzed. Error bars denote SD (n=16 total biological replicates). Significance analyses were performed by Student's *t*-test (two-tailed, equal variances): *p ≤ 0.05, □p ≤ 0.05, and ▪p ≤ 0.05 compared to +Pi, Col-0+Pi, and Col-0-Pi, respectively.

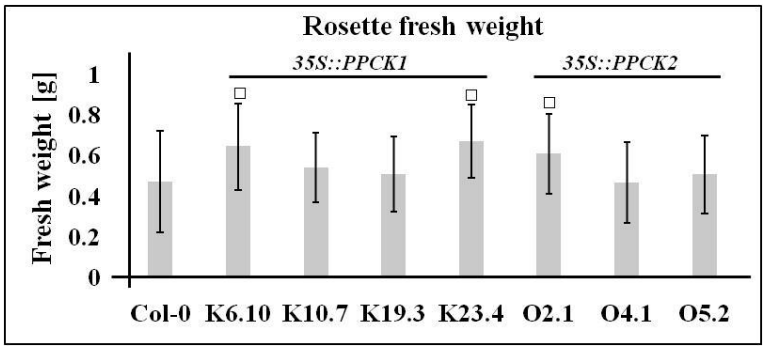

Supplementary Figure 7-13: Comparison of rosette fresh weight of plants overexpressing *PPCK1* and *PPCK2* to WT

Seedlings were germinated for 10 days on +Pi containing agar media on plates, and then transferred to pots and allowed to grow for additional 21 days in phytochamber before harvest. Error bars denote SD (n=40 biological replicates). Significance analysis was performed by Student's *t*-test (two-tailed, equal variances): □p ≤ 0.05 compared to WT (Col-0).

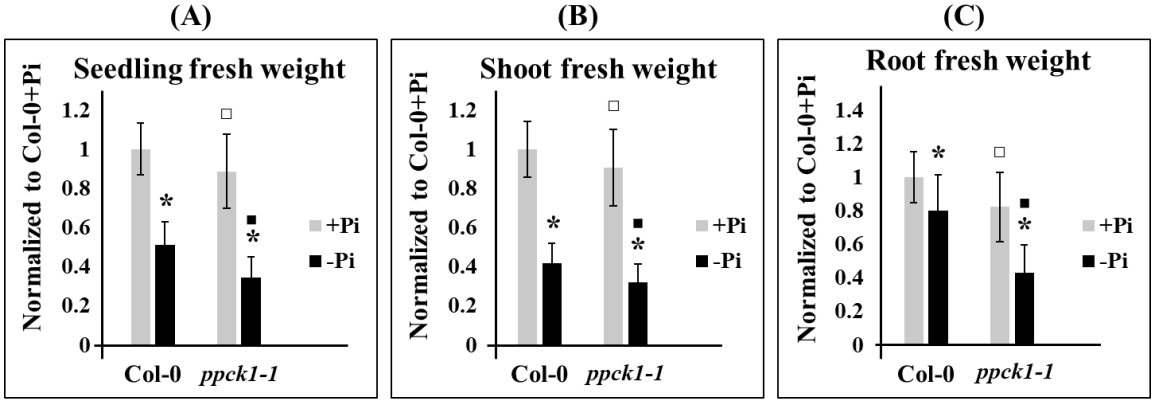

Supplementary Figure 7-14: Comparison between fresh weight of *ppck1-1* and WT seedlings

Normalized (A) seedling, (B) shoot, and (C) root fresh weight of *ppck1-1* seedlings grown under Pi-sufficient and Pi-deficient conditions compared to WT (Col-0). Seedlings were germinated for 6 days on +Pi agar plates, transferred to +Pi (500 µM) or –Pi (5 µM) conditions, and allowed to grow for additional 5 days before harvest. Data are normalized to Col-0+Pi. Shown are the cumulative data of 14 independent germination experiments. For each experiment, four biological replicates (two pooled seedlings per replicate) were analyzed. Error bars denote SD (n=56 total biological replicates). Significance analyses were performed by Student's *t*-test (two-tailed, equal variances): *p ≤ 0.05, □p ≤ 0.05, and ▪p≤ 0.05 compared to +Pi condition, Col-0+Pi, and Col-0-Pi, respectively.

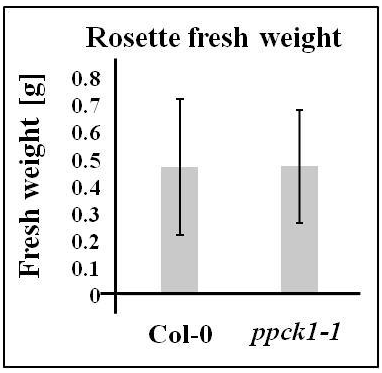

Supplementary Figure 7-15: Comparison of rosette fresh weight between *ppck1-1* and WT plants

Seedlings were germinated for 10 days on +Pi containing agar media on plates, and then transferred to pots and allowed to grow for additional 21 days in phytochamber before harvest. Error bars denote SD (n=40 total biological replicates). Significance analysis was performed by Student's *t*-test (two-tailed, equal variances): □p ≤ 0.05 compared to WT (Col-0).

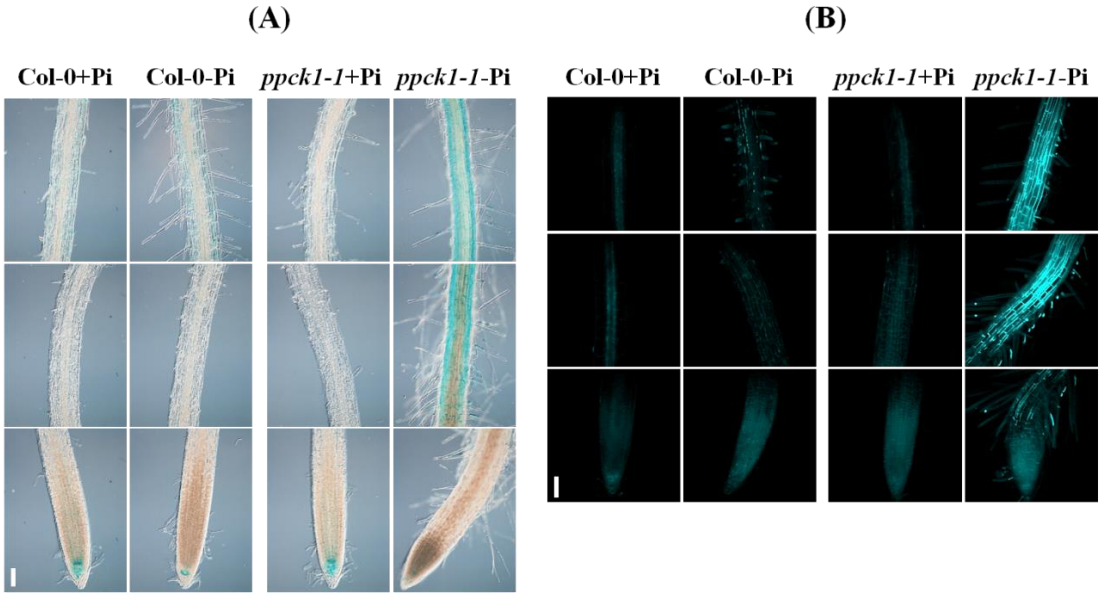

Supplementary Figure 7-16: Iron accumulation and callose deposition in Pi-depleted primary roots of *ppck1-1* seedlings

(A) Iron accumulation and (B) callose deposition in primary roots of *ppck1-1* seedlings compared to WT (Col-0). Seedlings were germinated for 6 days on +Pi agar plates, transferred to +Pi (500 µM) or –Pi (5 µM) conditions, and allowed to grow for additional 4 days prior to Perls or Callose staining. The top, center, and bottom panels depict the mature root zone, early differentiation zone, and root apical region, respectively. Representative images from one out of three independent experiments are shown. Scale bars represent 100 µm.

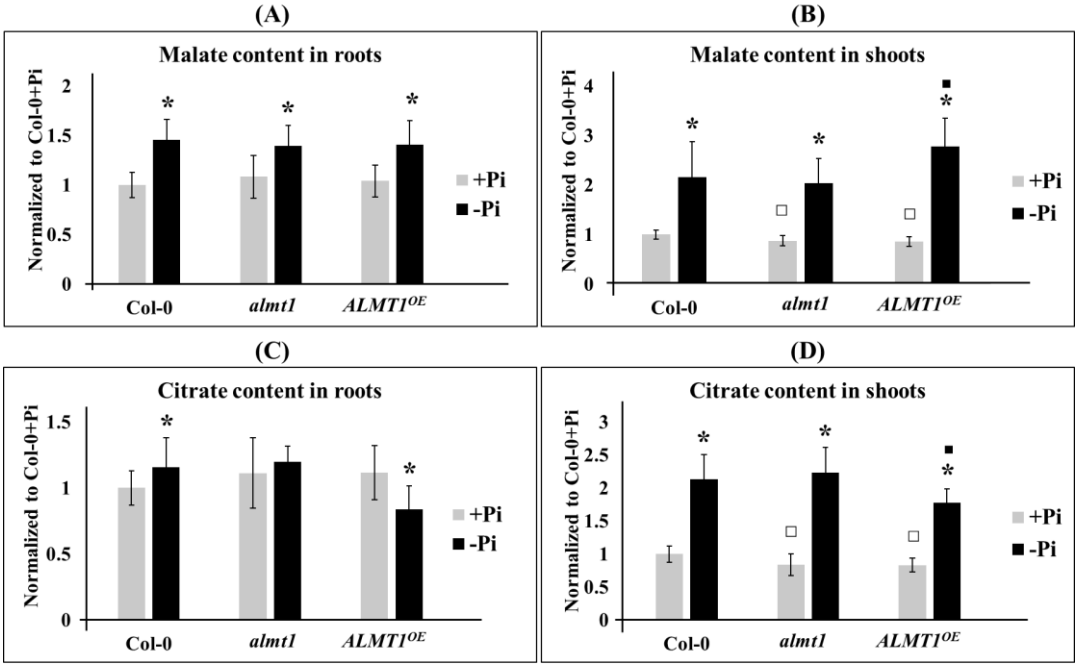

Supplementary Figure 7-17: Normalized malate and citrate content in *almt1* and *ALMT1^{OE}* compared to WT

Normalized content of (A) malate in roots, (B) malate in shoots, (C) citrate in roots, and (D) citrate in shoots of *almt1* and *ALMT1^{OE}* grown under Pi-sufficient and Pi-deficient conditions compared to WT (Col-0). Seedlings were germinated for 6 days on +Pi agar plates, transferred to +Pi (500 µM) or –Pi (5 µM) conditions, and allowed to grow for additional 5 days before harvest. Data are normalized to the levels detected in Col-0+Pi. Shown are the cumulative data of 4 independent germination experiments. For each experiment, four biological replicates (two pooled seedlings per replicate) were analyzed. Error bars denote SD (n=16 total biological replicates). Significance analyses were performed by Student's *t*-test (two-tailed, equal variances): *p ≤ 0.05, □p ≤ 0.05, and ▪p≤ 0.05 compared to +Pi condition, Col-0+Pi, and Col-0-Pi, respectively.

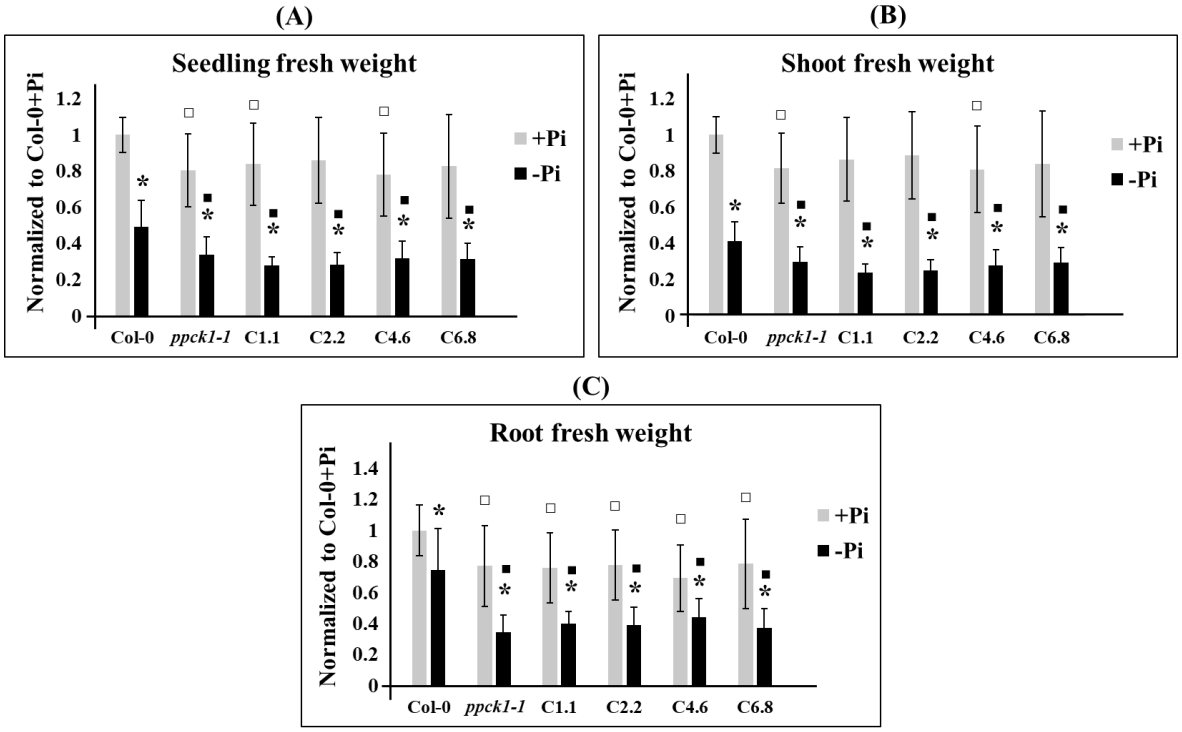

Supplementary Figure 7-18: Comparison of fresh weight of *pPPCK1$_{long}$::gDNA/ppck1-1* lines to WT and *ppck1-1*

Comparison of (A) seedling, (B) shoot, and (C) root fresh weight of C-lines grown under Pi-sufficient and Pi-deficient conditions to WT (Col-0) and *ppck1-1* seedlings. Seedlings were germinated for 6 days on +Pi agar plates, transferred to +Pi (500 µM) or –Pi (5 µM) conditions, and allowed to grow for additional 5 days before harvest. Data are normalized to Col-0+Pi. Shown are the cumulative data of 3 independent germination experiments. For each experiment, four biological replicates (two pooled seedlings per replicate) were analyzed. Error bars denote SD (n=12 total biological replicates). Significance analyses were performed by Student's *t*-test (two-tailed, equal variances): *p ≤ 0.05, □p ≤ 0.05, ▪p≤ 0.05, ○p ≤ 0.05, and •p ≤ 0.05 compared to +Pi, Col-0+Pi, Col-0-Pi, *ppck1-1*+Pi, and *ppck1-1*-Pi, respectively.

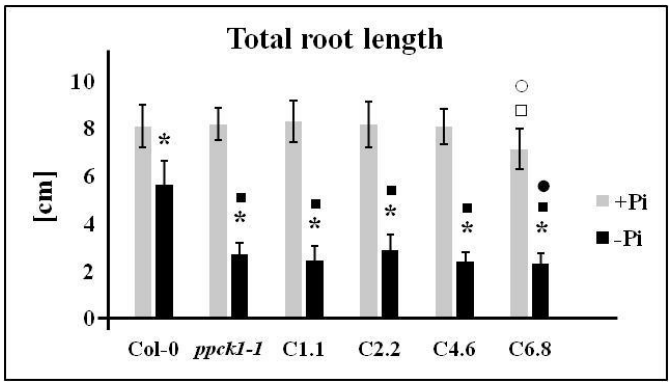

Supplementary Figure 7-19: Comparison of total root length of *pPPCK1$_{long}$::gDNA/ppck1-1* lines to WT and *ppck1-1*

Seedlings were germinated for 6 days on +Pi agar plates, transferred to +Pi (500 µM) or –Pi (5 µM) conditions, and allowed to grow for additional 9 days before root length measurement. Data from one representative out of three independent experiments are shown. Error bars denote SD (n=25 biological replicates). Significance analyses were performed by Student's *t*-test (two-tailed, equal variances): *p ≤ 0.05, □p ≤ 0.05, ▪p≤ 0.05, ○p ≤ 0.05, and •p ≤ 0.05 compared to +Pi, Col-0+Pi, Col-0-Pi, *ppck1-1*+Pi, and *ppck1-1*-Pi, respectively.

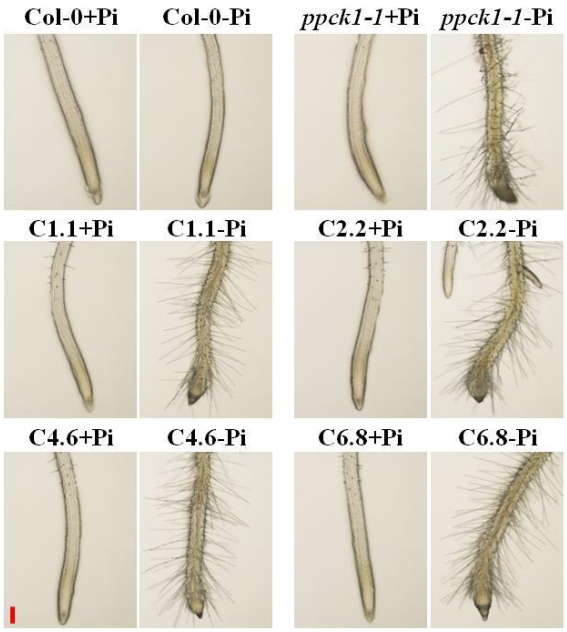

Supplementary Figure 7-20: Comparison of root-tip morphology of Pi-starved *pPPCK1$_{long}$::gDNA/ppck1-1* lines to WT and *ppck1-1* seedlings

Seedlings were germinated for 6 days on +Pi agar plates, transferred to +Pi (500 µM) or –Pi (5 µM) conditions, and allowed to grow for additional 4 days before imaging. Images were taken with Nikon SMZ1270 microscope. Representative image from one out of three independent experiments are shown. Scale bars represent 0.2 mm.

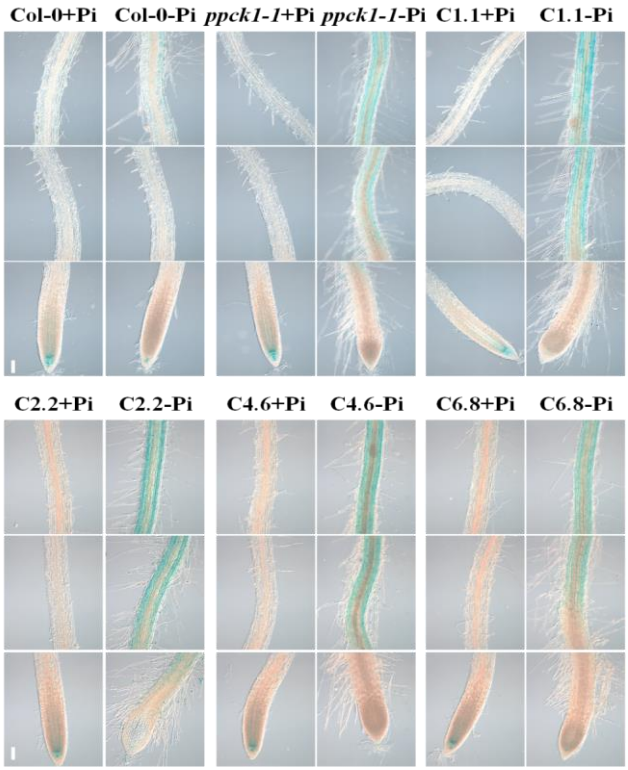

Supplementary Figure 7-21: Comparison of iron deposition in primary roots of Pi-depleted *pPPCK1$_{long}$::gDNA/ppck1-1* lines to WT and *ppck1-1* seedlings

Seedlings were germinated for 6 days on +Pi agar plates, transferred to +Pi (500 µM) or –Pi (5 µM) conditions, and allowed to grow for additional 4 days prior to Perls staining. The top, center, and bottom panels depict the mature root zone, early differentiation zone, and root apical region, respectively. Representative images from one out of three independent experiments are shown. Scale bars represent 100 µm.

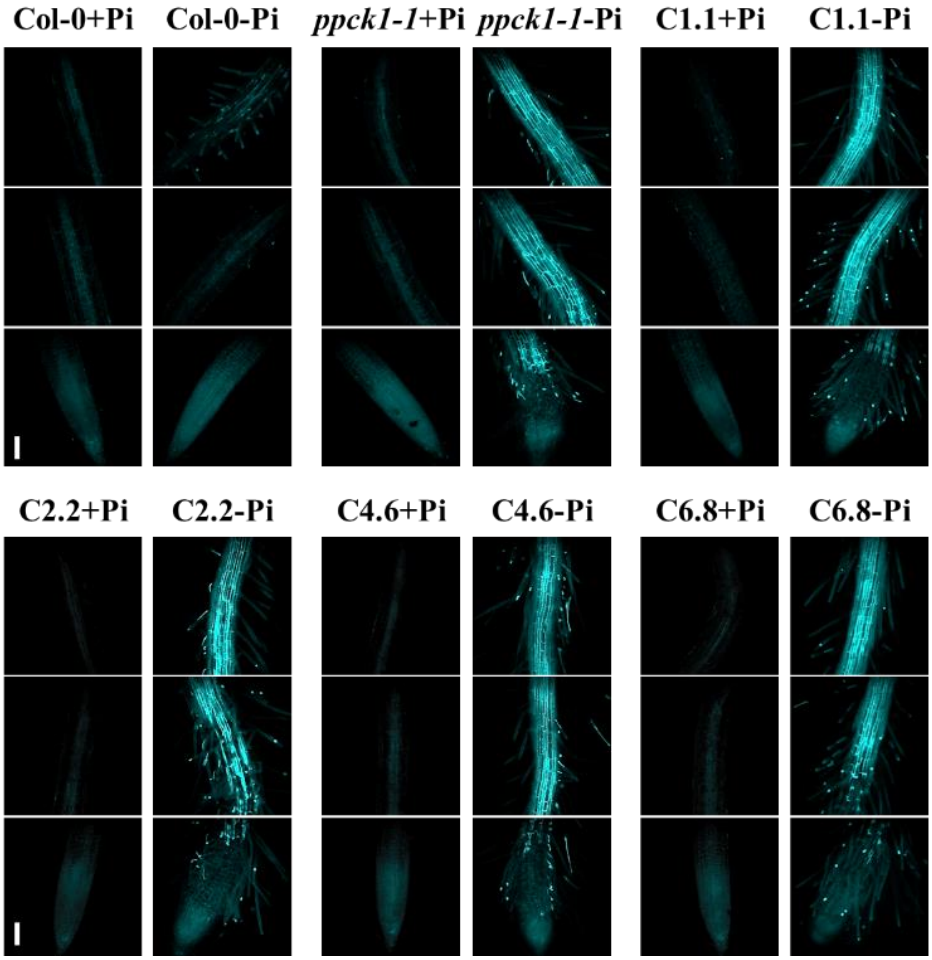

Supplementary Figure 7-22: Comparison of callose deposition in primary roots of Pi-starved *pPPCK1$_{long}$::gDNA/ppck1-1* lines to WT and *ppck1-1* seedlings

Seedlings were germinated for 6 days on +Pi agar plates, transferred to +Pi (500 µM) or –Pi (5 µM) conditions, and allowed to grow for additional 4 days prior to callose staining. The top, center, and bottom panels depict the mature root zone, early differentiation zone, and root apical region, respectively. Representative images from one out of three independent experiments are shown. Scale bars represent 100 µm.

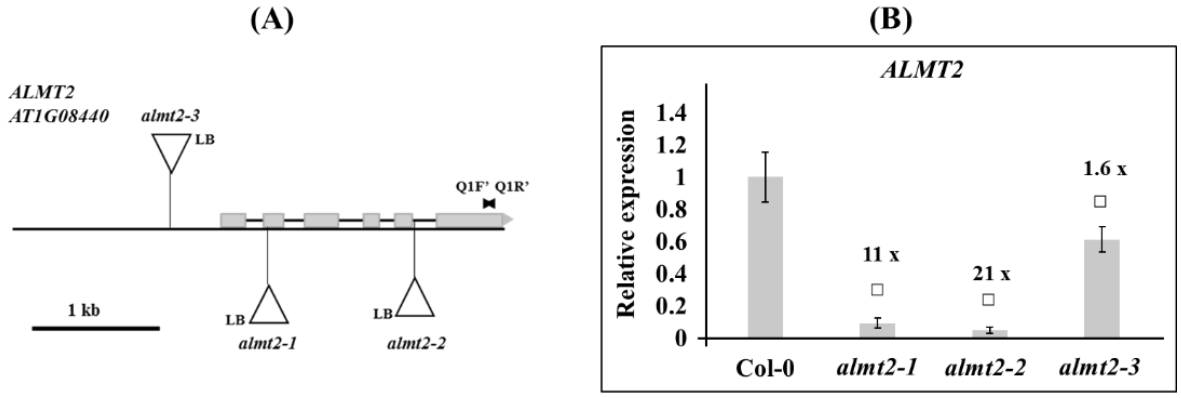

Supplementary figure 7-23: Characterization of T-DNA insertion mutants of *ALMT2*

(A) Gene model and position of T-DNA insertions in three independent lines, *almt2-1*, *almt2-2*, and *almt2-3.* Grey boxes indicate the exons and black line between exons indicate the introns. Position of T-DNA insertions are indicated with triangles. Arrows indicate the position of primers used for amplification of *ALMT2* transcripts for RT-qPCR analysis (B) *ALMT2* transcript levels in *almt2-1, almt2-2, and almt2-3* lines compared to the levels detected in WT (Col-0) by RT-qPCR analysis. Total RNA was extracted from 7 days old seedlings. *PP2A* was used as a reference gene and the relative expression levels were normalized to the levels detected in WT (Col-0). Error bars denote SD (n=3 biological replicates). Data from one representative out of two independent experiments are shown. Significance analyses were performed by Student's *t*-test (two-tailed, equal variances): □p ≤ 0.05 compared to WT (Col-0).

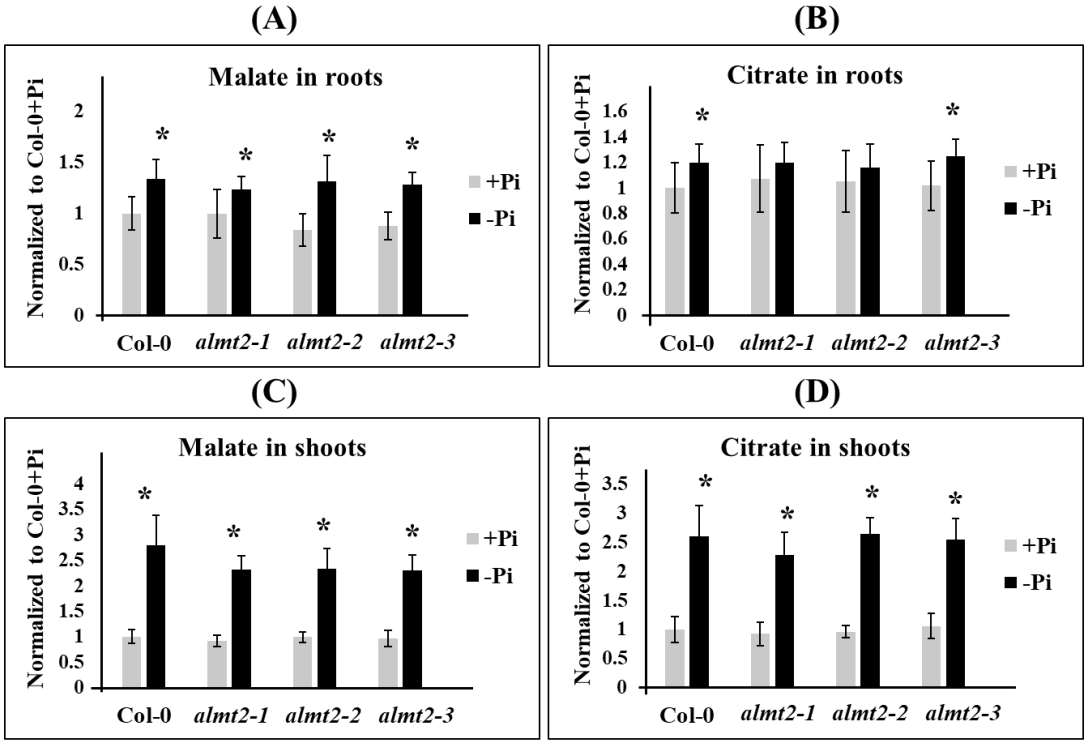

Supplementary Figure 7-24: Normalized content of malate and citrate in *almt2* lines compared to WT

Normalized content of (A) malate in roots, (B) citrate in roots, (C) malate in shoots, and (D) citrate in shoots of T-DNA insertion lines for *ALMT2*, grown under Pi-sufficient and Pi-deficient conditions compared to WT (Col-0). Seedlings were germinated for 6 days on +Pi agar plates, transferred to +Pi (500 µM) or –Pi (5 µM) conditions, and allowed to grow for additional 5 days before harvest. Data are normalized to the levels detected in Col-0+Pi. Shown are the cumulative data of two independent germination experiments. For each experiment, four biological replicates (two pooled seedlings per replicate) were analyzed. Error bars denote SD (n=08). Significance analyses were performed by Student's *t*-test (two-tailed, equal variances): *p ≤ 0.05; □p ≤ 0.05; and •p ≤ 0.05 compared to +Pi, Col-0+Pi, and Col-0-Pi, respectively.

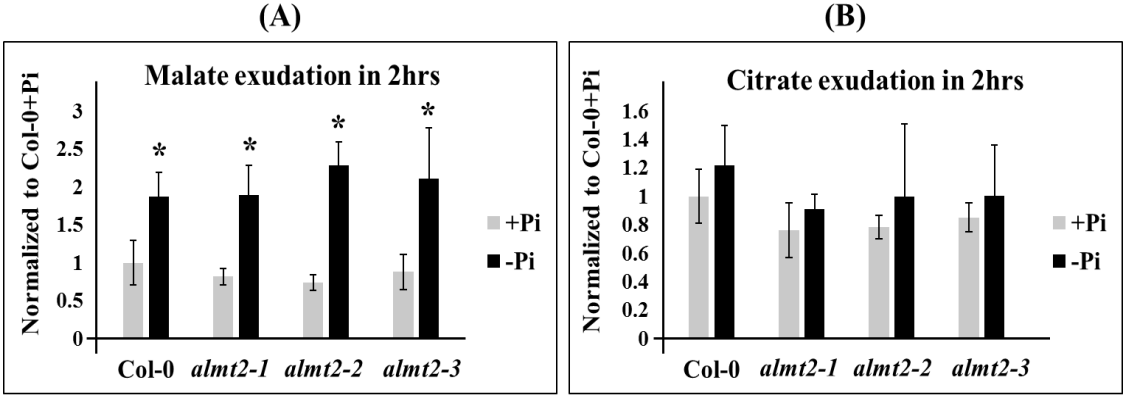

Supplementary figure 7-25: Normalized malate and citrate content in root exudates of *almt2* lines compared to WT

Normalized content of (A) malate and (B) citrate in root exudates of *almt2* lines grown under Pi-sufficient and Pi-deficient conditions compared to WT (Col-0). Seedlings were germinated for 6 days on +Pi agar plates, transferred to +Pi (500 µM) or –Pi (5 µM) conditions, and allowed to grow for additional 4 days. Subsequently, the root systems of three intact seedlings were incubated in 300 µl water, and exudates were collected after 2 h. Data are normalized to the levels detected in Col-0+Pi. Shown are the cumulative data of two independent germination experiments. For each experiment, four biological replicates (the exudates of three pooled root systems per replicate) were analyzed. Error bars denote SD (n=08 total biological replicates). Significance analyses were performed by Student's *t*-test (two-tailed, equal variances): *p ≤ 0.05, □p ≤ 0.05, and ▪p≤ 0.05 compared to +Pi condition, Col-0+Pi, and Col-0-Pi, respectively.

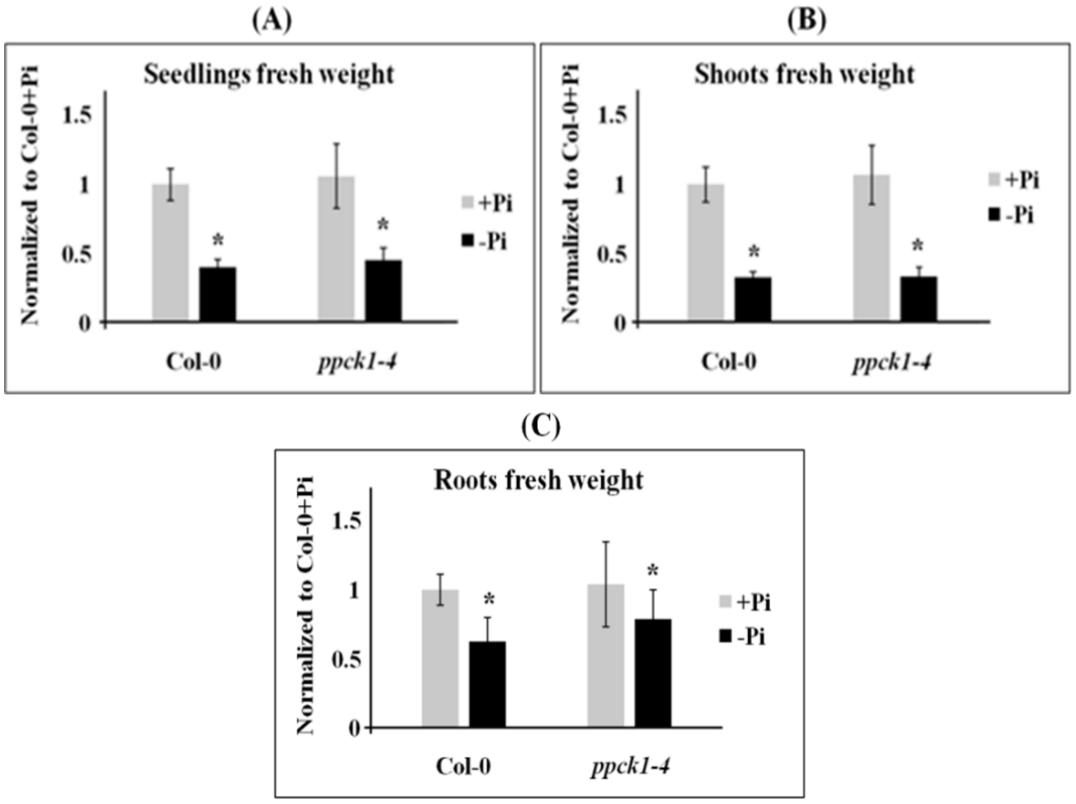

Supplementary Figure 7-26: Comparison between fresh weight of *ppck1-4* and WT seedlings

Normalized (A) seedling, (B) shoot, and (C) root fresh weight of *ppck1-4* plants grown under Pi-sufficient and Pi-deficient conditions compared to WT (Col-0). Seedlings were germinated for 6 days on +Pi agar plates, transferred to +Pi (500 µM) or –Pi (5 µM) conditions, and allowed to grow for additional 5 days before harvest. Data are normalized to Col-0+Pi. Shown are the cumulative data of 3 independent germination experiments. For each experiment, four biological replicates (two pooled seedlings per replicate) were analyzed. Error bars denote SD (n=12 total biological replicates). Significance analyses were performed by Student's *t*-test (two-tailed, equal variances): *p ≤ 0.05, □p ≤ 0.05, and ▪p≤ 0.05 compared to +Pi condition, Col-0+Pi, and Col-0-Pi, respectively.

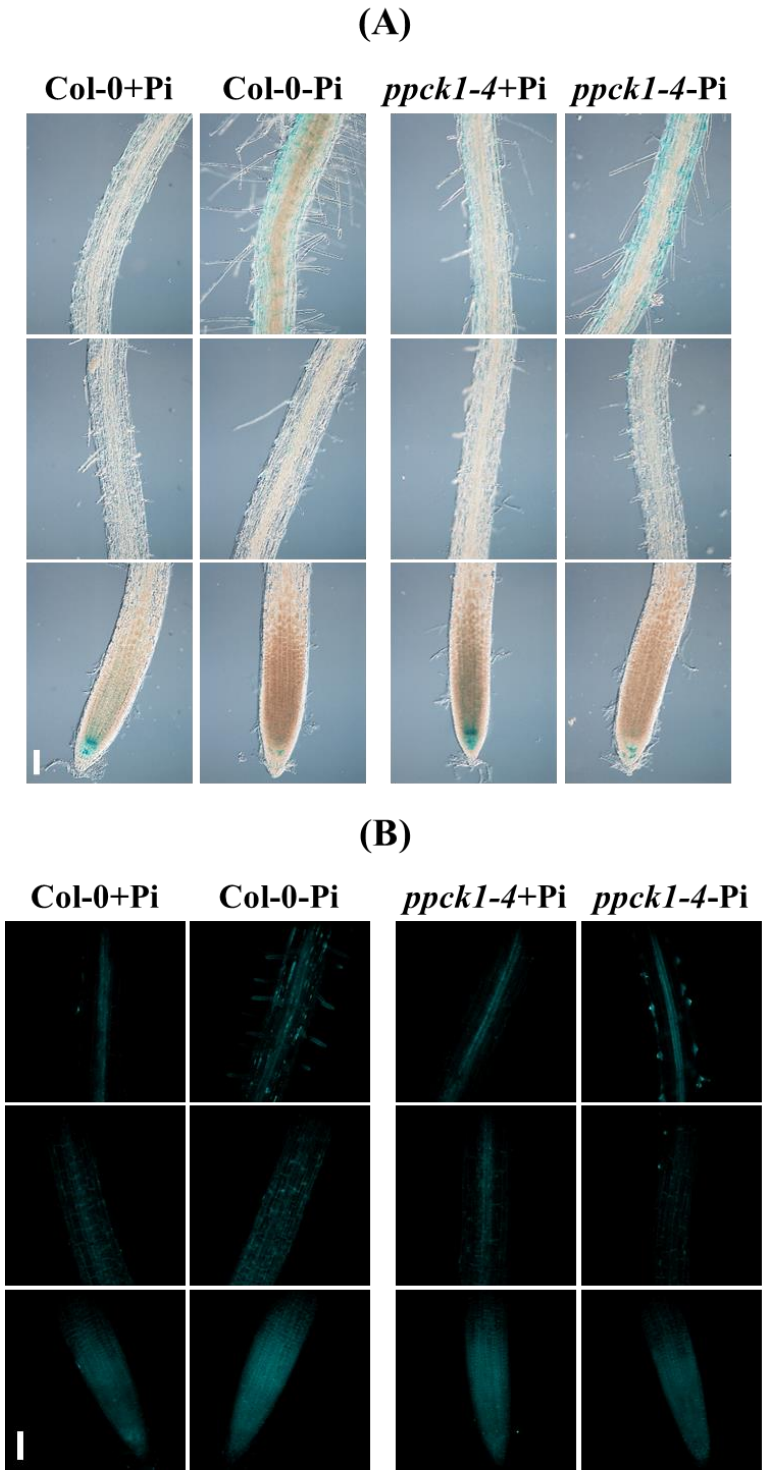

Supplementary figure 7-27: Iron accumulation and callose deposition in Pi-depleted primary roots of *ppck1-4* seedlings

(A) Iron accumulation and (B) callose deposition in primary roots of *ppck1-4* seedlings compared to WT (Col-0). Seedlings were germinated for 6 days on +Pi agar plates, transferred to +Pi (500 µM) or –Pi (5 µM) conditions, and allowed to grow for additional 4 days prior to Perls or Callose staining. The top, center, and bottom panels depict the mature root zone, early differentiation zone, and root apical region, respectively. Representative images from one out of three independent experiments are shown. Scale bars represent 100 µm.

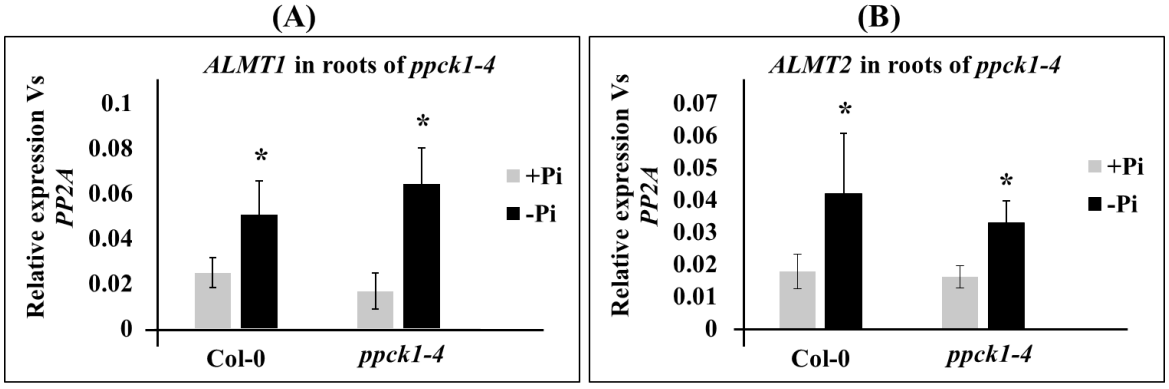

Supplementary figure 7-28: Expression analysis of *ALMT1* and *ALMT2* in roots of *ppck1-4* seedlings by RT-qPCR

Transcript levels of (A) *ALMT1* and (B) *ALMT2* in roots of Pi-sufficient and Pi-deficient *ppck1-4* seedlings compared to the levels detected in WT (Col-0). Seedlings were germinated for 6 days on +Pi agar plates, transferred to +Pi (500 µM) or –Pi (5 µM) conditions, and allowed to grow for additional 5 days before harvest for total RNA extraction. Data from one representative out of three independent experiments are shown. Error bars denote SD (n=4 total biological replicates). Significance analyses were performed by Student's *t*-test (two-tailed, equal variances): *p ≤ 0.05, □p ≤ 0.05, and ▪p≤ 0.05 compared to +Pi condition, Col-0+Pi, and Col-0-Pi, respectively.

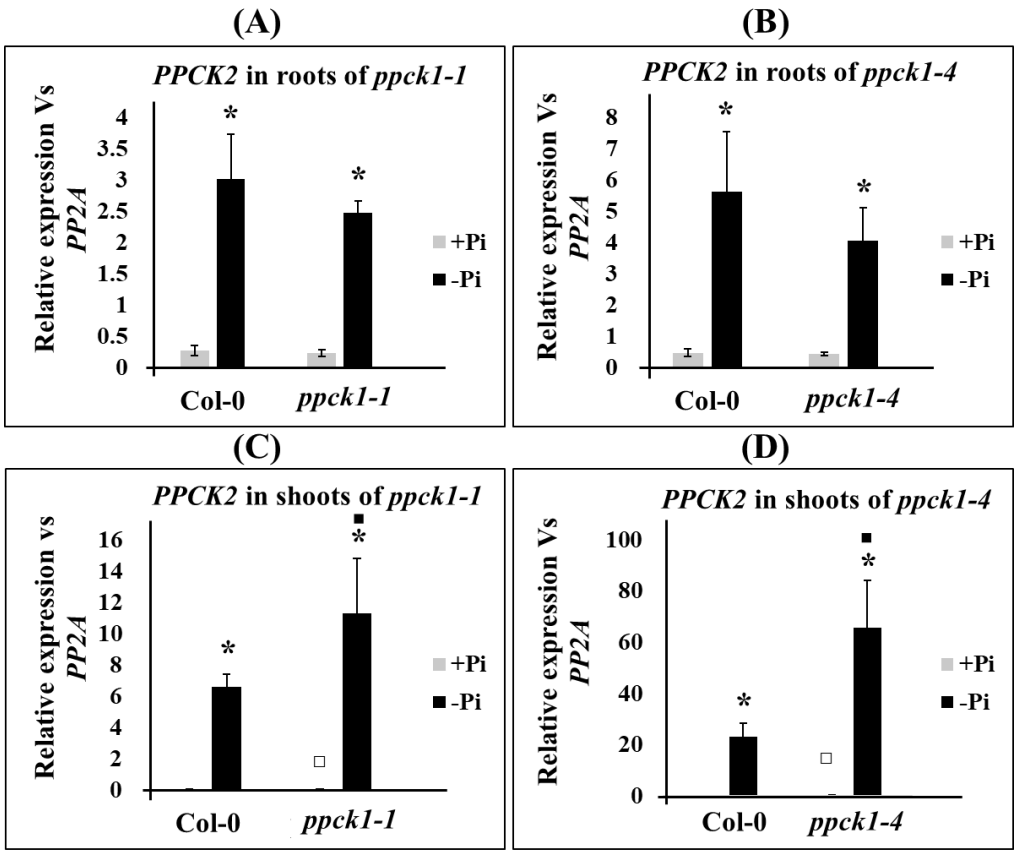

Supplementary figure 7-29: Expression analysis of *PPCK2* in *ppck1-1* and *ppck1-4* seedlings by RT-qPCR

Transcript levels of *PPCK2* in (A) roots of *ppck1-1*, (B) roots of *ppck1-4*, (C) shoots of *ppck1-1*, and (D) shoots of *ppck1-4* seedlings grown under Pi-sufficient and Pi-deficient conditions compared to the levels detected in WT (Col-0). Seedlings were germinated for 6 days on +Pi agar plates, transferred to +Pi (500 µM) or –Pi (5 µM) conditions, and allowed to grow for additional 5 days before harvest for total RNA extraction. Data from one representative out of three independent experiments are shown. Error bars denote SD (n=4 total biological replicates). Significance analyses were performed by Student's *t*-test (two-tailed, equal variances): *p ≤ 0.05, □p ≤ 0.05, and ▪p≤ 0.05 compared to +Pi condition, Col-0+Pi, and Col-0-Pi, respectively.

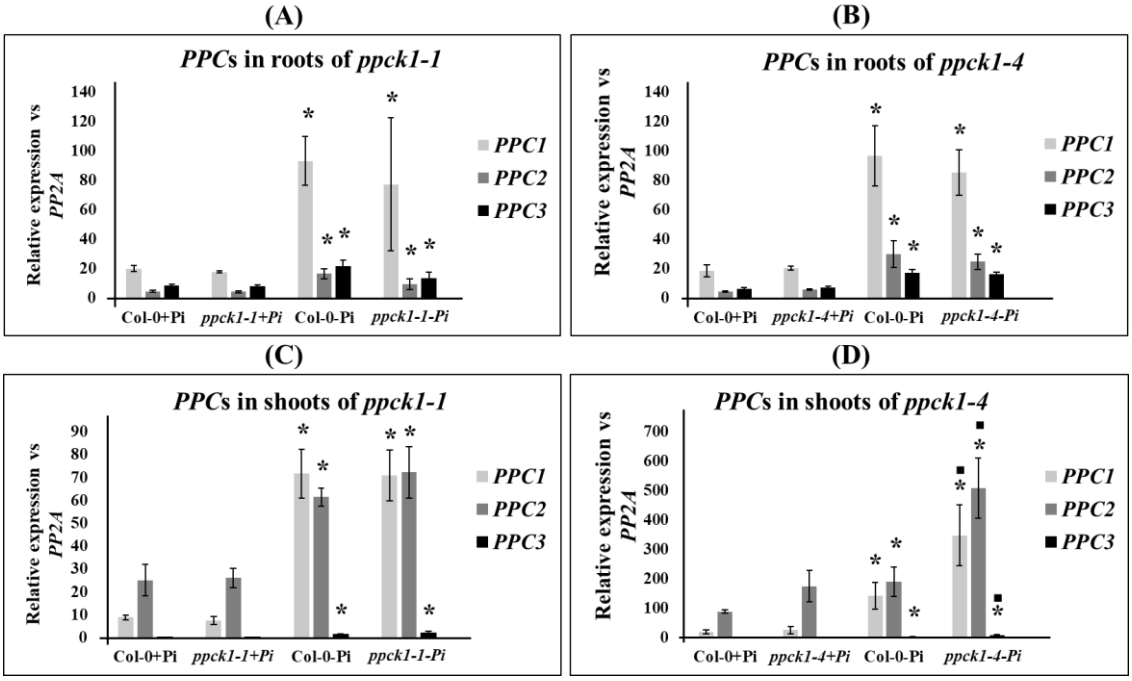

Supplementary figure 7-30: Expression analysis of *PPC*s in *ppck1-1* and *ppck1-4* seedlings by RT-qPCR

Transcript levels of *PPCs* in (A) roots of *ppck1-1*, (B) roots of *ppck1-4*, (C) shoots of *ppck1-1*, and (D) shoots of *ppck1-4* seedlings grown under Pi-sufficient and Pi-deficient conditions compared to the levels detected in WT (Col-0). Seedlings were germinated for 6 days on +Pi agar plates, transferred to +Pi (500 µM) or –Pi (5 µM) conditions, and allowed to grow for additional 5 days before harvest for total RNA extraction. Data from one representative out of three independent experiments are shown. Error bars denote SD (n=4 total biological replicates). Significance analyses were performed by Student's *t*-test (two-tailed, equal variances): *p ≤ 0.05, □p≤ 0.05, and •p≤ 0.05 compared to +Pi condition, Col-0+Pi, and Col-0-Pi, respectively.

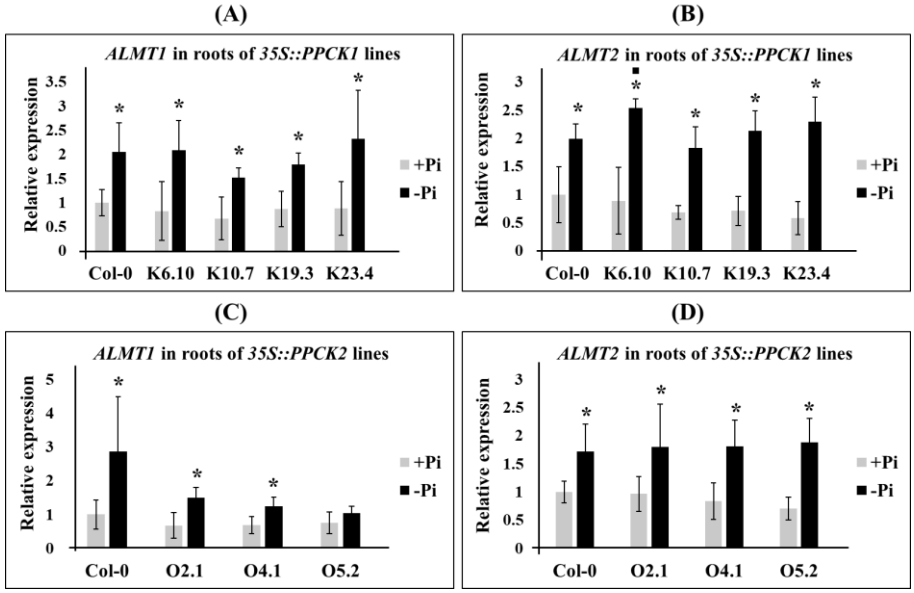

Supplementary figure 7-31: Expression analysis of *ALMT1* and *ALMT2* in roots of plants overexpressing *PPCK1* and *PPCK2* by RT-qPCR

Transcript levels of (A) *ALMT1* in *35S::PPCK1*, (B) *ALMT2* in *35S::PPCK1*, (C) *ALMT1* in *35S::PPCK2*, and (D) *ALMT2* in *35S::PPCK2* lines grown under Pi-sufficient and Pi-deficient conditions compared to the levels detected in WT (Col-0). Seedlings were germinated for 6 days on +Pi agar plates, transferred to +Pi (500 µM) or –Pi (5 µM) conditions, and allowed to grow for additional 5 days before harvest for total RNA extraction. Data from one representative out of three independent experiments are shown. Error bars denote SD (n=3 total biological replicates). Significance analyses were performed by Student's *t*-test (two-tailed, equal variances): *p ≤ 0.05, □p ≤ 0.05, and •p≤ 0.05 compared to +Pi condition, Col-0+Pi, and Col-0-Pi, respectively.

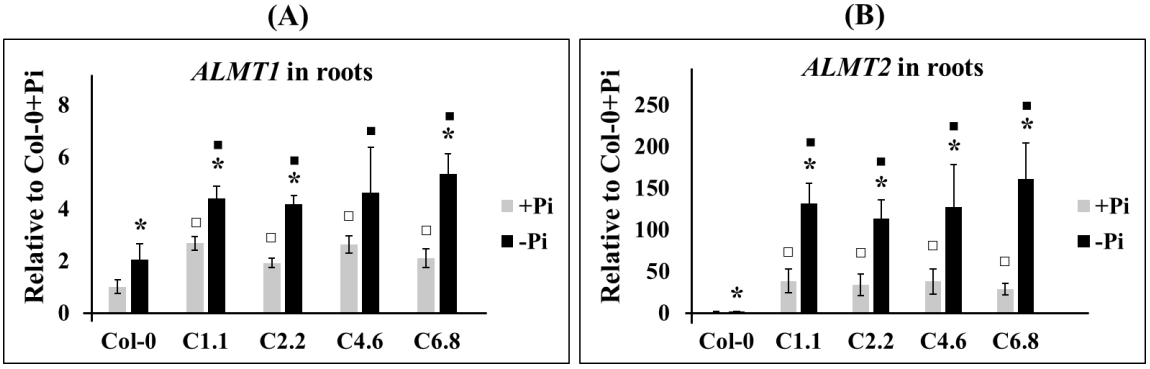

Supplementary figure 7-32: Expression analysis of *ALMT1* and *ALMT2* in roots of *pPPCK1$_{long}$::gDNA/ppck1-1* lines

Transcript levels of (A) *ALMT1* and (B) *ALMT2* in roots of C-lines grown under Pi-sufficient and Pi-deficient conditions compared to the levels detected in WT (Col-0). Seedlings were germinated for 6 days on +Pi agar plates, transferred to +Pi (500 µM) or –Pi (5 µM) conditions, and allowed to grow for additional 5 days before harvest for total RNA extraction. Data from one representative out of three independent experiments are shown. Error bars denote SD (n=3 total biological replicates). Significance analyses were performed by Student's *t*-test (two-tailed, equal variances): *p≤ 0.05, □p≤ 0.05, and ▪p≤ 0.05 compared to +Pi condition, Col-0+Pi, and Col-0-Pi, respectively.

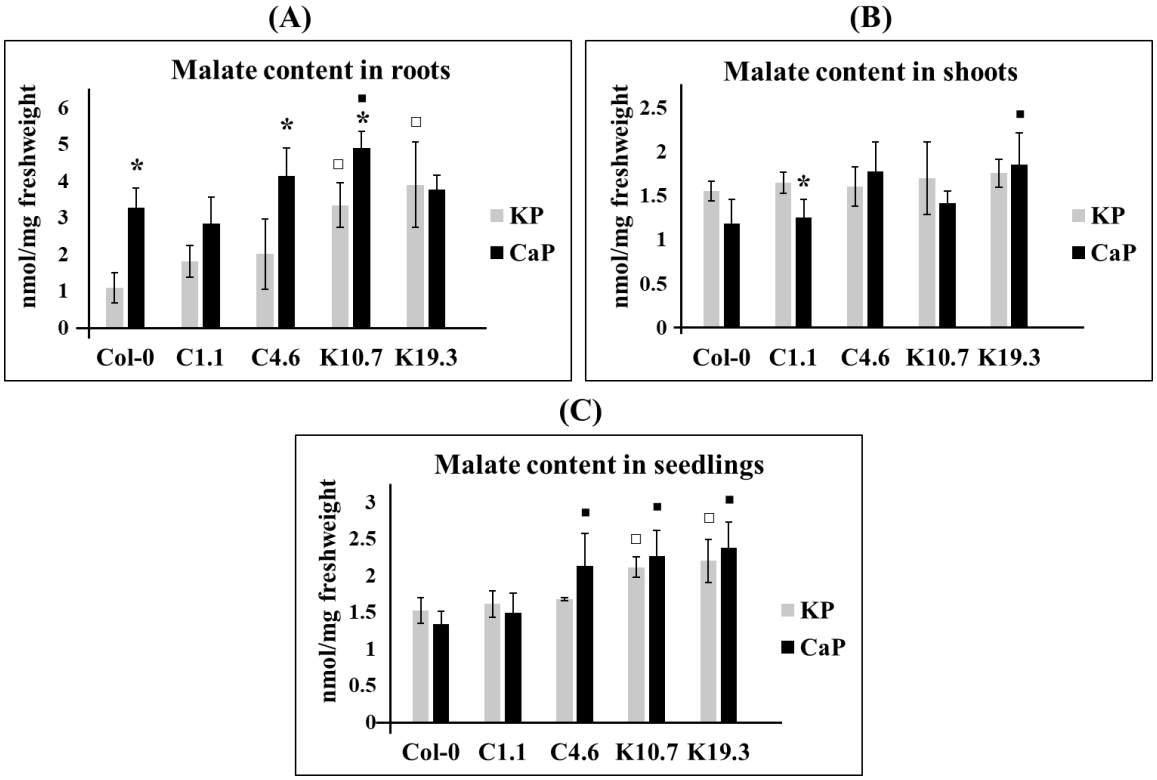

Supplementary figure 7-33: Malate content in *pPPCK1$_{long}$::gDNA/ppck1-1* and *35S::PPCK1* lines compared to WT when grown on insoluble Pi source, calcium phosphate

Malate content in (A) roots, (B) shoots, and (C) seedlings of C-lines (overexpression of *PPCK1* and *ALMT1*/*ALMT2*) and K-lines (overexpression of *PPCK1*), when grown on soluble Pi (potassium phosphate-KP) and insoluble Pi source (calcium phosphate-CaP) compared to WT (Col-0). Seedlings were germinated on agar plates containing either 1.25 mM KH_2PO_4 or 1.25 mM $Ca_3(PO_4)_2$ as Pi-source and allowed to grow for 11 days before harvest. Both media were used at a final pH of 7.6. This experiment was performed only once with four biological replicates (two pooled seedlings per replicate). Error bars denote SD (n=04 total biological replicates). Significance analyses were performed by Student's *t*-test (two-tailed, equal variances): *p ≤ 0.05, □p ≤ 0.05, and ▪p≤ 0.05, compared to KP, Col-0-KP, and Col-0-CaP, respectively.

Supplementary table 7-1: Comparison of metabolite levels in roots of *35::PPCK1* lines to the levels detected in WT
Metabolite levels in roots of K-lines were compared to WT roots grown under (A) Pi-sufficient and (B) Pi-deficient conditions. Data are normalized to the levels detected in WT+Pi. Shown are the cumulative data of 3 independent germination experiments. For each experiment, four biological replicates (two pooled seedlings per replicate) were analyzed (n=12 total biological replicates). Significance analyses were performed by Student's *t*-test (two tailed, two sample equal variance). Number in bold indicates significant difference between the transgenic lines and WT with p<0.05. Light grey and dark grey cell highlight the metabolites which were significantly increased and decreased, respectively in the lines compared to WT.

(A) +Pi-Roots								
Metabolites	# K6.10		# K10.7		# K19.3		# K23.4	
	fold Vs WT+Pi	*t*-test Vs WT+Pi	fold Vs WT+Pi	*t*-test Vs WT+Pi	fold Vs WT+Pi	*t*-test Vs WT+Pi	fold Vs WT+Pi	*t*-test Vs WT+Pi
A	0.700	**3.1E-04**	0.733	**1.4E-03**	0.938	5.0E-01	0.727	**2.7E-03**
C	0.995	9.5E-01	1.060	3.9E-01	1.498	**1.0E-02**	1.114	3.0E-01
D	1.246	**8.4E-03**	1.387	**5.7E-04**	1.523	**9.7E-05**	1.412	**4.6E-05**
E	1.024	6.3E-01	1.079	9.9E-02	1.260	**3.2E-03**	1.073	1.9E-01
F	0.808	**2.2E-02**	0.776	**3.4E-02**	0.862	2.4E-01	0.759	**3.4E-03**
G	0.779	1.0E-01	0.739	1.4E-01	1.339	3.3E-01	0.725	**4.4E-02**
H	1.196	2.7E-01	1.191	2.7E-01	1.534	**3.9E-02**	1.503	**3.6E-02**
I	0.925	5.3E-01	0.980	8.8E-01	1.337	1.7E-01	1.066	6.1E-01
K	1.004	9.8E-01	1.013	9.3E-01	1.218	2.8E-01	1.084	5.5E-01
L	0.993	9.5E-01	1.026	8.2E-01	1.386	1.2E-01	1.083	3.9E-01
M	0.932	3.5E-01	1.027	8.0E-01	1.280	1.5E-01	0.962	6.7E-01
N	1.151	3.6E-01	1.111	3.8E-01	1.604	**6.0E-03**	1.175	3.0E-01
P	1.059	3.8E-01	1.103	1.4E-01	1.435	5.5E-02	1.143	9.2E-02
Q	1.031	6.7E-01	1.118	1.1E-01	1.489	**1.2E-03**	1.114	2.4E-01
R	0.825	1.9E-01	0.802	1.1E-01	1.384	1.2E-01	1.054	7.1E-01
S	0.954	6.5E-01	0.943	5.4E-01	1.150	2.7E-01	0.988	9.0E-01
T	1.014	8.8E-01	1.029	6.8E-01	1.442	**1.9E-02**	1.145	1.6E-01
V	0.795	**1.9E-02**	0.836	9.4E-02	1.247	2.0E-01	0.892	2.9E-01
W	0.919	5.4E-01	0.807	1.3E-01	1.028	8.8E-01	1.004	9.8E-01
Y	0.974	8.1E-01	1.067	6.3E-01	1.254	1.7E-01	1.143	3.0E-01
Orn	1.265	3.4E-01	1.393	4.1E-01	2.311	1.6E-01	0.834	3.2E-01
Citru	0.968	8.0E-01	1.094	4.1E-01	2.556	1.4E-01	0.979	8.1E-01
fum	1.119	9.5E-02	1.116	1.8E-01	1.188	**1.3E-02**	1.048	4.6E-01
aco	2.071	2.3E-01	2.020	2.7E-01	1.716	3.0E-01	1.773	2.7E-01
akg	1.359	**5.9E-04**	1.391	**1.3E-02**	1.349	**2.3E-02**	1.231	1.3E-01
suc	1.225	**6.4E-04**	1.234	**6.6E-04**	1.258	**1.4E-03**	1.179	**3.2E-02**
(B) -Pi-Roots								
A	0.824	1.2E-01	0.888	2.9E-01	1.105	3.5E-01	0.822	1.3E-01
C	1.032	8.1E-01	1.098	4.4E-01	1.254	5.4E-02	1.087	5.3E-01
D	0.966	7.2E-01	1.008	9.2E-01	1.088	3.5E-01	0.985	8.7E-01
E	1.043	6.0E-01	1.085	2.4E-01	1.173	**8.2E-03**	0.979	7.5E-01
F	0.921	5.8E-01	0.762	**3.6E-02**	1.094	4.3E-01	0.755	**3.3E-02**
G	0.844	3.4E-01	0.933	7.1E-01	1.103	5.1E-01	0.800	2.1E-01
H	2.619	8.5E-02	2.982	8.8E-02	6.333	**1.8E-02**	0.791	3.2E-01
I	1.200	2.7E-01	1.173	2.9E-01	1.361	**3.3E-02**	1.296	2.1E-01
K	1.153	4.8E-01	1.122	5.4E-01	1.355	7.6E-02	0.948	7.9E-01
L	1.200	1.9E-01	1.276	7.3E-02	1.412	**7.8E-03**	1.233	2.2E-01
M	0.922	4.8E-01	1.036	7.7E-01	1.312	**1.9E-02**	0.880	2.4E-01
N	1.183	3.2E-01	1.215	2.2E-01	1.480	**1.3E-02**	1.220	2.3E-01
P	0.936	5.6E-01	1.208	1.3E-01	1.119	3.6E-01	1.063	6.0E-01
Q	1.127	4.3E-01	1.143	3.3E-01	1.336	**4.7E-02**	1.065	6.5E-01
R	1.296	1.7E-01	1.263	1.9E-01	1.226	1.8E-01	1.068	6.8E-01
S	1.027	8.1E-01	1.017	8.8E-01	1.147	2.1E-01	1.029	8.2E-01
T	1.055	6.7E-01	1.101	4.3E-01	1.258	**3.6E-02**	1.075	5.9E-01
V	1.369	9.6E-02	1.379	8.1E-02	1.663	**3.6E-03**	1.209	4.8E-01
W	1.081	6.0E-01	1.003	9.8E-01	1.243	1.5E-01	0.945	7.1E-01
Y	1.094	5.0E-01	1.123	3.7E-01	1.300	5.1E-02	1.041	7.9E-01
Orn	0.789	8.4E-02	0.655	**3.6E-03**	1.122	3.0E-01	0.500	**5.2E-05**
Citru	1.075	7.1E-01	1.462	1.4E-01	1.464	1.7E-01	1.171	3.9E-01
fum	0.899	4.9E-01	0.941	5.8E-01	1.020	8.7E-01	1.029	8.5E-01
aco	1.188	5.1E-01	2.364	1.2E-01	1.718	1.8E-01	1.798	1.7E-01
akg	1.407	5.6E-02	1.720	**1.0E-03**	1.108	4.4E-01	1.557	**3.6E-03**
suc	0.899	3.5E-01	0.992	9.4E-01	0.964	7.2E-01	0.918	4.4E-01

Supplementary table 7-2: Comparison of metabolite levels in roots of *35S::PPCK2* lines to the levels detected in WT
Metabolite levels in roots of O-lines were compared to WT roots grown under (A) Pi-sufficient and (B) Pi-deficient conditions. Data are normalized to the levels detected in WT+Pi. Shown are the cumulative data of 2 independent germination experiments. For each experiment, four biological replicates (two pooled seedlings per replicate) were analyzed (n=08). Significance analyses were performed by Student's *t*-test (two tailed, two sample equal variance). Number in bold indicates significant difference between the transgenic lines and WT with p<0.05. Light and dark grey cell highlight the metabolites which were significantly increased and decreased, respectively in the lines compared to WT.

(A) +Pi-Roots						
Metabolites	**# O2.1**		**# O4.1**		**# O5.2**	
	fold Vs WT+Pi	***t*-test Vs WT+Pi**	**fold Vs WT+Pi**	***t*-test Vs WT+Pi**	**fold Vs WT+Pi**	***t*-test Vs WT+Pi**
A	1.206	9.4E-02	1.435	**4.4E-03**	1.308	**1.0E-02**
C	0.988	9.1E-01	1.060	5.6E-01	1.149	1.4E-01
D	1.187	**2.8E-02**	1.217	**2.2E-02**	1.612	**4.2E-07**
E	1.053	4.6E-01	1.133	7.1E-02	1.228	**3.5E-03**
F	0.871	**1.8E-02**	0.883	1.7E-01	0.828	**2.5E-03**
G	0.837	1.9E-01	1.034	7.6E-01	0.756	**1.3E-02**
H	1.468	1.5E-01	1.935	**2.6E-03**	0.928	6.2E-01
I	1.092	4.9E-01	1.185	1.5E-01	1.095	3.3E-01
K	1.099	3.1E-01	1.282	**5.2E-03**	1.234	**1.3E-02**
L	1.039	6.3E-01	1.125	1.6E-01	1.103	6.3E-02
M	1.013	8.8E-01	1.021	8.0E-01	0.997	9.7E-01
N	1.280	2.3E-01	1.473	5.1E-02	1.465	**1.7E-02**
P	0.986	8.6E-01	1.141	7.0E-02	1.234	5.2E-02
Q	1.126	3.9E-01	1.215	7.9E-02	1.234	**3.3E-02**
R	1.099	4.6E-01	1.608	**1.7E-02**	1.443	**2.0E-02**
S	0.957	6.0E-01	1.152	**4.0E-02**	1.077	3.9E-01
T	1.021	8.1E-01	1.223	7.2E-02	1.177	5.0E-02
V	1.143	1.7E-01	1.195	1.3E-01	1.096	3.8E-01
W	0.925	4.6E-01	0.936	5.3E-01	1.018	8.1E-01
Y	1.213	7.8E-02	1.172	**4.0E-02**	1.362	**6.0E-04**
Orn	1.085	6.1E-01	1.247	4.3E-01	1.212	3.2E-01
Citru	1.112	4.0E-01	1.253	1.1E-01	1.126	2.4E-01
fum	0.998	9.8E-01	1.273	**2.5E-02**	1.249	**2.0E-02**
aco	0.752	**3.1E-02**	0.739	**7.6E-03**	0.669	**1.2E-04**
akg	0.786	**5.2E-03**	1.230	**2.3E-02**	1.201	5.1E-02
suc	0.740	**1.0E-04**	0.987	8.4E-01	0.959	5.1E-01
(B) -Pi-Roots						
A	1.117	4.3E-01	1.427	**8.4E-03**	1.174	1.8E-01
C	0.840	1.6E-01	1.021	8.8E-01	0.816	1.4E-01
D	0.956	6.0E-01	1.075	4.4E-01	1.135	1.2E-01
E	1.066	5.2E-01	1.190	1.4E-01	1.229	**1.9E-02**
F	0.971	8.1E-01	1.098	5.2E-01	1.002	9.8E-01
G	0.865	3.9E-01	1.132	5.5E-01	0.928	6.7E-01
H	6.647	**2.4E-02**	6.303	**3.2E-02**	4.534	**2.1E-02**
I	1.097	3.6E-01	1.151	2.2E-01	0.965	7.2E-01
K	0.858	3.4E-01	1.345	8.2E-02	0.923	5.9E-01
L	1.114	3.4E-01	1.353	5.9E-02	0.977	8.2E-01
M	0.971	8.4E-01	1.100	5.5E-01	0.861	3.4E-01
N	0.882	3.8E-01	1.112	5.9E-01	1.038	8.2E-01
P	1.141	2.1E-01	1.931	**4.9E-04**	1.689	**9.6E-05**
Q	0.968	8.6E-01	1.220	3.2E-01	1.366	1.3E-01
R	0.967	6.3E-01	1.288	**1.1E-02**	0.937	4.5E-01
S	1.116	2.9E-01	1.217	**4.0E-02**	0.943	3.6E-01
T	0.935	5.7E-01	1.028	8.5E-01	0.886	3.4E-01
V	1.204	5.5E-01	1.541	1.2E-01	1.188	5.1E-01
W	1.080	5.5E-01	1.432	5.5E-02	1.129	4.8E-01
Y	1.090	4.4E-01	1.202	1.1E-01	1.075	5.2E-01
Orn	0.897	7.0E-01	1.347	2.1E-01	1.081	7.3E-01
Citru	1.018	9.3E-01	1.148	5.8E-01	1.062	7.9E-01
fum	1.098	5.5E-01	1.083	5.0E-01	1.098	5.4E-01
aco	0.842	2.2E-01	0.811	1.5E-01	0.932	6.9E-01
akg	1.015	9.2E-01	1.255	**3.6E-02**	1.112	4.8E-01
suc	0.921	3.9E-01	1.136	8.3E-02	0.900	2.7E-01

Supplementary table 7-3: Comparison of metabolite levels in shoots of *35S::PPCK1* lines to the levels detected in WT
Metabolite levels in shoots of K-lines were compared to WT grown under (A) Pi-sufficient and (B) Pi-deficient conditions. Data are normalized to the levels detected in WT+Pi. Shown are the cumulative data of 3 independent germination experiments. For each experiment, four biological replicates (two pooled seedlings per replicate) were analyzed (n=12). Significance analyses were performed by Student's *t*-test (two tailed, two sample equal variance). Number in bold indicates significant difference between the transgenic lines and WT with p<0.05. Light grey and dark grey cell highlight the metabolites which were significantly increased and decreased, respectively in the lines compared to WT.

(A) +Pi-Shoots								
Metabolites	# K6.10		# K10.7		# K19.3		# K23.4	
	fold Vs WT+Pi	*t*-test Vs WT+Pi	fold Vs WT+Pi	*t*-test Vs WT+Pi	fold Vs WT+Pi	*t*-test Vs WT+Pi	fold Vs WT+Pi	*t*-test Vs WT+Pi
A	0.891	1.7E-01	0.856	6.6E-02	0.863	8.0E-02	0.836	**2.9E-02**
C	0.952	5.7E-01	0.996	9.5E-01	0.994	9.3E-01	1.006	9.0E-01
D	1.179	8.7E-02	1.248	**2.7E-02**	1.225	**1.3E-02**	1.197	**4.7E-02**
E	1.025	8.1E-01	1.025	7.7E-01	1.069	3.4E-01	0.951	4.3E-01
F	0.849	9.9E-02	0.803	**2.0E-02**	0.700	**2.9E-04**	0.863	2.4E-01
G	1.065	8.0E-01	0.618	**3.2E-02**	0.613	**6.5E-03**	0.597	**2.4E-03**
H	1.281	**3.4E-02**	1.112	4.6E-01	1.137	3.1E-01	1.146	3.2E-01
I	0.888	1.5E-01	0.842	**2.4E-02**	0.796	**4.7E-03**	0.992	9.2E-01
K	1.079	5.2E-01	1.070	5.1E-01	1.119	3.1E-01	1.146	7.9E-02
L	0.967	6.9E-01	0.864	5.7E-02	0.889	9.4E-02	1.017	8.2E-01
M	1.068	3.1E-01	1.028	7.6E-01	0.989	8.4E-01	0.953	6.0E-01
N	0.947	5.2E-01	1.129	7.0E-02	1.029	6.9E-01	1.121	8.4E-02
P	1.060	5.1E-01	1.103	2.7E-01	1.014	8.0E-01	1.027	6.5E-01
Q	1.040	6.1E-01	1.202	**1.7E-02**	1.133	7.4E-02	1.149	1.1E-01
R	0.922	4.4E-01	1.089	3.6E-01	0.935	5.7E-01	1.192	6.7E-02
S	0.858	1.1E-01	0.772	**1.5E-02**	0.823	5.5E-02	0.766	**7.9E-03**
T	0.986	8.6E-01	0.994	9.4E-01	0.998	9.8E-01	1.015	7.8E-01
V	0.888	1.3E-01	0.872	5.6E-02	0.893	9.6E-02	1.004	9.5E-01
W	1.099	3.6E-01	0.904	2.8E-01	0.766	**4.3E-03**	0.962	7.1E-01
Y	1.243	5.6E-02	1.134	4.1E-01	1.114	5.2E-01	1.065	6.3E-01
Orn	1.219	3.4E-01	1.078	7.5E-01	0.696	1.9E-01	0.655	**3.4E-02**
Citru	0.832	5.2E-02	1.042	6.0E-01	0.908	3.3E-01	1.254	9.0E-02
fum	1.186	1.8E-01	1.414	**9.3E-07**	1.386	**2.4E-02**	1.255	**4.4E-02**
aco	0.978	8.6E-01	1.048	6.6E-01	1.084	4.6E-01	1.094	2.9E-01
akg	0.827	**1.1E-02**	0.763	**4.8E-06**	0.969	5.9E-01	0.763	**2.2E-04**
suc	1.044	4.2E-01	0.997	9.5E-01	1.136	8.2E-02	0.971	6.6E-01
(B)-Pi-Shoots								
A	1.246	1.0E-01	1.436	**1.1E-02**	1.231	1.3E-01	1.417	**2.2E-02**
C	1.128	1.8E-01	1.210	8.0E-02	1.106	3.4E-01	1.277	**1.4E-02**
D	0.905	1.1E-01	0.878	5.5E-02	0.876	**3.7E-02**	0.863	**3.3E-02**
E	0.954	6.2E-01	1.013	8.9E-01	1.005	9.6E-01	0.946	5.8E-01
F	1.098	7.1E-01	1.123	6.5E-01	1.041	8.9E-01	1.257	3.5E-01
G	1.518	1.9E-01	1.447	2.5E-01	1.696	1.5E-01	2.030	1.3E-01
H	1.245	2.1E-01	1.397	9.6E-02	1.355	**3.2E-02**	1.426	**4.8E-02**
I	1.266	6.6E-02	1.240	1.7E-01	1.078	4.8E-01	1.334	**7.8E-03**
K	1.572	8.1E-02	1.378	2.3E-01	1.137	3.8E-01	1.373	2.3E-01
L	1.660	**1.9E-02**	1.480	7.8E-02	1.145	2.8E-01	1.731	**6.4E-03**
M	0.894	7.4E-01	0.907	7.6E-01	0.808	5.2E-01	0.822	5.7E-01
N	1.282	1.0E-01	1.438	7.0E-02	1.295	8.1E-02	1.430	**4.7E-02**
P	1.485	1.0E-01	2.228	**1.5E-02**	1.342	2.7E-01	1.673	1.2E-01
Q	1.211	4.3E-01	1.130	6.0E-01	1.240	4.0E-01	1.289	2.8E-01
R	1.664	9.2E-02	1.702	5.6E-02	1.310	3.0E-01	1.690	8.1E-02
S	0.966	8.7E-01	1.168	4.3E-01	0.992	9.7E-01	1.092	6.7E-01
T	1.138	1.3E-01	1.167	1.1E-01	1.103	3.1E-01	1.216	**4.0E-02**
V	1.241	**4.9E-02**	1.203	1.6E-01	1.117	2.3E-01	1.331	**9.3E-03**
W	2.097	**5.2E-04**	1.870	**1.5E-03**	1.582	**1.9E-02**	2.161	**6.0E-04**
Y	1.945	**3.4E-02**	1.706	9.7E-02	1.471	7.5E-02	1.904	**1.7E-02**
Orn	1.139	6.6E-01	1.134	7.3E-01	0.824	5.7E-01	1.042	9.0E-01
Citru	1.286	**2.1E-02**	1.371	**3.8E-02**	0.709	**2.9E-02**	1.310	5.1E-02
fum	0.851	6.4E-02	0.831	**4.5E-02**	0.869	2.7E-01	0.921	3.2E-01
aco	1.096	3.9E-01	1.280	**1.8E-02**	1.754	5.3E-02	1.437	**6.1E-03**
akg	0.770	1.5E-01	0.873	5.1E-01	1.112	5.7E-01	0.773	1.8E-01
suc	1.179	1.4E-01	1.231	**5.0E-02**	1.145	1.4E-01	1.191	1.1E-01

Supplementary table 7-4: Comparison of metabolite levels in shoots of *35S*::*PPCK2* lines to the levels detected in WT

Metabolite levels in shoots of O-lines were compared to WT grown under (A) Pi-sufficient and (B) Pi-deficient conditions. Data are normalized to the levels detected in WT+Pi. Shown are the cumulative data of 2 independent germination experiments. For each experiment, four biological replicates (two pooled seedlings per replicate) were analyzed (n=08). Significance analyses were performed by Student's *t*-test (two tailed, two sample equal variance). Number in bold indicates significant difference between the transgenic lines and WT with p<0.05. Light and dark grey cell highlight the metabolites which were significantly increased and decreased, respectively in the lines compared to WT.

(A) +Pi-Shoots						
Metabolites	**# O2.1**		**# O4.1**		**# O5.2**	
	fold Vs WT+Pi	***t*-test Vs WT+Pi**	**fold Vs WT+Pi**	***t*-test Vs WT+Pi**	**fold Vs WT+Pi**	***t*-test Vs WT+Pi**
A	1.009	9.4E-01	0.831	**3.0E-02**	0.809	**2.5E-02**
C	1.026	6.8E-01	0.887	5.9E-02	1.068	3.2E-01
D	1.210	**2.5E-02**	1.095	3.2E-01	1.316	**2.1E-02**
E	0.992	9.3E-01	0.849	**3.9E-02**	1.014	8.3E-01
F	0.974	8.5E-01	0.715	**2.7E-03**	0.898	5.0E-01
G	0.727	1.2E-01	0.709	**4.3E-02**	0.537	**3.3E-03**
H	0.965	6.2E-01	0.835	1.6E-01	0.995	9.7E-01
I	1.097	2.4E-01	0.930	3.6E-01	1.214	**1.6E-02**
K	1.237	7.9E-02	0.914	4.8E-01	1.122	3.1E-01
L	1.080	3.4E-01	0.802	**6.8E-03**	1.062	6.1E-01
M	0.931	5.3E-01	0.791	**1.8E-02**	0.886	1.3E-01
N	1.277	**3.3E-03**	1.014	8.5E-01	1.171	**3.4E-02**
P	1.037	5.6E-01	0.912	1.2E-01	1.058	3.6E-01
Q	0.938	4.7E-01	1.052	5.7E-01	1.120	1.4E-01
R	2.147	**1.3E-02**	1.108	5.3E-01	1.447	**1.3E-02**
S	0.846	1.4E-01	0.844	1.2E-01	0.664	**1.7E-03**
T	1.016	8.2E-01	0.866	**3.9E-02**	1.076	2.9E-01
V	1.048	4.3E-01	0.956	6.3E-01	1.144	**3.0E-02**
W	0.892	3.8E-01	0.833	8.5E-02	1.182	3.8E-01
Y	0.933	4.4E-01	0.734	**2.5E-02**	0.914	3.2E-01
Orn	0.908	6.8E-01	0.500	**1.7E-02**	0.658	9.2E-02
Citru	1.077	5.3E-01	0.948	4.4E-01	1.051	5.5E-01
fum	1.022	7.9E-01	1.606	**1.8E-05**	1.600	**9.3E-04**
aco	0.942	4.1E-01	1.033	6.2E-01	1.039	6.0E-01
akg	0.589	**9.9E-06**	0.739	**3.7E-03**	0.796	**2.6E-02**
suc	0.797	**6.6E-04**	1.036	5.3E-01	0.984	8.2E-01
(B) -Pi-Shoots						
A	0.848	**3.8E-02**	1.130	1.4E-01	0.822	**1.7E-02**
C	0.915	3.4E-01	1.061	5.5E-01	0.828	**3.6E-02**
D	0.916	5.1E-02	0.913	7.8E-02	0.982	7.7E-01
E	0.856	2.6E-01	1.026	8.6E-01	0.971	8.1E-01
F	1.114	4.9E-01	1.085	6.0E-01	0.601	**1.3E-02**
G	0.740	2.9E-01	1.957	1.1E-01	0.591	1.4E-01
H	0.844	2.0E-01	1.244	**4.0E-02**	0.823	8.5E-02
I	1.319	1.7E-01	1.636	**2.2E-02**	0.950	7.7E-01
K	1.361	3.0E-01	1.244	3.6E-01	0.983	9.4E-01
L	1.532	2.0E-01	1.771	1.0E-01	0.716	1.9E-01
M	0.844	6.1E-01	0.910	7.8E-01	0.744	3.8E-01
N	0.962	7.5E-01	1.283	5.7E-02	0.925	4.0E-01
P	1.404	**1.6E-02**	2.398	**4.1E-03**	1.707	**8.6E-04**
Q	1.052	7.3E-01	1.399	6.1E-02	1.144	4.5E-01
R	1.253	6.0E-01	1.160	7.2E-01	0.959	9.2E-01
S	0.669	5.0E-02	0.829	3.4E-01	0.554	**1.7E-02**
T	0.920	3.8E-01	1.070	5.4E-01	0.838	8.1E-02
V	1.163	3.1E-01	1.533	**1.8E-02**	0.951	7.4E-01
W	1.819	**5.1E-03**	1.464	**4.1E-02**	0.726	**4.4E-02**
Y	1.773	1.2E-01	1.477	1.8E-01	0.819	4.0E-01
Orn	0.805	5.4E-01	0.612	1.5E-01	0.861	6.7E-01
Citru	1.059	6.0E-01	0.882	1.5E-01	0.785	**1.2E-02**
fum	1.289	**6.0E-03**	1.484	**3.5E-04**	1.527	**1.6E-04**
aco	1.093	4.5E-01	1.179	1.4E-01	1.100	4.3E-01
akg	0.700	**6.0E-03**	1.346	1.0E-01	1.035	8.6E-01
suc	1.109	3.5E-01	1.412	**2.4E-03**	1.065	5.3E-01

Supplementary table 7-5: Comparison of metabolite levels in *ppck1-1* seedlings to the levels detected in WT
Metabolite levels in (A) roots and (B) shoots of *ppck1-1* seedlings grown under Pi-sufficient and deficient conditions. Data are normalized to the levels in WT+Pi. Shown are the cumulative data of 8 independent germination experiments. For each experiment, four biological replicates (two pooled seedlings per replicate) were analyzed (n=32). Significance analyses were performed by Student's *t*-test (two-tailed, equal variances). Number in bold indicates significant difference between *ppck1-1* and WT with p<0.05. Light and dark grey cell highlight the metabolites which were significantly increased and reduced, respectively in *ppck1-1* compared to WT.

(A) Roots				
Metabolites	+Pi		-Pi	
	fold Vs WT+Pi	*t*-test Vs WT+Pi	fold Vs WT-Pi	*t*-test vs WT-Pi
A	1.366	**1.7E-05**	1.990	**4.5E-10**
C	1.084	5.8E-02	1.924	**2.1E-09**
D	1.018	6.6E-01	1.203	**7.6E-03**
E	1.076	**4.0E-02**	1.139	**1.2E-02**
F	1.127	**3.3E-02**	2.725	**2.5E-13**
G	1.168	**4.8E-02**	1.533	**3.9E-06**
H	1.203	**9.6E-03**	1.965	**2.0E-05**
I	1.302	**2.7E-03**	2.270	**5.0E-08**
K	1.304	**3.9E-04**	2.517	**7.6E-12**
L	1.122	6.6E-02	2.121	**4.3E-10**
M	1.197	**1.3E-04**	1.706	**2.1E-11**
N	1.158	**3.8E-02**	1.615	**6.3E-06**
P	1.017	7.6E-01	1.584	**1.5E-03**
Q	1.201	**4.4E-05**	1.591	**7.4E-07**
R	1.268	**3.5E-03**	1.363	**4.0E-03**
S	1.364	**1.1E-10**	1.737	**1.5E-09**
T	1.137	**6.2E-03**	1.876	**2.5E-09**
V	1.104	1.2E-01	1.796	**6.5E-08**
W	1.201	6.6E-02	2.764	**2.7E-07**
Y	1.379	**2.8E-06**	2.533	**5.0E-14**
Orn	1.723	**2.1E-04**	1.783	**3.4E-04**
Citru	1.223	**5.8E-04**	1.587	**8.6E-05**
fum	0.709	**6.6E-13**	0.992	9.0E-01
aco	1.078	5.4E-01	1.336	1.3E-01
akg	0.649	**1.2E-12**	0.420	**2.9E-15**
suc	0.749	**7.1E-10**	1.368	**6.0E-05**
(B) Shoots				
A	1.042	2.5E-01	1.462	**1.3E-05**
C	1.047	1.6E-01	1.256	**7.0E-04**
D	1.226	**8.4E-04**	1.000	9.9E-01
E	1.086	**3.6E-02**	1.139	**9.7E-03**
F	0.874	**3.8E-03**	1.147	2.8E-01
G	1.023	7.3E-01	2.329	**6.1E-05**
H	1.052	5.2E-01	1.301	**6.6E-03**
I	1.050	1.8E-01	1.129	2.6E-01
K	1.087	1.5E-01	1.404	**6.8E-03**
L	1.065	2.2E-01	1.127	4.6E-01
M	1.054	2.4E-01	1.157	**4.0E-02**
N	1.191	**4.1E-05**	1.524	**1.7E-09**
P	1.051	1.7E-01	1.222	4.3E-01
Q	1.044	3.1E-01	1.310	**1.6E-04**
R	1.113	3.8E-01	1.263	2.2E-01
S	1.183	**1.3E-03**	1.295	**1.2E-04**
T	1.062	8.3E-02	1.279	**4.6E-05**
V	1.042	2.1E-01	1.104	2.1E-01
W	0.894	**1.7E-02**	1.368	5.5E-02
Y	1.104	9.5E-02	1.380	**4.2E-02**
Orn	0.983	9.0E-01	1.763	1.2E-01
Citru	1.230	**1.9E-04**	1.327	6.0E-02
fum	0.902	**1.3E-02**	0.865	**2.6E-02**
aco	0.812	**5.2E-03**	1.201	6.3E-02
akg	0.777	**1.4E-05**	0.871	4.7E-01
suc	0.801	**2.1E-08**	1.170	**2.6E-02**

Supplementary table 7-6: Comparison of metabolite levels in roots of *pPPCK1$_{long}$::gDNA/ppck1-1* grown under Pi-sufficient condition to the levels detected in WT and *ppck1-1* roots

Metabolite levels in roots of C-lines grown under Pi-sufficient condition were compared to (A) WT and (B) *ppck1-1* roots. Seedlings were germinated for 6 days on +Pi agar plates, transferred to +Pi (500 µM) or –Pi (5 µM) conditions, and allowed to grow for additional 5 days before harvest. Data are normalized to the levels detected in WT+Pi. Shown are the cumulative data of 2 independent germination experiments. For each experiment, four biological replicates (two pooled seedlings per replicate) were analyzed (n=08). Significance analyses were performed by Student's *t*-test (two-tailed, equal variances). Number in bold indicates significant difference between the transgenic lines and WT with p<0.05. Light and dark grey cell highlight the metabolites which were significantly increased and decreased, respectively in the lines compared to WT.

(A) +Pi-Roots (Compared to WT)								
Metabolites	# C1.1		# C2.2		# C4.6		# C6.8	
	fold Vs WT+Pi	*t*-test Vs WT+Pi	fold Vs WT+Pi	*t*-test Vs WT+Pi	fold Vs WT+Pi	*t*-test Vs WT+Pi	fold Vs WT+Pi	*t*-test Vs WT+Pi
A	1.251	1.8E-01	1.206	2.6E-01	1.245	**2.9E-02**	1.166	8.7E-02
C	1.105	2.2E-01	1.116	1.9E-01	1.220	**1.7E-02**	1.045	6.5E-01
D	1.262	**1.0E-02**	1.334	**7.2E-03**	1.422	**1.0E-04**	1.335	**1.5E-03**
E	1.113	1.3E-01	1.050	4.4E-01	1.202	**4.8E-02**	1.149	9.8E-02
F	1.366	1.5E-01	2.360	5.3E-02	1.885	**3.9E-02**	1.269	**1.5E-02**
G	1.951	1.0E-01	1.929	7.8E-02	1.909	5.5E-02	1.261	5.4E-02
H	1.153	3.3E-01	1.597	**1.5E-02**	0.960	7.0E-01	1.678	1.7E-01
I	1.241	1.0E-01	1.726	**8.8E-03**	1.409	**3.8E-02**	1.506	**4.4E-02**
K	2.598	**3.3E-02**	2.193	7.2E-02	2.741	**3.3E-02**	2.240	**7.2E-04**
L	1.182	2.4E-01	1.587	8.1E-02	1.424	7.2E-02	1.442	**1.5E-02**
M	1.515	8.3E-02	1.779	6.0E-02	1.352	**1.3E-02**	1.185	6.2E-02
N	1.166	1.2E-01	1.241	1.4E-01	1.365	**4.8E-02**	1.094	5.2E-01
P	1.388	**3.5E-02**	1.313	5.2E-02	1.674	**9.2E-05**	1.311	**4.1E-03**
Q	1.298	**9.6E-04**	1.279	**1.2E-03**	1.540	**2.8E-04**	1.256	**1.5E-02**
R	1.049	6.7E-01	1.147	2.3E-01	1.115	3.1E-01	1.240	1.8E-01
S	1.355	**1.9E-02**	1.276	1.1E-01	1.213	**2.7E-02**	1.314	**1.7E-02**
T	1.167	**4.6E-02**	1.121	1.7E-01	1.327	**3.3E-03**	1.072	4.5E-01
V	1.035	8.0E-01	1.320	2.1E-01	1.228	2.5E-01	1.204	1.7E-01
W	1.516	**1.5E-02**	2.262	**3.6E-02**	1.442	7.2E-02	1.656	**3.2E-02**
Y	1.765	6.6E-02	2.589	7.1E-02	2.065	**2.7E-02**	1.846	**1.7E-02**
Orn	1.278	3.4E-01	1.058	7.9E-01	1.729	1.8E-01	1.654	2.0E-01
Citru	1.049	7.5E-01	0.942	2.8E-01	1.365	8.0E-02	1.341	1.7E-01
fum	0.739	**1.9E-03**	0.704	**1.3E-03**	0.716	**1.4E-03**	0.652	**3.1E-05**
aco	0.600	**5.2E-03**	0.612	**4.3E-03**	0.553	**3.6E-03**	0.644	**1.9E-03**
akg	0.680	**5.1E-04**	0.901	1.3E-01	0.790	5.4E-02	0.704	**1.5E-02**
suc	0.915	2.5E-01	0.976	7.9E-01	0.958	6.1E-01	0.866	8.5E-02
(B) +Pi-Roots (Compared to *ppck1-1*)								
Metabolites	fold Vs *ppck1-1*+Pi	*t*-test Vs *ppck1-1*+Pi	fold Vs *ppck1-1*+Pi	*t*-test Vs *ppck1-1*+Pi	fold Vs *ppck1-1*+Pi	*t*-test Vs *ppck1-1*+Pi	fold Vs *ppck1-1*+Pi	*t*-test Vs *ppck1-1*+Pi
A	1.047	8.3E-01	1.010	9.6E-01	1.042	7.3E-01	0.976	8.2E-01
C	1.164	1.2E-01	1.176	1.1E-01	1.285	**8.9E-03**	1.101	4.4E-01
D	1.341	**2.0E-02**	1.418	**2.2E-02**	1.512	**7.3E-04**	1.419	**5.5E-03**
E	1.028	7.0E-01	0.970	6.1E-01	1.111	3.3E-01	1.061	5.2E-01
F	1.001	1.0E+00	1.730	3.1E-01	1.382	3.8E-01	0.930	4.9E-01
G	1.254	6.3E-01	1.240	6.1E-01	1.227	5.9E-01	0.811	1.8E-01
H	0.900	6.0E-01	1.247	3.5E-01	0.750	1.0E-01	1.310	5.7E-01
I	0.895	3.7E-01	1.246	2.9E-01	1.017	9.2E-01	1.087	6.9E-01
K	2.006	1.4E-01	1.694	2.6E-01	2.117	1.4E-01	1.730	**1.8E-02**
L	1.038	7.8E-01	1.393	3.2E-01	1.251	3.3E-01	1.267	1.3E-01
M	1.230	5.1E-01	1.445	3.5E-01	1.098	5.7E-01	0.962	7.8E-01
N	1.062	6.5E-01	1.131	5.2E-01	1.244	2.8E-01	0.997	9.9E-01
P	1.576	5.9E-02	1.492	6.5E-02	1.901	**1.1E-03**	1.489	**5.8E-03**
Q	1.186	6.0E-02	1.169	7.1E-02	1.408	**1.8E-02**	1.148	2.3E-01
R	0.888	2.8E-01	0.971	7.9E-01	0.945	5.7E-01	1.050	7.7E-01
S	0.951	7.4E-01	0.895	5.5E-01	0.852	1.6E-01	0.923	5.5E-01
T	1.264	**3.6E-02**	1.213	1.0E-01	1.436	**9.3E-03**	1.161	2.6E-01
V	1.037	7.8E-01	1.324	3.5E-01	1.231	3.6E-01	1.207	2.0E-01
W	1.066	7.2E-01	1.590	2.8E-01	1.014	9.5E-01	1.164	5.5E-01
Y	1.115	7.3E-01	1.636	3.8E-01	1.306	4.2E-01	1.167	5.4E-01
Orn	0.519	8.4E-02	0.430	**4.4E-02**	0.702	3.2E-01	0.672	2.7E-01
Citru	0.719	1.0E-01	0.645	**7.2E-03**	0.936	6.9E-01	0.919	6.6E-01
fum	1.102	3.6E-01	1.049	6.9E-01	1.067	5.8E-01	0.971	7.8E-01
aco	0.694	1.3E-01	0.709	1.2E-01	0.640	8.2E-02	0.745	1.3E-01
akg	1.026	8.7E-01	1.361	**1.6E-02**	1.193	3.0E-01	1.063	7.5E-01
suc	1.161	1.6E-01	1.240	7.1E-02	1.216	8.5E-02	1.100	3.8E-01

Supplementary table 7-7: Comparison of metabolite levels in roots of *pPPCK1$_{long}$::gDNA/ppck1-1* grown under Pi-deficient condition to the levels detected in WT and *ppck1-1* roots

Metabolite levels in roots of C-lines grown under Pi-deficient condition were compared to (A) WT and (B) *ppck1-1* roots. Seedlings were germinated for 6 days on +Pi agar plates, transferred to +Pi (500 µM) or –Pi (5 µM) conditions, and allowed to grow for additional 5 days before harvest. Data are normalized to the levels detected in WT+Pi. Shown are the cumulative data of 2 independent germination experiments. For each experiment, four biological replicates (two pooled seedlings per replicate) were analyzed (n=08). Significance analyses were performed by Student's *t*-test (two-tailed, equal variances). Number in bold indicates significant difference between the transgenic lines and WT with p<0.05. Light and dark grey cell highlight the metabolites which were significantly increased and decreased, respectively in the lines compared to WT.

(A) -Pi-Roots (Compared to Col-0)								
Metabolites	# C1.1		# C2.2		# C4.6		# C6.8	
	fold Vs WT-Pi	*t*-test Vs WT-Pi	fold Vs WT-Pi	*t*-test Vs WT-Pi	fold Vs WT-Pi	*t*-test Vs WT-Pi	fold Vs WT-Pi	*t*-test Vs WT-Pi
A	1.328	**2.6E-02**	1.121	3.9E-01	1.450	**3.4E-02**	1.437	**1.6E-02**
C	1.452	**3.8E-03**	1.482	**1.6E-02**	1.604	**7.4E-04**	1.747	**2.0E-03**
D	1.199	2.6E-01	1.174	2.8E-01	1.317	2.0E-01	1.307	1.4E-01
E	1.122	4.2E-01	1.035	7.0E-01	1.003	9.7E-01	1.194	5.5E-02
F	1.952	**1.5E-04**	1.824	**4.2E-03**	2.894	**1.1E-02**	1.940	**1.4E-03**
G	1.200	1.8E-01	1.296	1.1E-01	1.897	5.1E-02	1.330	**3.9E-02**
H	1.531	1.6E-01	1.561	1.8E-01	1.362	2.1E-01	1.567	8.6E-02
I	1.565	**1.9E-02**	1.659	**1.3E-02**	1.771	**4.8E-04**	2.065	**1.6E-02**
K	1.608	**1.1E-02**	1.627	**2.8E-02**	2.076	**1.3E-02**	1.959	**5.6E-03**
L	1.472	**7.7E-03**	1.447	**2.8E-02**	1.535	**2.2E-03**	1.630	**2.7E-02**
M	1.355	**2.3E-02**	1.490	**1.7E-02**	1.554	**4.3E-02**	1.302	**3.0E-02**
N	1.398	**3.4E-02**	1.237	1.3E-01	1.292	1.1E-01	1.614	**1.9E-03**
P	1.642	**1.3E-03**	1.488	**2.3E-02**	1.943	**4.6E-03**	1.489	**7.8E-03**
Q	1.536	**2.7E-03**	1.511	**1.8E-02**	1.454	**1.7E-02**	1.832	**2.8E-05**
R	1.318	**3.5E-03**	1.583	**6.1E-04**	1.186	1.2E-01	1.317	**4.0E-02**
S	1.163	1.7E-01	1.204	9.5E-02	1.412	6.9E-02	1.265	**1.8E-02**
T	1.515	**3.0E-03**	1.565	**1.0E-02**	1.424	**3.6E-03**	1.796	**8.9E-04**
V	1.324	**4.7E-02**	1.297	7.2E-02	1.449	**1.3E-02**	1.726	**6.7E-03**
W	1.951	**1.9E-03**	1.981	**2.0E-02**	1.978	**7.4E-05**	2.220	**1.3E-02**
Y	1.991	**4.5E-05**	2.051	**2.1E-03**	2.521	**4.3E-03**	2.181	**3.1E-04**
Orn	1.923	**7.1E-03**	3.249	**5.7E-03**	1.162	4.5E-01	1.724	**1.4E-03**
Citru	1.872	**1.3E-03**	2.192	**2.2E-02**	1.589	**4.8E-02**	2.805	**1.0E-02**
fum	1.400	**4.1E-03**	1.288	**1.5E-02**	1.245	**1.9E-02**	1.320	**1.7E-03**
aco	1.223	2.3E-01	0.997	9.9E-01	1.749	1.4E-01	0.864	5.9E-01
akg	0.717	**3.3E-03**	0.786	**5.3E-03**	0.719	**3.5E-03**	0.587	**9.9E-07**
suc	1.304	**3.3E-02**	1.248	7.4E-02	1.290	9.4E-02	1.285	9.4E-02
(B) -Pi-roots (Compared to *ppck1-1*)								
Metabolites	fold Vs *ppck1-1*-Pi	*t*-test Vs *ppck1-1*-Pi	fold Vs *ppck1-1*-Pi	*t*-test Vs *ppck1-1*-Pi	fold Vs *ppck1-1*-Pi	*t*-test Vs *ppck1-1*-Pi	fold Vs *ppck1-1*-Pi	*t*-test Vs *ppck1-1*-Pi
A	0.535	**1.3E-03**	0.452	**8.2E-04**	0.584	**1.1E-02**	0.579	**7.0E-03**
C	0.708	**5.0E-03**	0.722	**3.3E-02**	0.782	**3.1E-02**	0.851	2.7E-01
D	1.108	5.4E-01	1.085	5.5E-01	1.218	4.4E-01	1.209	3.4E-01
E	0.913	6.4E-01	0.843	2.1E-01	0.817	1.4E-01	0.972	8.2E-01
F	0.806	1.4E-01	0.754	1.5E-01	1.196	6.5E-01	0.802	2.2E-01
G	0.742	6.3E-02	0.801	2.1E-01	1.173	6.5E-01	0.822	1.8E-01
H	0.437	**1.9E-03**	0.446	**4.4E-03**	0.389	**1.0E-04**	0.447	**6.0E-04**
I	0.689	**4.6E-02**	0.731	9.9E-02	0.780	6.8E-02	0.910	7.2E-01
K	0.943	6.6E-01	0.955	7.8E-01	1.218	4.5E-01	1.149	4.9E-01
L	0.818	1.4E-01	0.805	1.9E-01	0.853	1.9E-01	0.906	6.4E-01
M	0.776	8.7E-02	0.853	3.6E-01	0.890	6.1E-01	0.746	**4.3E-02**
N	0.703	**4.3E-02**	0.622	**8.4E-03**	0.650	**2.2E-02**	0.812	1.5E-01
P	1.691	**4.1E-04**	1.532	**2.2E-02**	2.000	**1.7E-02**	1.533	**4.1E-03**
Q	0.723	**2.8E-02**	0.711	6.0E-02	0.685	**2.5E-02**	0.863	2.0E-01
R	1.008	9.0E-01	1.211	7.9E-02	0.907	3.2E-01	1.007	9.6E-01
S	0.723	**1.1E-02**	0.748	**1.9E-02**	0.877	5.2E-01	0.786	**1.8E-02**
T	0.729	**2.5E-02**	0.753	1.0E-01	0.685	**5.1E-03**	0.864	3.3E-01
V	0.859	2.3E-01	0.842	2.0E-01	0.940	6.2E-01	1.120	5.1E-01
W	0.645	**1.2E-02**	0.655	7.0E-02	0.654	**2.2E-03**	0.734	2.0E-01
Y	0.793	**4.8E-02**	0.817	2.5E-01	1.005	9.9E-01	0.869	3.4E-01
Orn	0.814	1.2E-01	1.376	1.3E-01	0.492	**1.5E-03**	0.730	**5.7E-03**
Citru	0.883	2.6E-01	1.033	8.8E-01	0.749	1.3E-01	1.323	2.8E-01
fum	1.257	5.5E-02	1.157	1.8E-01	1.118	2.7E-01	1.185	7.1E-02
aco	0.974	9.1E-01	0.794	4.3E-01	1.394	3.7E-01	0.688	2.6E-01
akg	1.452	6.6E-02	1.590	**1.0E-02**	1.454	7.0E-02	1.189	3.6E-01
suc	0.859	3.0E-01	0.822	1.9E-01	0.850	3.3E-01	0.847	3.2E-01

Supplementary table 7-8: Comparison of metabolite levels in shoots of *pPPCK1$_{long}$::gDNA/ppck1-1* grown under Pi-sufficient condition to the levels detected in WT and *ppck1-1* shoots

Metabolite levels in shoots of C-lines grown under Pi-sufficient condition were compared to (A) WT and (B) *ppck1-1* shoots. Seedlings were germinated for 6 days on +Pi agar plates, transferred to +Pi (500 µM) or –Pi (5 µM) conditions, and allowed to grow for additional 5 days before harvest. Data are normalized to the levels detected in WT+Pi. Shown are the cumulative data of 2 independent germination experiments. For each experiment, four biological replicates (two pooled seedlings per replicate) were analyzed (n=08). Significance analyses were performed by Student's *t*-test (two-tailed, equal variances). Number in bold indicates significant difference between the transgenic lines and WT with p<0.05. Light and dark grey cell highlight the metabolites which were significantly increased and decreased, respectively in the lines compared to WT.

(A) +Pi-Shoots (Compared to Col-0)								
	# C1.1		# C2.2		# C4.6		# C6.8	
Metabolites	fold Vs WT+Pi	*t*-test Vs WT+Pi	fold Vs WT+Pi	*t*-test Vs WT+Pi	fold Vs WT+Pi	*t*-test Vs WT+Pi	fold Vs WT+Pi	*t*-test Vs WT+Pi
A	0.949	4.2E-01	0.950	4.4E-01	1.055	6.3E-01	1.071	2.6E-01
C	1.174	6.7E-02	1.120	**3.6E-02**	1.219	**8.2E-03**	1.090	1.0E-01
D	1.298	**2.0E-03**	1.342	**9.6E-05**	1.488	**2.3E-06**	1.551	**4.6E-04**
E	1.178	**1.1E-02**	1.168	**6.9E-04**	1.240	**1.9E-03**	1.288	**2.3E-05**
F	1.020	8.7E-01	0.832	**2.9E-02**	0.949	4.1E-01	0.782	**3.5E-04**
G	0.718	**1.1E-03**	0.578	**4.1E-05**	0.709	**5.6E-03**	0.566	**1.3E-04**
H	1.176	8.6E-02	1.024	7.7E-01	1.080	4.5E-01	0.934	3.8E-01
I	1.186	1.7E-01	1.077	1.6E-01	1.238	**1.2E-03**	1.169	**5.6E-03**
K	1.287	6.4E-02	1.358	**1.7E-02**	1.741	**3.3E-04**	1.646	**2.8E-06**
L	1.222	2.8E-01	1.076	5.7E-01	1.355	**2.8E-02**	1.242	**2.3E-02**
M	1.110	4.0E-01	1.059	5.8E-01	1.193	6.6E-02	1.079	5.9E-01
N	1.245	**3.8E-02**	1.268	**8.5E-03**	1.421	**5.5E-03**	1.304	**2.0E-02**
P	1.176	**1.4E-02**	1.163	**8.1E-03**	1.292	**1.7E-04**	1.202	**4.9E-03**
Q	1.241	**1.1E-02**	1.235	**4.1E-04**	1.417	**8.2E-04**	1.168	**4.9E-02**
R	1.331	1.3E-01	1.231	5.2E-01	1.317	3.2E-01	1.152	5.9E-01
S	1.045	6.3E-01	0.964	5.7E-01	0.988	9.4E-01	0.939	3.5E-01
T	1.173	7.8E-02	1.159	**9.4E-03**	1.224	**1.4E-03**	1.091	1.1E-01
V	1.125	2.6E-01	1.148	1.0E-01	1.323	**3.2E-03**	1.287	**2.1E-02**
W	0.954	6.3E-01	0.860	9.3E-02	1.070	3.7E-01	0.942	4.5E-01
Y	1.075	6.2E-01	0.992	9.4E-01	1.342	6.5E-02	1.148	8.9E-02
Orn	0.296	8.9E-02	0.268	7.8E-02	0.720	4.4E-01	0.290	8.4E-02
Citru	1.055	6.0E-01	1.281	**9.0E-03**	1.204	9.4E-02	1.087	5.2E-01
fum	0.804	**2.2E-03**	1.014	9.0E-01	0.888	1.2E-01	0.869	4.3E-01
aco	0.720	**8.5E-03**	0.744	9.7E-02	0.946	5.2E-01	0.921	6.0E-01
akg	1.438	2.5E-01	1.845	9.4E-02	2.407	7.4E-02	1.904	9.7E-02
suc	0.838	**4.9E-02**	0.908	3.2E-01	0.981	8.1E-01	0.883	3.2E-01
(B) +Pi-Shoots (Compared to *ppck1-1*)								
Metabolites	fold Vs *ppck1-1*+Pi	*t*-test Vs *ppck1-1*+Pi	fold Vs *ppck1-1*+Pi	*t*-test Vs *ppck1-1*+Pi	fold Vs *ppck1-1*+Pi	*t*-test Vs *ppck1-1*+Pi	fold Vs *ppck1-1*+Pi	*t*-test Vs ppck1-1+Pi
A	0.848	**3.4E-02**	0.849	**4.4E-02**	0.943	6.9E-01	0.957	5.0E-01
C	1.094	4.3E-01	1.044	5.1E-01	1.136	1.7E-01	1.016	8.1E-01
D	1.248	**3.6E-02**	1.290	**4.2E-03**	1.430	**2.9E-04**	1.491	**1.3E-02**
E	0.992	9.0E-01	0.983	6.0E-01	1.044	5.3E-01	1.084	8.5E-02
F	1.018	9.2E-01	0.831	1.0E-01	0.947	5.3E-01	0.781	**4.0E-03**
G	0.592	**9.3E-04**	0.477	**1.2E-04**	0.585	**4.2E-03**	0.467	**5.2E-04**
H	1.323	7.3E-02	1.152	2.6E-01	1.215	2.6E-01	1.051	6.6E-01
I	0.998	9.9E-01	0.906	1.8E-01	1.041	5.9E-01	0.984	8.1E-01
K	1.202	3.0E-01	1.268	1.5E-01	1.626	**1.2E-02**	1.537	**4.0E-04**
L	1.273	3.8E-01	1.121	5.3E-01	1.412	8.1E-02	1.294	5.1E-02
M	1.058	7.3E-01	1.009	9.5E-01	1.137	2.8E-01	1.028	8.9E-01
N	1.047	7.1E-01	1.067	5.1E-01	1.195	2.3E-01	1.097	4.9E-01
P	1.069	3.5E-01	1.058	3.2E-01	1.174	**1.8E-02**	1.093	2.0E-01
Q	1.008	9.2E-01	1.004	9.4E-01	1.151	1.9E-01	0.949	5.5E-01
R	1.881	**4.9E-02**	1.741	3.5E-01	1.862	2.1E-01	1.628	2.9E-01
S	0.760	**2.2E-02**	0.701	**1.7E-04**	0.718	1.0E-01	0.682	**1.5E-04**
T	1.092	4.5E-01	1.078	2.3E-01	1.139	6.7E-02	1.016	8.0E-01
V	1.113	4.5E-01	1.136	2.5E-01	1.309	**2.9E-02**	1.274	1.0E-01
W	0.934	6.3E-01	0.842	1.9E-01	1.047	6.8E-01	0.922	4.8E-01
Y	0.947	7.6E-01	0.874	3.2E-01	1.183	3.7E-01	1.012	8.8E-01
Orn	0.629	5.4E-02	0.571	**6.4E-03**	1.532	6.9E-02	0.617	**8.0E-03**
Citru	0.669	**1.0E-03**	0.813	**2.6E-03**	0.763	**7.0E-03**	0.689	**6.8E-03**
fum	1.001	9.8E-01	1.263	7.2E-02	1.105	2.6E-01	1.082	6.8E-01
aco	0.844	2.2E-01	0.872	5.0E-01	1.107	3.4E-01	1.079	6.7E-01
akg	1.480	2.1E-01	1.900	6.7E-02	2.479	**4.9E-02**	1.960	6.9E-02
suc	1.085	3.7E-01	1.176	1.2E-01	1.270	**1.1E-02**	1.144	3.2E-01

Supplementary table 7-9: Comparison of metabolite levels in shoots of *pPPCK1$_{long}$::gDNA/ppck1-1* grown under Pi-deficient condition to the levels detected in WT and *ppck1-1* shoots

Metabolite levels in shoots of C-lines grown under Pi-deficient condition were compared to (A) WT and (B) *ppck1-1* shoots. Seedlings were germinated for 6 days on +Pi agar plates, transferred to +Pi (500 µM) or –Pi (5 µM) conditions, and allowed to grow for additional 5 days before harvest. Data are normalized to the levels detected in WT+Pi. Shown are the cumulative data of 2 independent germination experiments. For each experiment, four biological replicates (two pooled seedlings per replicate) were analyzed (n=08). Significance analyses were performed by Student's *t*-test (two-tailed, equal variances). Number in bold indicates significant difference between the transgenic lines and WT (Col-0) with p<0.05. Light and dark grey cell highlight the metabolites which were significantly increased and decreased, respectively in the lines compared to WT.

(A) -Pi-Shoots (Compared to Col-0)								
	# C1.1		# C2.2		# C4.6		# C6.8	
Metabolites	fold Vs WT-Pi	*t*-test Vs WT-Pi	fold Vs WT-Pi	*t*-test Vs WT-Pi	fold Vs WT-Pi	*t*-test Vs WT-Pi	fold Vs WT-Pi	*t*-test Vs WT-Pi
A	0.962	7.0E-01	0.975	7.5E-01	0.921	3.3E-01	1.049	5.9E-01
C	1.089	4.7E-01	1.085	2.5E-01	1.172	5.2E-02	1.048	5.1E-01
D	1.190	2.2E-01	1.103	4.3E-01	1.091	4.3E-01	1.014	9.1E-01
E	1.311	**5.0E-03**	1.195	**4.0E-02**	1.245	**1.6E-02**	1.158	1.7E-01
F	0.881	6.0E-01	0.793	3.8E-01	0.849	4.9E-01	0.954	8.6E-01
G	1.653	1.4E-01	0.981	8.8E-01	1.180	2.4E-01	1.749	**1.3E-03**
H	1.216	2.6E-01	0.947	7.7E-01	1.041	8.4E-01	1.217	1.8E-01
I	1.062	5.4E-01	0.929	4.4E-01	1.006	9.7E-01	1.165	2.1E-01
K	1.245	6.1E-02	1.107	3.3E-01	1.249	8.4E-02	1.454	**1.1E-02**
L	0.851	2.6E-01	0.718	**3.5E-02**	0.755	1.1E-01	0.817	2.1E-01
M	1.102	5.1E-01	1.063	7.1E-01	1.021	8.9E-01	0.984	9.3E-01
N	1.534	**1.1E-02**	1.279	6.8E-02	1.463	**1.5E-02**	1.260	7.8E-02
P	1.085	6.1E-01	0.710	9.7E-02	1.270	4.1E-01	0.552	**6.4E-03**
Q	1.700	**6.8E-03**	1.559	**5.5E-03**	1.716	**2.3E-03**	1.363	**2.6E-02**
R	1.754	8.3E-02	1.467	2.1E-01	1.578	1.3E-01	1.078	7.7E-01
S	0.896	1.9E-01	0.798	**1.5E-02**	0.877	1.7E-01	0.969	7.3E-01
T	1.262	**1.2E-02**	1.126	**4.9E-02**	1.185	**1.6E-02**	1.056	3.6E-01
V	0.999	9.9E-01	0.845	9.3E-02	0.987	9.0E-01	0.957	6.6E-01
W	1.166	4.4E-01	1.011	9.6E-01	1.086	6.7E-01	1.134	5.7E-01
Y	1.141	4.9E-01	0.936	7.1E-01	1.016	9.4E-01	1.326	1.8E-01
Orn	2.146	**4.4E-02**	1.829	**1.9E-02**	1.734	**1.3E-02**	1.664	**4.3E-02**
Citru	1.075	7.4E-01	1.130	5.0E-01	1.244	1.0E-01	0.950	7.8E-01
fum	1.095	5.5E-01	1.128	4.2E-01	1.214	2.2E-01	0.846	3.6E-01
aco	0.908	6.5E-01	1.258	1.2E-01	0.951	7.5E-01	1.043	7.7E-01
akg	1.515	2.1E-01	1.780	1.0E-01	1.512	1.4E-01	0.709	2.4E-01
suc	1.217	2.6E-01	1.126	4.7E-01	1.054	7.6E-01	1.180	3.6E-01
(B) -Pi-Shoots (Compared to *ppck1-1*)								
Metabolites	fold Vs *ppck1-1*-Pi	*t*-test Vs *ppck1-1*-Pi	fold Vs *ppck1-1*-Pi	*t*-test Vs *ppck1-1*-Pi	fold Vs *ppck1-1*-Pi	*t*-test Vs *ppck1-1*-Pi	fold Vs *ppck1-1*-Pi	*t*-test Vs *ppck1-1*-Pi
A	0.557	**4.5E-03**	0.565	**1.4E-03**	0.534	**8.3E-04**	0.608	**4.5E-03**
C	0.755	6.5E-02	0.752	**3.5E-03**	0.813	**3.6E-02**	0.727	**2.1E-03**
D	1.845	**2.1E-02**	1.711	**1.9E-02**	1.691	**9.3E-03**	1.573	**4.5E-02**
E	1.325	**3.4E-02**	1.207	1.2E-01	1.258	6.8E-02	1.170	3.1E-01
F	0.697	1.6E-01	0.627	9.2E-02	0.671	1.1E-01	0.755	3.0E-01
G	0.337	**9.8E-03**	0.200	**7.0E-04**	0.241	**1.0E-03**	0.357	**2.9E-03**
H	0.701	**4.0E-02**	0.546	**2.9E-03**	0.600	**2.0E-02**	0.701	**1.1E-02**
I	0.943	5.7E-01	0.825	6.4E-02	0.892	4.8E-01	1.034	8.0E-01
K	1.155	2.2E-01	1.027	7.8E-01	1.159	2.9E-01	1.349	7.1E-02
L	1.119	4.2E-01	0.945	6.3E-01	0.993	9.7E-01	1.074	5.2E-01
M	1.315	**4.8E-02**	1.269	1.7E-01	1.219	1.8E-01	1.175	3.7E-01
N	1.078	6.7E-01	0.899	4.7E-01	1.029	8.6E-01	0.885	3.9E-01
P	3.002	**9.2E-04**	1.966	**3.6E-02**	3.514	6.2E-02	1.528	**7.1E-03**
Q	1.144	5.3E-01	1.050	7.8E-01	1.155	4.5E-01	0.917	6.0E-01
R	2.218	8.9E-02	1.854	1.5E-01	1.995	1.1E-01	1.363	2.8E-01
S	0.705	**7.8E-03**	0.628	**1.6E-03**	0.690	**1.1E-02**	0.762	**4.6E-02**
T	0.888	2.2E-01	0.792	**1.1E-03**	0.834	**1.7E-02**	0.743	**2.8E-04**
V	1.041	5.9E-01	0.881	1.1E-01	1.029	8.0E-01	0.998	9.8E-01
W	1.008	9.8E-01	0.874	6.0E-01	0.938	8.0E-01	0.980	9.4E-01
Y	1.015	9.6E-01	0.833	4.7E-01	0.904	7.7E-01	1.179	5.9E-01
Orn	1.329	3.0E-01	1.132	5.0E-01	1.074	6.8E-01	1.031	8.8E-01
Citru	0.749	2.3E-01	0.786	2.2E-01	0.866	3.6E-01	0.661	9.9E-02
fum	1.333	8.4E-02	1.374	5.3E-02	1.478	**2.7E-02**	1.029	8.8E-01
aco	1.357	3.2E-01	1.882	**5.8E-03**	1.423	1.3E-01	1.559	**4.5E-02**
akg	1.449	3.9E-01	1.703	2.3E-01	1.447	3.4E-01	0.678	3.9E-01
suc	1.410	**2.6E-02**	1.304	5.5E-02	1.221	1.5E-01	1.367	**4.8E-02**

Supplementary table 7-10: Comparison of metabolite levels in *ppck1-4* seedlings to the levels detected in WT
Metabolite levels in (A) roots and (B) shoots of *ppck1-4* seedlings grown under Pi-sufficient and deficient conditions were compared to the levels detected in WT (Col-0). Seedlings were germinated for 6 days on +Pi agar plates, transferred to +Pi (500 µM) or –Pi (5 µM) conditions, and allowed to grow for additional 5 days before harvest. Data are normalized to the levels detected in WT+Pi. Shown are the preliminary data of one experiment. Four biological replicates (two pooled seedlings per replicate) were analyzed (n=04). Significance analyses were performed by Student's *t*-test (two-tailed, equal variances). Number in bold indicates significant difference between *ppck1-4* and WT with p<0.05. Light and dark grey cell highlight the metabolites which were significantly increased and reduced, respectively in the mutants compared to WT.

(A) Roots				
Metabolites	**+Pi**		**-Pi**	
	fold Vs WT+Pi	***t*-test Vs WT+Pi**	**fold Vs WT-Pi**	***t*-test vs WT-Pi**
A	1.379	1.2E-01	1.083	7.3E-01
C	0.848	5.1E-01	0.945	7.7E-01
D	0.995	9.4E-01	0.843	3.2E-01
E	1.079	2.4E-01	0.805	9.7E-02
F	1.013	9.5E-01	1.479	3.9E-01
G	1.327	2.6E-01	1.374	3.7E-01
H	1.615	3.2E-01	0.685	2.0E-01
I	1.497	3.4E-01	1.178	5.7E-01
K	0.921	7.4E-01	1.157	5.8E-01
L	1.016	9.5E-01	0.935	8.2E-01
M	1.814	1.1E-01	1.034	8.9E-01
N	0.934	6.9E-01	0.808	2.6E-01
P	1.010	9.3E-01	0.762	5.1E-02
Q	0.910	4.1E-01	0.791	8.2E-02
R	0.696	3.4E-01	0.887	5.7E-01
S	1.465	5.1E-02	0.958	8.6E-01
T	0.952	7.2E-01	0.873	4.9E-01
V	1.414	5.8E-02	0.937	7.5E-01
W	0.991	9.7E-01	0.957	9.3E-01
Y	1.013	9.6E-01	0.945	7.9E-01
Orn	2.373	**6.6E-03**	2.424	7.8E-02
Citru	1.292	3.1E-01	1.415	3.6E-01
fum	0.787	**7.2E-03**	0.728	**1.2E-03**
aco	0.899	1.9E-01	0.975	8.0E-01
akg	0.915	2.2E-01	0.473	**9.9E-05**
suc	0.802	**2.7E-03**	0.788	**6.7E-03**
(B) Shoots				
A	0.990	9.3E-01	1.445	**1.9E-02**
C	0.765	**1.9E-02**	1.377	**1.3E-02**
D	1.002	9.8E-01	1.045	5.1E-01
E	0.932	2.4E-01	1.106	2.9E-01
F	1.081	5.8E-01	1.369	1.7E-01
G	0.959	8.2E-01	1.160	4.9E-01
H	1.497	1.4E-01	0.899	6.1E-01
I	1.000	1.0E+00	0.769	2.4E-01
K	0.841	2.3E-01	1.169	5.3E-01
L	0.967	8.4E-01	1.343	4.7E-01
M	1.001	9.9E-01	1.141	5.3E-01
N	1.040	7.9E-01	1.430	**2.6E-02**
P	0.979	7.3E-01	1.055	8.1E-01
Q	0.852	9.5E-02	1.053	7.2E-01
R	0.692	2.1E-01	1.167	5.2E-01
S	1.013	9.1E-01	1.161	4.4E-01
T	0.814	**1.6E-02**	1.404	**2.7E-02**
V	1.183	3.4E-01	1.114	3.8E-01
W	1.169	3.5E-01	1.599	5.1E-02
Y	1.139	6.8E-01	1.059	6.9E-01
Orn	0.682	1.5E-01	1.177	7.3E-01
Citru	1.031	8.6E-01	1.236	1.3E-01
fum	0.912	2.2E-01	0.771	8.8E-02
aco	0.901	2.9E-01	1.163	2.2E-01
akg	0.880	1.9E-01	0.472	**9.2E-03**
suc	0.814	**3.1E-02**	1.159	3.2E-01

Supplementary table 7-11: Comparison of metabolite levels in *ALMT1*^{OE} grown under Pi-sufficient and Pi-deficient conditions to the levels detected in WT

Metabolite levels in (A) roots and (B) shoots of *ALMT1*^{OE} grown under Pi-sufficient and deficient conditions were compared to the levels detected in WT (Col-0). Seedlings were germinated for 6 days on +Pi agar plates, transferred to +Pi (500 µM) or –Pi (5 µM) conditions, and allowed to grow for additional 5 days before harvest. Data are normalized to the levels detected in WT+Pi. Shown are the preliminary data of one germination experiment. Four biological replicates (two pooled seedlings per replicate) were analyzed (n=04). Significance analyses were performed by Student's *t*-test (two-tailed, equal variances). Number in bold indicates significant difference between *ALMT1*^{OE} and WT with p<0.05. Light and dark grey cell highlight the metabolites which were significantly increased and reduced, respectively in the mutants compared to WT.

(A) Roots				
	+Pi		**-Pi**	
	fold Vs WT+Pi	***t*-test Vs WT+Pi**	**fold Vs WT-Pi**	***t*-test vs WT-Pi**
A	1.013	9.3E-01	2.070	**1.9E-02**
C	0.952	6.7E-01	2.126	**1.4E-02**
D	1.177	1.5E-01	1.731	**2.0E-02**
E	0.950	6.1E-01	1.259	1.6E-01
F	0.759	**4.3E-02**	3.304	**4.8E-04**
G	0.791	9.5E-02	1.739	**1.4E-02**
H	0.739	9.6E-02	3.422	**1.7E-03**
I	1.206	3.8E-01	3.829	**8.0E-04**
K	1.482	**7.5E-03**	2.991	**7.8E-03**
L	1.084	6.0E-01	3.014	**3.3E-03**
M	1.006	9.6E-01	1.732	**6.4E-03**
N	1.002	9.8E-01	2.607	**1.9E-03**
P	1.349	8.3E-02	2.766	**3.4E-02**
Q	0.881	2.9E-01	2.110	**1.4E-02**
R	1.409	8.7E-02	1.110	5.9E-01
S	0.831	1.6E-01	1.916	**7.8E-03**
T	0.855	2.7E-01	1.915	**1.3E-02**
V	0.959	7.6E-01	2.625	**4.1E-03**
W	0.825	2.9E-01	2.472	**6.8E-03**
Y	0.970	6.3E-01	3.090	**2.6E-03**
Orn	1.532	**3.1E-02**	3.029	**4.5E-04**
Citru	0.766	9.3E-02	2.709	**1.5E-02**
fum	0.814	**1.3E-03**	1.469	**1.1E-03**
aco	0.921	3.6E-01	1.047	7.8E-01
akg	1.201	**1.1E-02**	0.345	**6.1E-08**
suc	1.027	6.2E-01	1.329	**2.1E-02**
(B) Shoots				
A	0.871	1.7E-01	1.176	2.3E-01
C	0.969	6.1E-01	1.033	8.1E-01
D	1.330	**3.6E-03**	1.200	1.4E-01
E	0.959	5.3E-01	1.212	5.4E-02
F	0.756	9.0E-02	1.305	1.6E-01
G	0.750	2.4E-01	1.284	1.9E-01
H	0.723	2.9E-01	1.682	8.6E-02
I	0.996	9.5E-01	1.137	4.1E-01
K	1.190	**3.1E-02**	2.256	**1.5E-02**
L	0.931	6.3E-01	1.647	8.5E-02
M	1.157	3.6E-01	1.552	**4.2E-04**
N	0.999	9.9E-01	1.046	7.1E-01
P	1.117	8.7E-02	1.973	**1.3E-03**
Q	0.896	1.7E-01	1.008	9.5E-01
R	0.843	6.7E-01	1.419	**2.9E-02**
S	0.723	**4.8E-02**	0.907	**1.3E-02**
T	1.064	2.5E-01	1.070	6.0E-01
V	1.157	**2.1E-02**	0.972	8.0E-01
W	0.757	8.3E-02	2.144	**3.4E-03**
Y	0.860	4.2E-01	2.845	**1.0E-03**
Orn	0.764	4.9E-01	3.022	**7.0E-04**
Citru	1.180	7.8E-02	1.264	7.2E-02
fum	0.942	4.0E-01	0.923	3.1E-01
aco	1.076	3.3E-01	0.965	6.2E-01
akg	0.737	**4.4E-04**	1.310	**4.9E-02**
suc	0.842	**2.9E-02**	1.275	**1.8E-02**

Supplementary table 7-12: T-DNA insertion lines analyzed in this study

Gene	Locus	T-DNA insertion line	Additional information
PPCK1	At1G08650	GK_614F02_021894	*ppck1-1*; Feria et al., 2016; a 2nd site insertion affecting the expression of both *ALMT1* and *ALMT2* was detected in this line.
		SAIL_30_D02	*ppck1-2*; could not be genotyped
		SALK_116510.36.25	*ppck1-3*; exhibits same mRNA levels as WT
		SALKseq_138855.1	*ppck1-4*
		WiscDsLox477_480C13	*ppck1-5*; this mutant is in Col-2 background
		WiscDsLoxHs090_07H	
PPCK2	At3G04530	SALK_102132.37.95.x	*ppck2-1*; Feria et al., 2016; overexpression of *PPCK2*
		SALK_023356.42.45.X	*ppck2-2*; could not be genotyped
		GABI_196F01	*ppck2-3*; overexpression of *PPCK2*
		SAILseq_210_F08.1	*ppck2-4*; could not be genotyped
PPC1	At1G53310	SALK_088836.37.15.X	*ppc1-1*; Shi et al., 2015
		SALK_106414.23.50.X	
		SALK_070605C	
PPC2	At2G42600	SALK_128516.14.90.X	*ppc2-1*; Feria et al., 2016
		SALK_025005.49.75.X	*ppc2-2*; Shi et al., 2015
PPC3	At3G14940	SALK_031519C	*ppc3-1*; Feria et al., 2016; exhibit same mRNA level as WT
		SALK_143289.54.75.X	*ppc3-2*
ALMT1	At1G08430	SALK_009629C	*ALMT1$_{KO}$*
ALMT2	AT1G08440	SALK_108715C	*almt2-1*
		SAIL_1285_G09	*almt2-2*
		SALK_010570C	*almt2-3*
STOP1	AT1G34370	SALK_114108	a 2nd site insertion was detected
PHR1	At4G28610	SALK_067629C	
PHL1	At5G29000	SALK_079505C	

Supplementary table 7-13: Primers used for genotyping

LP, RP, and LB denotes Left primer, Right primer, and Left Border primer respectively.

Annealing temperature used for primers amplifying wild-type and mutant bands are separated by semicolon.

Locus	T-DNA insertion line	Primer	5'→3' sequence	Annealing temperature
PPCK1 (AT1G08650)	GK_614F02_021894	LP-PPCK1-GK(3) RP-PPCK1-GK(3) LB-GK-o8409	TCAGACGGCGTCGTTCGC TCCTCTCTACATTACCGTCTCTACC ATATTGACCATCATACTCATTGC	57°C; 53°C
	SALK_116510.36.25	LP-PPCK1-GK(3) RP-PPCK1-GK(3) LB1.3	TCAGACGGCGTCGTTCGC TCCTCTCTACATTACCGTCTCTACC ATTTTGCCGATTTCGGAAC	57°C; 54° C
	SALKseq_138855.1	K1-SPst-P1seqF RP-PPCK1-5(d) LB1.3	TACAAAGTACAAACCTTCTCCAAGT TCCTTTTACTCACCCCACATG ATTTTGCCGATTTCGGAAC	55°C; 52°C
	WiscDsLoxHs090_07H	LP-PPCK1-5(e) RP-PPCK1-5(e) LB4-Wisc	TCTGTTTCTCCTGCTCTTTGG AGGTAGAGCCGACTCAAGAGG TGATCCATGTAGATTTCCCGGACATGAAG	55°C; 60°C
	WiscDsLox477_480C13	LP-PPCK1-5(f) RP-PPCK1-5(f) LT6-Wisc	CTTAATGCTTGTTCGGCTGAG ACAAACCTTCTCCAAGTAAACTTC AATAGCCTTTACTTGAGTTGGCGTAAAAG	55°C; 58°C
PPCK2 (At3G04530)	SALK_102132.37.95.x	LP-PPCK2 RP-PPCK2 LB1.3	ATACGGGTAAGACGACCATTC CTGATTCTGATAACCTCCCCC ATTTTGCCGATTTCGGAAC	54°C; 54°C
	GABI_196F01	LP-PPCK2-6e RP-PPCK2-6e LB-GK-o8409	AGCATCTCTAGATGCTTTCGG CTCCGTCTCTATACACTCGCG ATATTGACCATCATACTCATTGC	55°C; 55°C
PPC1 (At1G53310)	SALK_088836.37.15.X	LP-SALK_088836 RP-SALK_088836 LB1.3	TGCTTATCGCCGTAGGA AAATCATAACCGGGAGTTAAA ATTTTGCCGATTTCGGAAC	50°C; 50°C
PPC2 (At2G42600)	SALK_128516.14.90.X	LP-PPC2-SALK1 RP-PPC2-SALK1 LB1.3	AAGGCCAAATGTTGACACTTG GCAAGATGAAATGAGAGCAGG ATTTTGCCGATTTCGGAAC	53°C; 53°C
	SALK_025005.49.75.X	LP-PPC2-SALK2 RP-PPC2-SALK2 LB1.3	GATACCATTCATGGGCAATTG TTTGGATTCAGTTTCACGAGC ATTTTGCCGATTTCGGAAC	53°C; 53°C
PPC3 (At3G14940)	SALK_031519C	LP-PPC3-SALK1 RP-PPC3-SALK1 LB1.3	TAGCTCCTGCTTGTCATCAGG GAATTTGGTTCCTTCTCCCAC ATTTTGCCGATTTCGGAAC	54°C; 54°C
	SALK_143289.54.75.X	LP-PPC3-SALK2 RP-PPC3-SALK2 LB1.3	CTGCATCTTTCCCTGAATCTG GAACTGCACAGGAACTCAAGG ATTTTGCCGATTTCGGAAC	53°C; 53°C
ALMT1 (At1G08430)	SALK_009629C	LP-ALMT1 RP-ALMT1 LB1.3	GAAATTATTTGGGGAAGCTGC TCTTTACCCATGGGAAAAACC ATTTTGCCGATTTCGGAAC	53°C; 53°C
ALMT2 (AT1G08440)	SALK_108715C	LP-ALMT2-26(a) RP-ALMT2-26(a) LB1.3	ATATTCGTCCCCAAATTCTGC TAAATAACGACGATCCATCCG ATTTTGCCGATTTCGGAAC	52°C; 52°C
	SAIL_1285_G09	LP-ALMT2-26(b) RP-ALMT2-26(b) LB1-SAIL	TCCACTGAGATCTCTCCATGC ACTTTTCGCCCCACAAAATAC GCCTTTTCAGAAATGGATAAATAGCCTTGCTTCC	54°C; 57° C
	SALK_010570C	LP-ALMT2-26(d) RP-ALMT2-26(d) LB1.3	AAATCTCTCTGCTGTGGAGGG AGCATGCACTACTCTTCTCGG ATTTTGCCGATTTCGGAAC	55°C; 55°C
STOP1 (AT1G34370)	SALK_114108	stop1_LP(2) stop1_RP(2) LB1.3	TTCATTGGTGAGAACGACTCC ATCTTCTTGTTGGTCGTGGTG ATTTTGCCGATTTCGGAAC	55°C; 55°C
Stop1[48](From Prof. Thierry Desnos)	Dominant negative EMS mutant	FP-Stop1dCAPS RP-Stop1dCAPS	CACACGCCTGCAATCCCTCTTGAAGAGAC AAAACATATCCTCCCATCAGTCATTCCACGCT	63°C
PHR1 (At4G28610)	SALK_067629C	LP-PHR1 RP-PHR1 LB1.3	GAGAGACCTCACACGCACTTC CTTTCTGGCGAACCTGTAGTG ATTTTGCCGATTTCGGAAC	55°C; 51°C
PHL1 (At5G29000)	SALK_079505C	LP-PHL1 RP-PHL1 LB1.3	GTGGAGACGTTTCTGCACTTC GGAGTAAGGGTGGACTCATCC ATTTTGCCGATTTCGGAAC	56°C; 51°C

Supplementary table 7-14: Transgenic lines generated during the course of this study

SL. No.	Transgenic lines	Purpose
1	*pPPCK1$_{long}$::GFP-GUS*	Tissue specific localization
2	*pPPCK1$_{short}$::GFP-GUS*	Tissue specific localization
3	*pPPCK2$_{long}$::GFP-GUS*	Tissue specific localization
4	*pPPCK2$_{short}$::GFP-GUS*	Tissue specific localization
5	*pPPCK1$_{short}$::gDNA/ppck1*	Complementation of *ppck1-1*
6	*pPPCK1$_{short}$::gDNA-GFP/ppck1*	Complementation of *ppck1-1*
7	*pPPCK1$_{long}$::gDNA/ppck1*	Complementation of *ppck1-1*
8	*pPPCK1$_{long}$::gDNA-GFP/ppck1*	Complementation of *ppck1-1*
9	*35S::GFP-PPCK1*	Subcellular localization and overexpression of *PPCK1*
10	*35S::PPCK1-GFP*	Subcellular localization and overexpression of *PPCK1*
11	*35S::PPCK1*	Overexpression of *PPCK1*
12	*UB10::GFP-PPCK1*	Subcellular localization and overexpression of *PPCK1*
13	*UB10::PPCK1-GFP*	Subcellular localization and overexpression of *PPCK1*
14	*UB10::PPCK1*	Overexpression of *PPCK1*
15	*35S::GFP-PPCK2*	Subcellular localization and overexpression of *PPCK2*
16	*35S::PPCK2-GFP*	Subcellular localization and overexpression of *PPCK2*
17	*35S::PPCK2*	Overexpression of *PPCK2*
18	*UB10::GFP-PPCK2*	Subcellular localization and overexpression of *PPCK2*
19	*UB10::PPCK2-GFP*	Subcellular localization and overexpression of *PPCK2*
20	*UB10::PPCK2*	Overexpression of *PPCK2*

Supplementary table 7-15: Primers used for amplification of products for Directional TOPO cloning

FP and RP denotes forward and reverse primer respectively.

Target	Product size	Primer	5'→3' sequence
PPCK1-CDS+STOP	855 bp	FP-PPCK1-CDS	CACCATGACTTGCAGCCAAAC
		RP-PPCK1-CDS+STOP	CTAGATGAATCTCTCCTCTGTTTCTCCT
PPCK1-CDS-STOP	852 bp	FP-PPCK1-CDS	CACCATGACTTGCAGCCAAAC
		RP-PPCK1-CDS-STOP	GATGAATCTCTCCTCTGTTTCTCC
pPPCK1$_{short}$	1029 bp	FP-SHORT PROMOTER PPCK1	CACCGGAGGAGCAAGAAGTAGATAG
		RP-PROMOTER PPCK1	AATATCACTTTCTTAATATTTTTTGTTTTGTG
pPPCK1$_{long}$	2468 bp	FP-LONG PROMOTER PPCK1	CACCATACAAAAGACATGAACTG
		RP-PROMOTER PPCK1	AATATCACTTTCTTAATATTTTTTGTTTTGTG
pPPCK1$_{short}$*::gPPCK1 +STOP*	2056 bp	FP-SHORT PROMOTER PPCK1	CACCGGAGGAGCAAGAAGTAGATAG
		RP-PPCK1-CDS+STOP	CTAGATGAATCTCTCCTCTGTTTCTCCT
pPPCK1$_{short}$*::gPPCK1 -STOP*	2053 bp	FP-SHORT PROMOTER PPCK1	CACCGGAGGAGCAAGAAGTAGATAG
		RP-PPCK1-CDS-STOP	GATGAATCTCTCCTCTGTTTCTCC
pPPCK1$_{long}$*::PPCK1 +stop codon*	3495 bp	FP-LONG PROMOTER PPCK1	CACCATACAAAAGACATGAACTG
		RP-PPCK1-CDS+STOP	CTAGATGAATCTCTCCTCTGTTTCTCCT
pPPCK1$_{long}$*::PPCK1-stop codon*	3493 bp	FP-LONG PROMOTER PPCK1	CACCATACAAAAGACATGAACTG
		RP-PPCK1-CDS-STOP	GATGAATCTCTCCTCTGTTTCTCC
PPCK2-CDS+STOP	837 bp	FP-PPCK2-CDS	CACCATGACCAGAG AATTCG
		RP-PPCK2-CDS+STOP	CTAATTGCTTTGGAGGTTTCCAAC
PPCK2-CDS-STOP	834 bp	FP-PPCK2-CDS	CACCATGACCAGAG AATTCG
		RP-PPCK2-CDS-STOP	ATTGCTTTGGAGGTTTCCAACGT
pPPCK2$_{short}$	1235 bp	FP-SHORT PROMOTER PPCK2	CACCGTTTTCAGCAATTTGCTTATTT
		RP-PROMOTER PPCK2	CGGAATATTCCTTTTTTCTTGTTGT
pPPCK2$_{long}$	2699 bp	FP-LONG PROMOTER PPCK2	CACCTTAGAACATTTGGTCATATTTGTGG
		RP-PROMOTER PPCK2	CGGAATATTCCTTTTTTCTTGTTGT

Supplementary table 7-16: Primers used for colony PCR

FP and RP denotes forward and reverse primer respectively.

Expression cassette in Agrobacterium	Primers	5'→ 3' sequence
pEXP-pUB-N-GFP-Dest-PPCK1-CDS+STOP	FP-PPCK1-CDS RP-PPCK1-CDS+STOP	CACCATGACTTGCAGCCAAAC CTAGATGAATCTCTCCTCTGTTTCTCCT
pEXP-pB7WGF2-PPCK1-CDS+STOP	FP-PPCK1-CDS RP-PPCK1-CDS+STOP	CACCATGACTTGCAGCCAAAC CTAGATGAATCTCTCCTCTGTTTCTCCT
pEXP-pB7WG2-PPCK1-CDS+STOP	FP-PPCK1-CDS RP-PPCK1-CDS+STOP	CACCATGACTTGCAGCCAAAC CTAGATGAATCTCTCCTCTGTTTCTCCT
pEXP-pUB-Dest-PPCK1-CDS+STOP	FP-PPCK1-CDS RP-PPCK1-CDS+STOP	CACCATGACTTGCAGCCAAAC CTAGATGAATCTCTCCTCTGTTTCTCCT
pEXP-pUB-N-GFP-Dest-PPCK2-CDS+STOP	FP-PPCK2-CDS RP-PPCK2-CDS+STOP	CACCATGACCAGAG AATTCG CTAATTGCTTTGGAGGTTTCCAAC
pEXP-pB7WGF2-PPCK2-CDS+STOP	FP-PPCK2-CDS RP-PPCK2-CDS+STOP	CACCATGACCAGAG AATTCG CTAATTGCTTTGGAGGTTTCCAAC
pEXP-pB7WG2-PPCK2-CDS+STOP	FP-PPCK2-CDS RP-PPCK2-CDS+STOP	CACCATGACCAGAG AATTCG CTAATTGCTTTGGAGGTTTCCAAC
pEXP-pUB-Dest-PPCK2-CDS+STOP	FP-PPCK2-CDS RP-PPCK2-CDS+STOP	CACCATGACCAGAG AATTCG CTAATTGCTTTGGAGGTTTCCAAC
pEXP-pBGWFS7-pPPCK1$_{short}$	FP- SHORT PROMOTER- PPCK1 RP-PROMTER-PPCK1	CACCGGAGGAGCAAGAAGTAGATAG AATATCACTTTCTTAATATTTTTTGTTTTGTG
pEXP-pBGWFS7-pPPCK1$_{long}$	K1-LP-P1seqF K1-LP-P3seqR	TTCATCAACTGGGCATACATGAGC GGAGATAATCCCTGCAAGTAAG
pEXP-pBGWFS7-pPPCK2$_{short}$	FP-SHORT-PROMOTER-PPCK2 RP- PROMOTER-PPCK2	CACCGTTTTCAGCAATTTGCTTATTT CGGAATATTCCTTTTTTCTTGTTGT
pEXP-pBGWFS7-pPPCK2$_{long}$	K2-LP-P1seqF K2-LP-P2seqR	CATCTTGATTTGGCTCACTGC TCGTCTTACCCGTATAGATGC
pEXP-pUB-C-GFP-PPCK1-CDS-STOP	FP-PPCK1-CDS RP-PPCK1-CDS-STOP	CACCATGACTTGCAGCCAAAC GATGAATCTCTCCTCTGTTTCTCC
pEXP-pB7FWG2-PPCK1-CDS-STOP	FP-PPCK1-CDS RP-PPCK1-CDS-STOP	CACCATGACTTGCAGCCAAAC GATGAATCTCTCCTCTGTTTCTCC
pEXP-pUB-C-GFP-PPCK2-CDS-STOP	FP-PPCK2-CDS RP-PPCK2-CDS-STOP	CACCATGACCAGAG AATTCG ATTGCTTTGGAGGTTTCCAACGT
pEXP-pB7FWG2-PPCK2-CDS-STOP	FP-PPCK2-CDS RP-PPCK2-CDS-STOP	CACCATGACCAGAG AATTCG ATTGCTTTGGAGGTTTCCAACGT
pEXP-pB7WG-pPPCK1::gPPCK1+STOP	K1-SPst-P1seqF RP-PPCK1-CDS+STOP	TACAAAGTACAAACCTTCTCCAAGT CTAGATGAATCTCTCCTCTGTTTCTCCT
pEXP-pB7FWG,0-pPPCK1short::gPPCK1-STOP	K1-SPst-P1seqF RP-PPCK1-CDS-STOP	TACAAAGTACAAACCTTCTCCAAGT GATGAATCTCTCCTCTGTTTCTCC
pEXP-pB7WG-pPPCK1$_{long}$::PPCK1+STOP	K1-LPst-P1seqF K1-LPst-P4seqR	GAGCTTATCATATGCCTTCTCAAG CATTCTCAACAGATCCAGATTTGT
pEXP-pB7FWG,0-pPPCK1$_{long}$::PPCK1-STOP	K1-LPst-P1seqF K1-LPst-P4seqR	GAGCTTATCATATGCCTTCTCAAG CATTCTCAACAGATCCAGATTTGT

Supplementary table 7-17: Primers used for sequencing of pENTR clones

FP and RP denotes forward and reverse primer respectively.

Target	Primer	5'→ 3' sequence
PPCK1	K1-LP-P1seqF	TTCATCAACTGGGCATACATGAGC
PPCK1	K1-LP-P2seqF	ATAGGCAACAGTAAGAAGCTCATC
PPCK1	K1-LP-P3seqR	GGAGATAATCCCTGCAAGTAAG
PPCK1	K1-SPst-P1seqF	TACAAAGTACAAACCTTCTCCAAGT
PPCK1	K1-SPst-P2seqR	AGATGGAGAGAGTCGAATCAG
PPCK1	K1-LPst-P1seqF	GAGCTTATCATATGCCTTCTCAAG
PPCK1	K1-LPst-P2seqR	CCATGAAGATGGAGAGAGTCG
PPCK1	K1-LPst-P3seqF	GCAGCATCAAGAGAAAGTACCTG
PPCK1	K1-LPst-P4seqR	CATTCTCAACAGATCCAGATTTGT
PPCK2	K2-Lp-P1seqF	CATCTTGATTTGGCTCACTGC
PPCK2	K2-Lp-P2seqR	TCGTCTTACCCGTATAGATGC
PPCK2	K2-Lp-P3seqF	TGTATGCGTCGGCTAATTTG
PPCK2	K2-SPstop-P1seqF	GGACAGACATTTGAATATTGAAG
PPCK2	K2-SPstop-P2seqR	CGTAGAGATCGAAGATCCTGATG
PPCK2	M13 F	GTAAAACGACGGCCAG
PPCK2	M13 R	CAGGAAACAGCTATGAC

Supplementary table 7-18: Restriction enzymes used to digest entry and destination cassette

Cloning cassette	Restriction enzymes used for digestion	Product size
Entry cassette		
pENTR-PPCK1-CDS+STOP	BamHI and NotI	831 bp, 2604 bp
pENTR-PPCK1-CDS-STOP	BamHI and NotI	831 bp, 2601 bp
pENTR-PPCK2-CDS+STOP	NotI and PstI	796 and 2621 bp
pENTR-PPCK2-CDS-STOP	NotI and PstI	796 and 2618 bp
PENTR-pPPCK1$_{long}$	NotI and ScaI	1878 bp and 3170 bp
PENTR-pPPCK1$_{short}$	NotI and ScaI	439 and 3170 bp
PENTR-pPPCK1$_{short}$::gPPCK1+STOP	NotI and BamHI	2032 and 2604 bp
PENTR-pPPCK1$_{short}$::gPPCK1-STOP	NotI and BamHI	2032 and 2604 bp
pENTR-pPPCK2$_{short}$	NotI and HindIII	1096 and 2719 bp
pENTR-pPPCK2$_{short}$::gPPCK2+STOP	NotI and HindIII	1096 and 3630 bp
pENTR-pPPCK2$_{short}$::gPPCK2-STOP	NotI and HindIII	1096 and 3627 bp
PENTR-pPPCK1$_{long}$::gPPCK1+STOP	NotI and BamHI	3471 and 2604 bp
PENTR-pPPCK1$_{long}$::gPPCK1-STOP	NotI and BamHI	3471 and 2601bp
pENTR-pPPCK2$_{long}$	NotI and XbaI	1752 and 3527 bp
Destination cassette		
pEXP-pUB-N-GFP-Dest-PPCK1-CDS+STOP	NcoI and SacI	1465, 527, 8476, and 261bp
pEXP-pB7WGF2-PPCK1-CDS+STOP	HindIII and BamHI	2655, 7860, and 345 bp
pEXP-pB7WG2-PPCK1-CDS+STOP	HindIII and BamHI	1938, 7860, and 345 bp
pEXP-pUB-Dest-PPCK1-CDS+STOP	NcoI and SacI	738, 527, 8528, and 261 bp
pEXP-pUB-N-GFP-Dest-PPCK2-CDS+STOP	BamHI and NdeI	1931,3651,2489, and 2640 bp
pEXP-pB7WGF2-PPCK2-CDS+STOP	BamHI and ScaI	552 bp, 7658, and 2632 bp
pEXP-pB7WG2-PPCK2-CDS+STOP	BamHI and NdeI	1733, 2489, 3652, and 2251 bp
pEXP-pUB-Dest-PPCK2-CDS+STOP	BamHI and PmlI	495, 1256, and 8285 bp
pEXP-pBGWFS7-pPPCK1$_{short}$	BamHI and ScaI	544, 3656, and 7661 bp
pEXP-pBGWFS7-pPPCK1$_{long}$	BamHI and ScaI	1983, 3656, and 7661 bp
pEXP-pBGWFS7-pPPCK2$_{short}$	BamHI and ScaI	1263, 3143, and 7661 bp
pEXP-pBGWFS7-pPPCK2$_{long}$	BamHI and HindIII	418, 2247, and 10866 bp
pEXP-pUB-C-GFP-PPCK1-CDS-STOP	EcoRI and NdeI	2489, 1979, and 6300 bp
pEXP-pB7FWG2-PPCK1-CDS-STOP	AscI and SacI	585, 1397, and 8879 bp
pEXP-pUB-C-GFP-PPCK2-CDS-STOP	NotI and PstI	796, 1100, 4011, 1290, 1532, and 2021 bp
pEXP-pB7FWG2-PPCK2-CDS-STOP	BamHI and ScaI	552, 7658, and 2633 bp
pEXP-pB7WG-pPPCK1short::gPPCK1+STOP	AscI and NdeI	2489, 3952, 2148, and 1763 bp
pEXP-pB7FWG,0-pPPCK1short::gPPCK1-STOP	AscI and NdeI	2489, 4669, and 3841 bp
pEXP-pB7WG-pPPCK1$_{long}$::PPCK1+STOP	EcoRI and PvuI	1865, 2922, 1017, and 5987 bp
pEXP-pB7FWG,0-pPPCK1$_{long}$::PPCK1-STOP	EcoRI and PvuI	1865, 3636, 1017, and 5920 bp

Supplementary table 7-19: Primers used in RT-PCR and RT-qPCR

FP and RP denote forward and reverse primer respectively.

Template	Locus	Primer	5'→3' sequence
PPC1	At1G53310	FP-PPC1-QRT	AGCTTAACCCGACTAGCGAATA
		RP-PPC1-QRT	TTAACCGGTGTTTTGTAGACCAG
PPC2	At2G42600	FP-PPC2-QRT	AGGGTATCGCTGCTGGTATG
		RP-PPC2-QRT	GCGTACGGGATAGGAGTTGG
PPC3	At3G14940	FP-PPC3-QRT	GCAATCAAGCAAATCAGCACA
		RP-PPC3-QRT	AGATAAGTGTGTCCTCAAGTCC
PPCK1	At1G08650	FP-PPCK1-QRT	GCTTATCATCTCTCTCGGTGGT
		RP-PPCK1-QRT	TTACATGCCCGACACTCCTC
		FP-K1-QRT(2)	AAAGCCTCTCTCTCCGACGA
		RP-K1-QRT(2)	CATGAGCTTAGGCTCGTTGTC
		FP-PPCK1-SRT (RT-PCR)	GTGAGGGAGAGACCACCGAA
		RP-PPCK1-SRT (RT-PCR)	CCGACACTCCTCCATACTTGTT
PPCK2	At3G04530	FP-PPCK2-QRT	TCTGTATCATCGGAAGCGAAGG
		RP-PPCK2-QRT	CGCCGAGAAACATCACGACA
ALMT1	At1G08430	FP-ALMT1-QRT	GGTCGTGCCATGCCAATAGA
		RP-ALMT1-QRT	ACGTCATGTAAAACTGTGACAACA
ALMT2	AT1G08440	FP-ALMT2-QRT	GGTGACGTTGACACATCAAACA
		RP-ALMT2-QRT	CACTGAGATCTCTCCATGCGAT
STOP1	AT1G34370	FP-STOP1-QRT	TGCTTATTGCGAATGCCTGTG
		RP-Stop1-QRT	AG TATCTGAAACAGACTCACCAACA
PHR1	At4G28610	FP-PHR1-QRT	CACAGCCAAAGCGTCCCAAA
		RP-PHR1-QRT	ACTCCGAGATTATCCAGCAAAAGA
PHL1	At5G29000	FP-PHL1-QRT	CAGCATCAAGGAAACGTGTCAG
		RP-PHL1-QRT	ACATGTTTCGTCAAACGAGATCAA
PP2A	AT1G13320	FP-PP2A-QRT	AGCCAACTAGGACGGATCTGGT
		RP-PP2A-QRT	GCTATCCGAACTTCTGCCTCATTA
CNADMDH1	AT1G04410	FP-C-NAD-MDH1-QRT	TGATGAGCTCTTCGATAATGGGT
		RP-C-NAD-MDH1-QRT	ACACAATAACACCATTCCTCACA
MMDH1	AT1G53240	FP-MMDH1-QRT	ACCTCCTCCTTCATCGGGTT
		RP-MMDH1-QRT	GGTTTCACTAATGGAGGCACA
MMDH2	AT3G15020	FP-MMDH2-QRT	TCTGCTCTTGAGGAACCAACC
		RP-MMDH2-QRT	ACATAGCAGCACAACAGCTTG
PNAD-MDH	AT3G47520	FP-pNAD-MDH-QRT	ACGGAGATGTCTACGAGTGC
		RP-pNAD-MDH-QRT	ACCCGTGATGCAAAGAAAGGA
CNADMDH2	AT5G43330	FP-C-NAD-MDH2-QRT	AGATGGATTTGACAGCAGAGGAG
		RP-C-NAD-MDH2-QRT	GAGAGGCATGAGTAAGCGAGG
CNADMDH3	AT5G56720	FP-C-NAD-MDH3-QRT	CCGGTTATCTGTGAGAAAGGGA
		RP-C-NAD-MDH3-QRT	TCTCCCTCGAAAACTCGTCT
NADPMDH	AT5G58330	FP-NADP-MDH-QRT	GGGGAAGTTTGATTTTTGCAGGA
		RP-NADP-MDH-QRT	ACAGCTAACAACCCGGAAGAG
ACTIN2	AT3G18780	FP-ACTIN2-SRT (RT-PCR)	CAAAGACCAGCTCTTCCATC
		RP-ACTIN2-SRT (RT-PCR)	CTGTGAACGATTCCTGGACCT

Supplementary table 7-20: MS parameters for MRM-transitions of organic acids (Ziegler et al., 2016)

Organic acid	MRM transitions	Retention time, min	Segment	Ionization energy, eV	Collision energy, eV
Succinate-D4	267→177 267→251	5.01	1	-135	5 5
Succinate	263→173 263→247	5.05			5 5
Fumarate	261→245 261→171	5.50			5 10
Malate	351→233 351→189	7.55	2	-135	5 15
Malate-D3	354→236 351→192	7.53			5 15
α-ketoglutarate	320→244 320→230	8.65	3	-135	5 10
Aconitate	391→211 391→301	10.55			5 15
Citrate-D4	485→276 485→367	11.03	4	-135	5 15
Citrate	481→273 481→363	11.04			5 15

ACKNOWLEDGEMENT

Coming to Halle for pursuing PhD was a life changing experience for me. It not only developed me as a scientist but also evolved me into a responsible person. This PhD would not have been achievable without the support and guidance that I received from so many people from different walks of my life.

My foremost gratitude goes to my mentor **Dr. Jörg Ziegler** for his invaluable guidance and unending support. His committed supervision and constant encouragement helped me enormously during my research. I thank him for always being so supportive of my work.

I am very grateful to **Prof. Dr. Steffen Abel** for accepting me as a PhD student in the department of Molecular Signal Processing and for the valuable discussions that positively helped in shaping this thesis. A special thanks to him for reviewing my thesis as well. I would also like to express my gratitude to **Prof. Dr. Ingo Heilmann (MLU, Halle, Germany)** and **Prof. Paul B. Larsen (UC, Riverside, USA)** for investing their time and energy to review my thesis. Many thanks to thesis committee members for evaluating my PhD research.

I have great pleasure in acknowledging the insights given by **Dr. Katharina Bürstenbinder** and **Dr. Selma Gago Zachert** on this project. My heartfelt thanks to **Dr. Christin Naumann** for reading my thesis and for her feedback to shape it even better.

A positive environment is very much needed in the place of work and I owe a very deep sense of gratitude to all my former and present lab members - **Pascal**, **Maria**, **Lena**, **Gina**, **Nancy**, and **Kathrin** for their help and support and for keeping the atmosphere of the lab very cheerful, which helped me to carry out my work with a lot of enthusiasm. I am thankful to every colleague of the **MSV department** for their thoughtful advices on my project and for creating a blissful environment in the department.

I greatly acknowledge the funding from the **Erasmus Mundus BRAVE Programme of the European Union**. My sincere gratitude to BRAVE coordinators **Dr. Andreas Voloudakis (AUA, Greece)**, **Prof. Dr. Sven Erik Behrens (MLU, Germany)**, and coordinators from India, especially **Dr. Basanta K. Borah** who worked tirelessly to make this programme a great success. I also want to thank **MLU, Halle-Wittenberg** for supporting me with PhD finalization grant.

My gratitude is towards all my friends, here in Halle and in India, for their inspiring and kind words which lifted my spirit up whenever I felt low. A very special thanks to **Somnath** for being my best friend and for all his advices and support during my thesis writing stage.

I am forever indebted to my parents (**Ma**, **deta**, and **Dangoma**) for their unconditional love and blessings and for always believing in me. I am very grateful to them for being my biggest source of strength and inspiration. I would also like to express my gratitude to my wonderful siblings (**Lakhimi**, **Runumi**, **Manju**, and **Roshan**) for always being there for me, for their constant motivation, and support while taking critical decisions in my life. Many thanks to **Meethu** and **Happy** for delighting me every time with their happy faces. I am very grateful to **Neeraj** for being by my side always.

Lastly, my sincerest thanks are to '**Lord Krishna**' for giving me the strength and courage to sail through this challenging period successfully.

CURRICULUM VITAE

Name: Ranju Chutia

Nationality: Indian

Date of Birth: 16.11.1990

Place of birth: Sabarmati, India

Education

2014-present	**PhD Candidate** Leibniz Institute of Plant Biochemistry, Halle (Saale) Dissertation thesis : Manipulation of malate biosynthesis and exudation in *Arabidopsis thaliana* Supervisor: Prof. Dr. Steffen Abel
2012-2014	**Master of Science (Agri. Biotechnology)** Assam Agricultural University, Jorhat, India Thesis: Population polymorphism study of tulsi (*Ocimum* sp.) in Assam Supervisor: Dr. Basanta K. Borah
2008-2012	**Bachelor of Science (Agriculture)** Assam Agricultural University, Jorhat, India

Conference and workshop attendances

11th Plant Science Student Conference	IPB, Halle, Germany, 2015
12th Plant Science Student Conference	IPK, Gatersleben, Germany, 2016
30th Conference on Molecular Biology of Plants	Dabringhausen, Germany, 2016
10th International metabolomics workshop	Leiden, Netherlands, 2017

List of publications

1) **Chutia R**, Abel S, Ziegler J. Iron and Phosphate Deficiency Regulators Concertedly Control Coumarin Profiles in Arabidopsis thaliana Roots during Iron, Phosphate, and Combined Deficiencies. Frontiers in plant science. 2019; 10:113.
doi: 10.3389/fpls.2019.00113.

2) Ziegler J, Schmidt S, **Chutia R**, Müller J, Böttcher C, Strehmel N, Scheel D, Abel S. Non-targeted profiling of semi-polar metabolites in Arabidopsis root exudates uncovers a role for coumarin secretion and lignification during the local response to phosphate limitation. Journal of experimental botany. 2015; 67(5): 1421-32.
doi:10.1093/jxb/erv539.

STATUTORY DECLARATION

Hiermit erkläre ich an Eides statt, dass ich mich mit der vorliegenden wissenschaftlichen Arbeit erstmals um die Erlangung des Doktorgrades bewerbe, die Arbeit selbständig und ohne fremde Hilfe verfasst, nur die angegebenen Quellen und Hilfsmittel genutzt und die den benutzten Werken wörtlich oder inhaltlich entnommenen Stellen als solche kenntlich gemacht habe.

Halle (Saale), den Ranju Chutia